UCLA
UCLA Electronic Theses and Dissertations

**Title**
Investigation of the roles of Coq8p, a putative kinase, and alternate ring precursors in coenzyme Q biosynthesis

**Permalink**
https://escholarship.org/uc/item/89b7p4mr

**Author**
Xie, Letian

**Publication Date**
2014

Peer reviewed|Thesis/dissertation

eScholarship.org Powered by the California Digital Library
University of California

UNIVERSITY OF CALIFORNIA

Los Angeles

# Investigation of the roles of Coq8p, a putative kinase, and alternate ring precursors in coenzyme Q biosynthesis

A dissertation submitted in partial satisfaction of the requirement for the degree Doctor of Philosophy in Biochemistry and Molecular Biology

by

Letian Xie

2014

**ABSTRACT OF THE DISSERTATION**

Investigation of the roles of Coq8p, a putative kinase, and alternate ring precursors in coenzyme Q biosynthesis

by

Letian Xie

Doctor of Philosophy in biochemistry and Molecular Biology

University of California, Los Angeles, 2014

Professor Catherine F. Clarke, Chair

Coenzyme Q (ubiquinone or Q) is an essential redox-active, polyisoprenylated benzoquinone lipid essential for electron and proton transport in the mitochondrial respiratory chain. Eleven genes products, Coq1-Coq9, Yah1 and Arh1, are required for Q biosynthesis in yeast *Saccharomyces cerevisiae*.

Chapter 2 details the investigation of the biological function of Coq8 and its human homolog ADCK3. Expression of ADCK3 harboring an amino-terminal yeast mitochondrial leader sequence successfully rescued growth of *coq8* mutants on non-fermentable carbon source, partially restored Q biosynthesis and the phosphorylation states of Coq3, Coq5, and Coq7.

Chapter 3 investigates the use of over-expression of *COQ8* as a tool to study Q biosynthesis pathway in *S. cerevisiae.* Over-expression of the Coq8 protein restores the steady state

levels of the unstable Coq proteins. This stabilization results in the accumulation of several novel $Q_6$ biosynthetic intermediates. Several of the new intermediates contain a C4-amine and provide information on the deamination reaction that takes place when *para*-aminobenzoci acid is used as a ring precursor in Q biosynthesis.

Chapter 4 studies the use of *para*-aminobenzoic acid, and resveratrol as alternative aromatic ring precursors in Q biosynthesis in *E. coli, S. cerevisiae,* mouse and human cells. In contrast to *S. cerevisiae*, neither *E. coli* nor mammalian cells could utilize pABA as ring precursors in Q biosynthesis. However, *E. coli* cells labeled with $^{13}C_6$-pABA generated several novel N-containing early intermediates, suggesting UbiA, UbiD,X, and Ubil are capable of using pABA as substrates. *E. coli, S. cerevisiae,* human and mouse cells cultured in the presence of $^{13}C_6$-resveratrol were able to synthesize $^{13}C_6$-Q. Thus, future evaluation of the physiological and pharmacological responses to dietary polyphenols should consider their metabolism to Q.

The dissertation of Letian Xie is approved.

Steven G. Clarke

Yibin Wang

Catherine F. Clarke, Committee Chair

University of California, Los Angeles

2014

**To my mom and dad, whom I love deeply.**

**谢谢你们**

## Table of Contents


| | | |
|---|---|---|
| List of Tables and Figures | | viii |
| Acknowledgments | | xi |
| Vita | | xiv |
| Chapter 1 | An introduction to Coenzyme Q | 1 |
| | References | 10 |
| Chapter 2 | Expression of Human atypical kinase ADCK3 rescues coenzyme Q biosynthesis and phosphorylation of Coq polypeptides in yeast *coq8* mutants | 11 |
| | References | 25 |
| Chapter 3 | Overexpression of the Coq8 Kinase in *Saccharomyces cerevisiae coq* Null Mutants Allows for Accumulation of Diagnostic Intermediates of the Coenzyme $Q_6$ Biosynthetic Pathway | 28 |
| | References | 38 |
| Chapter 4 | Investigation of alternative ring precursors of Coenzyme Q in *E. coli, S. cerevisiae,* mouse and human cells | 40 |
| | References | 55 |
| Chapter 5 | Perspectives | 68 |
| | References | 74 |
| Appendix I | *para*-Aminobenzoic Acid is a Precursor in Coenzyme $Q_6$ Biosynthesis in *Saccharomyces cerevisiae* | 76 |

| | | |
|---|---|---|
| Appendix II | *COQ6* mutations in human patients produce nephrotic syndrome with sensorineural deafness | 88 |
| Appendix III | Probucol ameliorates renal and metabolic sequelae of primary CoQ deficiency in *Pdss2* mutant mice | 100 |
| Appendix IV | Focal segmental glomerulosclerosis is associated with a *PDSS2* haplotype and, independently, with a decreased content of coenzyme $Q_{10}$ | 118 |
| Appendix V | *ADCK4* mutations promote steroid-resistant nephrotic syndrome through $CoQ_{10}$ biosynthesis disruption | 129 |

## List of Tables and Figures


| | | | |
|---|---|---|---|
| **Chapter 1** | Figure 1 | Coeznyme $Q_6$ biosynthesis in yeast *S. cerevisiae* | 8 |
| | Figure 2 | Biosynthetic pathway of $CoQ_8$ in *Escherichia coli* | 9 |
| **Chapter 2** | Table 1 | Genotype and sources of *S. cerevisiae* strains | 16 |
| | Table 2 | Plasmid constructs used in this study | 17 |
| | Figure 1 | Coq8p is a peripheral membrane protein, associated with the mitochondrial inner membrane on the matrix side | 19 |
| | Figure 2 | The Lysine216 in kinase subdomain II of Coq8 is required for the rescue of glycerol growth in yeast *coq8* null mutant | 19 |
| | Figure 3 | The yeast Coq8-K216A polypeptide is not present at normal steady-state levels | 19 |
| | Figure 4 | Seven yeast *coq8* mutant strains have normal steady-state levels of the Coq8 polypeptide | 20 |
| | Table 4 | Amino acid and nucleotide substitutions of *coq8* alleles | 20 |
| | Figure 5 | Amino acid alignment of Abc1/Coq8p homologs | 21 |
| | Figure 6 | Expression of the human ADCK3 polypeptide rescues the growth of yeast *coq8* mutants on non fermentable carbon source media | 22 |
| | Figure 7 | Expression of the human ADCK3 polypeptide | 22 |

| | | | |
|---|---|---|---|
| | | partially restores $Q_6$ content in yeast *coq8* mutants | |
| | Figure 8 | Expression of the human ADCK3 polypeptide in yeast *coq8* mutants partially restores steady-state levels of some of the yeast Coq polypeptides | 22 |
| | Figure 9 | Expression of the human ADCK3 polypeptide in yeast *coq8* mutants partially restores the phosphorylation state of the yeast Coq3 polypeptide | 23 |
| | Figure 10 | Expression of the human ADCK3 polypeptide in yeast *coq8* mutants partially restores the phosphorylation state of the yeast Coq5 and Coq7 polypeptides | 23 |
| | Figure 11 | The carboxyl terminal segment of Coq8 homologs and the amino terminal segment of RsbU homologs share a region of high identity | 24 |
| **Chapter 3** | Figure 1 | *S. cerevisiae* $Q_6$ biosynthetic pathway | 31 |
| | Table 1 | Genotype and source of yeast strains | 31 |
| | Table 2 | Plasmid constructs used in this study | 32 |
| | Figure 2 | Overexpression of Coq8 in several Δ*coq* strains restores steady state levels of Coq4, Coq7, and Coq9 | 32 |
| | Figure 3 | Overexpression of Coq8 restores steady state levels of Coq polypeptides in isolated mitochondria | 33 |
| | Figure 4 | Overexpression of Coq8-G130D does not restore steady state levels of Coq polypeptides | 33 |

| | | | |
|---|---|---|---|
| | Figure 5 | Δ*coq7 and* Δ*coq5* strains overexpressing Coq8 accumulate the respective Q intermediates, $DMQ_6$ and $DDMQ_6$ | 34 |
| | Figure 6 | Bypass of the respiratory growth defect of the Δ*coq7* strain with alternate ring precursors | 35 |
| | Figure 7 | Δ*coq3* and Δ*coq4* strains overexpressing Coq8 or a coq4-1 strain accumulate early $Q_6$ biosynthetic intermediates | 36 |
| | Figure 8 | Coq9 is important for Coq6 and Coq7 hydroxylation steps and for removal of the amino substituent | 37 |
| **Chapter 4** | Figure 1A | Q biosynthesis in yeast *S. cerevisiae* | 59 |
| | Figure 1B | Q biosynthesis in *E. coli* | 60 |
| | Figure 2 | pABA is not a precursor to $Q_{10}$ in mammalian cells | 61 |
| | Figure 3 | pABA is not a precursor to $Q_8$ in *E. coli* | 62 |
| | Figure 4 | pABA related intermediates in *E. coli.* Q biosynthesis | 63 |
| | Figure 5 | Resveratrol is a ring precursor to Q biosynthesis in yeast *S. cerevisiae* and mammalian cells | 65 |
| | Figure 6 | Increase concentration of resveratrol did not alter total Q levels in mammalian cells | 66 |
| | Figure 7 | *E. coli* ubiC mutant utilizes resveratrol better as a ring precursor to Q biosynthesis | 67 |

## Acknowledgments

Eight years ago when I was a newly transferred undergraduate student, Dr. Catherine F. Clarke gave me the opportunity to explore the world of research. Since then, her guidance, kindness, patience and innovative research ideas have accompanied me through my junior and senior years, as well as my whole graduate career. I am very grateful for the research freedom and endless support provided by Cathy – I virtually worked on every single projects that I was interested in. She has taught me to become a dedicated researcher, a determined mentor, and a better son.

I started my first research project roughly six months after I joined Cathy's laboratory. I would like to thank Dr. Beth Marbois for helping me achieving that. Not only she was my mentor in the research world, but also one of my best friend. She taught me everything form the basic of biochemical research to the techniques and skills of using mass spectrometer – something I relied very heavily during my graduate career. I am grateful for the friendship and assistance of past and present members of the Clarke lab. I especially wish to thank Chris Allan – my colleague as well as my formal roommate- for being the go-to person in the lab when Cathy's not around. Chris's great share of lab business responsibilities allowed me to spend significantly more time on research. I am immensely grateful for having Dr. Theresa Nguyen as my colleague and friend for the past six years – we practically started and finished our journey of graduate school together. I wish to thank Cuiwen He and Sue Hui Tsui for creating the perfect lab environment in YH5073 and allowing my endless borrowing of their reagents. I wish to thank Dr. Ryoichi Saiki, Dr. Adam Lunceford, and Dr. Fernando Gomez for their advices on research. And extra and special thank you to Yuchen Shi, Shota Watanabe, Jiayan Chen, Jeniffer

Tang, Emily Weng and Alice Hsu – all those enthusiastic undergraduate researches who contributed significantly to essentially every single research project and publication of mine. I am also very grateful for having Dr. Alexander Patananan from Dr. Steven G. Clarke's lab as my colleague and friend – I learned so much from his multi-tasking research and presentation expertise.

I wish to thank members of my thesis committee, Dr. Catherine F. Clarke, Dr. Steven G Clarke, Dr. Yibin Wang, Dr. Joesph A. Loo, and Dr. Michael Teitell for their immeasurable feedback and support during my graduate career and the writing of this dissertation. I also wish to recognize colleagues and collaborators who contributed to the research that comprises this thesis: Dr. Edward Hsieh, Shota Watanabe, Chris Allan, Jia Yan Chen, Dr. UyenPhuong Tran for the work of human ADCK3 (Chapter 2); Jeniffer Tang, Jia Yan Chen, from Clarke's lab at UCLA and Mohammad Ozeir and Dr. Fabien Pierrel from Charge de Recherche CNRS, France for the work of Coq8 overexpression (Chapter 3); Cuiwen He, Emily Weng from Clarke's lab, Dr. Steven Bensinger and Dr. Kevin Williams from Bensinger's lab at UCLA for the pABA and resveratrol research (Chapter 4); Dr. Beth Marbois, Samuel Choi, Kathleen Hirano, Kyle Hyman for the first discovery of pABA as ring precursor to Q biosynthesis in yeast (Appendix I); Zimin Ji from Clarke's lab at UCLA and Saskia Heeringa and Dr. Friedhelm Hildebrandt from University of Michigan for the *COQ6* project (Appendix II); Dr. Falk from The Children's Hospital of Philadelphia and Dr. Gasser from University of Pennsylvania for the work on probucol (Appendix III); Dr. Gasser from University of Pennsylvania and Dr. Jeffrey Kopp from National institute of health for the *PDSS2* project (Appendix IV); Shazia Ashraf and Dr. Friedhelm Hildebrandt from University of Michigan for the work of *ADCK4*(Appendix V); Drs.

Gregg Czerwieniec, Greg Kitrov, Xin Cong, Melissa Sondej and Jane Strouse from the UCLA MIC for their assistances with the 2D-IEF and mass spectrometry. I also wish to thank all my friends and colleagues in the department of Chemistry and Biochemistry ad UCLA.

I also would like to thank all the funding sources that supported me during my graduate career: UCLA Cellular and Molecular Biology Training Grant; Audree Fowler Protein Fellowship; and Chemistry and Biochemistry Departmental Fellowship.

In the end, I would like to thank and celebrate my family. My mom and Dad supported me tirelessly in all my studies for the past 10 years. Although we might have disagreements, but I am very certain that it was because of their deep love. Lastly, I thank Jia for her support on everything since our unbelievable first met. I thank her for her understanding and caring, and I thank her, for her appearance in my life.

## Vita

| | |
|---|---|
| 2005 | Associate in Arts<br>*Administration Honor*<br>Pasadena City College<br>Pasadena, CA |
| 2006 | National Science Foundation Computer Science, Engineering, and Mathematics Scholarship<br>Pasadena City College<br>Pasadena, CA |
| 2008 | B.S. Biochemistry<br>*cum laude*<br>University of California, Los Angeles<br>Los Angeles, CA |
| 2008 | Merck Index Reward<br>University of California, Los Angeles<br>Los Angeles, CA |
| 2008-2014 | Research Assistant<br>Department of Chemistry and Biochemistry<br>University of California, Los Angeles<br>Los Angeles, CA |
| 2009-2014 | Teaching Assistant<br>Department of Chemistry and Biochemistry<br>University of California, Los Angeles<br>Los Angeles, CA |
| 2010-2013 | The Cellular and Molecular Biology Fellow<br>University of California, Los Angeles<br>Los Angeles, CA |
| 2013 | Robert A. Smith Research Award<br>Department of Chemistry and Biochemistry<br>University of California, Los Angeles<br>Los Angeles, CA |
| 2013 | Audree Fowler Fellow<br>Department of Chemistry and Biochemistry<br>University of California, Los Angeles<br>Los Angeles, CA |

2014 Departmental Fellow
Department of Chemistry and Biochemistry
University of California, Los Angeles
Los Angeles, CA

## PUBLICATIONS

**Letian Xie,** Kevin Williams, Emily Weng, Beth Marbois, Steve Bensinger, Catherine F. Clarke, "Alternative ring precursors in Coenzyme Q biosynthesis in *E. coli*, *S. cerevisiae,* mouse, and human." ***In preparation.***

Cuiwen He, **Letian Xie**, Christopher Allan, UyenPhuong Tran, and Catherine F. Clarke, "Coenzyme Q supplementation or over-expression of the yeast Coq8 putative kinase stabilize multi-subunit Coq polypeptide complexes in yeast *coq* null mutants". Biochim Biophys Acta, 2014 Apr 4; 1841 (4):630-44.

Shazia Ashraf, Heon Yung Gee, Stephanie Woerner, **Letian Xie**, […], Corinne Antignac, and Friedhelm Hildebrandt. "Exome resequencing reveals *ADCK4* mutations as novel causes of steroid-resistant nephrotic syndrome". J. Clin. Invest. 2013 Dec 2; 123(12):5179-89

David Gasser, Cheryl Winkler, […], **Letian Xie**, Beth Marbois, Catherine F. Clarke, and Jeffery B. Kopp. "Focal Segmental Glomerulosclerosis is Associated with a PDSS2 haplotype and Independently , with a Decreased Content of Coenzyme Q10", Am J Physiol Renal Physiol. 2013 Oct 15; 305(8):F1228-38

**Letian Xie,** Mohammad Ozeir, […], Catherine F. Clarke, and Fabien Pierrel. "Over-expression of the Coq8 kinase in *Saccharomyces cerevisiae* coq null mutants allows for accumulation of diagnostic intermeidates of the Coenzyme $Q_6$ biosynthetic pathway." J Biol Chem. 2012 July 6;287(28):23571-81.

Falk MJ, Polyak E, Zhang Z, […], **Letian Xie,** Chen JY, Marbois B, Nissim I, Clarke CF, Gasser DL. "Probucol ameliorates renal and metabolic sequelae of primary CoQ deficiency in Pdss2 mutant mice". EMBO Mol Med. 2011 Jul;3(7):410-27.

**Letian Xie**, Edward J. Hsieh, Shota Watanabe, Chris M. Allan, UyenPhuong C. Tran, and Catherine F. Clarke, "Expression of the human atypical kinase ADCK3 rescues Coenzyme Q biosynthesis and phosphorylation of Coq polypeptides in yeast *coq8* mutants." Biochim Biophys Acta. 2011 May; 1811(5):348-60.

Saskia Heeringa, Gil Chernin, […], **Letian Xie** […], Friedhelm Hildebrandt, "*COQ6* mutations in human patients produce nephrotic syndrome with sensorineural deafness ". J Clin Invest. 2011 May 2; 121(5):2013-24.

Beth Marbois, **Letian Xie,** Samuel Choi, Kathleen Hirano, Kyle Hyman, and Catherine F. Clarke. "Para-Aminobenzoic Acid Is A Precursor in Coenzyme $Q_6$ Biosynthesis in *Saccharomyces cerevisiae"*. J Biol Chem. 2010 Sep 3; 285(36):27827

# Chapter 1

## An introduction to Coenzyme Q

Coenzyme Q (Q, ubiquinone, CoQ) was first isolated and characterized by Festenstein et al. back in 1955(1), and Crane et al. identified that Q functions in the mitochondrial respiratory chain (2). The structure of Q was determined the following year by Wolf et al. (3). Q is a polyisoprenylated benzoquinone lipid essential for electron and proton transport in the mitochondrial respiratory chain and in the plasma membrane of *E. coli* (4). The isoprene tail of Q varies in different species, for example, *Saccharomyces cerevisiae* possess six isoprene units ($Q_6$), *Escherichia coli* contains eight isoprene units ($Q_8$), mice and *Arabidopsis thaliana* contain $Q_9$, and human and fission yeast *Schizosaccharomyces pombe* have $Q_{10}$ (5).

In eukaryotes, the primary function of Q is to serve as an electron carrier that accepts electrons from complex I and complex II, and transfers the electrons to complex III. This is achieved by its redox-active benzoquinone head group, which can undergo three oxidation states. The oxidized quinone can accept one electron and one proton, and becomes semiquinone ($QH^{\bullet}$), which can be converted to ubiquinol ($QH_2$) upon accepting another electron and proton (4). Electrons are passed from $QH_2$ to complex III via Q cycle, a two-cycle process that oxidizes $QH_2$ back to Q. There are two Q binding sites in complex III, $Q_o$ and $Q_I$. In the first cycle, $QH_2$ first binds to the $Q_o$ site and transfers the first electron to an iron-sulfur cluster and eventually passes to cytochrome *c*. The second electron is transferred to two cytochrome *b* units and eventually to Q to form the $QH^{\bullet}$. In the second cycle, another $QH_2$ binds to the $Q_o$ site, transferring one electron to the iron-sulfur cluster again, and another electron to the cytochrome *b* and eventually to the $QH^{\bullet}$ generated during the first cycle, forming a new $QH_2$ to complete the Q cycle. Four protons are transferred across the membrane during this process(6).

Reactive oxygen species (ROS) generated by the mitochondrial electron transport chain is considered to be the major source of oxygen radicals and $H_2O_2$. These free radicals formed in the cells are able to damage lipids, proteins and DNA, a process considered as oxidative stress (7). The reduced form of Q, $QH_2$, has been shown to serve as an antioxidant since it was discovered to inhibit lipid peroxidation in vitro (8). $QH_2$ also serves as a co-antioxidant that regenerates Vitamin E.

In *S. cerevisiae*, at least eleven gene products, Coq1-Coq9, Arh1 and Yah1 are essential for Q biosynthesis(9). Yeast mutants lacking any one of these gene products do not grow on non-fermentable carbon source. Genetic and molecular evidence have shown that Coq3, Coq4, Coq5, Coq6, and Coq7 form a high molecular mass protein complex that is essential for Q biosynthesis(9,10). Deletion of one of the *COQ* genes destabilizes the Coq protein complex and consequently destabilizes the remaining other Coq polypeptides. For instance, a *coq3 null* mutant has barely detectable levels of Coq4, Coq6, Coq7, and Coq9 polypeptides (11).

4-hydroxy-benzoic acid was considered as the primary aromatic ring precursor in Q biosynthesis in yeast(12). Recently it was reported that para-aminobenzoic acid (pABA)could serve as an alternate ring precursor (12,13) (Fig 1). Coq1 catalyzes the first step in yeast Q biosynthesis by synthesizing the polyisoprene tail. The human homologs HsPDSS1 and HsPDSS2 act together to catalyze synthesize the tail. Coq2 in yeast attaches the polyisoprene tail to either 4HB or pABA. HsCOQ2 in human catalyze the same reaction. Coq6 in yeast and HsCOQ6 are required for the hydroxylation of the C5 position of the ring in a flavin-dependent

manner. In yeast, the activity of Coq6 requires ferrodoxin Yah1 and feerodoxin reductase Arh1. Coq3 in yeast and HscCOQ3 in human then methylate the C5 hydroxyl. Yet to be determined enzymes catalyze the decarboxylation of the ring and the hydroxylation at C1. Coq5 in yeast and HsCOQ5 in human catalyze the *C*-methylation at C2 position, using AdoMet as the methyl donor, producing demethoxy-$QH_2$. Coq7 in yeast and HsCOQ7 in human then hydroxylate the C6 position, generating demethyl-$QH_2$, which is then methylated by Coq3 in yeast and HsCOQ3 in human to create the final product $QH_2$.

Coq4, Coq8, and Coq9 are not represented in the pathway described above. These gene products are required for Q biosynthesis and deletion of the genes encoding Coq4, Coq8, or Coq9 destabilizes the Coq protein complex and abolishes Q biosynthesis. Coq4, a peripheral protein associated with the inner mitochondria membrane on the matrix side, has been shown to have close interaction with Coq3 via pull-down experiments (14), and it has been postulated that it could be the potential decarboxylase.

*COQ8* was initially identified as *ABC1*(activator of the $bc_1$ complex) in a screen for suppressors of defects in cytochrome *b* translation (15). A later study by Do *et al.* identified *COQ8* as the same gene as *ABC1*(16). This study discovered that yeast *coq8* mutants lacked Q, and the mutant phenotype of *coq8 null* can be rescued by the addition of exogenous Q. Yeast Coq8, *E. Coli* UbiB, and human ADCK3 are identified by Leonard *et al.* as members of an atypical kinase family (17), as potential protein kinases containing motifs I, II, VIB and VII. Human homologs of Coq8, ADCK1-5, were identified by Lagier-Tourene *et al.* as potentail novel kinases, containing six (I, II, III, VIb, VII, and VIII) of the twelve characteristic canonical

protein kinase motifs (18). These findings suggest that Coq8 is a putative protein kinase required in yeast Q biosynthesis.

Coq9 was also discovered to be peripheral membrane protein on the matrix side of the mitochondrial inner membrane(19). Coq9 has several homologs in eukaryotes and alpha-proteobacteria, but it has no homology to proteins with known functions. Neither does Coq9 have a known motif or domain. Thus, the function of Coq9 is still undetermined. The results presented in Chapter 3 suggest Coq9 is required for function of Coq7 and for the deaminiation of nitrogen containing Q-intermediates.

In addition to the nine *COQ* genes already discussed, another *COQ* gene, *COQ10,* is involved in Q biosynthesis in yeast. The Coq10 polypeptide contains a steroidogenic acute regulatory protein-related lipid transfer (START) domain (20). The *coq10* null mutant grew much slower on non-fermentable carbon source and was sensitive to polyunsaturated fatty acids. Although Q is present in *coq10* null mutant yeast, the *de novo* synthesis rate of Q was decreased in the *coq10 null* mutant (21). In the same study, Allan *et al*. demonstrated that Coq10 homolog from *C. crescentus* binds Q with a high affinity in vitro, suggesting that Coq10 might be involved in the delivery of Q from the biosynthesis site to the electron transport chain.

The Q biosynthesis pathway in *E. coli* shares the same initial steps with yeast and human (Fig 2). IspB catalyzes the first step that synthesizes the polyisoprene tail and UbiA attaches the tail to the aromatic ring precursor (22). However, instead of hydroxylation at C5 position for the third step, UbiD, and UbiX are required for the decarboxylation step, which occurs prior to the

first hydroxylation step in the *E. coli* pathway. UbiI hydroxylates the C5 position, followed by C5 *O*-methylation by UbiG, The *E. coli* and eukaryotic biosynthetic pathways then converge at the UbiH step; UbiH is required to add the C1-hydroxyl group, and UbiE catalyzes the *C*-methylation at C2, forming demethoxy-$Q_8$ ($DMQ_8$). UbiF adds the last hydroxyl group at C6, forming demethyl-$Q_8$ and UbiG returns for the last methylation producing the final product $Q_8$(22).

Progress made in characterization of Coq8 and its function in Q biosynthesis is discussed in chapter 2. Over-expression of human ADCK3 bearing an amino-terminal mitochondrial leader sequence successfully rescued Q biosynthesis in two yeast *coq8* point mutants and the *coq8 null* mutant. Using 2D-isoelectric focusing followed by SDS PAGE analysis, we showed that Coq3, Coq5, and Coq7 are phosphorylated in a Coq8 dependent manner. Mutations in *COQ8* abolish certain phosphorylation states of Coq3, Coq5, and Coq7, and such phenotype can be rescued with the overexpression of yeast *COQ8* or human ADCK3. These results indicate a profound conservation of protein kinase function in Q biosynthesis between yeast and human.

It was difficult to map out the Q biosynthetic pathway because most of the *coq* null mutants failed to accumulate characteristic intermediates, and instead accumulated the early Q-intermediates 3-hexaprenyl-4-hydroxybenzoic acid (HHB) or 3-hexaprenyl-4-aminobenzoic acid (HAB). In chapter 3, novel Q-intermediates were discovered to accumulate in yeast *coq5, coq6, coq7* and *coq9* nul*l* mutants harboring multi-copy *COQ8*. The over-expression of *COQ8* in *coq3, coq4, coq5, coq6, coq7* and *coq9* null mutants stabilizes the Coq protein complex essential for Q biosynthesis, allowing the accumulation of novel diagnostic intermediates. The results significantly illuminated the Q biosynthesis pathway in yeast *S. cerevisiae*.

Marbois *et al.* reported in 2010 that pABA was an alternative ring precursor in Coenzyme $Q_6$ biosynthesis in *S. cerevisiae(12)*. The result was surprising since pABA was a precursor to folate biosynthesis and the addition of pABA to *E. coli* and human culture inhibited Q biosynthesis. In chapter 4, the fate of pABA and resveratrol in Q biosynthesis in *E. coli* and mammalian culture are discussed. Using $^{13}C_6$-4HB, $^{13}C_6$-pABA, and $^{13}C_6$-resveratrol and LC/MS/MS, it was determined that resveratrol could be used as an aromatic ring precursor of Q in *E. coli,* yeast, and mammalian cells, while pABA is a ring precursor only in yeast Q biosynthesis. The results in chapter 4 open the possibilities that other potential small molecule natural products or neutraceuticals may serve as alternate ring precursors in Q biosynthesis.

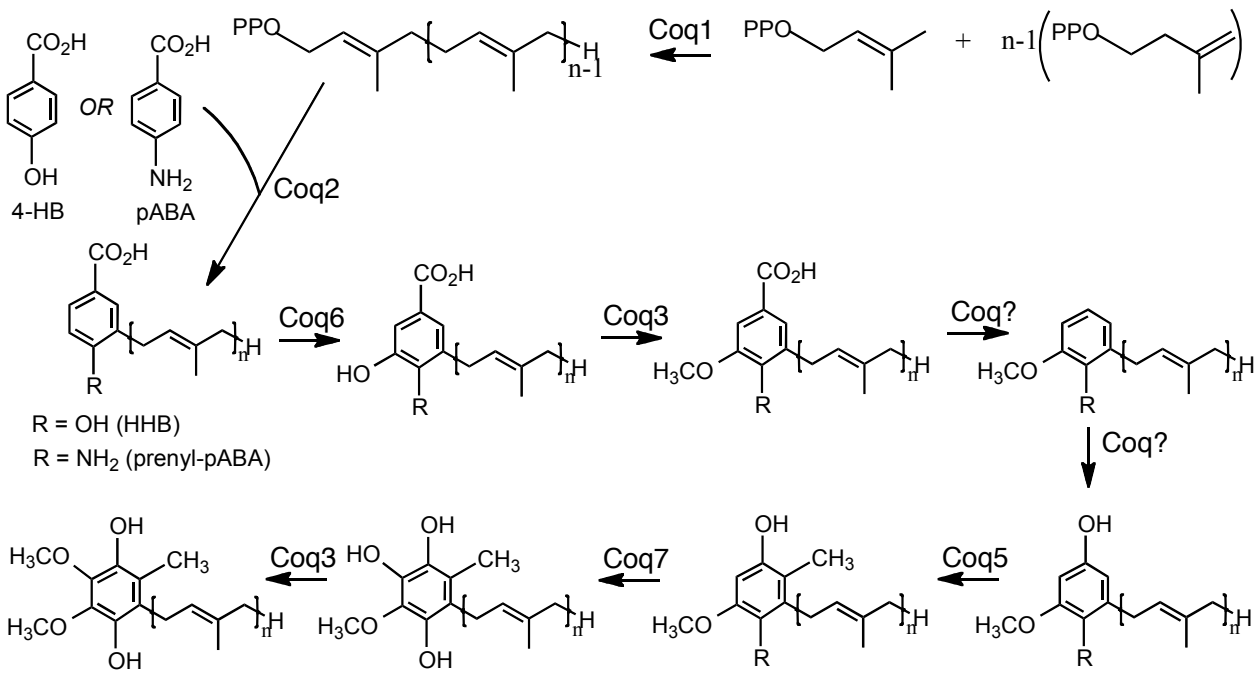



**Figure 1. Coenzyme $Q_6$ biosynthesis in yeast *S. cerevisiae.*** Coq1 assembles the polyisoprenyl-diphosphate tail, which is added to the aromatic ring precursor either 4-HB or pABA by Coq2 prenyltransferase. Coq6 hydroxylates the C5 position followed by Coq3 *O*-methylation by Coq3. Uncharacterized enzyme(s) catalyzes the decarboxylation and C1-hydroxylation of the ring, and Coq5 performs the *C*- methylation at the C2 position. Coq7 adds another hydroxyl at C6, followed by the methylation again catalyzed

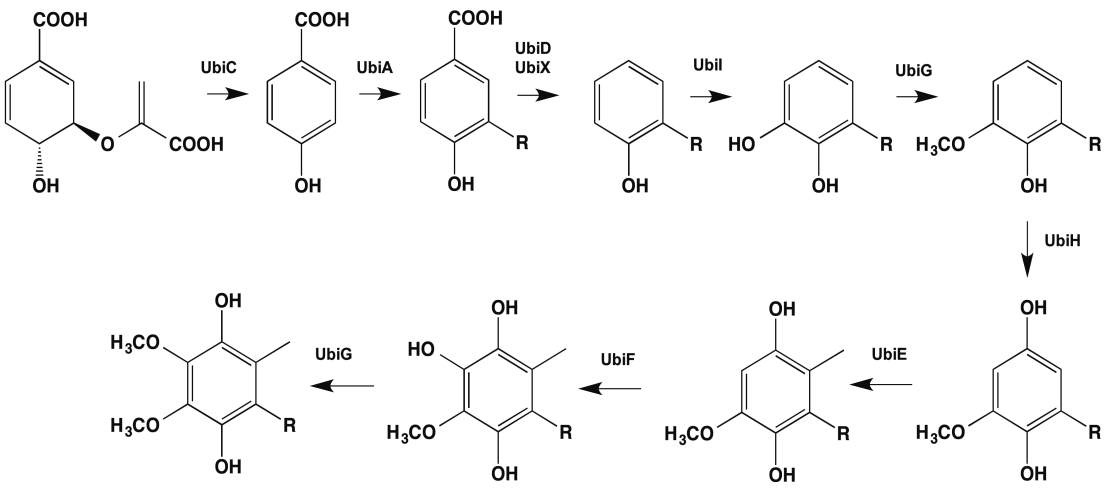



**Figure 2. Biosynthetic pathway of $CoQ_8$ in *Escherichia coli.*** R represents the octaprenyl tail. UbiC converts chorismate to 4HB, and UbiA attaches the octaprenyl tail to the aromatic ring. UbiD and UbiX catalyze the decarboxylation and UbiI adds the first hydroxyl to the ring, followed by the first *O*-methylation catalyzed by UbiG. UbiH adds the second hydroxyl at C1 position, followed by C2 *C*-methylation catalyzed by UbiE. UbiF adds the final hydroxyl at C6 position, followed by the second *O*-methylatio*n* catalyzed by UbiG to synthesize the find product $Q_8H_2$.

**References**


1. Festenstein, G. N., Heaton, F. W., Lowe, J. S., and Morton, R. A. (1955) A constituent of the unsaponifiable portion of animal tissue lipids (lambda max. 272 m mu). *Biochem J* **59**, 558-566
2. Crane, F. L., Hatefi, Y., Lester, R. L., and Widmer, C. (1957) Isolation of a quinone from beef heart mitochondria. *Biochim Biophys Acta* **25**, 220-221
3. D.E. Wolf, C. H. H., N.R. Trenner, B.H. Arison, C.H. Shunk, B.O. Linn, J.F. McPherson, K. Folkers,. (1958) Coenzyme Q. I. Structure studies on the coenzyme Q group. *J. Am. Chem. Soc.* **80**, 4750-4752
4. Bentinger, M., Tekle, M., and Dallner, G. (2010) Coenzyme Q--biosynthesis and functions. *Biochem Biophys Res Commun* **396**, 74-79
5. Kawamukai, M. (2009) Biosynthesis and bioproduction of coenzyme Q10 by yeasts and other organisms. *Biotechnology and applied biochemistry* **53**, 217-226
6. Sacksteder, C. A., Kanazawa, A., Jacoby, M. E., and Kramer, D. M. (2000) The proton to electron stoichiometry of steady-state photosynthesis in living plants: A proton-pumping Q cycle is continuously engaged. *Proc Natl Acad Sci U S A* **97**, 14283-14288
7. Halliwell, B., and Gutteridge, J. M. C. (2007) *Free radicals in biology and medicine*, 4th ed., Oxford University Press, Oxford ; New York
8. Bentinger, M., Brismar, K., and Dallner, G. (2007) The antioxidant role of coenzyme Q. *Mitochondrion* **7 Suppl**, S41-50
9. He, C. H., Xie, L. X., Allan, C. M., Tran, U. C., and Clarke, C. F. (2014) Coenzyme Q supplementation or over-expression of the yeast Coq8 putative kinase stabilizes multi-

subunit Coq polypeptide complexes in yeast coq null mutants. *Biochim Biophys Acta* **1841**, 630-644

10. Gin, P., and Clarke, C. F. (2005) Genetic evidence for a multi-subunit complex in coenzyme Q biosynthesis in yeast and the role of the Coq1 hexaprenyl diphosphate synthase. *J Biol Chem* **280**, 2676-2681
11. Xie, L. X., Ozeir, M., Tang, J. Y., Chen, J. Y., Jaquinod, S. K., Fontecave, M., Clarke, C. F., and Pierrel, F. (2012) Overexpression of the Coq8 kinase in Saccharomyces cerevisiae coq null mutants allows for accumulation of diagnostic intermediates of the coenzyme Q6 biosynthetic pathway. *J Biol Chem* **287**, 23571-23581
12. Marbois, B., Xie, L. X., Choi, S., Hirano, K., Hyman, K., and Clarke, C. F. (2010) para-Aminobenzoic acid is a precursor in coenzyme Q6 biosynthesis in Saccharomyces cerevisiae. *J Biol Chem* **285**, 27827-27838
13. Pierrel, F., Hamelin, O., Douki, T., Kieffer-Jaquinod, S., Muhlenhoff, U., Ozeir, M., Lill, R., and Fontecave, M. (2010) Involvement of mitochondrial ferredoxin and para-aminobenzoic acid in yeast coenzyme Q biosynthesis. *Chemistry & biology* **17**, 449-459
14. Marbois, B., Gin, P., Faull, K. F., Poon, W. W., Lee, P. T., Strahan, J., Shepherd, J. N., and Clarke, C. F. (2005) Coq3 and Coq4 define a polypeptide complex in yeast mitochondria for the biosynthesis of coenzyme Q. *J Biol Chem* **280**, 20231-20238
15. Bousquet, I., Dujardin, G., and Slonimski, P. P. (1991) ABC1, a novel yeast nuclear gene has a dual function in mitochondria: it suppresses a cytochrome b mRNA translation defect and is essential for the electron transfer in the bc 1 complex. *EMBO J* **10**, 2023-2031

16. Do, T. Q., Hsu, A. Y., Jonassen, T., Lee, P. T., and Clarke, C. F. (2001) A defect in coenzyme Q biosynthesis is responsible for the respiratory deficiency in Saccharomyces cerevisiae abc1 mutants. *J Biol Chem* **276**, 18161-18168

17. Leonard, C. J., Aravind, L., and Koonin, E. V. (1998) Novel families of putative protein kinases in bacteria and archaea: evolution of the "eukaryotic" protein kinase superfamily. *Genome research* **8**, 1038-1047

18. Lagier-Tourenne, C., Tazir, M., Lopez, L. C., Quinzii, C. M., Assoum, M., Drouot, N., Busso, C., Makri, S., Ali-Pacha, L., Benhassine, T., Anheim, M., Lynch, D. R., Thibault, C., Plewniak, F., Bianchetti, L., Tranchant, C., Poch, O., DiMauro, S., Mandel, J. L., Barros, M. H., Hirano, M., and Koenig, M. (2008) ADCK3, an ancestral kinase, is mutated in a form of recessive ataxia associated with coenzyme Q10 deficiency. *American journal of human genetics* **82**, 661-672

19. Hsieh, E. J., Gin, P., Gulmezian, M., Tran, U. C., Saiki, R., Marbois, B. N., and Clarke, C. F. (2007) Saccharomyces cerevisiae Coq9 polypeptide is a subunit of the mitochondrial coenzyme Q biosynthetic complex. *Arch Biochem Biophys* **463**, 19-26

20. Barros, M. H., Johnson, A., Gin, P., Marbois, B. N., Clarke, C. F., and Tzagoloff, A. (2005) The Saccharomyces cerevisiae COQ10 gene encodes a START domain protein required for function of coenzyme Q in respiration. *J Biol Chem* **280**, 42627-42635

21. Allan, C. M., Hill, S., Morvaridi, S., Saiki, R., Johnson, J. S., Liau, W. S., Hirano, K., Kawashima, T., Ji, Z., Loo, J. A., Shepherd, J. N., and Clarke, C. F. (2013) A conserved START domain coenzyme Q-binding polypeptide is required for efficient Q biosynthesis, respiratory electron transport, and antioxidant function in Saccharomyces cerevisiae. *Biochim Biophys Acta* **1831**, 776-791

22. Aussel, L., Pierrel, F., Loiseau, L., Lombard, M., Fontecave, M., and Barras, F. (2014) Biosynthesis and physiology of coenzyme Q in bacteria. *Biochim Biophys Acta* **1837**, 1004-1011

# Chapter 2

## Expression of Human atypical kinase ADCK3 rescues coenzyme Q biosynthesis and phosphorylation of Coq polypeptides in yeast *coq8* mutants

Biochimica et Biophysica Acta 1811 (2011) 348–360

Contents lists available at ScienceDirect

Biochimica et Biophysica Acta

journal homepage: www.elsevier.com/locate/bbalip

# Expression of the human atypical kinase ADCK3 rescues coenzyme Q biosynthesis and phosphorylation of Coq polypeptides in yeast *coq8* mutants

Letian X. Xie, Edward J. Hsieh [1], Shota Watanabe, Christopher M. Allan, Jia Y. Chen, UyenPhuong C. Tran [2], Catherine F. Clarke *

*Department of Chemistry and Biochemistry and the Molecular Biology Institute, University of California, Los Angles, Los Angeles, CA 90095-1569, USA*

ARTICLE INFO

*Article history:*
Received 1 December 2010
Received in revised form 17 January 2011
Accepted 28 January 2011
Available online 4 February 2011

*Keywords:*
Coenzyme Q
Ubiquinone
*Saccharomyces cerevisiae*
Mitochondria
Lipid metabolism
Protein kinase

ABSTRACT

Coenzyme Q (ubiquinone or Q) is a lipid electron and proton carrier in the electron transport chain. In yeast *Saccharomyces cerevisiae* eleven genes, designated *COQ1* through *COQ9*, *YAH1* and *ARH1*, have been identified as being required for Q biosynthesis. One of these genes, *COQ8* (*ABC1*), encodes an atypical protein kinase, containing six (I, II, III, VIB, VII, and VIII) of the twelve motifs characteristically present in canonical protein kinases. Here we characterize seven distinct Q-less *coq8* yeast mutants and show that unlike the *coq8* null mutant, each maintained normal steady-state levels of the Coq8 polypeptide. The phosphorylation states of Coq polypeptides were determined with two-dimensional gel analyses. Coq3p, Coq5p, and Coq7p were phosphorylated in a Coq8p-dependent manner. Expression of a human homolog of Coq8p, ADCK3(CABC1) bearing an amino-terminal yeast mitochondrial leader sequence, rescued growth of yeast *coq8* mutants on medium containing a nonfermentable carbon source and partially restored biosynthesis of $Q_6$. The phosphorylation state of several of the yeast Coq polypeptides was also rescued, indicating a profound conservation of yeast Coq8p and human ADCK3 protein kinase function in Q biosynthesis.

© 2011 Elsevier B.V. All rights reserved.

## 1. Introduction

Coenzyme Q (ubiquinone or Q) is an essential lipid component and plays a well-known role in respiratory electron and proton transport in energy metabolism. Q, the oxidized quinone, accepts electrons from NADH via complex I or succinate via complex II, and the reduced hydroquinone ($QH_2$) is oxidized by complex III where the electrons are transferred to cytochrome *c*. Q also functions as the electron acceptor in a number of metabolic oxidation reactions including amino acid catabolism and fatty acid beta oxidation via acyl-CoA dehydrogenases [1], glycerol-3-phosphate, dihydroorotate [2], and the oxidation of sulfide [3]. $QH_2$ is an important lipid-soluble chain-terminating antioxidant [4] and may also function as a co-antioxidant to maintain levels of vitamin E in membranes of cells and lipoproteins [5]. Q and Q analogs have been shown to be capable of inhibiting, activating, or occupying sites of the mitochondrial permeability transition pore [6–8]. The mitochondrial permeability transition pore is involved in apoptosis through the opening of a non-selective channel that disrupts membrane potential and causes hypotonic swelling of the inner membrane, a process that appears to be conserved from yeast to plants and animals [9,10].

Cells utilize isoprenoid biosynthetic pathways (mevalonate or methylerythritol) to produce the polyisoprenyl tail of $Q_n$, where *n* designates the number of isoprene units; $Q_{10}$, $Q_9$, $Q_8$ and $Q_6$ in human, *Caenorhabditis elegans*, *Escherichia coli*, and *Saccharomyces cerevisiae*, respectively [11]. Coq1p in *S. cerevisiae*, IspB in *E. coli*, or a complex of PDSS1 and PDSS2 in human cells synthesize the polyisoprene diphosphate tail precursor of $Q_n$. The aromatic ring precursors supplying the quinone ring of Q include 4-hydroxybenzoic acid (4-HB) derived from either chorismic acid or tyrosine [12]. Recently, para-aminobenzoic acid (pABA) was discovered to function as a ring precursor of Q in *S. cerevisiae* [13,14]. Coq2p is required for the prenylation of either 4-HB or pABA to form 3-hexaprenyl-4-hydroxy benzoic acid or 3-hexaprenyl-4-amino-benzoic acid [13]. *S. cerevisiae* requires at least nine additional polypeptides (Coq3-Coq9, Yah1, and Arh1) for biosynthesis of $Q_6$ [11,14,15].

Although much progress has been made in determining the enzymatic functions of the Coq proteins, the functions of Coq4p and Coq9p in Q biosynthesis are not known, and new information on the putative kinase function of Coq8p is described in this work. In *S. cerevisiae*, Coq4p and Coq9p are members of a high molecular mass multi-subunit mitochondrial complex together with the *O*-methyltransferase Coq3p, the *C*-methyltransferase Coq5p, and the hydroxylases Coq6p and Coq7p, required for ring modifications forming Q [16–18]. A

*Abbreviations:* 2D-IEF/SDS-PAGE, two-dimensional isoelectric focusing/sodium dodecyl sulfate-polyacrylamide gel electrophoresis; Q, coenzyme Q; ORF, open reading frame

* Corresponding author. Fax: +1 310 206 5213.
*E-mail address:* cathy@chem.ucla.edu (C.F. Clarke).
[1] Current address: University of Washington, Department of Genome Sciences, 3720 15th Ave. NE, Seattle, WA 98195-5065, USA.
[2] Current address: University of California, San Diego, Department of Pathology, 200W. Arbor Dr. #8416, San Diego, CA 92103-8416, USA.

1388-1981/$ – see front matter © 2011 Elsevier B.V. All rights reserved.
doi:10.1016/j.bbalip.2011.01.009

zinc-binding motif identified in Coq4p was postulated to be important for Coq4p function as a scaffolding protein [17]. Recently, Rea et al. [19] derived a model of yeast Coq4p by taking advantage of the structure determined by the Northeast Structural Genomics consortium of a Coq4p homolog from *Nostoc* sp. *PCC7120* (Alr8543) that crystallized with a bound geranylgeranyl monophosphate and a magnesium ion. The predicted Coq4p structure is consistent with the idea that Coq4p may bind the polyisoprene tail of a Q-intermediate, possibly serving as an important anchor for the Q-multisubunit biosynthetic complex.

The yeast *COQ8* gene was originally identified as *ABC1* (activator of the $bc_1$ complex) in a multicopy suppression screen of a specific *cbs2* mutant allele (*cbs2-223*) and proposed to function as a cytochrome *b* chaperone [20], necessary for $bc_1$ complex function [21]. However, the decrease in $bc_1$ complex in *coq8* mutants can be explained fully by the requirement of *COQ8* for Q biosynthesis [22]. Yeast *coq8* mutants lack $Q_6$ and the growth defect in media containing a nonfermentable carbon source can be rescued by the addition of exogenous $Q_6$ to the growth medium. The suppression of the *cbs2* mutation was shown to be due to a neighboring tRNA and not to *COQ8* [23]. *E. coli* UbiB and *Providencia stuartii* AarF are prokaryotic Coq8 homologs required for Q biosynthesis; mutants accumulate octaprenyl-phenol, the Q-intermediate expected from a block at the first hydroxylase step [24,25]. Patients with mutations in *ADCK3*/*CABC1* (a homolog of yeast *COQ8*) exhibit progressive neurological disorders with childhood onset cerebellar ataxia and atrophy and have decreased $Q_{10}$ content in muscle, fibroblast, and lymphoblast cells [26] [27]. Thus, in prokaryotes, yeast, and human cells, the principal and conserved function of the Coq8 polypeptide is its requirement for Q biosynthesis.

Yeast Coq8p, *E. coli* UbiB, and human ADCK3 are members of an atypical kinase family, first identified by Leonard et al. [28], as potential protein kinases harboring motifs I, II, VIB and VII. Subsequent analyses identified ADCK1-5 as novel human kinases [29], containing six (I, II, III, VIB, VII, and VIII) of the twelve motifs characteristically present in canonical protein kinases [27]. Patients with $Q_{10}$ deficiencies harboring mutations in *ADCK3* indicated it is required for $Q_{10}$ biosynthesis in humans. In these studies, expression of human ADCK3 did not rescue yeast *coq8* mutants. However, introduction of the human mutations into the corresponding yeast *COQ8* gene impaired growth of yeast on nonfermentable carbon sources and resulted in decreased $Q_6$ content [26,27]. These findings suggested that yeast Coq8p and human ADCK3 may function as kinase required for Q biosynthesis. There is also evidence that Coq8p may function to regulate Q biosynthesis, as overexpression of yeast Coq8p has been shown to rescue a yeast *coq9* nonsense mutant [18,30], a yeast *coq10* null mutant [31,32], and to restore synthesis of $DMQ_6$ in a *coq7* null mutant [33]. Tauche et al. [34] utilized two-dimensional IEF-SDS PAGE and tagged forms of yeast Coq polypeptides and determined that phosphorylation of yeast Coq3p is dependent on Coq8. They also demonstrated that the phosphorylation state of Coq3 affects its association with the Coq high molecular mass polypeptide complex. Thus, Coq8p appears to be essential for the formation of a multi-subunit Q-biosynthetic complex. It is intriguing that the first O-methylation step catalyzed by yeast Coq3 was identified as a potential regulated site of Q biosynthesis in response to high glucose, and it was speculated that a cAMP-dependent protein kinase might be involved in mediating this regulation [35].

In this study we have analyzed mutations in Coq8 that result in Q-biosynthetic defects. Initially, we employed site-directed mutagenesis to target the catalytic lysine in kinase motif II of Coq8p. Although yeast *coq8* null mutants expressing the Coq8-K216A polypeptide lacked $Q_6$, the Coq8-K216A polypeptide was not stable, and the phenotype of this strain mirrored the *coq8* null mutant. Several Coq polypeptides are unstable in the *coq8* null mutant (including Coq4p, Coq6p, Coq7p and Coq9p) [18]. To assess the role of Coq8p as a potential kinase, our goal was to analyze *coq8* mutants that retained normal steady-state levels of Coq8p. Therefore, we examined the collection of yeast *coq8* mutants in order to identify those that retained normal steady-state levels of Coq8p. Seven distinct yeast *coq8* amino acid substitution mutants have been characterized and a subset of these mutants used to investigate the phosphorylation state of Coq3 and other Coq polypeptides. We show that expression of human ADCK3 bearing an amino-terminal mitochondrial leader sequence in yeast *coq8* mutants rescues both synthesis of $Q_6$ and the phosphorylation state of several of the yeast Coq polypeptides, indicating a profound conservation of protein kinase function in Q biosynthesis.

## 2. Materials and methods

### 2.1. Strains and growth media

The yeast strains used in this study are listed in Table 1. Growth media were prepared as described [36]. Media included YPD (1% yeast extract, 2% peptone, 2% dextrose), YPG (1% yeast extract, 2% peptone, 3% glycerol) and YPGal + 0.1% Dextrose (1% yeast extract, 2% peptone, 2% galactose, 0.1% dextrose). SDC consisted of 0.18% yeast nitrogen base without amino acids, 2% dextrose, 0.14% $NaH_2PO_4$, 0.5% $(NH_4)_2SO_4$ and amino acids were added at final concentrations as described in Ref. [37]. SD-ade, SD-his, SD-leu, SD-met, SD-trp and SD-ura consisted of SDC media minus adenine, histidine, leucine, methionine, tryptophan and uracil respectively. Solid media contained 2% agar. All materials were obtained from Difco, Fisher or Sigma.

### 2.2. Sporulation and tetrad analysis

Diploid cells were grown to a cell concentration of $OD_{600} = 2.5$ in YPD. Yeast cells from 1 ml of culture were pelleted by centrifugation 12,000 × *g*, 30 seconds. The cell pellet was washed with sterile water and pelleted by centrifugation again. Cells were then resuspended in 1 ml sporulation medium (1% potassium acetate, 0.1% yeast extract, 0.05% dextrose) and incubated at 30 °C for 2 to 3 days. Cells were pelleted by centrifugation, and then resuspended in zymolyase buffer

**Table 1**
Genotypes and sources of *S. cerevisiae* strains.

| Strain | Genotype | Source |
|---|---|---|
| W303-1A | MAT a *ade2-1 his3-1,15 leu2-3,112 trp1-1 ura3-1* | R. Rothstein[a] |
| W303ΔABC1 | MAT a *ade2-1 his3-1,15 leu2-3,112 trp1-1 ura3-1 coq8::HIS3* | [22] |
| FY251 | MAT a *ura3-52 his3Δ200 leu2Δ1 trp1Δ63* | F. Winston[b] |
| FYΔABC1 | MAT a *ura3-52 his3Δ200 leu2Δ1 trp1Δ63 coq8::TRP1* | [22] |
| CH130-A1 | MAT a *his3-1,15 leu2-3,112 trp1-1 ura3-1 coq8-1* | [22] |
| CF130-2B | MAT α *his3Δ200 ura3-52 trp1Δ63 coq8-1* | C130[c] × FY251 |
| C177 | MAT α *met6 coq8-2* | A. Tzagoloff [c] |
| W177-3B | MAT a *his3-1,15 leu2-3,112 met6 ura3-1 coq8-2* | C177 × W303-1A |
| C183 | MAT α *met6 coq8-3* | A. Tzagoloff [c] |
| W183-2A | MAT a *his3-1,15 trp1-1 ura3-1 coq8-3* | C183 × W303-1A |
| C194 | MAT α *met6 coq8-4* | A. Tzagoloff [c] |
| W194-3A | MAT α *ade2-1 his3-1,15 met6 ura3-1 coq8-4* | C194 × W303-1A |
| C222 | MAT α *met6 coq8-5* | A. Tzagoloff [c] |
| W222-7D | MAT a *ade2-1 his3-1,15 leu2-3,112 ura3-1 coq8-5* | C222 × W303-1A |
| C240 | MAT α *met6 coq8-6* | A. Tzagoloff [c] |
| W240-1A | MAT a *leu2-3,112 ura3-1 coq8-6* | C240 × W303-1A |
| C275 | MAT α *met6 coq8-9* | A. Tzagoloff [c] |
| C308 | MAT α *met6 coq8-7* | A. Tzagoloff [c] |
| W308-4C | MAT α *ade2-1 his3-1,15 met6 trp1-1 ura3-1 coq8-7* | C308 × W303-1A |
| C315 | MAT α *met6 coq8-8* | A. Tzagoloff [c] |
| W315-4A | MAT α *trp1-1 ura3-1 coq8-8* | C315 × W303-1A |
| JM6 | MAT a, *his4* $\rho^0$ | [78] |
| JM8 | MAT α *ade1* $\rho^0$ | [78] |

[a] Dr. Rodney Rothstein, Department of Human Genetics, Columbia University.
[b] Dr. Fred Winston, C. Dollard, and S. Ricapero-Hovasse, Department of Genetics, Harvard University.
[c] Dr. Alex Tzagoloff, Department of Biological Sciences, Columbia University.

(1 M sorbitol, 50 mM Tris–Cl pH 7.5, 6 mg/ml zymolyase-20 T (MP Biomedicals)). Cells were incubated for 15 or 30 min at 30 °C. The zymolyase digestion was stopped by diluting the sample with four volumes of water and placing it on ice. The procedure for analysis and dissection of haploid spores was as described [36]. Yeast cells were transformed with plasmid DNA as described [38].

### 2.3. Subcloning of *COQ8* and *ADCK3*

The plasmids used in this study are listed in Table 2. To construct *COQ8* with a biotin accepting sequence at its C-terminus, a DNA segment was amplified with the primers pBC8-1 (5′ CGCGGAATTCACCAGCATTTTGGA-TAATTC 3′ −600 to −589 of *COQ8*) and pBC8-2 (5′ CGCGGAATTCAACTT-TATAGGCAAAAATCT 3′ +1503 to +1484 of *COQ8*). The DNA fragment was digested with EcoRI (sites underlined) and then ligated into the EcoRI site of the yeast/*E. coli* shuttle vector containing the biotinylated *Propionibacterium shermanii* transcarboxylase sequence, Yep352-Bio6 [39] [37] [40]. The resulting plasmid, pBT8-1, contains *COQ8* in frame with a carboxyl-terminal biotinylation site.

The plasmid MHS1011 containing human *ADCK3* cDNA was obtained from Open Biosystems. To generate a low-copy plasmid containing the open reading frame of *ADCK3* subcloned behind the *S. cerevisiae CYC1* promoter, MHS1011 was digested with XhoI and EcoRI. The DNA fragment containing *ADCK3* was purified with a Qiaquick Gel Extraction Kit (Qiagen) and the purified DNA treated with Klenow. A low-copy plasmid containing the *CYC1* promoter, pAH01 [41], was digested with HindIII, treated with Klenow and then treated with bacterial alkaline phosphatase. The purified DNA fragment containing *ADCK3* was then ligated into the treated pAH01 plasmid. The plasmid with *ADCK3* in the correct orientation was designated psCABC1. To generate a high-copy plasmid containing *ADCK3* subcloned behind the *CYC1* promoter, psCABC1 was digested with KpnI and SpeI to excise a DNA fragment containing the *CYC1* promoter and *ADCK3*. This DNA fragment was then ligated into the high-copy plasmid pCH1 [41], also digested with KpnI and SpeI. This plasmid was designated pmCABC1.

Two other yeast expression plasmids were constructed so that the ORF of human *ADCK3* would contain an amino-terminal mitochondrial-targeting leader sequence (from yeast *COQ3*), and expressed from the yeast *CYC1* promoter (see Table 2). A forward primer, ADCK3For (5′-clamp-Cla1-(+1 to +31)-3′ of *ADCK3*) and a reverse complement primer, ADCK3Rev (5′-clamp-Kpn1-(+1944 to +1927)-3′ of *ADCK3*) were used with MHS1011 as template DNA to generate a PCR-amplifed segment of DNA containing the ORF of *ADCK3*. The resulting DNA was digested with ClaI and KpnI and inserted into the corresponding restriction sites of pQM [41] or pRCM (Table 2), to generate plcADCK3 (low copy) and pmcADCK3 (multicopy), respectively.

**Table 2**
Plasmid constructs used in this study.

| Plasmid | Genes | Copy number | Source |
|---|---|---|---|
| pRS316 | Yeast shuttle vector only | Low copy | Sikorski and Hieter [79] |
| pRS426 | Yeast shuttle vector only | Multicopy | Christianson et al. [80] |
| pAH01 | Yeast vector with *CYC1* promoter | Low copy | Hsu et al. [81] |
| pCH1 | Yeast vector with *CYC1* promoter | Multicopy | Hsu et al. [81] |
| pQM | pAH01 with *COQ3* mito leader | Low copy | Hsu et al. [41] |
| pRCM | pCH1 with *COQ3* mito leader | Multicopy | Saiki and Morvaridi |
| p3HN4 | Yeast *ABC1/COQ8* | Low copy | Do et al. [82] |
| pK216A | Yeast *abc1/coq8-K216A* | Low copy | This work |
| p4HN4 | Yeast *ABC1/COQ8* | Multicopy | Hsieh et al. [23] |
| p4K216A | Yeast *abc1/coq8-K216A* | Multicopy | This work |
| pBT8-1 | Yeast *ABC1/COQ8*-biotin | Multicopy | This work |
| pBT8KA | Yeast *abc1/coq8-K216A*-biotin | Multicopy | This work |
| psCABC1 | pAH01/Human *CABC1/ADCK3* with *CYC1* promoter | Low copy | This work |
| pmCABC1 | pCH1/Human *CABC1/ADCK3* with *CYC1* promoter | Multicopy | This work |
| plcADCK3 | pQM/Human CABC1/*ADCK3* with *CYC1* promoter and *COQ3* mito leader | Low copy | This work |
| pmcADCK3 | pRCM/Human CABC1/*ADCK3* with *CYC1* promoter and *COQ3* mito leader | Multicopy | This work |

### 2.4. Site-directed mutagenesis

Primer mediated site-directed mutagenesis was performed as described [42]. Primer pairs used to generate *coq8-K216A* were KAbc1AF4 (5′ TCTTAAGAACTATACAGAACGGGAGAATTTC 3′ +55 to +89 bp) with KAbc1AR3 (5′ CAGGATATTGAATTGCGACAACCACTCTTT 3′ +661 to +632 bp) and KAbc1AF3 (5′ AAAGAGTGGTTGTCGCAATT-CAATATCCTG 3′ +632 to 661 bp) with KAbc1AR4 (5′ CATTTCG-TACGCCCCTTTCCTATCTCTCAATGTGG 3′ +1194 to 1160 bp). Nucleotides that are underlined are the mutated nucleotides. The PCR fragments were digested with AflII and BsiWI. The plasmids p3HN4 [22], p4HN4 [23] and pBT8-1 were treated with AflII and BsiWI to remove a fragment of *COQ8*. The AflII/BsiWI digested PCR fragment containing the K216A mutation was then ligated into the digested plasmids to generate pK216A, p4K216A and pBT8KA, respectively. pK216A and p4K216A are single copy and multicopy plasmids that contain the *coq8* gene with the K216A mutation. The pBT8KA plasmid contains the K216A mutation of *coq8* and a carboxyl-terminal biotinylation site.

### 2.5. Genomic DNA purification and sequencing

Yeast strains were grown overnight in 5 ml YPD at 30 °C. Yeast cells from 0.5 ml of culture were pelleted by centrifugation at 12,000×*g* for 1 min. Genomic DNA was purified using the Wizard Genomic DNA Kit (Promega). For sequencing, the *COQ8* locus was amplified in two overlapping segments. The first segment was amplified with the primers Abc1Seq-F (5′ ACTCGAGAAAAGCAATCTGGTAGATT-TATGGG 3′ −300 to −276 (underlined) relative to the *COQ8* ATG) and Abc1Seq-R (5′ CCTCGAGTTAAACTTTATAGGCAAAAATCTCTT 3′ +1506 to +1481 (underlined) relative to the *COQ8* ATG). The second segment was amplified with the primers KAbc1A-F1 (5′ CGTCTCTTAAGAACTA-TACAGAACG 3′ +55 to +74 relative to the *COQ8* ATG) and Abc1Seq-R2 (5′ TCTGTTTTATCTTTTTTTTTTGTTCTTCGAGATT 3′ +1640 to +1607 from the *COQ8* ATG). The UCLA Sequencing and Genotyping Core determined the nucleotide sequence of each of the PCR products.

### 2.6. Purification of mitochondria

Yeast cells were grown in 11 of YPGal+0.1% Dextrose and harvested at an $OD_{600}$ of approximately 1. Crude mitochondria were isolated and purified on a Histodenz (Sigma) gradient as described in Ref. [43]. Protein concentration was measured by bicinchoninic acid protein assay (Pierce).

### 2.7. Submitochondrial localization

Mitochondria were hypotonically shocked for 20 min on ice, with 5 volumes of 20 mM HEPES-KOH pH 7.4, to generate mitoplasts. Mitoplasts were pelleted by centrifugation (14,000×*g*, 10 min) and the supernatant saved as the intermembrane space fraction (IMS). Mitoplasts

were sonicated and the matrix (supernatant) and membrane (pellet) components separated by centrifugation (100,000×g, 30 min). Mitoplasts were also alkaline extracted with 0.1 M $Na_2CO_3$ pH 11.5 for 20 min at 4 °C, and subjected to centrifugation to separate matrix (supernatant), peripheral membrane (supernatant) and integral membrane (pellet) proteins. Proteinase K protection assays were as described [44]. Mitoplasts were pelleted and resuspended in isotonic buffer (0.6 M sorbitol, 20 mM HEPES-KOH pH 7.4) with or without the addition of 100 μg/ml proteinase K (Fisher Scientific) and 1% Triton X-100, for 1 h at 4 °C. Proteins were precipitated with 10% trichloroacetic acid and resuspended in SDS-PAGE sample buffer.

SDS-polyacrylamide denaturing gels were prepared containing 10% acrylamide as described [45].

### 2.8. 2D-Isoelectric focusing (IEF)/SDS-PAGE

IEF-PAGE was performed as described [34]. Approximately 200 μg of purified mitochondria from each strain were sedimented by centrifugation (14000×g, 10 min) at 4 °C, and resuspended in standard Rehydration Solution (7 M urea, 2 M thiourea, 4 % CHAPS, 0.5% Ampholytes 3–10, 0.0002% bromophenol blue) to a final concentration of 1.0 μg/μl. The sample was sedimented again (14000×g, 10 min) and de-streak reagent (GE Healthcare; final concentration of 1.25%) was added to the sample as a reducing agent. For in-gel hydration, 200 μl of diluted samples were applied to Immobiline DryStrips (GE Healthcare, 13 cm, pH 3–11 NL) and incubated overnight at room temperature. IEF was performed in the Bio-Rad Protean Isoelectric Focusing Cell (Bio-Rad) with four steps of voltage, (4 h at 100 V, 2 h at 250 V, 5 h gradient up to 4000 V, and a further 80,000 Volt-h at constant 4000 V) at 20 °C with a maximum current of 50 μA. The strips were equilibrated first for 20 min in Equilibration Buffer (75 mM Tris–HCl, pH 8.8, 6 M urea, 29.3% glycerol, 2% SDS, 0.002% bromophenol blue, 20 mg/ml dithiothreiotol), and then another 20 min in Equilibration Buffer with 25 mg/ml iodoacetamide. For the second dimension, the strips were applied to Criterion 8–16% PAGE gels in a Bio-Rad Criterion Dodeca Electrophoresis Cell. For phosphatase treatment, isolated mitochondria (200 μg protein) were resuspended in 19 μl λ-phosphatase buffer (New England Bio Labs; 50 mM HEPES, pH 7.4, 100 mM NaCl, 2 mM dithiothreitol, 0.01% Brij 35) containing complete EDTA-free Protease Inhibitor Cocktail (Roche). Samples were incubated for 45 min at 30 °C after addition of 1 μL λ-phosphatase (100 U/μL) (New England Bio Labs).

### 2.9. Immunoblot analyses

Proteins were transferred from SDS-polyacrylamide gels to polyvinylidene difuloride (PVDF) membrane, and then incubated in 2% non-fat milk and probed with primary antibodies (generated in rabbits) to yeast mitochondrial proteins at the following dilutions: Coq1p, 1:10,000; Coq2p, 1:1000; Coq3p, 1:1000; Coq4p, 1:1000; Coq5p, 1:10,000; Coq6p: 1:250; Coq7p: 1:1000; Coq8p: 1:100; Coq9p, 1:1000; secondary antibody goat anti-rabbit IgG, heavy and light chain specific peroxidase conjugate (Calbiochem) were used at 1:10,000. A mouse monoclonal antibody for Rip1p was used at 1:10,000 and the secondary antibody was goat anti-mouse peroxidase conjugate. Supersignal West Pico Chemiluminescent kit (Pierce) was used for detection of polypeptides on Western blots.

### 2.10. Lipid extraction and analysis

Yeast cells were grown in YPGal + 0.1% dextrose. Q was extracted from yeast whole cells as described [13,46]. Lipids were separated and analyzed essentially as described [13]. In brief, reverse-phase HPLC with tandem mass spectrometry was used to detect and quantify $Q_6$ and $Q_4$ was used as an internal standard. The mass spectrometer was an Applied Biosystems-MDS Sciex 4000 Q Trap (Hybrid triple-quad linear ion trap analyzer with Autosampler, and a Turbo-V source equipped with ESI and APCI sources).

## 3. Results

### 3.1. Coq8p is a peripheral membrane protein located on the matrix side of the inner membrane

Coq8p is localized to the mitochondria [22] and a c-myc-tagged form of Coq8p is located within the mitochondrial matrix [34]. Recent analyses of yeast Coq8p have identified a membrane spanning region [47]. Although the Coq8-c-myc tagged polypeptide was shown to rescue growth on glycerol [34], Q content was not reported. Other tagged forms of Coq polypeptides have been observed to rescue growth on glycerol, but the Q content is not restored to wild type [14], and in some cases the tagged form of the polypeptide was found to be mislocalized in the rescued yeast strains [48]. Thus it is important to localize the native form of the Coq8 polypeptide. We used antibodies recognizing Coq8p to determine the submitochondrial location of the untagged polypeptide. W303-1A yeast mitochondria were isolated and a hypotonic shock was performed to rupture the outer membrane, leaving the inner membranes intact, generating mitoplasts. Mitoplasts were sonicated to disrupt the remaining membranes, allowing separation of soluble matrix proteins and insoluble membrane associated proteins. Mitoplasts were also treated with alkaline buffer to extract proteins peripherally associated with the inner membrane [49]. Western blot analysis of these samples showed that Coq8p remained with the membrane components after sonication and was released into the supernatant after alkaline treatment, but not after sonication, indicating that Coq8p is a peripherally associated membrane protein (Fig. 1A). A proteinase K protection assay on purified mitochondria, or mitochondria subjected to hypotonic buffer to release intermembrane space components, identified Coq8p as located on the matrix side of the inner membrane (Fig. 1B). The results show that Coq8p is a peripherally associated membrane protein located on the matrix side of the inner membrane.

### 3.2. Mutation of the catalytic lysine-216 to alanine in Coq8p disrupts Q biosynthesis

Amino acid sequence analyses of yeast Coq8p, human ADCK3, and homologs have identified protein kinase motifs [27–29]. The lysine present in motif II is believed to be involved in the transfer of protons during phosphorylation [50]. Previous studies have shown that mutation of this lysine to alanine in a variety of other protein kinases results in the loss of kinase function, but preserves structure [51]. To determine the role of this conserved lysine in Coq8p function, site-directed mutagenesis was used to convert lysine-216 to alanine. The *coq8Δ* yeast strain, W303ΔABC1, was transformed with plasmids containing either wild type or *coq8-K216A* and tested for growth on plate media containing glycerol as sole nonfermentable carbon source. No growth was detected after 3 to 10 days of incubation of transformants expressing Coq8-K216A (Fig. 2). Identical results were obtained with another *coq8Δ* null mutant FYΔABC1, in a distinct genetic background (data not shown).

### 3.3. Steady-state polypeptide levels in coq8-K216A

Previous work has shown that deletions of any of the *COQ1–COQ9* genes results in a decrease in the steady-state levels of several of the other Coq polypeptides [18]. For example, *coq8* null mutants have decreased levels of Coq4, Coq6, Coq7, and Coq9 polypeptides [18], and the formation or integrity of the Q-biosynthetic complex is affected by the absence of Coq8p [34]. To determine the steady-state level of the Coq8-K216A polypeptide, mitochondria from yeast expressing Coq8p-K216A were purified and steady-state polypeptide levels were determined by Western blot. Polypeptide levels of Coq8p-

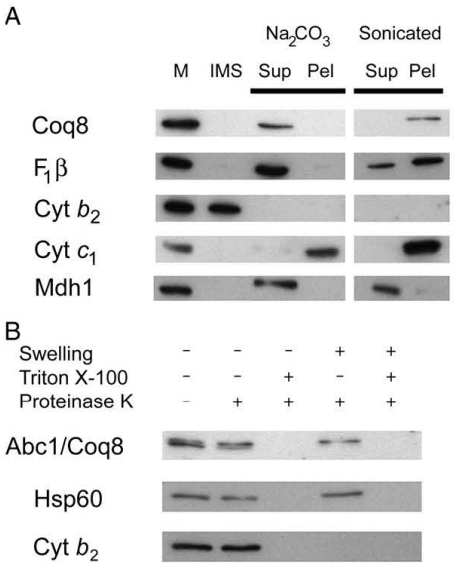



**Fig. 1.** Coq8p is a peripheral membrane protein, associated with the mitochondrial inner membrane on the matrix side. *A.* Coq8p is peripherally associated with mitochondria membranes. Nycodenz purified mitochondria (M) were hypotonically swelled to generate the intermembrane space (IMS) fraction and mitoplasts. Mitoplasts were then treated with 0.1 M $Na_2CO_3$ pH 11.5, or sonicated. The treated mitoplasts were centrifuged and the supernatant (Sup) and pellet (Pel) fractions were analyzed. *B.* Coq8p is located on the matrix side of the inner membrane. Mitochondria and mitoplasts were treated with Proteinase K with and without 1% Triton X-100. The β subunit of $F_1$-ATPase ($F_1\beta$) is a peripheral membrane protein [83], cytochrome $b_2$ (Cyt $b_2$) is located in the intermembrane space [84], cytochrome $c_1$ (Cyt $c_1$) is an integral membrane protein [85], malate dehydrogenase (Mdh1) [86] and Hsp60p [87] are localized to the matrix.

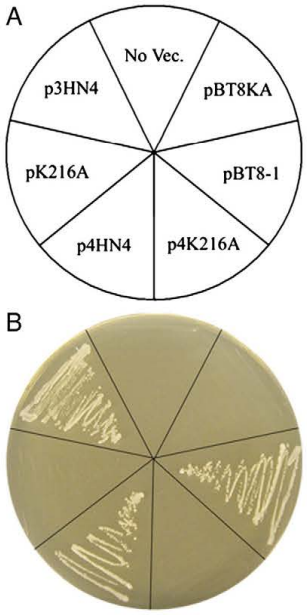



**Fig. 2.** The Lysine216 in kinase subdomain II of Coq8 is required for rescue of glycerol growth in a yeast *coq8* null mutant. The yeast *coq8* null mutant (W303ΔABC1) was transformed with plasmids containing either wild-type *COQ8* or *coq8-K216A*. p3HN4 (*COQ8*) and pK216A (*coq8-K216A*) are low-copy vectors; p4HN4 (*COQ8*), p4K216A (*coq8-K216A*), pBT8-1 (*COQ8*) and pBT8KA (*coq8-K216A*) are multicopy vectors. Yeast transformants were incubated 3 days on YPG plate media at 30 °C.

K216A when expressed from a low-copy plasmid are diminished relative to wild-type or the null mutant expressing wild-type Coq8 (W303ΔABC1:p3HN4) (Fig. 3), and steady-state levels of Coq4p are also decreased. Thus, it is not possible to discern whether low Coq4p levels are due to the absence of kinase activity, or to the low level of the Coq8p-K216A.

Previous studies have suggested that Q or a Q-biosynthetic intermediate may be necessary for Coq polypeptide complex stability [52,53]. For example, addition of $Q_6$ to growth media has been shown to increase steady-state levels of Coq3 and Coq4p polypeptides in *coq1* and *coq7* null mutants [52,53], and addition of $Q_6$ to yeast *coq7* null mutant cultures restores assembly of a biosynthetic complex enabling synthesis of $DMQ_6$, the penultimate intermediate in Q biosynthesis [33]. Addition of $Q_6$ to cultures of *coq8* null mutants has been shown to restore growth on media containing glycerol or ethanol as the sole nonfermentable carbon source [22]. However, addition of $Q_6$ to cultures of W303ΔABC1:pK216A yeast did not rescue steady-state Coq8 polypeptide levels. Similarly, addition of $Q_6$ did not restore the Q-biosynthetic complex in *coq8* null mutants [34]. Antibodies against the β subunit of the $F_1$-ATPase and the Complex III Rieske iron–sulfur complex, Rip1, were used to verify equivalent sample loading, and indicate that disruption of the Coq polypeptide complex has no effect on steady-state levels of representative components in mitochondrial respiratory complexes. In summary, the very low steady-state levels of the Coq8-K216A polypeptide produce the same limitations as the *coq8* null mutant; thus, we sought to identify *coq8* mutants that retained normal steady-state levels of Coq8p.

### *3.4. Characterization of yeast coq8 point mutants with normal steady-state level of Coq8p*

Eight different mutants in the G75/*coq8* complementation group [54] whose *coq8* gene defects had not previously been characterized were studied, with the goal of identifying mutants that retained

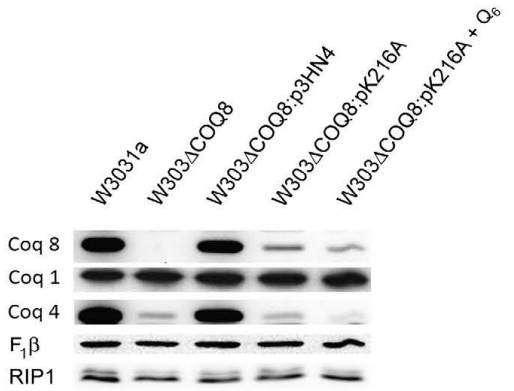



**Fig. 3.** The yeast Coq8-K216A polypeptide is not present at normal steady-state levels. Yeast were grown in 11 of YPGal medium with 0.1% dextrose and harvested at an $OD_{600nm}$ of approximately 4. W303ΔABC1:pK216A + $Q_6$ was grown in YPGal + 0.1% Dextrose media supplemented with 1.2 μM $Q_6$. Purified mitochondria from W303-1A, W303ΔABC1 and W303ΔABC1 harboring the designated plasmids were subjected to Western blot analysis.

steady-state levels of Coq8p. These mutants were obtained via mutagenesis of the parental wild-type strain D273-10B/A1 [55,56]. Each of the original *coq8* mutants within this collection of strains (Table 1) was shown to be defective for growth on ethanol and/or glycerol as a carbon source, indicating a defect in respiration. The respiratory deficiency stems from recessive mutations in a nuclear gene, as they were complemented by a $\rho^0$ strain with a normal complement of nuclear genes but lacking mitochondrial DNA (Table 1). Each strain was cultured and subjected to analysis by Western blot. Seven of the mutants expressed Coq8p polypeptide in amounts comparable to wild type, W303-1A (Fig. 4). The *coq8* loci in each of these seven mutants were amplified by PCR and sequence analysis revealed that each mutant harbored a unique nucleotide substitution mutation resulting in amino acid substitution (Table 3). Four of the mutations affect residues within known kinase motifs (*coq8-3*, A197V in motif I; *coq8-6*, D229N in motif III; and *coq8-8*, D346N and *coq8-4*, N348Y, both in motif VIB; Fig. 5). The remaining three mutations result in glycine to aspartate substitution and are present in regions of unknown function (*coq8-2*, G89D; *coq8-5*, G130D; and *coq8-7*, G475D; Fig. 5).

Derivatives of each of these seven *coq8* point mutant yeast strains were prepared by mating to W303-1A, sporulation, and dissection of tetrads to yield respiratory defective mutants with designated auxotrophies (Table 1). Each of the *coq8* mutant strains was rescued for growth on glycerol-medium following transformation with p3HN4 (low-copy yeast *COQ8*), while transformation with pRS426 (multi-copy yeast empty vector) failed to rescue growth. Two of the *coq8* point mutants were chosen for further characterization: the W222 point mutant (*coq8-5*; G130D) was chosen because it mirrors a human ADCK3 mutation (G272D) present in a conserved region of unknown function and that is associated with disease and a lower level of $Q_{10}$ content in skeletal muscle [26], and the W182 *coq8* point mutant (*coq8-3*; A197V) was selected because it is located within conserved kinase motif I, and we anticipated that it would disrupt kinase activity of Coq8p. The rescue of W183 and W222, harboring the respective *coq8-3* or *coq8-5* allele, is shown (Fig. 6). To determine the effect of the mutations on $Q_6$ content, lipids were extracted from wild-type and mutant yeast, and $Q_6$ levels were measured with a QT4000 mass spectrometer coupled in-line with reversed phase HPLC. $Q_6$ was not detected in W303ΔCOQ8, W183, or W222 harboring empty vector, pRS426. In contrast, $Q_6$ levels were restored in W303ΔCOQ8, W183, and W222 mutant yeast harboring the p3HN4 plasmid (low-copy yeast *ABC1/COQ8*) (Fig. 7). The rescue is less efficient in the point mutants (W183 and W222) than in the *coq8* null mutant, perhaps due to interference by the mutant Coq8 polypeptide.

### 3.5. Expression of the human ADCK3 polypeptide rescues yeast coq8 mutants

A human homolog *ADCK3* shows 38% amino acid sequence identity with *S. cerevisiae* Coq8p. However, the human *ADCK3* gene has not been shown to rescue the yeast *coq8* mutant. To determine if *ADCK3*

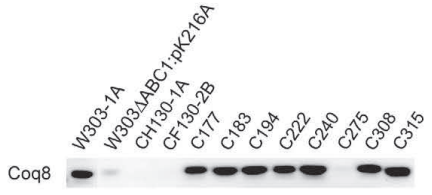



**Fig. 4.** Seven yeast *coq8* mutant strains have normal steady-state levels of the Coq8 polypeptide. The designated yeast strains were grown in YPD, lysed with 2% SDS and 425–600 μm glass beads (Sigma). Aliquots of whole cell lysates (corresponding to 0.1 $OD_{600}$ of yeast cells) were separated by SDS-PAGE and then transferred to a PVDF membrane for Western blot analyses with antibodies to Coq8p.

**Table 3**
Amino acid and nucleotide substitutions of *coq8* alleles.

| Strain (*abc1/coq8* allele) | Amino acid substitution (nucleic acid mutation)[a] |
|---|---|
| C130 (*coq8-1*) | Not determined |
| C177 (*coq8-2*) | G89D (G266A) |
| C183 (*coq8-3*) | A197V (C590T) |
| C194 (*coq8-4*) | N348Y (A1042T) |
| C222 (*coq8-5*) | G130D (G389A) |
| C240 (*coq8-6*) | D229N (G685A) |
| C275 (*coq8-9*) | Not determined |
| C308 (*coq8-7*) | G475D (G1424A) |
| C315 (*coq8-8*) | D346N (G1036A) |

[a] Positions of mutations are relative to the ATG start codon of *ABC1/COQ8*.

might be an ortholog of yeast *COQ8*, its corresponding cDNA was subcloned into yeast expression vectors. Prior studies showed that rescue of yeast *coq* mutants by heterologous *COQ* genes required expression from multicopy vectors [46,57]. In other cases, rescue by an *E. coli* homolog of Coq5p was observed for certain *coq5* point mutants but not *coq5* null mutants [58]. Neither low-copy nor high-copy plasmids expressing *ADCK3* from the yeast *CYC1* promoter (Table 2) were found to rescue yeast *coq8* mutants [59]. It seemed possible that the human ADCK3 polypeptide may not be efficiently transported to the yeast mitochondrial matrix. To remedy this potential problem, we then tested plasmids expressing *ADCK3* ORF with an amino-terminal yeast mitochondrial leader sequence (plcADCK3 and pmcADCK3). The resulting plasmids were transformed into a *coq8* null mutant (W303ΔABC1) as well as yeast strains containing the *coq8-3* (W183) and *coq8-5* (W222) mutant alleles. To test rescue, yeast *coq8* mutants harboring ADCK3 were plated on medium containing the nonfermentable carbon source, glycerol. Each of the *coq8* mutants tested was rescued by pmcADCK3, and rescue was also observed after 10 days with plcADCK3 (Fig. 6). The pmcADCK3 plasmid partially restored $Q_6$ content in yeast lipid extracts from transformed yeast (Fig. 7). Yeast *abc1/coq8* mutants transformed with pmcADCK3 contained a small amount of $Q_6$, while the same mutants transformed with the empty vector (pRS426) contained no detectable $Q_6$.

The long incubation time needed to observe the rescue of the W222 *coq8* mutant by low-copy ADCK3, and the *coq8* null mutant by multicopy ADCK3 probably reflects the time necessary to accumulate a sufficient amount of $Q_6$. Yeast growth is observed in the spot containing only 20,000 cells (2 μl of yeast cells at $A_{600nm} = 1.0$ or $1 \times 10^7$ cells/ml). Hence, it seems unlikely that spontaneous secondary mutations could account for the rescue on YPG, since they would not be expected to arise at such a high frequency. While there does not seem to be a strong correlation between the rescued growth in Fig. 6 and the $Q_6$ content shown in Fig. 7, it seems likely that the content of $Q_6$ as measured in YPGal liquid medium (Fig. 7) may not be indicative of the $Q_6$ content in cells tested for growth on YPGlycerol. In fact, yeast *coq7* mutants rescued with a heterologous gene and cultured on YPGal have been shown to have lower $Q_6$ content as compared to the same cells cultured on YPG [53]. In summary, human ADCK3 is an ortholog of yeast Coq8p, since its expression rescues both growth on nonfermentable carbon source and $Q_6$ biosynthesis in yeast *coq8* mutants.

### 3.6. Coq8p is required for steady-state levels of other Coq polypeptides

Previous studies have investigated the effects of deletions in the *COQ* genes on the steady-state protein levels of Coq1p–Coq10p [18]. To examine whether *coq8* point mutants destabilize other Coq polypeptides, mitochondria isolated from W183, W222, W303-1A (WT), and W303ΔABC1 were analyzed on immunoblots with antisera against the Coq1–Coq9 proteins (Fig. 8). Mitochondria from W183 and W222 contained steady-state levels of Coq8p, which was absent in W303ΔABC1. Steady-state levels of Coq1p, Coq2p, Coq3p, Coq5p,

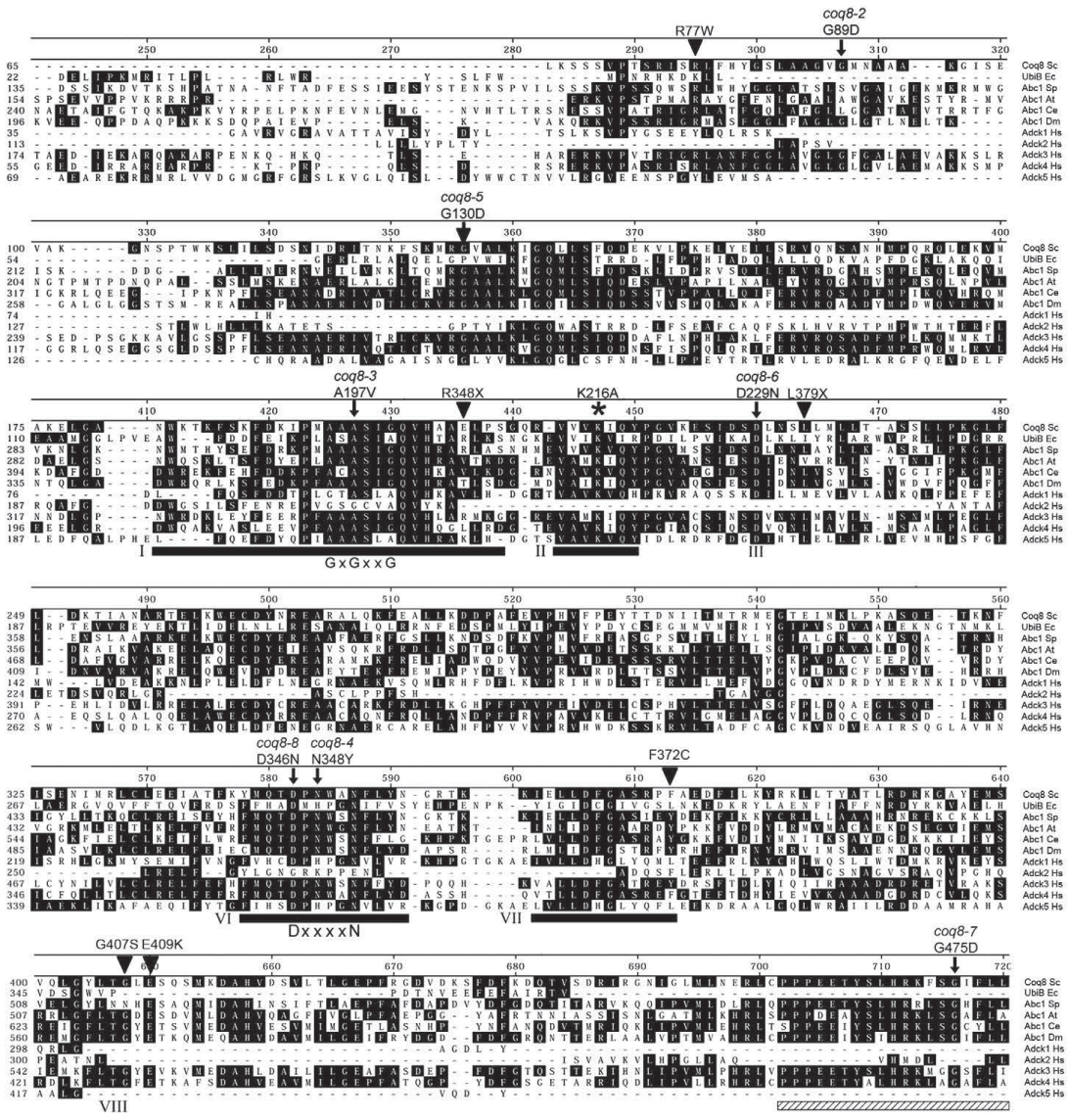



**Fig. 5.** Amino acid alignment of Abc1/Coq8p homologs. An alignment of Abc1/Coq8p and its homologs was created using DNASTAR™ Megalign. Clustal method was used with PAM250 residue weight table. Homologs are *E. coli* (GenBank™ accession number P27854), *S. pombe* (GenBank™ accession number CAA62818), *A. thaliana* (GenBank™ accession number AAC72875), *C. elegans* (GenBank™ accession number AAA62560), *D. melanogaster* (GenBank™ accession number AAA62560NP_572836) and humans (*ADCK1*, *ADCK2*, *ADCK3/CABC1*, *ADCK4* and *ADCK5*. GenBank™ accession numbers NP_065154, NP_443085, BAB91363, NP_079152 and NP_777582, respectively). *S. cerevisiae coq8* mutant alleles and their mutations identified in this study (Table 3) are indicated on the alignment by *arrows*. Mutations detected in CABC1/ADCK3 in human patients [26,27,73] are indicated with *triangles*. Kinase subdomains I, II, III, VIB, VII and VIII, the G-x-G-x-x-G glycine-rich region and the D-x-x-x-x-N catalytic loop are indicated. The invariant lysine of subdomain II is designated with an asterisk. A highly conserved motif in Coq8p with remarkable sequence identity to a region in the *Bacillus subtilis* protein RsbU is indicated by the hatched bar (▨). Numbers on the left indicate amino acid position relative to the start codon. Identical residues are shaded.

and Coq6p were observed in each of the *coq8* mutant strains. As reported by Tauche et al. [34], we observed that the presence of phosphatase inhibitors during mitochondria isolation preserved the steady-state levels of Coq3p. Interestingly, W183 contained steady-state levels of Coq4p and Coq7p, which were either dramatically decreased or absent in W222 and W303ΔCOQ8. All three *coq8* mutant strains had dramatically decreased levels of Coq9p compared to wild type. Expression of human *ADCK3* was able to restore steady-state level of Coq4p in W222, and steady-state level of Coq7p in both W222 and W303ΔCOQ8 strains. However, Coq9p level in the *ADCK3* transformed yeast remained significantly decreased compared to wild-type yeast.

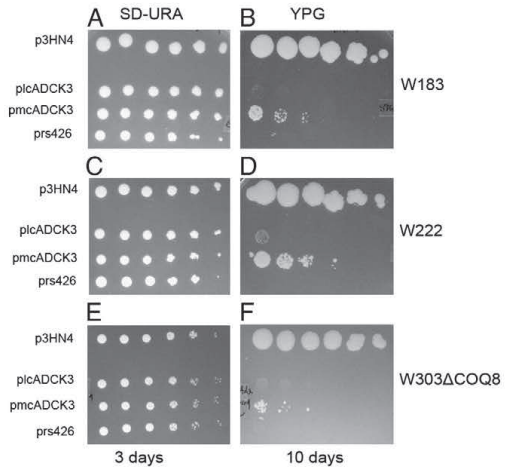



**Fig. 6.** Expression of the human ADCK3 polypeptide rescues the growth of yeast *coq8* mutants on nonfermentable carbon source media. Yeast *coq8* point mutants W183 and W222, and *coq8* null mutant (W303ΔABC1) were transformed with the designated plasmids: p3HN4, yeast low-copy *COQ8*; plcADCK3, low-copy ADCK3; pmcADCK3, multicopy ADCK3; or pRS426, empty vector. Each strain was cultured overnight in SD-Ura selective media, the optical density ($A_{600nm}$) was adjusted to 1.0, and 2 μl of 1:5 serial dilutions were spotted onto plate media, corresponding to a final $A_{600nm}$ of 1.0, 0.2, 0.04, 0.008, 0.0016, or 0.00032. *A*, *C*, and *E*, Growth is depicted on SD-Ura plates after 3 days of incubation at 30 °C; *B*, *D*, and *F*, YPG plates after 10 days of incubation at 30 °C.

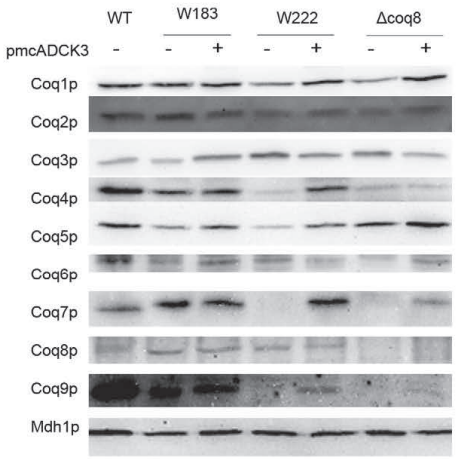



**Fig. 8.** Expression of the human ADCK3 polypeptide in yeast *coq8* mutants partially restores steady-state levels of some of the yeast Coq polypeptides. Mitochondria were isolated from wild-type yeast (W303-1A) or from the indicated *coq8* mutant yeast strains with or without pmcADCK3 (a multicopy plasmid with ADCK3). Isolated mitochondria (20 μg protein) from the designated yeast strains were separated by 10% SDS-PAGE and then transferred to a PVDF membrane for immunoblotting with antibodies to one of the Coq polypeptides (Coq1–Coq9), or to malate dehydrogenase (Mdh1), as a loading control.

### *3.7. Coq3p, Coq5p, and Coq7p are putative substrates of Coq8p*

Phosphorylation of Coq3p has been shown to depend on the presence of Coq8p [34]. 2D-IEF/SDS-PAGE was performed to address whether other Coq polypeptides might also serve as substrates for Coq8p. Purified mitochondria from wild-type W303-1A and from *coq8* mutants (W183, W222, and W303ΔCOQ8) were subjected to 2D-IEF/SDS-PAGE as described in Materials and methods. Whereas previous studies made use of a tagged version of Coq3p [34], we utilized antibodies to Coq3p to detect the polypeptide in its natural state (Fig. 9). The detection of Coq3p revealed two spots in wild type in the pH range of 5–6, which is consistent with the predicted isoelectric point of 5.44 for Coq3p (Table 1S). The leftward, more acidic spot was no longer present in the phosphatase-treated wild-type mitochondria, identifying it as a phosphorylated isoform of Coq3p. These studies confirm the observation that W303ΔABC1 contained only the unphosphorylated isoform of Coq3p [34] and allowed us to use Coq3p as an internal marker in these analyses. Interestingly, W183 does contain a small fraction of phosphorylated Coq3p, suggesting this point mutation did not completely eliminate the kinase activity of Coq8p. On the other hand, W222 contained only the unphosphorylated isoform of Coq3p, with migration patterns similar to the *coq8* null mutant. Expression of human ADCK3 was able to restore the phosphorylation state of Coq3p in both *coq8* null mutant and W222 point mutant, although to different degrees.

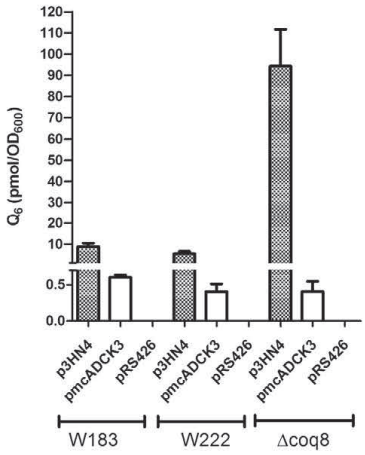



**Fig. 7.** Expression of the human ADCK3 polypeptide partially restores $Q_6$ content in yeast *coq8* mutants. Yeast cells were cultured in YPGal + 0.1% dextrose and collected at an optical density ($A_{600nm}$) of about 1.0. The content of $Q_6$ in yeast cell lipid extracts was determined by HPLC/MS-MS as described in Materials and methods. Yeast *coq8* mutants were transformed with plasmids expressing yeast *ABC1/COQ8* (low-copy, p3HN4), human CABC1/ADCK3 (multicopy, pmcADCK3), or empty vector control (multicopy, pRS426). Each bar represents a total of four measurements from two independent samples each with two injections. Standard deviations are represented with error bars. $Q_4$ was used as internal standard.

Detection of Coq5p and Coq7p with antibodies to these polypeptides revealed multiple spots for each (Fig. 10). For Coq5p, wild-type mitochondria contained at least four spots in the pH range of 5 to 6, consistent with the predicted isoelectric point of Coq5p (Table 1S). The two most acidic spots disappeared in wild-type mitochondria upon phosphatase treatment, indicating those two spots represent two different phosphorylation states of Coq5p. Interestingly, W183, W222, and W303ΔABC1 contained three spots, lacking the most acidic spot observed in wild type, indicating that Coq8p is responsible for the most acidic phosphorylated isoforms of Coq5p. This result suggests that there may be another kinase working together with Coq8p on Coq5p, which is responsible for some Coq5p phosphorylation. The phosphorylation pattern of Coq5p is restored to wild type when ADCK3 was expressed in the point mutants W222 and W183. For Coq7p, three spots were observed in wild-type mitochondria in the pH range of 7 to 8, consistent with the predicted isoelectric point of Coq7p (Table 1S). The left two spots disappeared upon phosphatase treatment, indicating those two

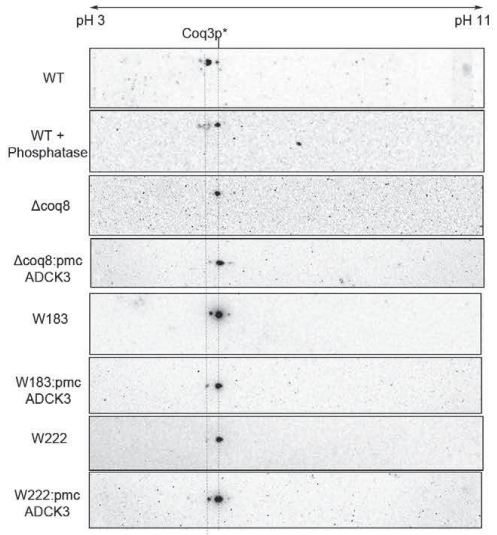



**Fig. 9.** Expression of the human ADCK3 polypeptide in yeast *coq8* mutants partially restores the phosphorylation state of the yeast Coq3 polypeptide. Isolated mitochondria (200 μg protein) from wild-type yeast (W303-1A), or from the designated *coq8* mutants, W183, W222, or W303ΔCOQ8, either without or with pmcADCK3 (as indicated), were separated by two-dimensional electrophoresis, with isoelectric focusing (IEF) in the first dimension and SDS-PAGE in the second dimension, followed by transfer to PVDF membranes for Western analysis. Where indicated, wild-type mitochondria were treated with phosphatase prior to rehydration and IEF. Coq3p was detected with anti-Coq3p antibody (1:1000 dilution). The two dashed lines indicate the positions of Coq3p isoforms. The pH range for IEF is indicated.

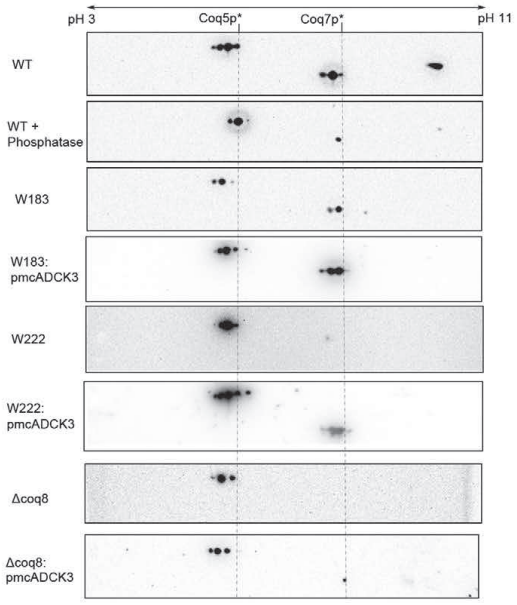



**Fig. 10.** Expression of the human ADCK3 polypeptide in yeast *coq8* mutants partially restores the phosphorylation state of the yeast Coq5 and Coq7 polypeptides. Isolated mitochondria (200 μg protein) from wild-type yeast (W303-1A), or from the designated *coq8* mutants, W183, W222, or W303ΔCOQ8, either without or with pmcADCK3 (as indicated), were analyzed as described in Fig 7. Where indicated, wild-type mitochondria were treated with phosphatase prior to rehydration and IEF. Coq5p and Coq7 were detected with the designated antibodies (1:1000 dilution). The dashed lines designate the alignment and relative positions of the Coq5p and Coq7p isoforms The pH range for IEF is indicated.

spots are phosphorylated isoforms of Coq7p. Coq7p is not detected in the *coq8* null mutant (Fig. 10) since it is destabilized in the W303ΔABC1 strain (Fig. 8). In contrast, the W183 point mutant contained two spots, lacking the most acidic spot as compared to the wild type. However, it is difficult to discern whether a distinct kinase acts on Coq7p, or whether the A197V point mutation in Coq8p of W183 fails to completely eliminate the kinase activity. As shown in Fig. 8, W222 mitochondria do not contain stable levels of Coq7p. Expression of human ADCK3 is able to restore the phosphorylation pattern of Coq7p in both *coq8* point mutants, but only the steady-state level of Coq7p is restored in *coq8* null mutant (Figs. 8 and 10).

## 4. Discussion

*S. cerevisiae* Coq8 polypeptide, and its human homolog ADCK3, have been shown to be required for biosynthesis of Q [22,26,27]. Yeast Coq8p is known to be required for the phosphorylation of the yeast Coq3 polypeptide, and this phosphorylation is important for the stability or formation of a multisubunit Coq polypeptide Q-biosynthetic complex [34]. In this work we have identified and utilized *coq8* mutants that retain normal steady-state levels of the Coq8 polypeptide and determined the effects of Coq8 point mutations on $Q_6$ content, Coq polypeptide steady-state levels, and the phosphorylated states of Coq3p, Coq5p, and Coq7p. The results suggest a profound functional conservation of kinase activity of human ADCK3, which when expressed in yeast *coq8* mutant strains rescues both $Q_6$ synthesis and phosphorylation of yeast Coq3, Coq5 and Coq7 polypeptide substrates.

Initially, we introduced a K216A substitution within kinase motif II of Coq8p, because the corresponding mutation of this residue in other kinases resulted in correctly folded but kinase-inactive enzymes [51]. However, levels of the K216A-Coq8 polypeptide were profoundly decreased as compared to wild-type Coq8p. Consequently, steady-state levels of the other Coq polypeptides were also decreased (for example Coq4p), as observed previously in *coq8* null mutants [18]. For this reason we screened a collection of yeast *coq8* mutants [54], with the goal of identifying *coq8* mutant strains that retained normal steady-state levels of the Coq8 polypeptide.

Seven distinct *coq8* missense mutations were characterized in yeast mutants that produced a wild-type steady-state level of Coq8p. Four of the seven yeast *coq8* mutations affect residues that reside within known kinase subdomains (Fig. 5). A197V is located in subdomain I, which surrounds the bound ATP [51]. This subdomain in the majority of eukaryotic protein kinases contains the amino acid sequence G-x-G-x-x-G, present in many nucleotide-binding proteins. This motif helps form a β-strand-turn-β-strand structure that holds the α and β phosphate groups of ATP [51]. In Coq8p, this motif contains two alanine residues in place of the first two glycine residues (A-A-A-S-I-G). While the A197V (underlined) might cause steric hindrance and interfere with binding of phosphate moieties, our results indicate that the yeast W183 (*coq8-3*) mutant harboring A197V-Coq8p retained some kinase activity. Another mutation affected the aspartate in subdomain III (D229N), believed to help stabilize interactions between the invariant lysine of subdomain II and the phosphate groups of ATP [60,61]. Disruption of the negative charge at that position would directly affect its ability to form a salt-bridge with the lysine. Two other mutations, D346N and N348Y, affected residues with kinase subdomain VIB, identified by the D-x-x-x-x-N motif that forms a catalytic loop. The invariant D residue of this loop is believed to be the catalytic base that accepts the proton from the amino acid substrate hydroxyl [51]. Thus D346N-Coq8p would be expected to slow or prevent phosphorylation. Distinct classes of eukaryotic protein

kinases uniformly retain the invariant terminal D and N residues of motif VIB but show variations of the "x" residues that mediate peptide substrate recognition [62–64]. For example, many serine and threonine kinases typically contain the sequence D-L-K-P-E-N, while tyrosine kinases contain D-L-R-A-A-N or D-L-A-A-R-N [65]. The sequence D-P-N-W-A-N constitutes another distinct motif that is highly conserved among the Coq8/ADCK3 homologs (Fig. 5). The yeast *coq8* mutation resulting in N348Y (underlined) would likely disrupt the structure of this catalytic loop.

Three *coq8* missense mutations (G89D, G130D, and G475D) are present in regions of unknown function. Both G89D and G130D are located near or in conserved regions. Patients harboring ADCK3 mutations resulting in R213W, G272V or G272D (corresponding to R77 and G130 in yeast Coq8, respectively) had deficiencies in muscle $Q_{10}$ content [26]. Introduction of the human mutations into the corresponding positions of yeast Coq8 (R77WCoq8, G130VCoq8, or G130DCoq8) and expression in yeast *coq8* null mutants was shown to result in greatly decreased or absent $Q_6$ content, respectively [26]. We confirm that the corresponding yeast *coq8* mutant harboring G130D-Coq8p lacked $Q_6$ and further determined that it failed to phosphorylate Coq3p and Coq7p and was deficient in phosphorylation of Coq5p.

The mutation in *coq8-7* (G475D) is near the sequence P-P-P-E-E-T-Y-S-L-H-R-K-x-x-G, identifying a remarkably conserved region among the Coq8 and human ADCK3 and ADCK4 homologs (Fig. 5). A BLAST search with this sequence identifies a similar segment in the *Bacillus subtilis* protein, RsbU. This sequence is well conserved near the amino-terminus of RsbU homologs (Fig. 11). In crystal structures of RsbU, this region forms an α-helix and several conserved residues (including P44 and E45 in *B. subtilis*) are required for interaction with a neighboring α-helix [66]. This interaction stabilizes the RsbU polypeptide (a phosphatase), allowing it to form a homodimer necessary for binding of RsbU to RsbT (a kinase). The RsbU/RsbT interaction (termed partner switching) is controlled by serine phosphorylation and mediates stress response to environmental and nutritional signals in *B. subtillis,* and contributes to pathogenicity and enhanced intracellular growth of *Staphylococcus aureus* and *Listeria monocytogenes* [67,68]. In Coq8p, this motif is located near the carboxyl-terminus. It is conceivable that in yeast Coq8 and human ADCK3, this region mediates a similar protein–protein interaction required for Q biosynthesis. Tauche et al. [34] determined that yeast Coq8p forms homomeric complexes. In fact, the rescue mediated by expression of wild-type yeast *COQ8* was much less robust in yeast *coq8* point mutants as compared to the *coq8* null mutant (Fig. 7), suggesting that dysfunctional Coq8p present in the point mutants may interfere with functional interaction(s) of wild-type Coq8p, either with itself or with partner polypeptides.

Tauche et al. [34] discovered that Coq3p is a putative phosphorylation substrate of Coq8p using a tagged version of Coq3p. Here, we utilized antibodies to the Coq3 polypeptide to confirm this result, and extended the studies by examining Coq polypeptide steady-state levels and phosphorylation status in wild-type, *coq8* null and two of the *coq8* point mutants that retained high steady-state levels of the Coq8 polypeptide.

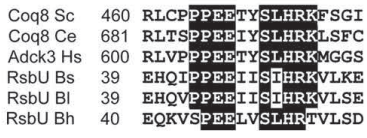



**Fig. 11.** The carboxyl terminal segment of Coq8 homologs and the amino terminal segment of RsbU homologs share a region of high identity. In RsbU the sequence designated by the black bar forms an alpha-helix, and side chains interact with a neighboring alpha-helix in a RsbU homodimer. Numbers indicate the amino acid position of the segment. The RsbU homologs shown are from *Bacillus subtilis* (GenBank accession number NP_388351), *Bacillus lichenformis* (GenBank accession number YP_077796), and *Bacillus halodurans* (GenBank accession number NP_241392). Shading indicates identical residues present in the majority of the sequences.

The *coq8* null mutant and W222 (*coq8-5*; G130D) were found to possess only the unphosphorylated isoform of Coq3p. However, W183 (*coq8-3*; A197V) retained phosphorylated Coq3p, suggesting that the A197V mutation did not eliminate the kinase activity of Coq8p and allowed phosphorylation of Coq3p. W183 retained high steady-state levels of Coq1 through Coq8 polypeptides, although levels of Coq9p were decreased relative to wild type. In contrast, W222 had dramatically lower levels of Coq4p and lacked Coq7p and Coq9p, a phenotype similar to the *coq8* null mutant. One interpretation is that phosphorylated forms of Coq3p are required to preserve stability of Coq4, Coq7 and Coq9 polypeptides. In contrast, the W222 mutant lacked phosphorylated forms of Coq3p, contributing to profound destabilization of Coq4, Coq7 and Coq9 polypeptides. Alternatively, the mutation in W183 that allows for detectable steady-state levels of Coq9p may in turn stabilize the other Coq polypeptides.

Coq7p and Coq5p were also found to be substrates of Coq8p. Wild-type yeast and the W183 *coq8-3* mutant each contained normal steady-state levels of Coq7p, and W183 retained one of the two phosphorylated Coq7 isoforms. In contrast, the *coq8* null and W222 mutant both lacked steady-state levels of Coq7p. We propose that the steady-state level of Coq7p depends on Coq8 kinase activity, and that phosphorylation of Coq7p prevented Coq7p from destabilization. Coq7 has been previously identified as a regulated step in Q biosynthesis [33]. We further demonstrated that Coq5p also contained multiple phosphorylated isoforms. However, not all of the phosphorylation states of Coq5p were Coq8p-dependent. Both the *coq8* null mutant and the W222 *coq8* point mutant lacked only the most acidic Coq5 spot in the 2D-IEF analyses. Three of the four Coq5 spots observed in wild-type mitochondria disappeared upon phosphatase treatment, suggesting that there is another kinase (or kinases) acting on Coq5p. Whether these phosphorylated isoforms of Coq5 are essential for Q synthesis still remains a question.

In these analyses we were not able to resolve phosphorylation states of several of the Coq polypeptides. Coq4p did not appear to be phosphorylated, since it migrated as one spot, and showed similar mobility with or without phosphatase treatment (data not shown). Coq2, Coq6, Coq8, Coq9 and Coq10 polypeptides were not detectable on 2D-IEF gels, even though they can be readily detected in isolated mitochondria by Western blot of SDS-PAGE gels. Although multiple spots of Coq1p were detected on 2D-IEF gels, no signal was detected following phosphatase treatment, thus the phosphorylation state of Coq1p is ambiguous (data not shown).

Steady-state levels of Coq9p mirrored those of Coq7p, and thus it is tempting to speculate that Coq8 may also phosphorylate Coq9p. In fact, Coq9p has been detected in a yeast phosphoproteome analysis and is phosphorylated at T34 [69]. Currently, this is the only reported phosphorylation site in any yeast Coq polypeptide [70]. The amino terminal sequence of Coq9 residue is not conserved in metazoan Coq9 sequences, and it is interesting that T34 may be located within the predicted mitochondrial leader sequence of yeast Coq9p (Table 1S). Overexpression of *COQ8* is known to suppress a nonsense ($Q_{151}$STOP) *coq9* mutant [18] and was attributed to a detectable presence of Coq9p due to read-through. Overexpression of *COQ8* restores the steady-state level of Coq4p in several *coq* null mutants, but not in the *coq9* null mutant [71]. While experiments have not revealed a complex between Coq8p and Coq9p [30], it is certainly possible that phosphorylation of Coq9p by Coq8p might be necessary to form a Q-biosynthetic complex and so preserve the otherwise unstable Coq polypeptides known to interact with Coq9, including Coq4p, Coq6p, and Coq7p. It is likely that such Coq8-mediated phosphorylation of Coq polypeptides might function to regulate $Q_6$ synthesis, and thus also account for the *COQ8* multicopy suppression of the *coq10* mutant [31,71].

Expression of the Coq8 human homolog, ADCK3, rescued the growth of yeast *coq8* mutants on nonfermentable carbon source and enabled synthesis of $Q_6$. Although ADCK3 (CABC1) has been localized to mitochondria [72], the rescue observed here required the addition of

an amino-terminal yeast mitochondrial leader sequence to ADCK3 (pmcADCK3). In the yeast W222 and *coq8* null mutants, pmcADCK3 rescued phosphorylation of Coq3p and Coq7p. The rescue afforded by pmcADCK3 was most dramatic in the W222 mutant because restoration of phosphorylated Coq3p and Coq7p coincided with significantly increased steady-state levels of Coq7p, Coq4p, and Coq9p. ADCK3 also restored the phosphorylation state of Coq5p in W222. The effect of pmcADCK3 on the steady-state level of Coq polypeptides was less significant in the *coq8* null mutant. We speculate that the presence of the Coq8-G130D polypeptide may facilitate the phosphorylation or stabilization of yeast Coq polypeptides by human ADCK3. It is important to note that detection of phosphorylation by 2D-IEF and Western blot can detect whether or not a protein is phosphorylated but does not indicate whether the polypeptide is correctly phosphorylated. While the rescue observed is dramatic, growth is much slower and the content of $Q_6$ is much lower in the ADCK3 rescued mutants as compared to mutants rescued with yeast *COQ8*. ADCK3 shares 38% sequence identity with yeast Coq8p (Fig. 5), thus the activity of ADCK3 might not be ideal for the yeast substrates.

Patients harboring missense, deletion, or nonsense mutations in both copies of *ADCK3* seem to have a distinct and milder presentation of symptoms as compared to patients with defects in other genes necessary for Q biosynthesis [26,27,73]. For example patients with severe mutations resulting in nonsense mediated decay of *ADCK3* mRNA, develop progressive cerebellar ataxia, but indicate that ADCK3 itself is not essential for life [73]. In contrast, patients with *PDSS1*, *PDSS2*, *COQ2*, or *COQ9* mutations generally exhibit a severe multisystemic infantile form of Q-deficiency, and develop renal disease [74]. In the clinical setting it is important to identify Q-deficiencies in patients as early as possible, since treatment with oral $Q_{10}$ can sometimes elicit dramatic improvement [74]. Partial rescue of kidney disease with oral $Q_{10}$ supplements has been observed in the *Pdss2* mouse model of kidney disease [75]. Yeast *coq8* null mutants are indistinguishable from the other yeast *coq* mutants (*coq1–coq7* and *coq9*); they lack Q, have severe respiratory deficiency, and exhibit similar sensitivity to oxidative stress [11,15]. Therefore, it seems likely that one or more of the other human homologs of *ADCK3* must also function in Q biosynthesis, perhaps supplying a partial overlap of function. Consistent with this idea is that fibroblasts cultured from patients with defects in ADCK3 have normal $Q_{10}$ content [26]. The best candidate appears to be *ADCK4*, since it shares highest sequence identity. However, the function of *ADCK4* in Q biosynthesis is not yet clear.

It is intriguing that plants contain numerous homologs of Coq8/ADCK3. *Arabidopsis thaliana ABC1A* is an ortholog of yeast Coq8p, and when expressed in yeast *coq8*(*abc1*) mutants, rescues the Q-deficient respiratory defect [76]. However, four distinct *A. thaliana* Coq8 homologs are present within plastoglobules, which are located within chloroplasts and appear to be important in lipid metabolism, including the synthesis and storage of other prenylated molecules such as plastoquinone, phylloquinone, and tocopherols [77]. It will be important to determine the function of plant Coq8(Abc1) homologs in the synthesis and regulation of these prenylated lipid molecules. Indeed, the stress sensitivity observed in *A. thaliana* strains harboring insertion mutations in the *AtOSA1* gene (a Coq8 homolog) is consistent with a defect in synthesis of one of the prenylated quinone antioxidant lipids [47].

In summary, there is a striking conservation of Q biosynthesis from yeast to humans [11,15]. This can now be extended to include the conserved function of yeast Coq8p and human ADCK3. Both yeast Coq8p and human ADCK3 appear to function as kinases recognizing conserved Coq polypeptide substrates, including Coq3p, Coq7p, and Coq5p. This phosphorylation is key to the formation or maintenance of a Q multisubunit complex [34] and may modulate biosynthesis of Q.

Supplementary materials related to this article can be found online at doi:10.1016/j.bbalip.2011.01.009.


## Acknowledgments

We are grateful to Dr. A. Tzagoloff for sending us the collection of yeast *coq8* point mutants and for the cytochrome $c_1$ antibodies. We thank Peter T. Lee for pBT8-1 and Drs. R. Saiki and S. Morvaridi for the gift of pRCM plasmid. We thank Dr. L. McAlister-Henn for malate dehydrogenase antibodies, Dr. B. Trumpower for antibodies to Rip1, and Dr. C. M. Koehler for antibodies to cytochrome $b_2$, Atp2, and Hsp60. This work is supported by the National Institutes of Health Grant GM45952 (to C.F.C.), and L.X.X. was supported by the Ruth L. Kirschstein National Service Award GM007185. The 2D gel work was performed in the Proteomic Facility at the UCLA Molecular Instrumentation Center, which was established with a grant from the W. M. Keck Foundation. The LC-MS/MS determination of quinones was supported in part by Grant Number S10RR024605 from the National Center for Research Resources. The content is solely the responsibility of the authors and does not necessarily represent the official views of the National Center for Research Resources or the National Institutes of Health.


## References


[1] S. Ghisla, C. Thorpe, Acyl-CoA dehydrogenases. A mechanistic overview, Eur. J. Biochem. 271 (2004) 494–508.
[2] G. Lenaz, A. De Santis, A survey of the function and specificity of ubiquione in the mitochondrial respiratory chain, in: G. Lenaz (Ed.), Coenzyme Q, John Wiley & Sons, Chichester, U.K., 1985, pp. 165–199.
[3] T.M. Hildebrandt, M.K. Grieshaber, Three enzymatic activities catalyze the oxidation of sulfide to thiosulfate in mammalian and invertebrate mitochondria, FEBS J. 275 (2008) 3352–3361.
[4] S. Hill, K. Hirano, V.V. Shmanai, B.N. Marbois, D. Vidovic, A.V. Bekish, B. Kay, V. Tse, J. Fine, C.F. Clarke, M.S. Shchepinov, Isotope-reinforced polyunsaturated fatty acids protect yeast cells from oxidative stress, Free Radic. Biol. Med. 50 (2010) 130–138.
[5] M. Bentinger, K. Brismar, G. Dallner, The antioxidant role of coenzyme Q, Mitochondrion 7S (2007) S41–S50.
[6] L. Papucci, N. Schiavone, E. Witort, M. Donnini, A. Lapucci, A. Tempestini, L. Formigli, S. Zecchi-Orlandini, G. Orlandini, G. Carella, R. Brancato, S. Capaccioli, Coenzyme Q10 prevents apoptosis by inhibiting mitochondrial depolarization independently of its free radical scavenging property, J. Biol. Chem. 278 (2003) 28220–28228.
[7] L. Walter, H. Miyoshi, X. Leverve, P. Bernard, E. Fontaine, Regulation of the mitochondrial permeability transition pore by ubiquinone analogs. A progress report, Free Radic. Res. 36 (2002) 405–412.
[8] F. Devun, L. Walter, J. Belliere, C. Cottet-Rousselle, X. Leverve, E. Fontaine, Ubiquinone analogs: a mitochondrial permeability transition pore-dependent pathway to selective cell death, PLoS ONE 5 (2010) e11792.
[9] D.R. Green, J.C. Reed, Mitochondria and apoptosis, Science 281 (1998) 1309–1312.
[10] L. Azzolin, S. von Stockum, E. Basso, V. Petronilli, M.A. Forte, P. Bernardi, The mitochondrial permeability transition from yeast to mammals, FEBS Lett. 584 (2010) 2504–2509.
[11] M. Kawamukai, Biosynthesis and bioproduction of coenzyme Q10 by yeasts and other organisms, Biotechnol. Appl. Biochem. 53 (2009) 217–226.
[12] R.E. Olson, H. Rudney, Biosynthesis of ubiquinone, Vitam. Horm. 40 (1983) 1–43.
[13] B. Marbois, L.X. Xie, S. Choi, K. Hirano, K. Hyman, C.F. Clarke, *para*-Aminobenzoic acid is a precursor in coenzyme Q6 biosynthesis in *Saccharomyces cerevisiae*, J. Biol. Chem. 285 (2010) 27827–27838.
[14] F. Pierrel, O. Hamelin, T. Douki, S. Kieffer-Jaquinod, U. Muhlenhoff, M. Ozeir, R. Lill, M. Fontecave, Involvement of mitochondrial ferredoxin and para-aminobenzoic acid in yeast coenzyme Q biosynthesis, Chem. Biol. 17 (2010) 449–459.
[15] U.C. Tran, C.F. Clarke, Endogenous synthesis of coenzyme Q in eukaryotes, Mitochondrion 7S (2007) S62–S71.
[16] B. Marbois, P. Gin, K.F. Faull, W.W. Poon, P.T. Lee, J. Strahan, J.N. Shepherd, C.F. Clarke, Coq3 and Coq4 define a polypeptide complex in yeast mitochondria for the biosynthesis of coenzyme Q, J. Biol. Chem. 280 (2005) 20231–20238.
[17] B. Marbois, P. Gin, M. Gulmezian, C.F. Clarke, The yeast Coq4 polypeptide organizes a mitochondrial protein complex essential for coenzyme Q biosynthesis, Biochim. Biophys. Acta 1791 (2009) 69–75.
[18] E.J. Hsieh, P. Gin, M. Gulmezian, U.C. Tran, R. Saiki, B.N. Marbois, C.F. Clarke, *Saccharomyces cerevisiae* Coq9 polypeptide is a subunit of the mitochondrial coenzyme Q biosynthetic complex, Arch. Biochem. Biophys. 463 (2007) 19–26.
[19] S.L. Rea, B.H. Graham, E. Nakamaru-Ogiso, A. Kar, M.J. Falk, Bacteria, yeast, worms, and flies: exploiting simple model organisms to investigate human mitochondrial diseases, Dev. Disabil. Res. Rev. 16 (2010) 200–218.
[20] I. Bousquet, G. Dujardin, P.P. Slonimski, *ABC1*, a novel yeast nuclear gene has a dual function in mitochondria: it suppresses a cytochrome *b* mRNA translation defect and is essential for the electron transfer in the $bc_1$ complex, EMBO J. 10 (1991) 2023–2031.
[21] G. Brasseur, G. Tron, G. Dujardin, P.P. Slonimski, P. Brivet-Chevillotte, The nuclear *ABC1* gene is essential for the correct conformation and functioning of the

cytochrome *bc1* complex and the neighbouring complexes II and IV in the mitochondrial respiratory chain, Eur. J. Biochem. 246 (1997) 103–111.
[22] T.Q. Do, A.Y. Hsu, T. Jonassen, P.T. Lee, C.F. Clarke, A defect in coenzyme Q biosynthesis is responsible for the respiratory deficiency in *Saccharomyces cerevisiae abc1* mutants, J. Biol. Chem. 276 (2001) 18161–18168.
[23] E.J. Hsieh, J.B. Dinoso, C.F. Clarke, A tRNA(TRP) gene mediates the suppression of *cbs2-223* previously attributed to *ABC1/COQ8*, Biochem. Biophys. Res. Commun. 317 (2004) 648–653.
[24] D.R. Macinga, G.M. Cook, R.K. Poole, P.N. Rather, Identification and characterization of *aarF*, a locus required for production of ubiquinone in *Providencia stuartii* and *Escherichia coli* and for expression of 2′-*N*-acetyltransferase in *P. stuartii*, J. Bacteriol. 180 (1998) 128–135.
[25] W.W. Poon, D.E. Davis, H.T. Ha, T. Jonassen, P.N. Rather, C.F. Clarke, Identification of *Escherichia coli ubiB*, a gene required for the first monooxygenase step in ubiquinone biosynthesis, J. Bacteriol. 182 (2000) 5139–5146.
[26] J. Mollet, A. Delahodde, V. Serre, D. Chretien, D. Schlemmer, A. Lombes, N. Boddaert, I. Desguerre, P. de Lonlay, H.O. de Baulny, A. Munnich, A. Rotig, CABC1 gene mutations cause ubiquinone deficiency with cerebellar ataxia and seizures, Am. J. Hum. Genet. 82 (2008) 623–630.
[27] C. Lagier-Tourenne, M. Tazir, L.C. Lopez, C.M. Quinzii, M. Assoum, N. Drouot, C. Busso, S. Makri, L. Ali-Pacha, T. Benhassine, M. Anheim, D.R. Lynch, C. Thibault, F. Plewniak, L. Bianchetti, C. Tranchant, O. Poch, S. DiMauro, J.L. Mandel, M.H. Barros, M. Hirano, M. Koenig, ADCK3, an ancestral kinase, is mutated in a form of recessive ataxia associated with coenzyme Q10 deficiency, Am. J. Hum. Genet. 82 (2008) 661–672.
[28] C.J. Leonard, L. Aravind, E.V. Koonin, Novel families of putative protein kinases in bacteria and archaea: evolution of the "eukaryotic" protein kinase superfamily, Genome Res. 8 (1998) 1038–1047.
[29] G. Manning, D.B. Whyte, R. Martinez, T. Hunter, S. Sudarsanam, The protein kinase complement of the human genome, Science 298 (2002) 1912–1934.
[30] A. Johnson, P. Gin, B.N. Marbois, E.J. Hsieh, M. Wu, M.H. Barros, C.F. Clarke, A. Tzagoloff, *COQ9*, a new gene required for the biosynthesis of coenzyme Q in *Saccharomyces cerevisiae*, J. Biol. Chem. 280 (2005) 31397–31404.
[31] M.H. Barros, A. Johnson, P. Gin, B.N. Marbois, C.F. Clarke, A. Tzagoloff, The *Saccharomyces cerevisiae COQ10* gene encodes a START domain protein required for function of coenzyme Q in respiration, J. Biol. Chem. 280 (2005) 42627–42635.
[32] C. Busso, E.B. Tahara, R. Ogusucu, O. Augusto, J.R. Ferreira-Junior, A. Tzagoloff, A.J. Kowaltowski, M.H. Barros, *Saccharomyces cerevisiae coq10* null mutants are responsive to antimycin A, FEBS J. (2010).
[33] S. Padilla, U.C. Tran, M. Jimenez-Hidalgo, J.M. Lopez-Martin, A. Martin-Montalvo, C.F. Clarke, P. Navas, C. Santos-Ocana, Hydroxylation of demethoxy-Q6 constitutes a control point in yeast coenzyme Q6 biosynthesis, Cell. Mol. Life Sci. 66 (2009) 173–186.
[34] A. Tauche, U. Krause-Buchholz, G. Rodel, Ubiquinone biosynthesis in *Saccharomyces cerevisiae*: the molecular organization of *O*-methylase Coq3p depends on Abc1p/Coq8p, FEMS Yeast Res. 8 (2008) 1263–1275.
[35] C.J. Sippel, R.R. Goewert, F.N. Slachman, R.E. Olson, The regulation of ubiquinone-6 biosynthesis by *Saccharomyces cerevisiae*, J. Biol. Chem. 258 (1983) 1057–1061.
[36] D. Burke, D. Dawson, T. Stearns, Methods in Yeast Genetics, Cold Spring Harbor Laboratory Press, Plainview, NY, 2000.
[37] R.J. Barkovich, A. Shtanko, J.A. Shepherd, P.T. Lee, D.C. Myles, A. Tzagoloff, C.F. Clarke, Characterization of the *COQ5* gene from *Saccharomyces cerevisiae*. Evidence for a *C*-methyltransferase in ubiquinone biosynthesis, J. Biol. Chem. 272 (1997) 9182–9188.
[38] R. Elble, A simple and efficient procedure for transformation of yeasts, Biotechniques 13 (1992) 18–20.
[39] S.H. Ackerman, J. Martin, A. Tzagoloff, Characterization of *ATP11* and detection of the encoded protein in mitochondria of *Saccharomyces cerevisiae*, J. Biol. Chem. 267 (1992) 7386–7394.
[40] D.M. Glerum, T.J. Koerner, A. Tzagoloff, Cloning and characterization of *COX14*, whose product is required for assembly of yeast cytochrome oxidase, J. Biol. Chem. 270 (1995) 15585–15590.
[41] A.Y. Hsu, W.W. Poon, J.A. Shepherd, D.C. Myles, C.F. Clarke, Complementation of *coq3* mutant yeast by mitochondrial targeting of the *Escherichia coli* UbiG polypeptide: evidence that UbiG catalyzes both *O*-methylation steps in ubiquinone biosynthesis, Biochemistry 35 (1996) 9797–9806.
[42] B. Cormack, Directed mutagenesis using the polymerase chain reaction, in: V.B. Chanda (Ed.), Current Protocols in Molecular Biology, vol. 1, John Wiley & Sons, 1997, pp. 8.5.1–8.5.10.
[43] B.S. Glick, L.A. Pon, Isolation of highly purified mitochondria from *Saccharomyces cerevisiae*, Meth. Enzymol. 260 (1995) 213–223.
[44] B.S. Glick, A. Brandt, K. Cunningham, S. Muller, R.L. Hallberg, G. Schatz, Cytochromes $c_1$ and $b_2$ are sorted to the intermembrane space of yeast mitochondria by a stop-transfer mechanism, Cell 69 (1992) 809–822.
[45] U.K. Laemmli, Cleavage of structural proteins during the assembly of the head of bacteriophage T4, Nature 227 (1970) 680–685.
[46] T. Jonassen, C.F. Clarke, Isolation and functional expression of human *COQ3*, a gene encoding a methyltransferase required for ubiquinone biosynthesis, J. Biol. Chem. 275 (2000) 12381–12387.
[47] M. Jasinski, D. Sudre, G. Schansker, M. Schellenberg, S. Constant, E. Martinoia, L. Bovet, AtOSA1, a member of the Abc1-like family, as a new factor in cadmium and oxidative stress response, Plant Physiol. 147 (2008) 719–731.
[48] G.I. Belogrudov, P.T. Lee, T. Jonassen, A.Y. Hsu, P. Gin, C.F. Clarke, Yeast *COQ4* encodes a mitochondrial protein required for coenzyme Q synthesis, Arch. Biochem. Biophys. 392 (2001) 48–58.
[49] Y. Fujiki, A.L. Hubbard, S. Fowler, P.B. Lazarow, Isolation of intracellular membranes by means of sodium carbonate treatment: application to endoplasmic reticulum, J. Cell Biol. 93 (1982) 97–102.
[50] M.P. Kamps, B.M. Sefton, Neither arginine nor histidine can carry out the function of lysine-295 in the ATP-binding site of p60src, Mol. Cell. Biol. 6 (1986) 751–757.
[51] S.K. Hanks, T. Hunter, Protein kinases 6. The eukaryotic protein kinase superfamily: kinase (catalytic) domain structure and classification, FASEB J. 9 (1995) 576–596.
[52] P. Gin, C.F. Clarke, Genetic evidence for a multi-subunit complex in coenzyme Q biosynthesis in yeast and the role of the Coq1 hexaprenyl diphosphate synthase, J. Biol. Chem. 280 (2005) 2676–2681.
[53] U.C. Tran, B. Marbois, P. Gin, M. Gulmezian, T. Jonassen, C.F. Clarke, Complementation of *Saccharomyces cerevisiae coq7* mutants by mitochondrial targeting of the *Escherichia coli* UbiF polypeptide: two functions of yeast Coq7 polypeptide in coenzyme Q biosynthesis, J. Biol. Chem. 281 (2006) 16401–16409.
[54] A. Tzagoloff, C.L. Dieckmann, *PET* genes of *Saccharomyces cerevisiae*, Microbiol. Rev. 54 (1990) 211–225.
[55] A. Tzagoloff, A. Akai, R.B. Needleman, Assembly of the mitochondrial membrane system. Characterization of nuclear mutants of *Saccharomyces cerevisiae* with defects in mitochondrial ATPase and respiratory enzymes, J. Biol. Chem. 250 (1975) 8228–8235.
[56] A. Tzagoloff, A. Akai, R.B. Needleman, G. Zulch, Assembly of the mitochondrial membrane system. Cytoplasmic mutants of *Saccharomyces cerevisiae* with lesions in enzymes of the respiratory chain and in the mitochondrial ATPase, J. Biol. Chem. 250 (1975) 8236–8242.
[57] Z. Vajo, L.M. King, T. Jonassen, D.J. Wilkin, N. Ho, A. Munnich, C.F. Clarke, C.A. Francomano, Conservation of the *Caenorhabditis elegans* timing gene *clk-1* from yeast to human: a gene required for ubiquinone biosynthesis with potential implications for aging, Mamm. Genome 10 (1999) 1000–1004.
[58] S.W. Baba, G.I. Belogrudov, J.C. Lee, P.T. Lee, J. Strahan, J.N. Shepherd, C.F. Clarke, Yeast *coq5 C*-methyltransferase is required for stability of other polypeptides involved in coenzyme Q biosynthesis, J. Biol. Chem. 279 (2004) 10052–10059.
[59] E.J. Hsieh, Characterization of the Coenzyme Q Biosynthetic Genes *ABC1/COQ8* and *COQ9* in Yeast *Saccharomyces cerevisiae*, Chemistry and Biochemistry, University of California, Los Angeles, Los Angeles, 2006, p. 126.
[60] S. Facchin, R. Lopreiato, S. Stocchetto, G. Arrigoni, L. Cesaro, O. Marin, G. Carignani, L.A. Pinna, Structure–function analysis of yeast piD261/Bud32, an atypical protein kinase essential for normal cell life, Biochem. J. 364 (2002) 457–463.
[61] M. Spitaler, A. Villunger, H. Grunicke, F. Uberall, Unique structural and functional properties of the ATP-binding domain of atypical protein kinase C-iota, J. Biol. Chem. 275 (2000) 33289–33296.
[62] S.S. Taylor, E. Radzio-Andzelm, T. Hunter, How do protein kinases discriminate between serine/threonine and tyrosine? Structural insights from the insulin receptor protein-tyrosine kinase, FASEB J. 9 (1995) 1255–1266.
[63] L.N. Johnson, E.D. Lowe, M.E. Noble, D.J. Owen, The Eleventh Datta Lecture. The structural basis for substrate recognition and control by protein kinases, FEBS Lett. 430 (1998) 1–11.
[64] S.K. Hanks, Genomic analysis of the eukaryotic protein kinase superfamily: a perspective, Genome Biol. 4 (2003) 111.
[65] S.K. Hanks, A.M. Quinn, T. Hunter, The protein kinase family: conserved features and deduced phylogeny of the catalytic domains, Science 241 (1988) 42–52.
[66] O. Delumeau, S. Dutta, M. Brigulla, G. Kuhnke, S.W. Hardwick, U. Volker, M.D. Yudkin, R.J. Lewis, Functional and structural characterization of RsbU, a stress signaling protein phosphatase 2C, J. Biol. Chem. 279 (2004) 40927–40937.
[67] A.C. Olivier, S. Lemaire, F. Van Bambeke, P.M. Tulkens, E. Oldfield, Role of rsbU and staphyloxanthin in phagocytosis and intracellular growth of *Staphylococcus aureus* in human macrophages and endothelial cells, J. Infect. Dis. 200 (2009) 1367–1370.
[68] J.H. Shin, M.S. Brody, C.W. Price, Physical and antibiotic stresses require activation of the RsbU phosphatase to induce the general stress response in *Listeria monocytogenes*, Microbiology 156 (2010) 2660–2669.
[69] A. Chi, C. Huttenhower, L.Y. Geer, J.J. Coon, J.E. Syka, D.L. Bai, J. Shabanowitz, D.J. Burke, O.G. Troyanskaya, D.F. Hunt, Analysis of phosphorylation sites on proteins from *Saccharomyces cerevisiae* by electron transfer dissociation (ETD) mass spectrometry, Proc. Natl Acad. Sci. USA 104 (2007) 2193–2198.
[70] C. Stark, T.C. Su, A. Breitkreutz, P. Lourenco, M. Dahabieh, B.J. Breitkreutz, M. Tyers, I. Sadowski, PhosphoGRID: a database of experimentally verified in vivo protein phosphorylation sites from the budding yeast *Saccharomyces cerevisiae*, Database (Oxford) 2010 (2010) bap026.
[71] M.A. Zampol, C. Busso, F. Gomes, J.R. Ferreira-Junior, A. Tzagoloff, M.H. Barros, Over-expression of *COQ10* in *Saccharomyces cerevisiae* inhibits mitochondrial respiration, Biochem. Biophys. Res. Commun. 402 (2010) 82–87.
[72] M. Iiizumi, H. Arakawa, T. Mori, A. Ando, Y. Nakamura, Isolation of a novel gene, *CABC1*, encoding a mitochondrial protein that is highly homologous to yeast activity of $bc_1$ complex, Cancer Res. 62 (2002) 1246–1250.
[73] M. Gerards, B. van den Bosch, C. Calis, K. Schoonderwoerd, K. van Engelen, M. Tijssen, R. de Coo, A. van der Kooi, H. Smeets, Nonsense mutations in CABC1/ADCK3 cause progressive cerebellar ataxia and atrophy, Mitochondrion 10 (2010) 510–515.
[74] C.M. Quinzii, M. Hirano, Coenzyme Q and mitochondrial disease, Dev. Disabil. Res. Rev. 16 (2010) 183–188.
[75] R. Saiki, A.L. Lunceford, Y. Shi, B. Marbois, R. King, J. Pachuski, M. Kawamukai, D.L. Gasser, C.F. Clarke, Coenzyme Q10 supplementation rescues renal disease in Pdss2kd/kd mice with mutations in prenyl diphosphate synthase subunit 2, Am. J. Physiol. Ren. Physiol. 295 (2008) F1535–F1544.
[76] B. Cardazzo, P. Hamel, W. Sakamoto, H. Wintz, G. Dujardin, Isolation of an *Arabidopsis thaliana* cDNA by complementation of a yeast abc1 deletion mutant deficient in complex III respiratory activity, Gene 221 (1998) 117–125.
[77] A.J. Ytterberg, J.B. Peltier, K.J. van Wijk, Protein profiling of plastoglobules in chloroplasts and chromoplasts. A surprising site for differential accumulation of metabolic enzymes, Plant Physiol. 140 (2006) 984–997.

[78] J.E. McEwen, C. Ko, B. Kloeckner-Gruissem, R.O. Poyton, Nuclear functions required for cytochrome *c* oxidase biogenesis in *Saccharomyces cerevisiae*. Characterization of mutants in 34 complementation groups, J. Biol. Chem. 261 (1986) 11872–11879.
[79] R.S. Sikorski, P. Hieter, A system of shuttle vectors and yeast host strains designed for efficient manipulation of DNA in *Saccharomyces cerevisiae*, Genetics 122 (1989) 19–27.
[80] T.W. Christianson, R.S. Sikorski, M. Dante, J.H. Shero, P. Hieter, Multifunctional yeast high-copy-number shuttle vectors, Gene 110 (1992) 119–122.
[81] A.Y. Hsu, W.W. Poon, J.A. Shepherd, D.C. Myles, C.F. Clarke, Complementation of coq3 mutant yeast by mitochondrial targeting of the *Escherichia coli* UbiG polypeptide: evidence that UbiG catalyzes both O-methylation steps in ubiquinone biosynthesis, Biochemistry 35 (1996) 9797–9806.
[82] T.Q. Do, A.Y. Hsu, T. Jonassen, P.T. Lee, C.F. Clarke, A defect in coenzyme Q biosynthesis is responsible for the respiratory deficiency in *Saccharomyces cerevisiae abc1* mutants, J. Biol. Chem. 276 (2001) 18161–18168.
[83] W.J. Chen, M.G. Douglas, Phosphodiester bond cleavage outside mitochondria is required for the completion of protein import into the mitochondrial matrix, Cell 49 (1987) 651–658.
[84] G. Daum, P.C. Bohni, G. Schatz, Import of proteins into mitochondria. Cytochrome *b2* and cytochrome *c* peroxidase are located in the intermembrane space of yeast mitochondria, J. Biol. Chem. 257 (1982) 13028–13033.
[85] A. Ohashi, J. Gibson, I. Gregor, G. Schatz, Import of proteins into mitochondria. The precursor of cytochrome *c1* is processed in two steps, one of them heme-dependent, J. Biol. Chem. 257 (1982) 13042–13047.
[86] L.M. Thompson, L. McAlister-Henn, Dispensable presequence for cellular localization and function of mitochondrial malate dehydrogenase from *Saccharomyces cerevisiae*, J. Biol. Chem. 264 (1989) 12091–12096.
[87] D.S. Reading, R.L. Hallberg, A.M. Myers, Characterization of the yeast HSP60 gene coding for a mitochondrial assembly factor, Nature 337 (1989) 655–659.

# Chapter 3

## Overexpression of the Coq8 Kinase in *Saccharomyces cerevisiae coq* Null Mutants Allows for Accumulation of Diagnostic Intermediates of the Coenzyme $Q_6$ Biosynthetic Pathway

# Overexpression of the Coq8 Kinase in *Saccharomyces cerevisiae coq* Null Mutants Allows for Accumulation of Diagnostic Intermediates of the Coenzyme $Q_6$ Biosynthetic Pathway*[S]

Received for publication, March 8, 2012, and in revised form, May 9, 2012 Published, JBC Papers in Press, May 16, 2012, DOI 10.1074/jbc.M112.360354

**Letian X. Xie**[‡1,2], **Mohammad Ozeir**[§¶‖2], **Jeniffer Y. Tang**[‡], **Jia Y. Chen**[‡], **Sylvie-Kieffer Jaquinod**[**], **Marc Fontecave**[§¶‖‡‡], **Catherine F. Clarke**[‡3], **and Fabien Pierrel**[§¶‖4]

*From the* [‡]*Department of Chemistry and Biochemistry and the Molecular Biology Institute, UCLA, Los Angeles, California 90095-1569, the* [§]*Commissariat à l'Energie Atomique, Institut de Recherches en Technologies et Sciences pour le Vivant, Laboratoire Chimie et Biologie des Métaux, F-38054 Grenoble, France, the* [¶]*CNRS, UMR5249, F-38054 Grenoble, France, the* [‖]*Université Joseph Fourier-Grenoble I, UMR5249, F-38041 Grenoble, France, the* [**]*Etude de la Dynamique des Protéomes, Laboratoire Biologie à Grande Echelle, U1038 INSERM/CEA/UJF, 38054 Grenoble Cedex 9, France, and the* [‡‡]*Collège de France, 11 Place Marcellin-Berthelot, 75005 Paris, France*

**Background:** Several steps of eukaryotic coenzyme Q biosynthesis are still in question.
**Results:** Yeast *coq* null mutants overexpressing the Coq8 kinase have stable Coq polypeptides and accumulate new Q intermediates that help diagnose the blocked step.
**Conclusion:** New functions for Coq polypeptides are proposed.
**Significance:** Identification of the blocked step allows for the use of alternate ring precursors that rescue Q biosynthesis in some mutants.

**Most of the Coq proteins involved in coenzyme Q (ubiquinone or Q) biosynthesis are interdependent within a multiprotein complex in the yeast *Saccharomyces cerevisiae*. Lack of only one Coq polypeptide, as in Δ*coq* strains, results in the degradation of several Coq proteins. Consequently, Δ*coq* strains accumulate the same early intermediate of the $Q_6$ biosynthetic pathway; this intermediate is therefore not informative about the deficient biosynthetic step in a particular Δ*coq* strain. In this work, we report that the overexpression of the protein Coq8 in Δ*coq* strains restores steady state levels of the unstable Coq proteins. Coq8 has been proposed to be a kinase, and we provide evidence that the kinase activity is essential for the stabilizing effect of Coq8 in the Δ*coq* strains. This stabilization results in the accumulation of several novel $Q_6$ biosynthetic intermediates. These Q intermediates identify chemical steps impaired in cells lacking Coq4 and Coq9 polypeptides, for which no function has been established to date. Several of the new intermediates contain a C4-amine and provide information on the deamination reaction that takes place when *para*-aminobenzoic acid is used as a ring precursor of $Q_6$. Finally, we used synthetic analogues of 4-hydroxybenzoic acid to bypass deficient biosynthetic steps, and we show here that 2,4-dihydroxybenzoic acid is able to restore $Q_6$ biosynthesis and respiratory growth in a Δ*coq7* strain overexpressing Coq8. The overexpression of Coq8 and the use of 4-hydroxybenzoic acid analogues represent innovative tools to elucidate the Q biosynthetic pathway.**

Coenzyme Q (ubiquinone or Q)[5] is a redox-active lipid essential for electron and proton transport in the mitochondrial respiratory chain. Q is also important in the mitochondrial inner membrane because it serves as an antioxidant, modulates the function of the mitochondrial membrane transition pore, and is a cofactor of uncoupling proteins (1). Q is composed of a fully substituted benzoquinone ring that is attached to a polyisoprenyl tail of various lengths (6 isoprenyl units in *Saccharomyces cerevisiae* hence $Q_6$ and 10 units in humans, hence $Q_{10}$). The eukaryotic Q biosynthetic pathway has been studied most thoroughly in *S. cerevisiae* where it implicates at least 11 proteins, Coq1–Coq9, Arh1, and Yah1 (2, 3).

Genetic and biochemical studies have shown that most Coq proteins are present in a high molecular mass, multisubunit $Q_6$

* This work was supported, in whole or in part, by National Institutes of Health Grant GM45952 (to C. F. C.). This work was also supported by Région Rhône-Alpes Program CIBLE 2009 (to F. P.) and National Science Foundation Grant 0919609 (to C. F. C.).

[S] This article contains supplemental Figs. S1–S6.

[1] Supported by Ruth L. Kirschstein National Institutes of Health Service Award GM007185.

[2] Both authors contributed equally to this work.

[3] To whom correspondence may be addressed: Dept. of Chemistry and Biochemistry, 607 Charles E. Young Dr. E, UCLA, Los Angeles, CA 90095-1569. Tel.: 310-825-0771; Fax: 310-206-5213; E-mail: cathy@chem.ucla.edu.

[4] To whom correspondence may be addressed. Tel.: 33-4-38-78-91-10; Fax: 33-4-38-78-91-24; E-mail: fabien.pierrel@cea.fr.

[5] The abbreviations used are: Q, ubiquinone or coenzyme Q; 4-AP, 3-hexaprenyl-4-aminophenol; $DDMQ_6$, oxidized form of demethyl-demethoxy-$Q_6H_2$; DHHB, 3-hexaprenyl-4,5-dihydroxybenzoic acid; 2,4-diHB, 2,4-dihydroxybenzoic acid; $DMQ_6$, demethoxy-$Q_6$; ECD, electrochemical detection; 4-HB, 4-hydroxybenzoic acid; HAB, 3-hexaprenyl-4-aminobenzoic acid; HHAB, 3-hexaprenyl-4-amino-5-hydroxybenzoic acid; HHB, 3-hexaprenyl-4-hydroxybenzoic acid; HMAB, 3-hexaprenyl-4-amino-5-methoxybenzoic acid; 4-HP, 3-hexaprenyl-4-hydroxyphenol; $IDMQ_6$, 4-imino-demethoxy-$Q_6$; MRM, multiple reaction monitoring; OE, overexpression; *p*ABA, *para*-aminobenzoic acid; RP-HPLC-MS/MS; reverse phase-HPLC-MS/MS; VA, vanillic acid (4-hydroxy-3-methoxybenzoic acid); DOGAL, Drop Out Galactose medium.

Downloaded from http://www.jbc.org/ at UCLA-Louise Darling Biomed. Lib. on July 2, 2014

biosynthetic complex in *S. cerevisiae* (4, 5). The absence of a single Coq polypeptide from the complex causes a drastic diminution of the steady state levels of some Coq proteins. For example, the steady state levels of Coq4, Coq6, Coq7, and Coq9 are decreased in each of the Δ*coq1*–Δ*coq9* null strains (6). As a result, the same early intermediate 3-hexaprenyl-4-hydroxybenzoic acid (HHB; Fig. 1, *path 1*) accumulates in each of the Δ*coq3*–Δ*coq9* strains. Certain point mutations resulting in amino acid substitutions seem to have less impact on the integrity of the Q biosynthetic complex than a null mutation; expression of the inactive Coq7-E194K polypeptide in a Δ*coq7* strain caused accumulation of the expected intermediate demethoxy-$Q_6$ ($DMQ_6$, Fig. 1) (7, 8). Apart from this example, the absence of accumulation of biosynthetic intermediates downstream of HHB in Δ*coq* strains has hindered our understanding of the Q biosynthetic pathway. Therefore, the precise order of certain biosynthetic steps is still elusive, and the function of Coq4 and Coq9 is not defined.

The yeast *COQ8* gene was formerly called *ABC1* and was thought to be essential for complex III function (9, 10). However, it was later shown that *COQ8* was required for $Q_6$ biosynthesis, and as such, its deletion only affected complex III activity indirectly (11). Coq8 is a matrix protein peripherally associated with the mitochondrial inner membrane (12) and belongs to the "atypical kinases" subgroup of the protein-kinase-like superfamily (13). Mutations in *ADCK3*, the human orthologue of *COQ8*, were shown to cause $Q_{10}$ deficiency and cerebellar ataxia (13, 14). In yeast, Coq8 is essential for phosphorylation of Coq3 and for its association with the Q biosynthetic complex (12, 15). In addition, several phosphorylated forms of Coq5 and Coq7 disappear in a yeast strain expressing the G130D mutant form of Coq8 (12), which mimics the pathogenic G272D mutation found in *ADCK3* (14). Therefore, Coq8 appears to be a kinase essential for the phosphorylation of several conserved Coq polypeptides and some of these phosphorylated forms likely play a role in the assembly or maintenance of the $Q_6$ biosynthetic complex. Recent studies indicate that overexpression of *COQ8* can have profound effects on $Q_6$ biosynthesis. Indeed, the overexpression of Coq8 (from now on referred to as Coq8 OE) in a Δ*coq7* strain promoted the accumulation of $DMQ_6$ (16), implying that all Coq proteins acting upstream of Coq7 in the biosynthetic pathway were stable and active. The effect of Coq8 OE is likely post-transcriptional because *COQ4* mRNA levels in the Δ*coq7* strain were not dependent on the level of Coq8 OE (16). Recently, the low steady state level of Coq4 encountered in Δ*coq2*, Δ*coq3*, Δ*coq5*, and Δ*coq7* strains was shown to be restored to wild-type levels by Coq8 OE (17). In the case of a Δ*coq6* strain, Coq8 OE allowed the specific accumulation of 3-hexaprenyl-4-hydroxyphenol (4-HP) (Fig. 1), which led us to identify Coq6 as the monooxygenase responsible for the C5-hydroxylation step (18). This example demonstrates that the accumulation of $Q_6$ biosynthetic intermediates in Δ*coq* strains and the identification of their chemical structure are important for understanding the function of Coq proteins.

In addition to the classic Q biosynthetic pathway emanating from 4-hydroxybenzoic acid (4-HB), *S. cerevisiae* also makes use of *para*-aminobenzoic acid (*p*ABA) as a ring precursor for $Q_6$ biosynthesis (Fig. 1, *path 2*) (3, 19). Coq2 is able to catalyze the prenylation of 4-HB to yield HHB, as well as the prenylation of *p*ABA to yield 3-hexaprenyl-4-aminobenzoic acid (HAB). We have hypothesized that Coq3–Coq9 enzymes modify both HAB and HHB and that the C4-amino group must be removed from the HAB-derived intermediates to produce $Q_6$ (3, 19). The deamination reaction likely occurs before the C6-hydroxylation step catalyzed by Coq7 because 4-imino-$DMQ_6$ ($IDMQ_6$) was proposed to be a precursor of $DMQ_6$ (19). Ring precursors other than 4-HB and *p*ABA can also be used *in vivo* by *S. cerevisiae* to synthesize $Q_6$. Indeed, 3,4-dihydroxybenzoic acid and vanillic acid bypass a deficiency in the Coq6-mediated C5-hydroxylation reaction and restore $Q_6$ biosynthesis in *coq6* or *yah1* mutant strains (18).

In this study, we show that Coq8 OE restores the steady state levels of the Coq proteins in most Δ*coq* strains. The stabilization of the Coq polypeptides leads to the accumulation of $Q_6$ biosynthetic intermediates that allow the diagnosis of the impaired step. We have used this property to demonstrate that several biosynthetic steps are impaired in the Δ*coq4* and Δ*coq9* strains and to gain insights into the deamination reaction. Finally, the use of alternate ring precursors promoted the restoration of $Q_6$ biosynthesis and respiratory growth for a Δ*coq7* strain.

## EXPERIMENTAL PROCEDURES

*Yeast Strains and Culture Conditions*—*S. cerevisiae* strains used in this study are listed in Table 1. *S. cerevisiae* strains were transformed with lithium acetate as described (20, 21). YNB without *p*ABA and folate (−*p*ABA−folate) was purchased from MP Biomedicals. Rich YP medium was prepared as described (22). Dextrose or lactate-glycerol was used at 2%. In preparation for analyses by HPLC-ECD, yeast cells were cultured as described (3) and grown for 18 h at 30 °C. Stock solutions of 4-HB analogues at 100 mM were prepared by slowly titrating NaOH (care was taken not to exceed pH 9) until complete dissolution. The solutions were then filter-sterilized, and aliquots were kept at −20 °C for several months. The 4-HB analogues were added to −*p*ABA−folate growth medium at the indicated concentrations. Alternatively, in preparation for analyses by HPLC-MS/MS, yeast cells were cultured in Drop Out Galactose medium (DOGAL) (19) and labeled as described. Briefly, 100 $A_{600}$ cells were collected from overnight culture and transferred to fresh medium in the presence of various aromatic ring precursors for 2–4 h at 30 °C. Cells were then collected by centrifugation and subject to LC-MS/MS analysis.

*Plasmids*—Plasmids used in this study are listed in Table 2. *COQ7* ORF with its own promoter and terminator was cloned into pRS425 using HindIII and XhoI. Sequencing was used to confirm cloning products.

*SDS-PAGE and Immunoblot Analysis*—Whole cell lysate and isolation of mitochondria were performed as described (12). Proteins were transferred from SDS-polyacrylamide gels to polyvinylidene difluoride (PVDF) membrane and then incubated with primary antibodies at the following dilutions: Coq1, 1:10,000; Coq3, 1:1000; Coq4, 1:1000; Coq5, 1:10,000; Coq6,

Downloaded from http://www.jbc.org/ at UCLA-Louise Darling Biomed. Lib. on July 2, 2014

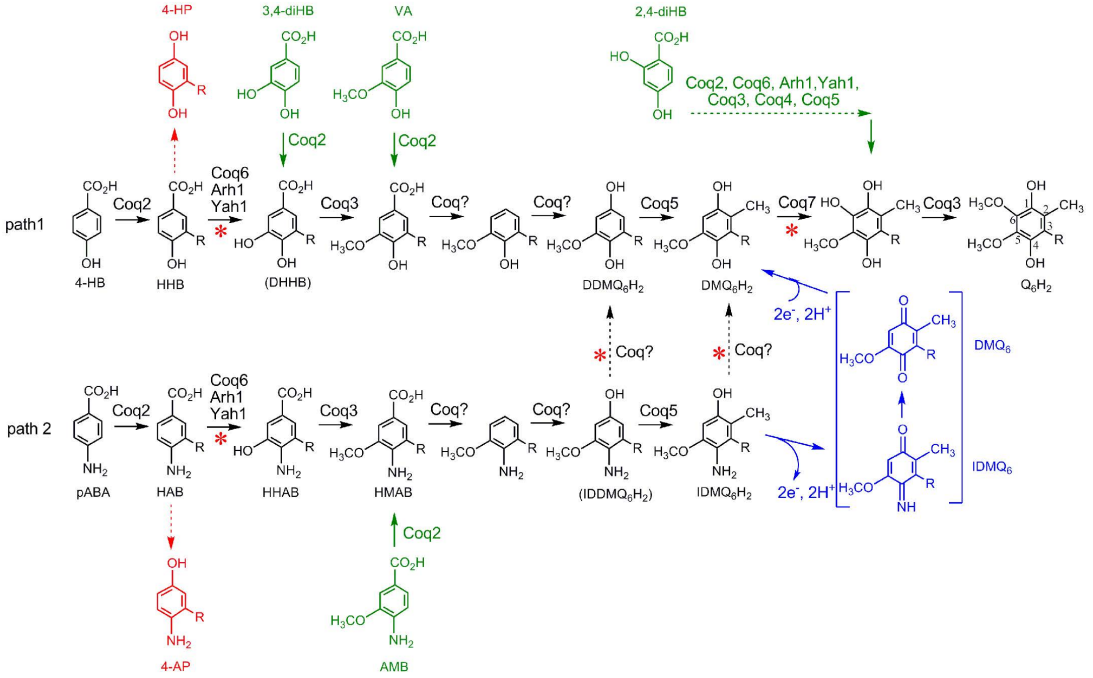



FIGURE 1. ***S. cerevisiae* $Q_6$ biosynthetic pathway.** Accumulation of $Q_6$ biosynthetic intermediates is caused by the overexpression of Coq8 in Δ*coq* strains. The classic Q biosynthetic pathway is shown in *path 1* emanating from 4-HB. Coq1 (not shown) synthesizes the hexaprenyl-diphosphate tail that is transferred by Coq2 to 4-HB to form HHB. *R* represents the hexaprenyl tail present in all intermediates from HHB to $Q_6$. Alternatively, in *path 2*, *p*ABA is prenylated by Coq2 to form HAB. Both HHB and HAB are early $Q_6$ intermediates, readily detected in each of the *coq* null strains (Δ*coq3*-Δ*coq9*). The numbering of the aromatic carbon atoms used throughout this study is shown on the reduced form of $Q_6$, $Q_6H_2$. Coq8 OE in certain Δ*coq* strains leads to the accumulation of the following compounds: *4-AP*, 3-hexaprenyl-4-aminophenol; *4-HP*, 3-hexaprenyl-4-hydroxyphenol; *HHAB*, 3-hexaprenyl-4-amino-5-hydroxybenzoic acid; *HMAB*, 3-hexaprenyl-4-amino-5-methoxybenzoic acid; *$DDMQ_6H_2$*, is the reduced form of demethyl-demethoxy-$Q_6$; *$IDMQ_6$*, 4-imino-demethoxy-$Q_6$; *$IDMQ_6H_2$*, 4-amino-demethoxy-$Q_6H_2$; *$DMQ_6$*, demethoxy-$Q_6$; *$DMQ_6H_2$*, demethoxy-$Q_6H_2$. *$IDDMQ_6H_2$*, 2-demethyl-4-amino-demethoxy-$Q_6H_2$, and *DHHB*, 3-hexaprenyl-4,5-dihydroxybenzoic acid, are shown in *parentheses* to indicate that they have not been detected in this study. *Black dotted arrows* (from *path 2* to *path 1*) designate the replacement of the C4-amine with a C4-hydroxyl and correspond to the C4-deamination/deimination reaction. A putative mechanism to replace the C4-imino group with the C4-hydroxy group is shown in *blue brackets* for $IDMQ_6$ but could also occur on 2-demethyl-4-amino-demethoxy-$Q_6$ (*$IDDMQ_6$*) (not shown). 4-AP and 4-HP, which are formed upon inhibition of the C5-hydroxylation catalyzed by Coq6, are shown in *red*. Analogues of 4-HB and *p*ABA allowing the bypass of certain steps in Q biosynthesis are indicated in *green*. Steps defective in the Δ*coq9* strain are designated with a *red asterisk*.

**TABLE 1**

**Genotype and source of yeast strains**

| Strain | Genotype | Source |
|---|---|---|
| W303-1A | MAT a *ade2-1 his3-1,15 leu2-3,112 trp1-1 ura3-1* | R. Rothstein[a] |
| W303Δ*coq1* | MAT a *ade2-1 his3-1,15 leu2-3,112 trp1-1 ura3-1 coq1::LEU2* | 23 |
| W303Δ*coq2* | MAT a *ade2-1 his3-1,15 leu2-3,112 trp1-1 ura3-1 coq2::HIS3* | 31 |
| CC303 | MAT α *ade2-1 his3-1,15 leu2-3,112 trp1-1 ura3-1 coq3::LEU2* | 32 |
| W303Δ*coq4* | MAT a *ade2-1 his3-1,15 leu2-3,112 trp1-1 ura3-1 coq4::TRP1* | 33 |
| W303Δ*coq5* | MAT a *ade2-1 his3-1,15 leu2-3,112 trp1-1 ura3-1 coq5::HIS3* | 34 |
| W303Δ*coq6* | MAT a *ade2-1 his3-1,15 leu2-3,112 trp1-1 ura3-1 coq6::LEU2* | 35 |
| W303Δ*coq7* | MAT α *ade2-1 his3-1,15 leu2-3,112 trp1-1 ura3-1 coq7::LEU2* | 36 |
| W303Δ*coq8* | MAT a *ade2-1 his3-1,15 leu2-3,112 trp1-1 ura3-1 abc1/coq8::HIS3* | 33 |
| BY4741 | MAT a *his3Δ1 leu2Δ0 met15Δ0 ura3Δ0* | 37 |
| BY4741Δ*coq9* | MAT a *coq9Δ::kanMX4 his3Δ1 leu2Δ0 met15Δ0 ura3Δ0* | 38[b] |
| C9-E1 | MAT a *ade2-1, coq4-1, trp1-1, ura3-1* | 39 |
| BY4741Δ*coq3* | MAT a *coq3Δ::kanMX4 his3Δ1 leu2Δ0 met15Δ0 ura3Δ0* | 38[b] |
| BY4742Δ*coq4* | MAT α *coq4Δ::kanMX4 his3Δ1 leu2Δ0 lys2Δ0 ura3Δ0* | 38[b] |
| BY4742Δ*coq9* | MAT α *coq9Δ::kanMX4 his3Δ1 leu2Δ0 lys2Δ0 ura3Δ0* | 38[b] |

[a] Dr. Rodney Rothstein, Dept. of Human Genetics, Columbia University.
[b] European *S. cerevisiae* Archive for Functional Analysis (EUROSCARF), available on-line.

1:200; Coq7, 1:1000; Coq8, 1:100; Coq9, 1:1000; and Pda1, 1:1000. Goat anti-rabbit IgG secondary antibodies (Calbiochem) were used at 1:10,000.

*Lipid Extraction and Detection of Electroactive Compounds by HPLC-ECD*—Cellular lipid extraction after addition of the $Q_4$ standard and detection of electroactive compounds by

Downloaded from http://www.jbc.org/ at UCLA-Louise Darling Biomed. Lib. on July 2, 2014

**TABLE 2**
Plasmid constructs used in this study

| Plasmid | Relevant genes | Copy number | Source |
|---|---|---|---|
| pRS316 | Yeast shuttle vector | Low copy | 40 |
| pRS426 | Yeast shuttle vector | Multicopy | 41 |
| p3HN4 | Yeast *ABC1/COQ8* | Low copy | 11 |
| p4HN4 | Yeast *ABC1/COQ8* | Multicopy | 42 |
| pFL44 Coq8 | Yeast *ABC1/COQ8* | Multicopy | 9 |
| pFL44 Coq8 G130D | Yeast *ABC1/COQ8 G130D* | Multicopy | 14 |
| pRS425 Coq7 | Yeast *COQ7* | Multicopy | This work |

HPLC-ECD with a 5011A analytical cell (E1, −550 mV; E2, +550 mV) were conducted as described (3). Hydroquinones present in samples were oxidized with a precolumn 5020 guard cell set in oxidizing mode (*E*, +650 mV).

*Lipid Extraction and RP-HPLC-MS/MS*—Lipid extractions of cells made use of $Q_4$ as internal standard, and all LC-MS/MS analysis were performed as described previously (19). Briefly, a 4000 QTRAP linear MS/MS spectrometer from Applied Biosystems (Foster City, CA) was used. Analyst version 1.4.2 software (Applied Biosystems) was used for data acquisition and processing. A binary HPLC solvent delivery system was used with a phenyl-hexyl column (Luna 5u, 100 × 4.60 mm, 5-$\mu$m, Phenomenex) for yeast extracts. The mobile phase consisted of Solvent A (methanol/isopropyl alcohol, 95:5, with 2.5 mM ammonium formate) and Solvent B (isopropyl alcohol, 2.5 mM ammonium formate). The percentage of Solvent B was increased linearly from 0 to 5% over 6 min, and the flow rate was increased from 600 to 800 $\mu$l/min. The flow rate and mobile phase were changed back to initial condition linearly by 7 min. All samples were analyzed in multiple reaction monitoring mode (MRM).

*Purification of Q Biosynthetic Intermediates and High Resolution Mass Spectrometry Measurements*—The compounds were purified from yeast cells as described previously (3). Samples in methanol were diluted with 90% acetonitrile and 0.2% formic acid and were infused into the nanospray source of a discovery ORBITRAP instrument (Thermo Fischer Scientific) at a flow rate of 0.5 $\mu$l/min for high resolution mass spectrometry analyses (3).

## RESULTS

*Overexpression of Coq8 Restores Steady State Levels of Coq Proteins in Mitochondria of Δcoq Strains*—Immunodetection on whole cell lysates revealed that Coq4, Coq7, and Coq9 steady state levels were increased by Coq8 OE in Δ*coq3* and Δ*coq5* strains (Fig. 2, *A* and *B*). Similarly, Coq8 OE increased steady state levels of Coq9 and Coq7 in the Δ*coq4* strain and Coq9 and Coq4 in the Δ*coq7* strain (Fig. 2*A*). Even though Coq8 OE resulted in comparable levels of Coq8 in all Δ*coq* strains tested, it failed to increase the steady state levels of Coq7 and Coq9 in Δ*coq1* and Δ*coq2* (Fig. 2*B*). The inefficiency of Coq8 OE in these two strains likely results from the absence of synthesis of prenylated $Q_6$ intermediates that have been hypothesized to be important for the stability of Coq4 and Coq6 (23). In the Δ*coq9* strain, Coq8 OE did not restore the steady state levels of either Coq4 or Coq7 (Fig. 2*A*).

Because the yeast Coq polypeptides localize to mitochondria (2), we verified that the proteins stabilized by Coq8 OE were present in this organelle. The Coq4, Coq7, and Coq9 proteins were readily detected in mitochondria prepared from Δ*coq5* and Δ*coq6* cells with Coq8 OE (Fig. 3*A*). Although previous studies indicated that the Coq3 polypeptide was labile in Δ*coq* strains (6), subsequent experiments performed in the presence of both protease and phosphatase inhibitors preserved steady state levels of Coq3 (12, 15). In agreement, Coq3 levels were unaffected in Δ*coq5* or Δ*coq6* cells (Fig. 3*A*). The Coq6 antibody reacts with many nonspecific polypeptides in yeast cell extracts, and therefore immunoblotting for Coq6 is best carried out on isolated mitochondria. The steady state level of Coq6 was also increased by Coq8 OE in Δ*coq3*, Δ*coq4*, and Δ*coq7*, although it did not reach wild-type levels (Fig. 3*B*). Steady state levels of the Coq1 polypeptide provide a loading control, because Coq1 is unaffected by null mutations in Δ*coq2*-Δ*coq9* (6).

*Moderate Overexpression of Kinase-active Coq8 Is Sufficient for the Stabilization of Coq Polypeptides*—The yeast W222 mutant (24) has a mutated *COQ8* gene that encodes a Coq8-G130D polypeptide that mimics the human G272D pathogenic mutation found in ADCK3 (14). W222 does not synthesize $Q_6$, has low levels of Coq4, Coq7, and Coq9, and has no detectable phosphorylated form of Coq3, suggesting that the G130D mutation completely abolishes the kinase activity of Coq8 (12).

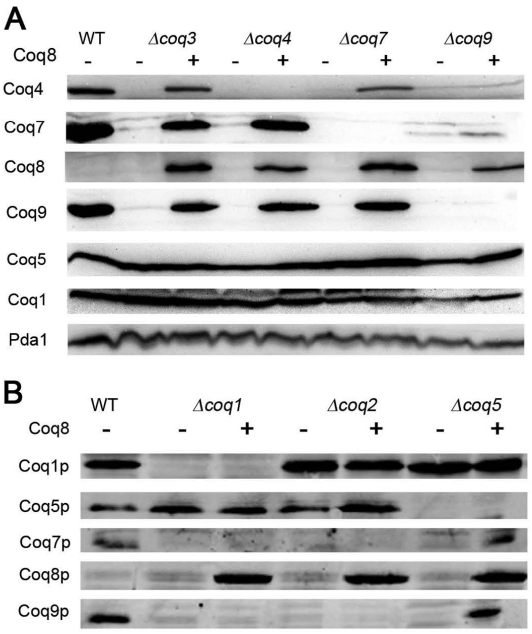



FIGURE 2. **Overexpression of Coq8 in several Δ*coq* strains restores steady state levels of Coq4, Coq7, and Coq9.** Whole cell lysates were prepared from W303-1B wild-type yeast (*WT*) or from the indicated Δ*coq* strains (all except Δ*coq9* in W303 genetic background) with (+) or without (−) p4HN4, a multicopy plasmid with yeast *COQ8* (Coq8). Yeast cells cultured in YPGal medium to mid-log (2–3 $A_{600\ nm}$) were harvested, and aliquots of 20 $A_{600\ nm}$ were lysed and analyzed by SDS-PAGE (10% acrylamide) followed by transfer to PVDF membrane and immunoblotting with antibodies to the designated Coq polypeptides or to Pda1, the α-subunit of pyruvate dehydrogenase. *A*, Pda1 serves as a loading control; *B*, Coq1 and/or Coq5 serve as loading controls.

Downloaded from http://www.jbc.org/ at UCLA-Louise Darling Biomed. Lib. on July 2, 2014

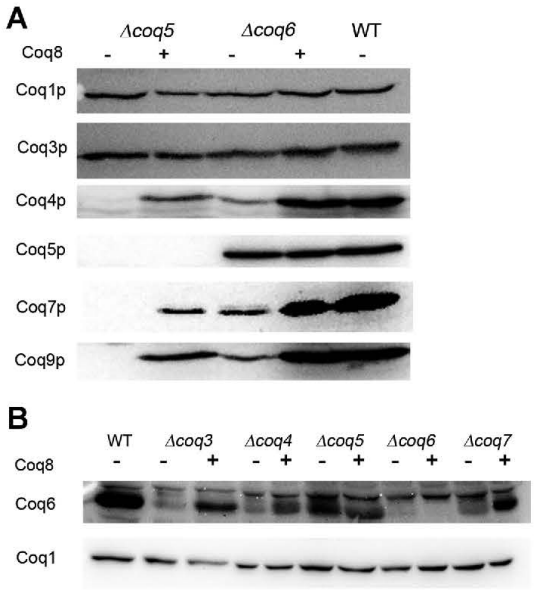



FIGURE 3. **Overexpression of Coq8 restores steady state levels of Coq polypeptides in isolated mitochondria.** Isolated mitochondria were purified with Opti-Prep gradients from W303-1B wild-type yeast (*WT*) or from the designated Δ*coq* strains (W303 genetic background) with (+) or without (−) p4HN4 (Coq8). Aliquots of mitochondrial protein (20 μg) were analyzed by SDS-PAGE followed by immunoblot analyses with antisera to the designated Coq polypeptides (*A*) or with antisera to Coq6 (*B*). Coq1 serves as a loading control.

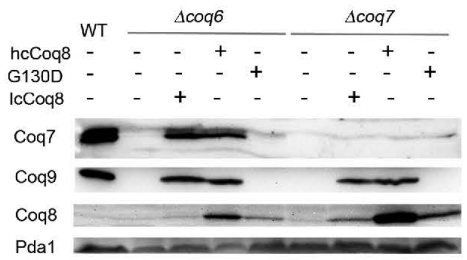



FIGURE 4. **Overexpression of Coq8-G130D does not restore steady state levels of Coq polypeptides.** Whole cell lysates were prepared as described in Fig. 2 from W303-1B wild-type yeast (*WT*) or from Δ*coq6* or Δ*coq7* strains (W303 genetic background) harboring either no plasmid; pFL44, a multicopy plasmid expressing Coq8 (hcCoq8); G130D, a multicopy plasmid with Coq8 containing the G130D mutation (G130D); or p3HN4, a low copy plasmid expressing Coq8 (lcCoq8). Yeast cells were cultured in SD−Ura medium to mid-log (2–3 $A_{600\,nm}$) phase and harvested, and aliquots of 20 $A_{600\,nm}$ were lysed and subjected to immunoblotting analyses with antisera to the designated Coq polypeptides. Pda1 serves as a loading control.

We tested the importance of the kinase activity of Coq8 for the stabilization of Coq proteins in Δ*coq* strains by overexpressing Coq8-G130D. The levels of Coq7 and Coq9 were restored in Δ*coq6* cells with Coq8 OE but remained undetectable with Coq8-G130D OE (Fig. 4). Similarly, Coq9 steady state levels were restored in Δ*coq7* cells with Coq8 OE but not with Coq8-G130D OE. Coq8-G130D steady state level was lower than that of wild-type Coq8 overexpressed from the same high copy vector (Fig. 4). Transformation of Δ*coq6* and Δ*coq7* cells with a centromeric plasmid containing the *COQ8* gene (lcCoq8) resulted in moderate expression of Coq8, which was sufficient to restore steady state levels of the Coq7 and Coq9 polypeptides (Fig. 4). Because the Coq8-G130D polypeptide also accumulates to a moderate level upon overexpression, we conclude that the kinase activity of Coq8 is necessary to cause the stabilization of the Coq polypeptides.

*Overexpression of Coq8 Promotes the Accumulation of Diagnostic Intermediates in Δcoq5 and Δcoq7 Strains*—Based on our observation that Coq8 OE stabilizes most Coq proteins in the collection of the Δ*coq* strains, we reasoned that these mutants may now accumulate $Q_6$ biosynthetic intermediates downstream of HHB. In fact, it has been shown that a Δ*coq7* strain known to accumulate HHB can be induced to proceed further and to accumulate $DMQ_6$ upon Coq8 OE (16). In this study, we have used HPLC separation coupled to either ECD or mass spectrometry (MS) to detect $Q_6$ intermediates in lipid extracts of the different strains tested. In our HPLC-ECD system, a pre-column electrode oxidizes the reduced hydroquinone intermediates present in the lipid extracts into their oxidized quinone form, accounting for the presence of only oxidized products in the HPLC column eluate. In the HPLC-MS/MS detection, the redox state of the intermediates is detected and affects the elution position. MRM allows the detection of the molecular ion of $Q_6$ intermediates in conjunction with the corresponding product ion base peak. A Δ*coq7* strain with Coq8 OE revealed that $DMQ_6$ was produced in a synthetic medium supplemented with either *p*ABA or 4-HB, although no electroactive compound was detected in the absence of Coq8 OE (Fig. 5*A* and data not shown). The synthesis of $DMQ_6$ from *p*ABA is consistent with our previous observations that $DMQ_6$, but not its imino-counterpart $IDMQ_6$, was the main intermediate synthesized when strains expressing either a partially inactive form of Coq7 (3) or a *coq7* point mutant (19) were grown in *p*ABA-containing medium.

An electro-active compound that eluted earlier than $DMQ_6$ was accumulated in a Δ*coq5* strain only upon Coq8 OE (Fig. 5*B*). The observed mass of the purified compound ($M + H^+$) *m/z* 547.4150 corresponds to that of demethyl-demethoxy-ubiquinone ($DDMQ_6$) ($[M + H]^+ = C_{37}H_{55}O_3^+$, 547.4151; −0.2 ppm), the expected substrate of Coq5. The identification of $DDMQ_6$ is further supported by the trap scan spectrum that showed a tropylium-like ion at *m/z* 153 characteristic of $Q_6$-related compounds (supplemental Fig. S1*A*). $DDMQ_6$ was synthesized by the Δ*coq5* strain with Coq8 OE when either 4-HB or *p*ABA was used as ring precursors (Fig. 5*B*). This result was further confirmed by detecting $^{13}C_6$-$DDMQ_6$ in Δ*coq5* with Coq8 OE grown either in the presence of $^{13}C_6$-*p*ABA or $^{13}C_6$-4-HB (Fig. 5*C* and supplemental Fig. S1*B*). As expected, no $Q_6$ biosynthetic intermediates besides HHB or HAB were detected in either Δ*coq5* or Δ*coq7* strains with Coq8-G130D OE (data not shown). Our results show that Coq8 OE in Δ*coq5* and Δ*coq7* strains leads to the biosynthesis of the expected $Q_6$ intermediates, $DDMQ_6$ and $DMQ_6$, respectively.

*Bypass of the Q Biosynthetic Deficiency in Δcoq7 Cells by 4-HB Analogue*—Based on our recent demonstration of the bypass of the deficient C5-hydroxylation reaction in a Δ*coq6*

Downloaded from http://www.jbc.org/ at UCLA-Louise Darling Biomed. Lib. on July 2, 2014

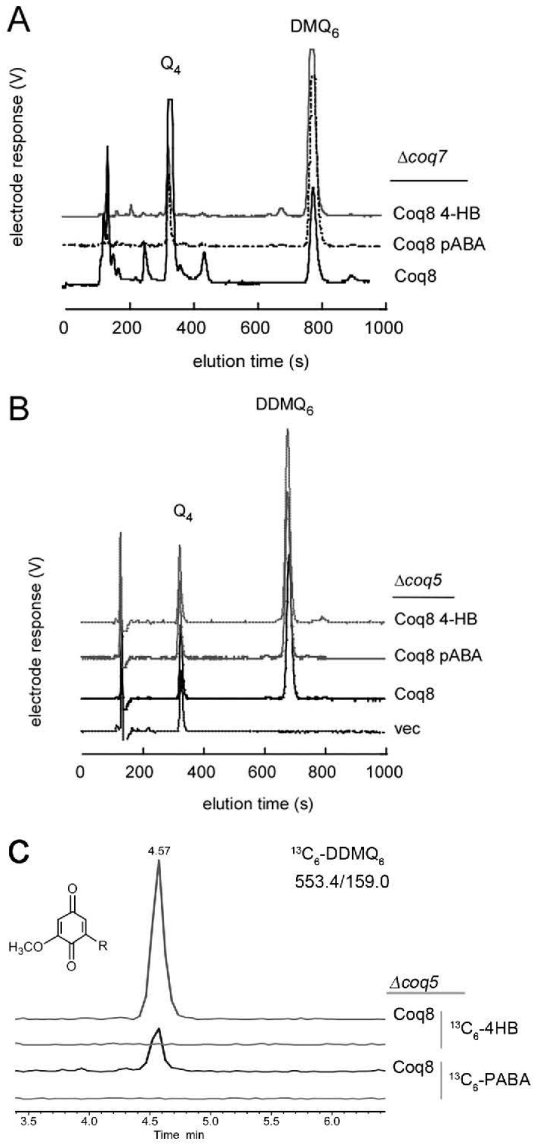



FIGURE 5. **Δ*coq7* and Δ*coq5* strains overexpressing Coq8 accumulate the respective Q intermediates, $DMQ_6$ and $DDMQ_6$.** *A*, Δ*coq7* cells (W303 genetic background) transformed with pFL44, an episomal vector encoding Coq8 (Coq8), were grown overnight in YNB-*p*ABA-folate 2% dextrose with no additions or with 5 μM 4-HB or *p*ABA. Lipid extracts of 4 mg of cells (no addition) or of 1.5 mg of cells (4-HB, *p*ABA) were analyzed by HPLC-ECD. The peaks corresponding to $DMQ_6$ and to the $Q_4$ standard are marked. *B*, Δ*coq5* cells (W303 genetic background) transformed either with pFL44 (Coq8) or an empty vector (*vec*) were grown overnight in YNB−*p*ABA−folate 2% dextrose containing either no addition or 5 μM 4-HB or *p*ABA. Lipid extracts of 10 mg of cells were analyzed by HPLC-ECD. *C*, Δ*coq5* cells (W303 genetic background) containing either no plasmid or p4HN4, an episomal vector encoding Coq8 (Coq8), were first grown in YPGal + 0.1% dextrose and then cultured in DOGAL + 0.1% dextrose−*p*ABA−folate−tyrosine overnight. Finally cells were collected and transferred to fresh DOGAL + 0.1% dextrose−*p*ABA−folate in the presence of either $^{13}C_6$-4HB or $^{13}C_6$-*p*ABA (10 μg/ml; 3 ml) and incubated for 2 h. Cells were collected (150 $A_{600\ nm}$), and lipid extracts were subjected to RP-HPLC-ESI/MS-MS as described under "Experimental Procedures," and detection of the precursor-to-product ion transition (553.4/159.0) was performed with MRM. The *traces* indicate arbitrary units, and the scale is the same for all traces within a panel.

strain by 3,4-dihydroxybenzoic acid and vanillic acid (VA) (Fig. 1) (18), we grew Δ*coq7* cells with Coq8 OE in the presence of 2,4-dihydroxybenzoic acid (2,4-diHB). In the presence of 2,4-diHB, cells contained a significant amount of $Q_6$, whereas growth in the presence of 4-HB only produced $DMQ_6$ (Fig. 6*A*). The product eluting at 780 s in 2,4-diHB-treated cells is not $DMQ_6$ because its UV-visible spectrum has a maximum at 265 nm different from that of $DMQ_6$ at 271 nm (data not shown). $Q_6$-deficient strains have a growth defect on respiratory carbon sources because the mitochondrial electron transport chain is interrupted. The quantity of $Q_6$ synthesized in the presence of 2,4-diHB was sufficient to allow respiratory growth on lactate-glycerol (Fig. 6*B*). $DMQ_6$ was incompetent at re-establishing the flow of electrons in the respiratory chain as shown by the absence of growth on respiratory medium containing 4-HB (Fig. 6*B*). Likewise, Coq8-G130D OE failed to rescue the respiratory growth defect of the Δ*coq7* strain in the presence of 2,4-diHB. These results show that it is possible to bypass the deficient C6-hydroxylation reaction in a Δ*coq7* strain with 2,4-diHB provided that Coq polypeptides are stabilized by Coq8 OE.

*Yeast Δcoq3 and Δcoq4 Cells Overexpressing Coq8 Accumulate Early Q Biosynthetic Intermediates*—We detected only HAB and HHB in a Δ*coq3* strain with Coq8 OE (data not shown). This was surprising to us because Coq4, Coq7, Coq9 (Fig. 2*A*), and Coq6 (Fig. 3*B*) are stable in a Δ*coq3* strain with Coq8 OE, and we therefore expected the accumulation of 3-hexaprenyl-4,5-dihydroxybenzoic acid (DHHB), the product of Coq6. VA bypassed the requirement for the C5-hydroxylase (Coq6) and the O5-methyltransferase (Coq3) and led to the accumulation of $DMQ_6$ in the Δ*coq3* strain with Coq8 OE (Fig. 7*A*). This result demonstrates that C1-decarboxylase, C1-hydroxylase, and Coq5 are active in the Δ*coq3* strain.

In a Δ*coq4* strain grown in the presence of $^{13}C_6$-*p*ABA, Coq8 OE caused the accumulation of a product whose mass is consistent with the $^{13}C_6$-labeled form of 3-hexaprenyl-4-amino-5-hydroxybenzoic acid (HHAB; Fig. 7*B*). HHAB was also detected in the *coq4-1* point mutant (Fig. 7*B*), and trap scan spectra confirmed both the unlabeled and $^{13}C_6$-labeled forms of HHAB (supplemental Fig. S2, *A* and *B*). The HHAB intermediate is not observed in *p*ABA-labeled wild-type yeast (data not shown). Upon culture with $^{13}C_6$-4HB, the corresponding anticipated intermediate, $^{13}C_6$-DHHB, was not detected in Coq4-deficient strains; only $^{13}C_6$-HHB was detected (data not shown). We also failed to detect DHHB in the Δ*coq4* strain with Coq8 OE even when the medium was supplemented with 3,4-dihydroxybenzoic acid (100 μg/ml; data not shown). The accumulation of HHAB suggested a deficient O5-methyltransferase activity, even though the Coq3 polypeptide is stable in the Δ*coq4* strain. Addition of VA to the Δ*coq4* strain with Coq8 OE failed to generate either $DMQ_6$ (Fig. 7*A*) or the predicted prenylation product, 3-hexaprenyl-4-hydroxy-5-methoxybenzoic acid

Downloaded from http://www.jbc.org/ at UCLA-Louise Darling Biomed. Lib. on July 2, 2014

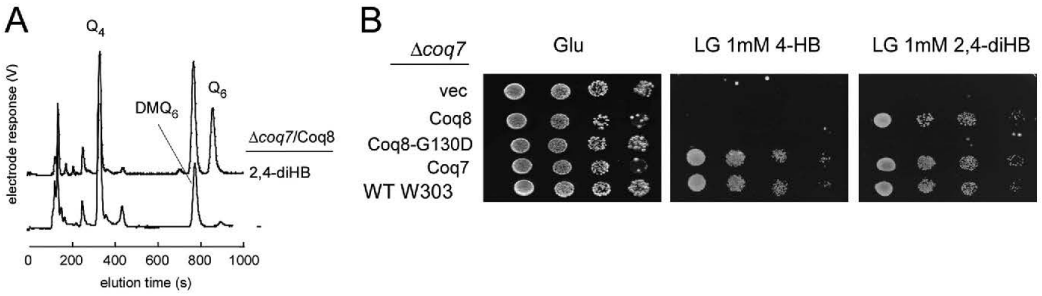



FIGURE 6. **Bypass of the respiratory growth defect of the Δ*coq7* strain with alternate ring precursors.** *A*, Δ*coq7* cells (W303 genetic background) transformed with an episomal vector coding for Coq8 (pFL44) were grown in YNB−*p*ABA−folate 2% dextrose containing 1 mM 2,4-dihydroxybenzoic acid (*2,4-diHB*) or not (−). Lipid extracts of 2 mg of cells were analyzed by HPLC-ECD. *B*, WT W303 cells or Δ*coq7* cells transformed either with an empty vector (*vec*), an episomal vector (pFL44) encoding Coq8 or Coq8-G130D, or with an episomal vector encoding Coq7 were grown in YNB−*p*ABA−folate 2% dextrose for 24 h, and serial dilutions were spotted onto agar plates. The plates contained either YP 2% dextrose (Glu) or synthetic medium−*p*ABA−folate supplemented with 2% lactate-2% glycerol (*LG*) containing either 4-HB or 2,4-dihydroxybenzoic acid (*2,4-diHB*) at 1 mM. The plates were incubated for 2 days (Glu) or 4 days (LG) at 30 °C.

(data not shown). Addition of 3-methoxy-4-aminobenzoic acid to the growth medium of the *coq4-1* point mutant led to the accumulation of 3-hexaprenyl-4-amino-5-methoxybenzoic acid (HMAB) (Fig. 7*C* and supplemental Fig. S3). HMAB is expected to accumulate in cells deficient for the C1-decarboxylation reaction. However, it is important to note that HMAB is also observed in wild-type yeast incubated in the presence of 3-methoxy-4-aminobenzoic acid (Fig. 7*C*). Therefore, a possible defect in the C1-decarboxylation reaction in the *coq4-1* point mutant cannot be probed by using 3-methoxy-4-aminobenzoic acid. Collectively, our data show that only early amino intermediates of the Q pathway accumulate in *coq4* yeast mutants and that the use of analogues of 4-HB or *p*ABA does not cause the accumulation of downstream intermediates contrary to what we obtained in Δ*coq3* (Fig. 7*A*) or Δ*coq7* (Fig. 6*A*) mutants. Therefore, in addition to the O5-methylation that we proved to be deficient in a *coq4* mutant, at least one other downstream biosynthetic step of the $Q_6$ pathway is impaired. This situation is consistent with a more general functional/structural role for Coq4 in the $Q_6$ biosynthetic complex (5).

*Yeast Δcoq9 Cells Overexpressing Coq8 Accumulate Intermediates Diagnostic of a Deficiency in C5- and C6-Hydroxylation Reactions*—Coq9 is essential for $Q_6$ biosynthesis but its molecular function is unknown (25). Upon Coq8 OE, we observed the accumulation of distinct electroactive compounds depending on whether *p*ABA or 4-HB was added to the growth medium of a Δ*coq9* strain (Fig. 8*A*). In the presence of 4-HB, two compounds were detected with UV-visible spectra (not shown) and retention times characteristic of $DMQ_6$ and of the oxidized form of 3-hexaprenyl-4-hydroxyphenol (4-HP). The identity of these intermediates was further confirmed by labeling with $^{13}C_6$-4-HB and by comparing the lipid extracts of Δ*coq9* cells with those of Δ*coq6* cells that are known to contain 4-HP (18) (525.4 to 129 transition at 2.66 min, see Fig. 8*B*) and to those of Δ*coq7* cells that contain $DMQ_6$ (567.6 to 173 transition at 4.86 min, see Fig. 8*C*). In the presence of *p*ABA (Fig. 8*A*), the compound eluting at 600 s corresponds to the oxidized form of 3-hexaprenyl-4-aminophenol (4-AP). The compound eluting at 860 s (Fig. 8*A*) was identified as 4-imino-demethoxyquinone ($IDMQ_6$) based on its observed mass $(M + H^+)$ *m/z* 560.44458 ($IDMQ_6$; $[M + H]^+ = C_{38}H_{58}NO_2^+$: 560.44675; −3.90 ppm) and its fragmentation spectrum with tropylium-like and chromenylium-like ions at *m/z* 166 and 206 (supplemental Fig. S4*A*), which are shifted with M + 6 (*m/z*) upon labeling with $^{13}C_6$-*p*ABA (supplemental Fig. S4*B*). The $^{13}C_6$-labeled form of 4-AP (524.4 to 128 transition at 2.86 min, Fig. 8*D*; trap scan spectra supplemental Fig. S5) was detected in Δ*coq6* and Δ*coq9* cells, and $^{13}C_6$-$IDMQ_6$ (566.6 to 172 transition at 4.76 min, Fig. 8*E*) was present in Δ*coq7* and Δ*coq9* cells. The ion with a 525.4 to 129 transition at 2.86 min in Δ*coq6* cells with Coq8 OE (Fig. 8*B*) is attributed to the +1 isotope of $^{13}C_6$-4-AP (compare Fig. 8, *B* and *D*). Likewise, the signal at 4.76 min (Fig. 8*C*) actually corresponds to the +1 isotope of $^{13}C_6$-$IDMQ_6$ (566.6 to 172 transition; compare Fig. 8, *C* and *E*). Our experiments show that Δ*coq9* cells with Coq8 OE accumulate 4-AP/4-HP that are diagnostic of a deficiency in the C5-hydroxylation catalyzed by Coq6 (18) and $DMQ_6$/$IDMQ_6$, which are formed consequently to a defect in the C6-hydroxylation reaction catalyzed by Coq7. Moreover, the C4-deamination (*black dotted arrows* in Fig. 1) of $Q_6$ biosynthetic intermediates originating from *p*ABA is not efficiently catalyzed in the absence of Coq9. In conclusion, deletion of *coq9* impacts on the activity of multiple Coq proteins Coq6, Coq7, and the putative deaminase.

We next attempted to bypass the biosynthetic defects of Δ*coq9* cells. Supplementation of the growth medium with VA caused the accumulation of $DMQ_6$ (supplemental Fig. S6), showing that even though the Coq6 deficiency could be bypassed, a strong block subsists at the level of Coq7. With 2,4-diOH, no $Q_6$ could be detected; instead a new electroactive compound at 730 s appeared (supplemental Fig. S6). The absence of $Q_6$ biosynthesis may be caused by the poor stability of several Coq polypeptides even with Coq8 OE (Fig. 2*A*). Indeed, the quantity of intermediates accumulated in the Δ*coq9* strain is lower than that obtained in Δ*coq6* and Δ*coq7* strains (Fig. 8, *B–D*), which have higher levels of Coq polypeptides compared with the Δ*coq9* strain (Fig. 2*A*). Finally, 2,3,4-trihydroxybenzoic acid, which could in theory bypass both C5- and C6-hydroxylations, was found to inhibit $Q_6$ biosynthesis in WT cells and was therefore not tested further (data not shown).

Downloaded from http://www.jbc.org/ at UCLA-Louise Darling Biomed. Lib. on July 2, 2014

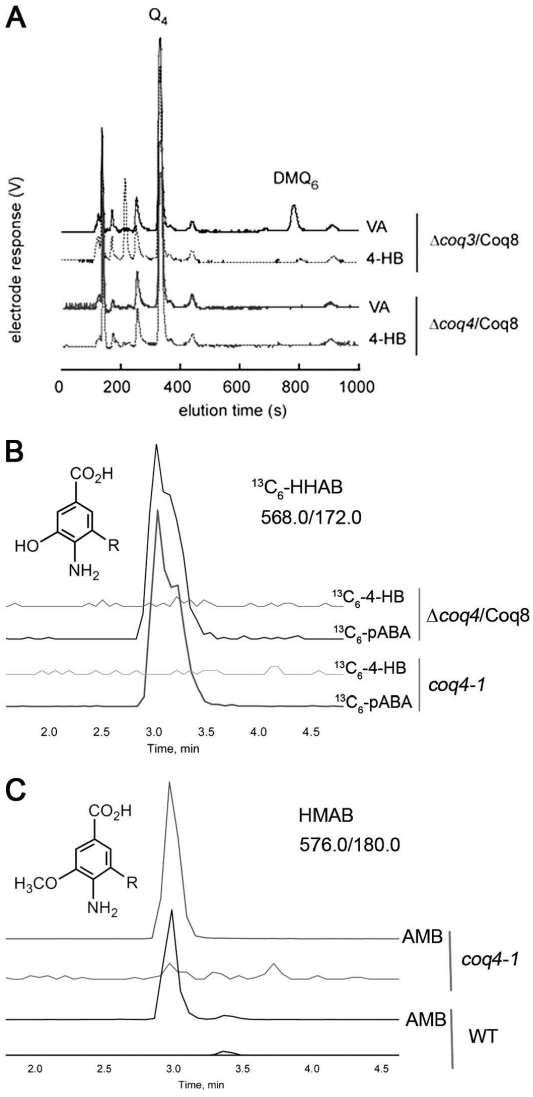



FIGURE 7. **Δ*coq3* and Δ*coq4* strains overexpressing Coq8 or a *coq4-1* strain accumulate early $Q_6$ biosynthetic intermediates.** *A,* yeast Δ*coq3* (BY4741 genetic background) and Δ*coq4* cells (BY4742 genetic background) transformed with pFL44, an episomal vector encoding Coq8 (Coq8), were grown in YNB−*p*ABA−folate 2% dextrose containing 100 μM VA or 100 μM 4-HB. Lipid extracts of 4 mg of cells were analyzed by HPLC-ECD. *B,* yeast Δ*coq4* cells (W303 genetic background) transformed with p4HN4, an episomal vector encoding Coq8, and *coq4-1* cells were grown in YPGal + 0.1% dextrose overnight and labeled in DOGAL + 0.1% dextrose−folate−*p*ABA in the presence of either $^{13}C_6$-4HB or $^{13}C_6$-*p*ABA (20 μg/ml; 3 ml) for 2 h. Lipid extracts of 100 $A_{600\,nm}$ of cells were analyzed by RP-HPLC-MS/MS as described under "Experimental Procedures," and detection of the precursor-to-product ion transition (568.0/172.0) was performed with MRM. *C,* yeast *coq4-1* mutant cells or wild-type yeast cells were grown in YPGal + 0.1% dextrose overnight and transferred into 3 ml of fresh DOGAL + 0.1% dextrose−folate−*p*ABA in the presence of 100 μg/ml 4-amino-3-methoxybenzoic acid (*AMB*). Lipid extracts of 100 $A_{600\,nm}$ of cells were analyzed by RP-HPLC-ESI/MS-MS as described under "Experimental Procedures," and detection of the precursor-to-product ion transition (576.0/180.0) was performed with MRM.

## DISCUSSION

Most of the Coq polypeptides involved in $Q_6$ biosynthesis in *S. cerevisiae* are part of a multiprotein complex. Among Coq proteins, only Coq2 is predicted to possess transmembrane domains. Organization of the Coq polypeptides in a $Q_6$ biosynthetic complex associated with the mitochondrial inner membrane helps rationalize how these proteins can gain access to their substrates, which are hexaprenylated lipophilic compounds likely embedded in the membrane (26). In the absence of any one of the Coq polypeptides (Δ*coq1*–Δ*coq9* strains), assembly of the $Q_6$ biosynthetic complex is impaired, which results in the degradation of Coq4, Coq6, Coq7, and Coq9. This situation is not unique for multiprotein complexes in *S. cerevisiae* and is also encountered for example with cytochrome *c* oxidase. Indeed, most Cox proteins are degraded in the absence of any of the three mitochondrially encoded core subunits Cox1–Cox3 (27). Our present study establishes that Coq8 OE stabilizes the levels of Coq4, Coq6, Coq7, and Coq9 in Δ*coq3*–Δ*coq7* strains and therefore generalizes to most Coq polypeptides this stabilizing effect that had been described previously for Coq4 (17). The stabilized proteins are active because they allowed accumulation of novel $Q_6$ biosynthetic intermediates in several Δ*coq* strains, suggesting that the $Q_6$ biosynthetic complex is at least partially assembled.

Coq8 has been proposed to possess a kinase activity (11) and has been shown to be necessary for the existence of phosphorylated forms of Coq3, Coq5, and Coq7 *in vivo* (12, 15). A G130D mutation in Coq8 abolishes the phosphorylated form of Coq3 suggesting that this mutation impairs the kinase activity (12). Our data with the G130D mutant indicate that the kinase activity of Coq8 is also important for the stabilization of Coq6 and Coq7 (Fig. 4) and probably also of Coq4 and Coq9. How does Coq8 OE stabilize Coq polypeptides that are otherwise degraded? A direct phosphorylation by Coq8 of the polypeptides could occur, especially in the case of Coq7 for which Coq8-dependent phosphorylated forms have been detected (12). However, a direct phosphorylation seems unlikely in the case of Coq4 because no phosphorylated forms of this protein could be detected (12). In addition, we do not currently know whether Coq6 and Coq9 are phosphorylated *in vivo* (12). So, to explain the effect of Coq8, we favor an hypothesis in which Coq8 OE increases the phosphorylation state of a particular Coq protein that modulates the assembly and/or stability of the $Q_6$ biosynthetic complex. An obvious candidate is Coq3, whose association with the $Q_6$ biosynthetic complex was shown to be dependent on Coq8 (15). However, stable Coq proteins are detected in a Δ*coq3* strain with Coq8 OE (Fig. 2*A*), establishing that phosphorylated Coq3 is not the only factor promoting the stabilization of the Coq polypeptides. Coq8-dependent phosphorylation(s) may be considered a positive regulator of $Q_6$ biosynthesis because it seems to favor assembly of the $Q_6$ biosynthetic complex that should lead to increased $Q_6$ biosynthesis. On the contrary, a regulatory phosphorylation with a negative impact on $Q_6$ biosynthesis has recently been described for Coq7 (28). In that study, an increase in the phosphorylated forms of Coq7 correlated with a decreased level of $Q_6$ and an increased level of $DMQ_6$, the substrate of Coq7. It was therefore

Downloaded from http://www.jbc.org/ at UCLA-Louise Darling Biomed. Lib. on July 2, 2014

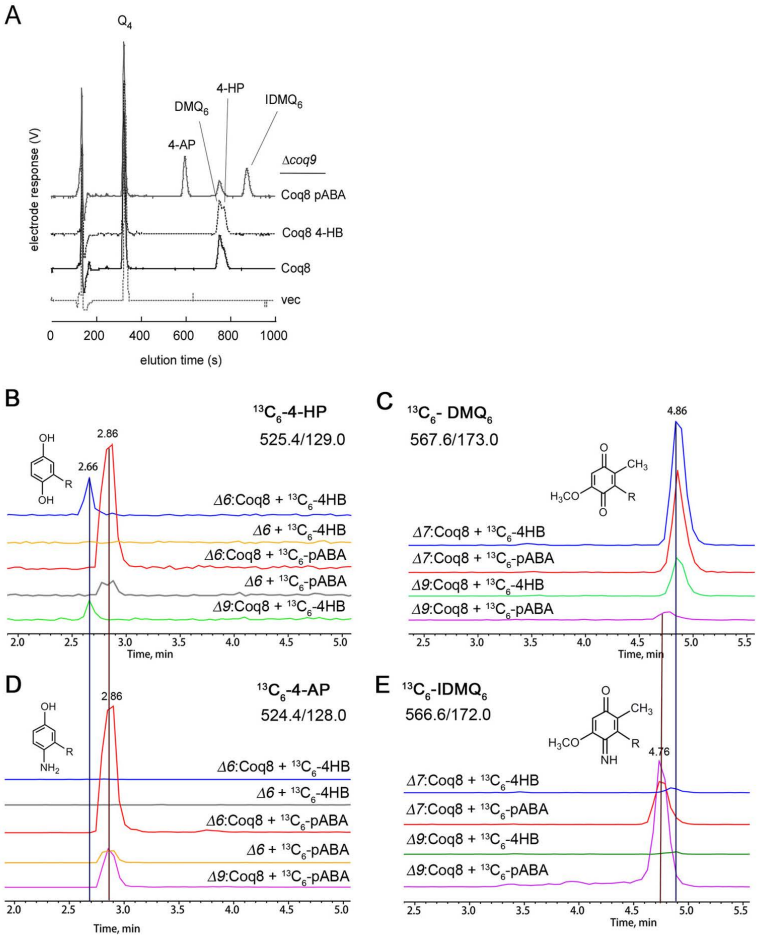



FIGURE 8. **Coq9 is important for Coq6 and Coq7 hydroxylation steps and for removal of the amino substituent.** *A*, Δ*coq9* cells (BY4742 genetic background) transformed either with an episomal vector coding for Coq8 (pFL44) or an empty vector (*vec*) were grown in YNB−*p*ABA−folate 2% dextrose containing or not 5 μM 4-HB or *p*ABA. Lipid extracts of 10 mg of cells were analyzed by HPLC-ECD. The peaks corresponding to $DMQ_6$, to $IDMQ_6$, or to the oxidized forms of 4-AP and of 4-HP are marked. *B–E*, yeast Δ*coq6*, Δ*coq7*, Δ*coq9*, in the absence or presence of p4HN4 (an episomal plasmid encoding Coq8) were cultured and prepared as described in Fig. 5. Yeast cell pellets (150 $A_{600\ nm}$ of cells) were subjected to RP-HPLC-MS/MS as described under "Experimental Procedures," and detection of the designated precursor-to-product ion transitions (525.4/129.0, 524.4/128.0, 567.6/173.0, 566.6/172.0) was performed with MRM.

concluded that phosphorylated Coq7 has diminished activity (28). It remains to be established which kinase is responsible for the phosphorylation of the regulatory sites of Coq7.

We exploited the stabilizing effect of Coq8 OE to understand more precisely the $Q_6$ biosynthetic pathway, especially the role played by Coq4 and Coq9. We observed the accumulation of several intermediates in strains lacking Coq9 or Coq4 contrary to strains lacking Coq5 or Coq7, which accumulate a single late-stage intermediate, the substrate of the missing enzyme. Consequently, the impairment of several biosynthetic steps in Δ*coq9* and Δ*coq4* cells points to a role of these proteins in the general function or organization of the $Q_6$ biosynthetic complex rather than to a role in the catalysis of a particular biosynthetic step. In Δ*coq9* cells with Coq8 OE, the accumulation of 4-AP/4-HP establishes that the C5-hydroxylation step catalyzed by Coq6 is limiting, but this C5-hydroxylation occurs to some extent as demonstrated by the accumulation of $IDMQ_6$/$DMQ_6$. These later intermediates reveal that the C6-hydroxylation catalyzed by Coq7 is also deficient. In fact, the C6-hydroxylation is completely impaired because addition of VA, which bypasses the C5-hydroxylation, resulted in increased accumulation of $DMQ_6$ without any production of detectable $Q_6$ or demethyl-$Q_6$ (supplemental Fig. S6). The role of Coq9 in the C5- and C6-hydroxylation reactions is not clear, but Coq9 appears to be important for the stability of Coq7 because steady state levels of Coq7 are not restored in Δ*coq9* cells with Coq8 OE. Nevertheless, Coq9 is not absolutely required for the stability of the $Q_6$ complex to which it has been shown to belong

Downloaded from http://www.jbc.org/ at UCLA-Louise Darling Biomed. Lib. on July 2, 2014

(6), because the accumulation of $DMQ_6$ implies that the Coq enzymes implicated in the $Q_6$ pathway upstream of Coq7 are stable and active, at least partially.

The Δ*coq4* strain was diagnosed to be impaired in multiple biosynthetic steps; Coq3, which catalyzes both the O5- and O6-methylation steps, does not function in the Δ*coq4* strain as established by the accumulation of HHAB. Furthermore, addition of VA did not generate $DMQ_6$ in the Δ*coq4* strain, contrary to what we observed in the Δ*coq3* strain (Fig. 7*A*), revealing that at least another biosynthetic step downstream of the O5-methylation is impaired. In agreement with these results, Coq4 was hypothesized to serve as an anchor for the $Q_6$ biosynthetic complex (5) and was recently proposed to bind the polyisoprenyl tail of $Q_6$ intermediates, therefore allowing sequential modification of the aromatic head group (29). It is of interest to note that a diploid yeast carrying a deletion of one allele of *COQ4* showed a diminished $Q_6$ content demonstrating that wild-type level of Coq4 is crucial for the function of the $Q_6$ biosynthetic complex (30). Human Coq4 may play an analogous role in organizing $Q_{10}$ biosynthesis because *COQ4* haploinsufficiency was recently shown to cause $Q_{10}$ deficiency in a patient (30).

It is interesting that $Q_6$ intermediates containing a catechol moiety (DHHB and demethyl-$Q_6$) could not be detected in this study despite the fact that we expected their synthesis in some of the strains tested. Indeed, we anticipated the formation of DHHB in a Δ*coq4* strain grown in the presence of 4-HB because this strain produced HHAB from *p*ABA. Also, the Δ*coq3* strain synthesized $DMQ_6$ but not demethyl-$Q_6$ from VA. In consequence, the catechol-containing $Q_6$ intermediates may be unstable and hence cannot accumulate in detectable amounts in *S. cerevisiae*.

*p*ABA is a precursor of $Q_6$ in *S. cerevisiae*, and the C4-amine must be replaced by a C4-hydroxyl along the $Q_6$ pathway (3, 19). Our data reveal several new elements regarding this C4-deamination (or deimination) reaction. First, Δ*coq6* and Δ*coq9* cells with Coq8 OE synthesized C4-aminated intermediates (4-AP and $IDMQ_6$) in the presence of *p*ABA but synthesized the C4-hydroxylated intermediates (4-HP and $DMQ_6$) in the presence of 4-HB. This result supports the notion that HHB and HAB follow the same biosynthetic steps up to $DMQ_6$/$IDMQ_6$ and are modified by the same Coq enzymes, which thus accommodate both C4-hydroxylated and C4-aminated $Q_6$ biosynthetic intermediates (*path 1* and *path 2*, Fig. 1). Second, the deamination reaction does not proceed via nonenzymatic hydrolysis because in this case, $IDMQ_6$, which was previously established to be a precursor of $DMQ_6$, should be converted into $DMQ_6$. Third, the C4-deamination/deimination reaction occurs efficiently in some mutants (Δ*coq5* and Δ*coq7*) but not in others (Δ*coq6*, Δ*coq9* and possibly Δ*coq4*). The deamination reaction may implicate Coq6 or Coq9 or an uncharacterized protein that may be inactive or unstable in Δ*coq6* and Δ*coq9* cells. In this latter case, a differential proteomic analysis of Δ*coq5* and Δ*coq7* cells on the one hand and Δ*coq6* and Δ*coq9* cells on the other hand may reveal the identity of the C4-deaminase. Fourth, the deamination reaction can occur prior to the C2-methylation catalyzed by Coq5 as supported by the accumulation of $DDMQ_6$ and not 2-demethyl-4-amino-demethoxy-$Q_6$ by the Δ*coq5* strain cultured in the presence of *p*ABA. The step at which the deamination reaction occurs in a WT strain is still in question. Indeed, it could take place prior to the C2-methylation or prior to the C6-hydroxylation catalyzed by Coq7 as suggested by the results establishing that $IDMQ_6$ is a precursor of $DMQ_6$ (19). In that study, the *coq7-1* point mutant and also wild-type yeast grown in the presence of *p*ABA accumulated lower quantities of $IDMQ_6$ compared with $DMQ_6$ (19), in agreement with results presented in this study. The real question now concerns the reasons of the synthesis of the minute amounts of $IDMQ_6$ detected in WT cells. Is it a "normal" intermediate that only accumulates in small quantities because it is efficiently converted into $DMQ_6$ or does $IDMQ_6$ represent a by-product formed when the deamination reaction that may occur prior to Coq5 is rate-limiting? Further experiments will address this question.

The accumulation of $Q_6$ intermediates in Δ*coq4* and Δ*coq9* cells with Coq8 OE shed some light on the biosynthetic defects in these strains and is a significant advance in our understanding of $Q_6$ biosynthesis. Furthermore, the use of the 2,4-diHB aromatic ring precursor together with Coq8 OE was shown to restore $Q_6$ biosynthesis in yeast Δ*coq7* cells. Finally, the accumulation of C4-aminated intermediates in some Δ*coq* strains provided new information regarding the deamination reaction. Overall, our study describes that Coq8 OE and the use of 4-HB analogues represent valuable tools to advance our comprehension of the $Q_6$ biosynthetic pathway by allowing for the unprecedented molecular dissection of the defect of particular Δ*coq* strains.

*Acknowledgments—We thank Dr. Geneviève Dujardin for the gift of the pFL44 COQ8 plasmid and Dr. Agnès Rötig for the gift of the pFL44 Coq8 G130D plasmid. Antibodies to yeast Pda1 were kindly supplied by Dr. J. Gordon Lindsay. We thank Dr. Beth Marbois for advice and expertise in detection and identification of Q intermediates. The LC-MS/MS determination of quinones was supported in part by National Institutes of Health Grant S10RR024605 from the NCRR.*

## REFERENCES

1. Bentinger, M., Tekle, M., and Dallner, G. (2010) Coenzyme Q-biosynthesis and functions. *Biochem. Biophys. Res. Commun.* **396,** 74–79
2. Tran, U. C., and Clarke, C. F. (2007) Endogenous synthesis of coenzyme Q in eukaryotes. *Mitochondrion* **7,** S62–S71
3. Pierrel, F., Hamelin, O., Douki, T., Kieffer-Jaquinod, S., Mühlenhoff, U., Ozeir, M., Lill, R., and Fontecave, M. (2010) Involvement of mitochondrial ferredoxin and *para*-aminobenzoic acid in yeast coenzyme Q biosynthesis. *Chem. Biol.* **17,** 449–459
4. Marbois, B., Gin, P., Faull, K. F., Poon, W. W., Lee, P. T., Strahan, J., Shepherd, J. N., and Clarke, C. F. (2005) Coq3 and Coq4 define a polypeptide complex in yeast mitochondria for the biosynthesis of coenzyme Q. *J. Biol. Chem.* **280,** 20231–20238
5. Marbois, B., Gin, P., Gulmezian, M., and Clarke, C. F. (2009) The yeast Coq4 polypeptide organizes a mitochondrial protein complex essential for coenzyme Q biosynthesis. *Biochim. Biophys. Acta* **1791,** 69–75
6. Hsieh, E. J., Gin, P., Gulmezian, M., Tran, U. C., Saiki, R., Marbois, B. N., and Clarke, C. F. (2007) *Saccharomyces cerevisiae* Coq9 polypeptide is a subunit of the mitochondrial coenzyme Q biosynthetic complex. *Arch. Biochem. Biophys.* **463,** 19–26
7. Padilla, S., Jonassen, T., Jiménez-Hidalgo, M. A., Fernández-Ayala, D. J., López-Lluch, G., Marbois, B., Navas, P., Clarke, C. F., and Santos-Ocaña, C. (2004) Demethoxy-Q, an intermediate of coenzyme Q biosynthesis, fails to support respiration in *Saccharomyces cerevisiae* and lacks antioxi-

Downloaded from http://www.jbc.org/ at UCLA-Louise Darling Biomed. Lib. on July 2, 2014

dant activity. *J. Biol. Chem.* **279,** 25995–26004
8. Tran, U. C., Marbois, B., Gin, P., Gulmezian, M., Jonassen, T., and Clarke, C. F. (2006) Complementation of *Saccharomyces cerevisiae coq7* mutants by mitochondrial targeting of the *Escherichia coli* UbiF polypeptide. Two functions of yeast Coq7 polypeptide in coenzyme Q biosynthesis. *J. Biol. Chem.* **281,** 16401–16409
9. Bousquet, I., Dujardin, G., and Slonimski, P. P. (1991) ABC1, a novel yeast nuclear gene has a dual function in mitochondria. It suppresses a cytochrome *b* messenger-RNA translation defect and is essential for the electron transfer in the *bc1* complex. *EMBO J.* **10,** 2023–2031
10. Brasseur, G., Tron, G., Dujardin, G., Slonimski, P. P., and Brivet-Chevillotte, P. (1997) The nuclear *ABC1* gene is essential for the correct conformation and functioning of the cytochrome $bc_1$ complex and the neighboring complexes II and IV in the mitochondrial respiratory chain. *Eur. J. Biochem.* **246,** 103–111
11. Do, T. Q., Hsu, A. Y., Jonassen, T., Lee, P. T., and Clarke, C. F. (2001) A defect in coenzyme Q biosynthesis is responsible for the respiratory deficiency in *Saccharomyces cerevisiae abc1* mutants. *J. Biol. Chem.* **276,** 18161–18168
12. Xie, L. X., Hsieh, E. J., Watanabe, S., Allan, C. M., Chen, J. Y., Tran, U. C., and Clarke, C. F. (2011) Expression of the human atypical kinase ADCK3 rescues coenzyme Q biosynthesis and phosphorylation of Coq polypeptides in yeast *coq8* mutants. *Biochim. Biophys. Acta* **1811,** 348–360
13. Lagier-Tourenne, C., Tazir, M., López, L. C., Quinzii, C. M., Assoum, M., Drouot, N., Busso, C., Makri, S., Ali-Pacha, L., Benhassine, T., Anheim, M., Lynch, D. R., Thibault, C., Plewniak, F., Bianchetti, L., Tranchant, C., Poch, O., DiMauro, S., Mandel, J. L., Barros, M. H., Hirano, M., and Koenig, M. (2008) ADCK3, an ancestral kinase, is mutated in a form of recessive ataxia associated with coenzyme $Q_{10}$ deficiency. *Am. J. Hum. Genet.* **82,** 661–672
14. Mollet, J., Delahodde, A., Serre, V., Chretien, D., Schlemmer, D., Lombes, A., Boddaert, N., Desguerre, I., de Lonlay, P., de Baulny, H. O., Munnich, A., and Rötig, A. (2008) *CABC1* gene mutations cause ubiquinone deficiency with cerebellar ataxia and seizures. *Am. J. Hum. Genet.* **82,** 623–630
15. Tauche, A., Krause-Buchholz, U., and Rödel, G. (2008) Ubiquinone biosynthesis in *Saccharomyces cerevisiae*. The molecular organization of *O*-methylase Coq3p depends on Abc1p/Coq8p. *FEMS Yeast Res.* **8,** 1263–1275
16. Padilla, S., Tran, U. C., Jiménez-Hidalgo, M., López-Martín, J. M., Martín-Montalvo, A., Clarke, C. F., Navas, P., and Santos-Ocaña, C. (2009) Hydroxylation of demethoxy-Q6 constitutes a control point in yeast coenzyme Q6 biosynthesis. *Cell. Mol. Life Sci.* **66,** 173–186
17. Zampol, M. A., Busso, C., Gomes, F., Ferreira-Junior, J. R., Tzagoloff, A., and Barros, M. H. (2010) Overexpression of *COQ10* in *Saccharomyces cerevisiae* inhibits mitochondrial respiration. *Biochem. Biophys. Res. Commun.* **402,** 82–87
18. Ozeir, M., Mühlenhoff, U., Webert, H., Lill, R., Fontecave, M., and Pierrel, F. (2011) Coenzyme Q biosynthesis: Coq6 is required for the C5-hydroxylation reaction and substrate analogues rescue Coq6 deficiency. *Chem. Biol.* **18,** 1134–1142
19. Marbois, B., Xie, L. X., Choi, S., Hirano, K., Hyman, K., and Clarke, C. F. (2010) *para*-Aminobenzoic acid is a precursor in coenzyme $Q_6$ biosynthesis in *Saccharomyces cerevisiae*. *J. Biol. Chem.* **285,** 27827–27838
20. Elble, R. (1992) A simple and efficient procedure for transformation of yeasts. *BioTechniques* **13,** 18–20
21. Burke, D., Dawson, D., and Stearns, T. (2000) *Methods in Yeast Genetics,* Cold Spring Harbor Laboratory Press, Cold Spring Harbor, NY
22. Sherman, F. (2002) Getting started with yeast. *Methods Enzymol.* **350,** 3–41
23. Gin, P., and Clarke, C. F. (2005) Genetic evidence for a multisubunit complex in coenzyme Q biosynthesis in yeast and the role of the Coq1 hexaprenyl diphosphate synthase. *J. Biol. Chem.* **280,** 2676–2681
24. Tzagoloff, A., and Dieckmann, C. L. (1990) Pet genes of *Saccharomyces cerevisiae*. *Microbiol. Rev.* **54,** 211–225
25. Johnson, A., Gin, P., Marbois, B. N., Hsieh, E. J., Wu, M., Barros, M. H., Clarke, C. F., and Tzagoloff, A. (2005) *COQ9*, a new gene required for the biosynthesis of coenzyme Q in *Saccharomyces cerevisiae*. *J. Biol. Chem.* **280,** 31397–31404
26. Olson, R. E., and Rudney, H. (1983) Biosynthesis of ubiquinone. *Vitam. Horm.* **40,** 1–43
27. Fontanesi, F., Soto, I. C., and Barrientos, A. (2008) Cytochrome *c* oxidase biogenesis. New levels of regulation. *IUBMB Life* **60,** 557–568
28. Martín-Montalvo, A., González-Mariscal, I., Padilla, S., Ballesteros, M., Brautigan, D. L., Navas, P., and Santos-Ocaña, C. (2011) Respiratory-induced coenzyme Q biosynthesis is regulated by a phosphorylation cycle of Cat5p/Coq7p. *Biochem. J.* **440,** 107–114
29. Rea, S. L., Graham, B. H., Nakamaru-Ogiso, E., Kar, A., and Falk, M. J. (2010) Bacteria, yeast, worms, and flies. Exploiting simple model organisms to investigate human mitochondrial diseases. *Dev. Disabil. Res. Rev.* **16,** 200–218
30. Salviati, L., Trevisson, E., Rodriguez Hernandez, M. A., Casarin, A., Pertegato, V., Doimo, M., Cassina, M., Agosto, C., Desbats, M. A., Sartori, G., Sacconi, S., Memo, L., Zuffardi, O., Artuch, R., Quinzii, C., Dimauro, S., Hirano, M., Santos-Ocaña, C., and Navas, P. (2012) Haploinsufficiency of *COQ4* causes coenzyme $Q_{10}$ deficiency. *J. Med. Genet.* **49,** 187–191
31. Ashby, M. N., Kutsunai, S. Y., Ackerman, S., Tzagoloff, A., and Edwards, P. A. (1992) COQ2 is a candidate for the structural gene encoding *para*-hydroxybenzoate:polyprenyltransferase. *J. Biol. Chem.* **267,** 4128–4136
32. Do, T. Q., Schultz, J. R., and Clarke, C. F. (1996) Enhanced sensitivity of ubiquinone-deficient mutants of *Saccharomyces cerevisiae* to products of autoxidized polyunsaturated fatty acids. *Proc. Natl. Acad. Sci. U.S.A.* **93,** 7534–7539
33. Hsu, A. Y., Do, T. Q., Lee, P. T., and Clarke, C. F. (2000) Genetic evidence for a multisubunit complex in the *O*-methyltransferase steps of coenzyme Q biosynthesis. *Biochim. Biophys. Acta* **1484,** 287–297
34. Barkovich, R. J., Shtanko, A., Shepherd, J. A., Lee, P. T., Myles, D. C., Tzagoloff, A., and Clarke, C. F. (1997) Characterization of the *COQ5* gene from *Saccharomyces cerevisiae*. Evidence for a *C*-methyltransferase in ubiquinone biosynthesis. *J. Biol. Chem.* **272,** 9182–9188
35. Gin, P., Hsu, A. Y., Rothman, S. C., Jonassen, T., Lee, P. T., Tzagoloff, A., and Clarke, C. F. (2003) The *Saccharomyces cerevisiae COQ6* gene encodes a mitochondrial flavin-dependent monooxygenase required for coenzyme Q biosynthesis. *J. Biol. Chem.* **278,** 25308–25316
36. Marbois, B. N., and Clarke, C. F. (1996) The *COQ7* gene encodes a protein in *Saccharomyces cerevisiae* necessary for ubiquinone biosynthesis. *J. Biol. Chem.* **271,** 2995–3004
37. Brachmann, C. B., Davies, A., Cost, G. J., Caputo, E., Li, J., Hieter, P., and Boeke, J. D. (1998) Designer deletion strains derived from *Saccharomyces cerevisiae* S288C: A useful set of strains and plasmids for PCR-mediated gene disruption and other applications. *Yeast* **14,** 115–132
38. Winzeler, E. A., Shoemaker, D. D., Astromoff, A., Liang, H., Anderson, K., Andre, B., Bangham, R., Benito, R., Boeke, J. D., Bussey, H., Chu, A. M., Connelly, C., Davis, K., Dietrich, F., Dow, S. W., El Bakkoury, M., Foury, F., Friend, S. H., Gentalen, E., Giaever, G., Hegemann, J. H., Jones, T., Laub, M., Liao, H., Liebundguth, N., Lockhart, D. J., Lucau-Danila, A., Lussier, M., M'Rabet, N., Menard, P., Mittmann, M., Pai, C., Rebischung, C., Revuelta, J. L., Riles, L., Roberts, C. J., Ross-MacDonald, P., Scherens, B., Snyder, M., Sookhai-Mahadeo, S., Storms, R. K., Véronneau, S., Voet, M., Volckaert, G., Ward, T. R., Wysocki, R., Yen, G. S., Yu, K., Zimmermann, K., Philippsen, P., Johnston, M., and Davis, R. W. (1999) Functional characterization of the *S. cerevisiae* genome by gene deletion and parallel analysis. *Science* **285,** 901–906
39. Belogrudov, G. I., Lee, P. T., Jonassen, T., Hsu, A. Y., Gin, P., and Clarke, C. F. (2001) Yeast *COQ4* encodes a mitochondrial protein required for coenzyme Q synthesis. *Arch. Biochem. Biophys.* **392,** 48–58
40. Sikorski, R. S., and Hieter, P. (1989) A system of shuttle vectors and yeast host strains designed for efficient manipulation of DNA in *Saccharomyces cerevisiae*. *Genetics* **122,** 19–27
41. Christianson, T. W., Sikorski, R. S., Dante, M., Shero, J. H., and Hieter, P. (1992) Multifunctional yeast high copy number shuttle vectors. *Gene* **110,** 119–122
42. Hsieh, E. J., Dinoso, J. B., and Clarke, C. F. (2004) A tRNA(TRP) gene mediates the suppression of *cbs2-223* previously attributed to *ABC1/COQ8*. *Biochem. Biophys. Res. Commun.* **317,** 648–653

Downloaded from http://www.jbc.org/ at UCLA-Louise Darling Biomed. Lib. on July 2, 2014

# Chapter 4

## Investigation of alternative ring precursors of coenzyme Q in *E. coli*, *S. cerevisiae*, mouse, and human cells

**Abstract**

Coenzyme Q (ubiquinone or Q) is an essential redox-active, polyisoprenylated benzoquinone lipid essential for electron and proton transport in the mitochondrial respiratory chain. The aromatic ring 4-hydroxybenzoic acid (4HB) is commonly depicted as the sole aromatic ring precursor in Q biosynthesis despite the recent finding that para-aminobenzoic acid (pABA) also served as a ring precursor in yeast Q biosynthesis. In this study, we employed $^{13}C_6$-4-hydroxy benzoic acid, $^{13}C_6$-para-amino benzoic acid, and $^{13}C_6$-resveratrol to investigate the use of these small molecules as aromatic ring precursors in Q biosynthesis in *E. coli,* yeast, human and mouse cells. In contrast to *S. cerevisiae*, neither *E. coli* nor mammalian cells cultured in the presence of $^{13}C_6$-pABA were able to form $^{13}C_6$-Q. However, *E. coli* cells labeled with $^{13}C_6$-pABA generated $^{13}C_6$-ring labeled forms of 3-octaprenyl-4-aminobenzoic acid, 2-octaprenyl-aniline, and 3-octaprenyl-2-aminophenol, suggesting UbiA, UbiD,X, and Ubil are capable of using pABA or pABA-derived intermediates as substrates. *E. coli, S. cerevisiae,* human and mouse cells cultured in the presence of $^{13}C_6$-resveratrol were able to synthesize $^{13}C_6$-Q. Future evaluation of the physiological and pharmacological responses to dietary polyphenols should consider their metabolism to Q.

## Introduction

Coenzyme Q (ubiquinone or Q) is a polyisoprenylated benzoquinone lipid essential for electron and proton transport in the mitochondrial respiratory chain and in the plasma membrane of *E. coli* [1]. The hydroquinone or reduced $QH_2$ functions as a chain-terminating lipid antioxidant and as a co-antioxidant to recycle Vitamin E [2]. Q is also involved in many other metabolic processes including fatty acid beta-oxidation, sulfide oxidization, pyrimidine metabolism, disulfide bond formation, sulfide oxidation, and pyrimidine metabolism [3-5]. Q is composed of a fully substituted benzoquinone ring that is attached to a polyisoprenyl tail with variable number of isoprenyl units (six for *Saccharomyces cerevisiae*, eight for *E. coli*, nine for mouse, and ten for human, hence $Q_{10}$).

Cells rely on *de novo* synthesis for sufficient amount of Q. In yeast *S. cerevisiae,* at least eleven gene products, Coq1-Coq9, Arh1, and Yah1 [6-9] are essential for Q biosynthesis. The Coq1 polypeptide synthesizes the polyprenyl tail and Coq2 attaches the tail to the aromatic ring (Fig. 1). The other Coq polypeptides catalyze ring modifications including *O*-methylation (Coq3), C-methylation (Coq5), hydroxylation (Coq6 and Coq7), while the functioning of Coq6 requires ferredoxin (Yah1) and ferredoxin reductase (Arh1)[9]. The roles of Coq3, Coq4, and Coq9 have not yet been determined although they are all essential for yeast Q biosynthesis. Schemes of coenzyme Q (ubiquinone or Q) biosynthesis generally depict 4HB as the biosynthetic aromatic ring precursor of Q [10]. 4HB is considered to derive from coumarate in yeast and from tyrosine in animal cells. Yeast can also use *para*-aminobenzoic acid (pABA) as an alternate ring precursor in the biosynthesis of coenzyme Q [9, 11]. This finding was surprising because pABA

was a well known precursor of folate, which is synthesized de novo by many microorganisms, but is a vitamin for humans. A new yeast $Q_6$ biosynthesis scheme was reported recently including detailed steps showing how yeast can convert either 4-hydroxylbenzoic acid (4HB) or *para*-aminobenzoic acid (pABA) into $Q_6$ [12].

The biosynthesis of $Q_8$ in *E. coli* requires eleven *ubi* genes; UbiC protein carries out the first committed step in the biosynthesis of $Q_8$, the conversion of chorismate to 4-HB (Fig. 2)[13, 14]. UbiA adds the octaprenyl tail to the 4HB ring, followed by the decarboxylation catalyzed by UbiD and UbiX. UbiI adds the first hydroxyl group at the C5 position, followed by *O*-methylation catalyzed by UbiG, the homolog of yeast Coq3. Additional ring modifications catalyzed by UbiH, UbiE, UbiF, UbiG and UbiJ generate the final product of $Q_8$.

A recent study reported that *para*-coumarate can be used for ubiquinone biosynthesis in Arabidopsis [15]. Due to the structural similarity to coumarate, a likely precursor of 4HB, the possibility of resveratrol serving as a ring precursor in Q biosynthesis was investigated. The in vivo metabolism of resveratrol can be monitored via stable isotopes with high accuracy and specificity via LC/MS-MS identification and quantification. Here we have made use of $^{13}C_6$-ring labeled resveratrol to track its fate in lipid extracts of yeast and animal cells.

In this study, we confirmed that human and *E. coli* cells do not utilize pABA as an aromatic ring precursor in the synthesis of Q; while resveratrol is a ring precursor of Q in *E. coli, S. cerevisiae,* human and mouse cells.

**Methods**

*Yeast Growth and Stable Isotope Labeling* – The *S. cerevisiae* strain used was W303-1B (MAT α, *ade2-1 his3-1,15 leu2-3,112 trp1-1 ura3-1*)[11]. YPD medium (2% glucose, 1% yeast extract, 1% peptone) was prepared as described[16]. Solid plate medium included 2% Bacto agar. Yeast colonies from YPD plate medium were first inoculated into 250 ml flasks containing 70 ml YPD liquid media. Following overnight incubation with shaking (250 rpm) at 30°C, yeast cells were transferred into fresh *D*rop *O*ut *D*extrose (DoD) medium [11]. DoD medium contained 2% dextrose, 6.8g/liter Bio101 yeast nitrogen base minus *p*ABA minus folate with ammonium sulfate (MP Biomedicals), and 5.83 mM sodium monophosphate (pH adjusted to 6.0 with NaOH). Amino acids and nucleotides were added as described previously [11]. Stable isotope-containing compounds included *p*-hydroxy[*aromatic*-$^{13}C_6$]benzoic acid ([$^{13}C_6$]4HB) from Cambridge Isotope Laboratories (Andover, MA). Resveratrol[4-hydroxyphenyl-$^{13}C_6$] ([$^{13}C_6$]resveratrol) and *p*-amino[*aromatic*-$^{13}C_6$]benzoic acid ([$^{13}C_6$]paba) were obtained from Sigma/ISOTEC (Miamisburg, OH). $^{13}C_6$-labeled aromatic ring precusors were added to fresh DoD medium and incubated with yeast cells (100 OD/ml) at 30$^{o}$C for 4 h. Cells were collected by centrifugation and pellets were stored at –20$^{o}$C. The wet weight of each cell pellet was determined by subtracting the weight of the tube from the total weight. Protein assays (BCA assay, Pierce) were performed on yeast cell lysates (1 g wet weight cells contains approximately 11 mg protein).

*E. coli growth and Stable Isotope Labeling* –

Bacterial strains HW272, MG1655, and *ubiC* were used. Cells were inoculated in 100 ml of Luria Broth for 16 h at 37°C. 50 $OD_{600}$ of cells form each sample were collected by centrifugation, and the collected pellets were resuspended in fresh LB medium in the presence of either 10 ug/ml of $^{13}C_6$-4HB, $^{13}C_6$-pABA, $^{13}C_6$-resveratrol, or equivalent volume of ethanol, and incubated at 37°C with shaking at 250 RPM. Cells were collected again by centrifugation after 4 h and stored at -20°C for LC/MS/MS lipid analysis.

*Animal Cell Culture and Stable Isotope Labeling* -

U251 human glioma and 3T3 mouse fibroblast cells were cultured in DMEM (Gibco). U87 human glioma cells were cultured in IMDM (Gibco). Human embryonic kidney 293T cells were cultured in DMEM with 1 mM sodium pyruvate (Gibco). All cells were passaged in the stated media supplemented with 10% Fetal Bovine Serum (Omega Scientific). Equal numbers of cells were plated approximately 12 h prior to treatment experiments. During treatment with stable isotope-labeled compounds, cells were cultured with 1% FBS unless otherwise stated. Cells were cultured with the designated stable isotope-labeled compound for 24 h, then washed with 1X PBS and released from the culture dish with 0.25% Trypsin-EDTA (Gibco). Aliquots of the released cells were stained with Trypan Blue and the number of cells counted with the Cellometer Auto T4 (Nexcelom Bioscience); aliquots (5%) were also removed for determination of protein content (BCA assay; Pierce). The remaining cells in the suspension were collected by centrifugation. Cell pellets were stored at –20°C.

*Lipid Extraction* – Cell pellets were thawed on ice, and then suspended in 1.2 ml of methanol followed by 1.8 ml of petroleum ether. $Q_4$ was added as an internal strandard for the

determination of $Q_6$ content in yeast lipid extracts. Diethoxy-$Q_{10}$[17] was used as an internal standard for determination of $Q_9$ and $Q_{10}$ in mammlian cell lipid extracts and $Q_8$ in *E. coli* cell lipid extracts. Samples were vortexed for 45 s, then the upper layer was removed to a new tube, and another 1.8 ml of petroleum either was added to the lower phase, and the sample was votexed again for 45 s. The upper layer was again removed and combined with the previous organic phase. The combined organic phase was dried under a stream of nitrogen gas and resuspended in 200 μl of ethanol (USP, Aaper Alcohol and Chemical Co., Shelbyville, KY).

*Reverse phase-high performace liquid chromatography and mass spectroscopy (HPLC-MS/MS)* – The HPLC-MS/MS analyses were performed as previously described for determination of $Q_6$ in yeast lipid extracts [8, 11], and and determination of $Q_9$ and $Q_{10}$ in mammalian lipid extracts [17, 18]. Briefly, a 4000 QTRAP linear MS/MS spectrometer from Applied Biosystems (Foster City, CA) was used. Applied Biosystem sofwatre, Analyst version 1.4.2, was used for data acquisition and processing. A binary HPLC solvent delivery system was used with either a Luna Phenyl-Hexyl column (particle size 5μm, 100 × 4.60 mm; Phenomenex) for yeast cell lipid extracts or a Luna Phenyl-Hexyl column (particle size 3μm, 50 × 2.00 mm; Phenomenex) for mammlian and bacteria cell lipid extracts. The mobile phase consisted of Solvent A (methanol:isopropanol, 95:5, with 2.5 mM ammonium formate) and Solvent B (isopropanol, 2.5 mM ammonium formate). For separation of yeast quinones, the percentage of Solvent B increased linearly from 0% to 5% over 6 min, and the flow rate increased from 600 μl/min to 800 μl/min. The flow rate and mobile phase were linearly changed back to initial condition by 7 min. For separation of bacteria and mammalian quinones, the percentage of Solvent B for the first 1.5 min was 0%, and increased linearly to 10% by two min. The percentage of Solvent B remain

unchanged for the next min and decreased linearly back to 0% by 6 min. A constant flow rate of 800 μl/min was used. All samples were analyzed in multiple reaction monitoring mode (MRM); MRM transitions were as follows: m/z 591/197.1 ($Q_6$); m/z 610/197.1 ($Q_6H_2$ with ammonium adduct); m/z 597/203.1 ($^{13}C_6$-$Q_6$); m/z 616/203.1 ($^{13}C_6$-$Q_6H_2$ with ammonium adduct); m/z 636/106 (OA); m/z 637/107 (OP); m/z 642/112 ($^{13}C_6$-OA); m/z 643/113 ($^{13}C_6$-OP); m/z 652/122 (OAP); m/z 658/128 ($^{13}C_6$-OAP); m/z 682/150 (OABA); m/z 688/156 ($^{13}C_6$-OABA); m/z 727/197.1 ($Q_8$); m/z 733/203.1 ($^{13}C_6$-$Q_8$); m/z 746/197.1 ($Q_8H_2$ with ammonium adduct); m/z 750/203.1 ($^{13}C_6$-$Q_8H_2$ with ammonium adduct); m/z 880.7/197.0 ($Q_{10}$ with ammonium adduct); m/z 882.7/197.0 ($Q_{10}H_2$ with ammonium adduct); m/z 886.7/203.0 ($^{13}C_6$-$Q_{10}$ with ammonium adduct); m/z 888.7/203 ($^{13}C_6$-$Q_{10}H_2$ with ammonium adduct); m/z 812.6/197 ($Q_9$ with ammonium adduct); m/z 455.6/197.1 ($Q_4$); m/z 908.7/225.1 (Diethoxy-$Q_{10}$ with ammonium adduct) and m/z 910.7/225.1 (Diethoxy-$Q_{10}H_2$ with ammonium adduct

**Results**

Para-amino benzoic acid was demonstrated as a ring precursor to Q biosynthesis in yeast *S. cerevisiae [9, 11]*. In other species, such as in mammalian cells, the dedicated precursors to Q biosynthesis are polyisoprene diphosphate, which provides the tail, and 4-hydroxy benzoic acid (4HB), which contributes to the ring [19, 20]. Thus, to investigate whether pABA is a precursor to Q in mammalian cells, U251 cells were cultured in the presence of 7uM, 70uM and 700uM of either $^{13}C_6$-4HB or $^{13}C_6$-pABA for 24 hrs prior to LC/MS/MS analysis of Q content (Fig.2). Treatments of all three concentrations of 4HB (7, 70, and 700 uM) lead to the accumulation of $^{13}C_6$-$Q_{10,}$ while U251 cells incubated with $^{13}C_6$-pABA under the same condition resulted no detectable $^{13}C_6$-$Q_{10}$. Treatments of various concentration of $^{13}C_6$-4HB did not alter the total $Q_{10}$ content; however 700 uM of $^{13}C_6$-pABA resulted in significantly lower total Q content in mammalian cells ($p<0.05$).

In addition to investigating mammalian cells, $^{13}C_6$-pABA and $^{13}C_6$-4HB were added to *E. coli* (HW272, MG1655, *ubiC*) cultured in LB medium at 10 ug/ml final concentration (Fig. 3). Similar to the U251 cells, all three *E. coli* strains incubated in the presence of 10 ug/ml $^{13}C_6$-4HB, but not $^{13}C_6$-pABA, accumulated significant amount of $^{13}C_6$-$Q_8$. Interestingly, *ubiC* mutants, which were incapable of *de novo* 4HB synthesis, were also unable to use pABA to synthesize Q. This result potentially excluded the possibility that pABA might be used as a secondary precursor to Q biosynthesis in *E. coli* under conditions of 4HB deficiency.

Before concluding that pABA does not serve as a ring precursor in the biosynthesis of $Q_8$, we first need to examine pABA uptake by the cells. LC/MS/MS detection of $^{13}C_6$-octaprenyl-pABA

(OAB) in $^{13}C_6$-pABA treated cells indicated that *E. coli* cells successfully absorbed $^{13}C_6$-pABA from the medium and prenlyated $^{13}C_6$-pABA, which was the very first step in the Q biosynthetic pathway catalyzed by UbiA [21] (Fig. 4A). Accumulated $^{13}C_6$-3-octaprenyl-4-aminobenzoic acid was then converted into $^{13}C_6$-2-octaprenyl-aniline(OA)(Fig. 4B). Note that the *ubiC* mutant contained significantly more amino-containing intermediates (Fig. 4A,B) even in the absence of pABA addition, presumably due to a deficiency in 4HB. Such situation was more obvious in the accumulation of the next-step intermediate $^{13}C_6$-3-octaprenyl-4-amino phenol (OAP) (Fig. 4D). The *ubiC* mutant accumulated 10 times more OAP than HW272 and MG1655 independent of the supplied $^{13}C_6$-pABA, suggesting that OAP might be the "dead-end" intermediate of the pABA side of the pathway. $^{13}C_6$-4HB treated and control cells contained none of these three amino-containing Q biosynthesis intermediates (Fig 4A,B,D), while $^{13}C_6$-2-octaprenyl phenol was only detected in $^{13}C_6$-4HB treated cells(Fig 4C). These results together suggest that no cross talk existed between these two branches of the pathway in the early steps.

If pABA could serve as an alternative ring precursor to Q biosynthesis in yeast, then the other question one would ask if whether there are more alternative ring precursors. Surprisingly, wild-type yeast could indeed use resveratrol as a ring precursor in the synthesis of $Q_6$ (Fig. 5a). W303 cells cultured in the presence of 68 uM, 282 uM, or 974 uM of $^{13}C_6$-resveratrol, accumulated increasing amounts of $^{13}C_6$-$Q_6$, while the ethanol control samples contained no detectable $^{13}C_6$-$Q_6$. Notably, the increasing amount of resveratrol did not alter the total Q content. We next examined whether other human or mouse cells could use resveratrol as a ring precursor to Q. All four mammalian cell lines we examined were able to convert resveratrol to Q, as shown by the accumulation of $^{13}C_6$-$Q_{10}$ (Fig. 5B-D) in three different human cell lines, or $^{13}C_6$-$Q_9$ (Fig. 5E) in

mouse 3T3 fibroblasts when cultured in the presence of 70 uM of $^{13}C_6$-resveratrol. Although cells cultured with $^{13}C_6$-4HB accumulated significantly more $^{13}C_6$-$Q_{10}$ than when cultured with $^{13}C_6$-resveratrol, the incorporation of $^{13}C_6$-resveratrol into Q (10%) was much higher than that observed in wild-type yeast cells (less than 1%). $^{13}C_6$-$Q_{10}$ content in U251 and 3T3 cells increased linearly in response to the higher concentration of $^{13}C_6$-resveratrol,while the total Q content still remain unaltered, as observed in yeast (Fig. 6). Unfortunately, higher concentration (>70 uM) of resveratrol induced cell death, thus we were not able to examine the amount of $^{13}C_6$-Q synthesized in the presence of high concentrations of $^{13}C_6$-resveratrol.

Surprisingly, *E. coli* also utilized resveratrol as an alternative ring precursor to Q, although to a lower extent as compared to yeast or human cells. HW272 and MG1655 cells cultured in LB medium in the presence of 10ug/ml $^{13}C_6$-resveratrol accumulated barely detectable amounts of $^{13}C_6$-$Q_8$ (Fig. 7A). In comparison, 10 ug/ml of $^{13}C_6$-4HB resulted in more than two thirds of the total Q content being $^{13}C_6$ labeled in HW272 and MG1655 cells. However, *ubiC* mutants, with defects in *de-novo* synthesis of 4HB, accumulated significantly more of $^{13}C_6$-$Q_8$ than HW272 and MG1655 when labeled with $^{13}C_6$-resveratrol. $^{13}C_6$-octaprenylphenol was only detected when all three *E. coli* strains cultured in the presence of $^{13}C_6$-4HB, and not with $^{13}C_6$-resveratrol, suggesting that step(s) at which resveratrol is used as a ring precursor may not depend on its conversion to 4HB.

**Discussion**

It was reported that para-amino benzoic acid was an alternative precursor to Q biosynthesis in yeast *S. cerevisae* [9, 11]. However, most biosynthetic schemes of Q biosynthesis continue to depict 4HB as the "sole" aromatic ring precursor. Our use of the stable isotope labeled ring precursors $^{13}C_6$-pABA and $^{13}C_6$-4HB, led to the identification of novel Q intermediates in yeast *coq5, coq6, coq7* and *coq9* null mutants, when Coq8 was over-expressed [8]. The finding that yeast cells could utilize pABA as a ring precursor in Q biosynthesis was rather surprising because pABA is a crucial intermediate in folate biosynthesis, and it was reported that the addition of pABA to either *E. coli* or human cells leads to a concentration-dependent inhibition of Q content [10, 22, 23]. A recent report showed that another aromatic ring compound, 4-nitrobenzoic acid, inhibited Q biosynthesis in mammalian cells by competing with 4HB for Coq2p [24]. However, it remained possibile that pABA might still be utilized as a ring precursor in Q biosynthesis. Therefore, we employed $^{13}C_6$-pABA to investigate its fate in mammalian and *E. coli* cells.

$^{13}C_6$-pABA labeling results revealed that pABA was not an aromatic ring precursor to Q biosynthesis in human, mouse or *E. coli* cells. The only nitrogen containing Q intermediate detected was the imino-demethoxy-$Q_9$ in 3T3 cells, which indicated that pABA was absorbed by cells and prenylated. In order to rule out the scenario that *E. coli* cells only utilize pABA as a ring precursor in Q biosynthesis when the primary ring precursor 4HB is not available, we incubated *ubiC* mutants, which have defects in the *de-novo* synthesis of 4HB, in the presence of $^{13}C_6$-pABA; however, even *ubiC* mutants weren't able to utilize pABA for $Q_8$ biosynthesis. Interestingly, multiple nitrogen containing Q biosynthetic intermediates resulted form $^{13}C_6$-

pABA were detected. Detection of $^{13}C_6$-3-octaprenyl-4-aminobenzoic acid (OAB) in all three strains (HW272, MG1655, and *ubiC*) confirmed $^{13}C_6$-pABA uptake (Fig. 4A). Further modifications of the $^{13}C_6$-OAB resulted $^{13}C_6$-2-octaprenyl-aniline and $^{13}C_6$-3-octaprenyl-4-aminophenol, indicating that amino ring substituent was tolerated by UbiA, UbiD/UbiX and Ubil in *E. coli* (Fig.4B, D) [14]. The accumulation of octaprenyl aminophenol in *ubiC* mutant regardless of the addition of $^{13}C_6$-pABA implies that OAP could be a dead-end intermediate derived from pABA. Neither HW272 nor MG1655 wild-type *E. coli* accumulated significant amounts of octaprenyl aminophenol, indicating that *E. coli* cells only process pABA through early steps in the Q biosynthesis pathway when 4HB content is low. We did not detect further down stream nitrogen containing Q biosynthetic intermediates using targeted and limited-untargeted LC/MS/MS approaches. However, the presence of additional N-containing Q intermediates downstream of octaprenyl aminophenol cannot be ruled out.

The beneficial health effects of resveratrol have led to vigorous research investigating its mechanisms of action. Many studies suggest that in addition to acting as an antioxidant, resveratrol elicits metabolic responses similar to dietary restriction. A wide spectrum of activities is attributed to stilbenoids produced by a variety of plants when under attack by pathogens [25]. A stilbenoid of recent fame, resveratrol acts as a chain breaking antioxidant, modulates cellular antioxidant enzymes and apoptosis, and has beneficial affects on neurodegenerative and cardiovascular diseases, eliciting metabolic responses similar to dietary restriction [26, 27]. Although there is much controversy regarding the lifespan extension effects of resveratrol [28], its effects on age-associated diseases in animal models has generated considerable enthusiasm for research on its mechanism of action [29]. Many questions remain regarding resveratrol biodistribution, its metabolism, and the biological effects of resveratrol metabolites [30].

It was rather surprising that resveratrol could serve as an aromatic ring precursor in Q biosynthesis in *E. coli,* yeast, and mammalian cells. Wild-type *E. coli* could barely utilize resveratrol for Q biosynthesis; significant incorporation of the resveratrol ring into Q8 was observed in ubiC mutants, with defects in synthesis of the primary ring precursor 4HB. In contrast, approximately ten percent of the total Q content in human and mouse cells harbored the ring derived from $^{13}C_6$-resveratrol after 24 hours of incubation. The maximum concentration of resveratrol tested was lower than either 4HB or pABA because resveratrol induces apoptotic cell death [31]. Thus, we monitored cell viability in our experiments and limited the amount of resveratrol tested in order to avoid induction of cell death.

The metabolism of resveratrol responsible for its incorporation into Q has not been determined. Animals harbor homologues of the carotenoid cleavage oxidase family, a group of enzymes that cleave one of the double bonds in carotenoids to produce retinal, or act on stilbenoids to produce the two ring aldehyde products [32]. Notably the 4' hydroxy group has been identified as crucial for antioxidant and neuroprotective effects of stilbenoids [33]. It seems likely that other stilbenoids may serve as ring precursors of Q. For example, processing of piceatannol (*trans*-3,5,3'4'-tetrahydroxystilbene) by a carotenoid cleavage oxidase family member [34], generates 3,4-dihydroxy-benzaldehyde, a ring precursor that would bypass the Coq6 hydroxylase step of Q biosynthesis upon Coq2-prenylation [35].

Of the more than one hundred clinical trials testing the efficacy of resveratrol or other polyphenols (clinical trials.gov), few determine the metabolic fate of the administered

supplement. When metabolism of resveratrol is studied, the focus is on aqueous soluble polar metabolites of resveratrol, including sulfated and glucuronidated conjugation products [36]. The new finding that a metabolic conversion of resveratrol into Q occurs in eukaryotes shows that exogenous antioxidants may be utilized as precursors to synthesize a wholly different class of molecule. The effects of resveratrol in mimicking calorie restriction [26, 27] may be due in part to its conversion to Q, a lipid known to induce anti-inflammatory responses [37], an essential component of mitochondrial energy metabolism and a potent lipid soluble antioxidant [10]. Investigation of the pharmacological responses to diverse dietary polyphenols (e.g. curcumin) should be expanded to include this molecular fate.

**References**


1. *Bentinger, M., M. Tekle, and G. Dallner, Coenzyme Q--biosynthesis and functions. Biochem Biophys Res Commun, 2010. **396**(1): p. 74-9.*
2. *Bentinger, M., K. Brismar, and G. Dallner, The antioxidant role of coenzyme Q. Mitochondrion, 2007. **7 Suppl**: p. S41-50.*
3. *Inaba, K., Disulfide bond formation system in Escherichia coli. J Biochem, 2009. **146**(5): p. 591-7.*
4. *Zhang, M., et al., High production of sulfide in coenzyme Q deficient fission yeast. Biofactors, 2008. **32**(1-4): p. 91-8.*
5. *Matsuo, Y., et al., Polypeptone induces dramatic cell lysis in ura4 deletion mutants of fission yeast. PLoS One, 2013. **8**(3): p. e59887.*
6. *Tran, U.C. and C.F. Clarke, Endogenous synthesis of coenzyme Q in eukaryotes. Mitochondrion, 2007. **7 Suppl**: p. S62-71.*
7. *Wang, Y. and S. Hekimi, Mitochondrial respiration without ubiquinone biosynthesis. Hum Mol Genet, 2013. **22**(23): p. 4768-83.*
8. *Xie, L.X., et al., Overexpression of the Coq8 kinase in Saccharomyces cerevisiae coq null mutants allows for accumulation of diagnostic intermediates of the coenzyme Q6 biosynthetic pathway. J Biol Chem, 2012. **287**(28): p. 23571-81.*
9. *Pierrel, F., et al., Involvement of mitochondrial ferredoxin and para-aminobenzoic acid in yeast coenzyme Q biosynthesis. Chem Biol, 2010. **17**(5): p. 449-59.*
10. *Turunen, M., J. Olsson, and G. Dallner, Metabolism and function of coenzyme Q. Biochim Biophys Acta, 2004. **1660**(1-2): p. 171-99.*

11. *Marbois, B., et al., para-Aminobenzoic acid is a precursor in coenzyme Q6 biosynthesis in Saccharomyces cerevisiae. J Biol Chem, 2010.* ***285****(36): p. 27827-38.*

12. *He, C.H., et al., Coenzyme Q supplementation or over-expression of the yeast Coq8 putative kinase stabilizes multi-subunit Coq polypeptide complexes in yeast coq null mutants. Biochim Biophys Acta, 2014.* ***1841****(4): p. 630-44.*

13. *Nichols, B.P. and J.M. Green, Cloning and sequencing of Escherichia coli ubiC and purification of chorismate lyase. J Bacteriol, 1992.* ***174****(16): p. 5309-16.*

14. *Aussel, L., et al., Biosynthesis and physiology of coenzyme Q in bacteria. Biochim Biophys Acta, 2014.* ***1837****(7): p. 1004-1011.*

15. *Block, A., et al., The Origin and Biosynthesis of the Benzenoid Moiety of Ubiquinone (Coenzyme Q) in Arabidopsis. Plant Cell, 2014.*

16. *Amberg, D.C., et al., Methods in yeast genetics : a Cold Spring Harbor Laboratory course manual. 2005 ed. 2005, Cold Spring Harbor, N.Y.: Cold Spring Harbor Laboratory Press. xvii, 230 p.*

17. *Falk, M.J., et al., Probucol ameliorates renal and metabolic sequelae of primary CoQ deficiency in Pdss2 mutant mice. EMBO Mol Med, 2011.* ***3****(7): p. 410-27.*

18. *Gasser, D.L., et al., Focal segmental glomerulosclerosis is associated with a PDSS2 haplotype and, independently, with a decreased content of coenzyme Q10. Am J Physiol Renal Physiol, 2013.* ***305****(8): p. F1228-38.*

19. *Olson, R.E. and H. Rudney, Biosynthesis of ubiquinone. Vitam Horm, 1983.* ***40****: p. 1-43.*

20. *Pennock, J.F., The biosynthesis of chloroplastidic terpenoid quinones and chromanols. Biochem Soc Trans, 1983.* ***11****(5): p. 504-10.*

21. *Gulmezian, M., et al., The role of UbiX in Escherichia coli coenzyme Q biosynthesis. Arch Biochem Biophys, 2007.* ***467****(2): p. 144-53.*

22. *Alam, S.S., A.M. Nambudiri, and H. Rudney, J-Hydroxybenzoate: polyprenyl transferase and the prenylation of 4-aminobenzoate in mammalian tissues. Arch Biochem Biophys, 1975.* ***171****(1): p. 183-90.*

23. *Hamilton, J.A. and G.B. Cox, Ubiquinone biosynthesis in Escherichia coli K-12. Accumulation of an octaprenol, farnesylfarnesylgeraniol, by a multiple aromatic auxotroph. Biochem J, 1971.* ***123****(3): p. 435-43.*

24. *Forsman, U., et al., 4-Nitrobenzoate inhibits coenzyme Q biosynthesis in mammalian cell cultures. Nat Chem Biol, 2010.* ***6****(7): p. 515-7.*

25. *Likhtenshtein, G., Stilbenes: Applications in Chemistry, Life Sciences and Materials Science. 2010, Weinheim: Wiley-VCH Verlag GmbH & Co. KGaA. 348.*

26. *Baur, J.A. and D.A. Sinclair, Therapeutic potential of resveratrol: the in vivo evidence. Nat Rev Drug Discov, 2006.* ***5****(6): p. 493-506.*

27. *Timmers, S., et al., Calorie restriction-like effects of 30 days of resveratrol supplementation on energy metabolism and metabolic profile in obese humans. Cell Metab, 2011.* ***14****: p. 612-622.*

28. *Burnett, C., et al., Absence of effects of Sir2 overexpression on lifespan in C. elegans and Drosophila. Nature, 2011.* ***477****(7365): p. 482-5.*

29. *Smoliga, J.M., O. Vang, and J.A. Baur, Challenges of Translating Basic Research Into Therapeutics: Resveratrol as an Example. J Gerontol A Biol Sci Med Sci, 2011.*

30. *Vang, O., et al., What is new for an old molecule? Systematic review and recommendations on the use of resveratrol. PLoS One, 2011.* ***6****(6): p. e19881.*

31. *Jiang, H., et al., Resveratrol-induced apoptotic death in human U251 glioma cells. Mol Cancer Ther, 2005.* ***4****(4): p. 554-61.*

32. *Marasco, E.K. and C. Schmidt-Dannert, Identification of bacterial carotenoid cleavage dioxygenase homologues that cleave the interphenyl alpha,beta double bond of stilbene derivatives via a monooxygenase reaction. Chembiochem, 2008.* ***9****(9): p. 1450-61.*

33. *Foti Cuzzola, V., et al., Role of Resveratrol and its Analogues in the Treatment of Neurodegenerative Diseases: Focus on Recent Discoveries. CNS Neurol Disord Drug Targets, 2011.* ***10****: p. 849-862.*

34. *Brefort, T., et al., Cleavage of resveratrol in fungi: characterization of the enzyme Rco1 from Ustilago maydis. Fungal Genet Biol, 2011.* ***48****(2): p. 132-43.*

35. *Ozeir, M., et al., Coenzyme q biosynthesis: coq6 is required for the c5-hydroxylation reaction and substrate analogs rescue coq6 deficiency. Chem Biol, 2011.* ***18****(9): p. 1134-42.*

36. *Walle, T., Bioavailability of resveratrol. Ann N Y Acad Sci, 2011.* ***1215****: p. 9-15.*

37. *Schmelzer, C., et al., The reduced form of coenzyme Q10 decreases the expression of lipopolysaccharide-sensitive genes in human THP-1 cells. J Med Food, 2011.* ***14****(4): p. 391-7.*

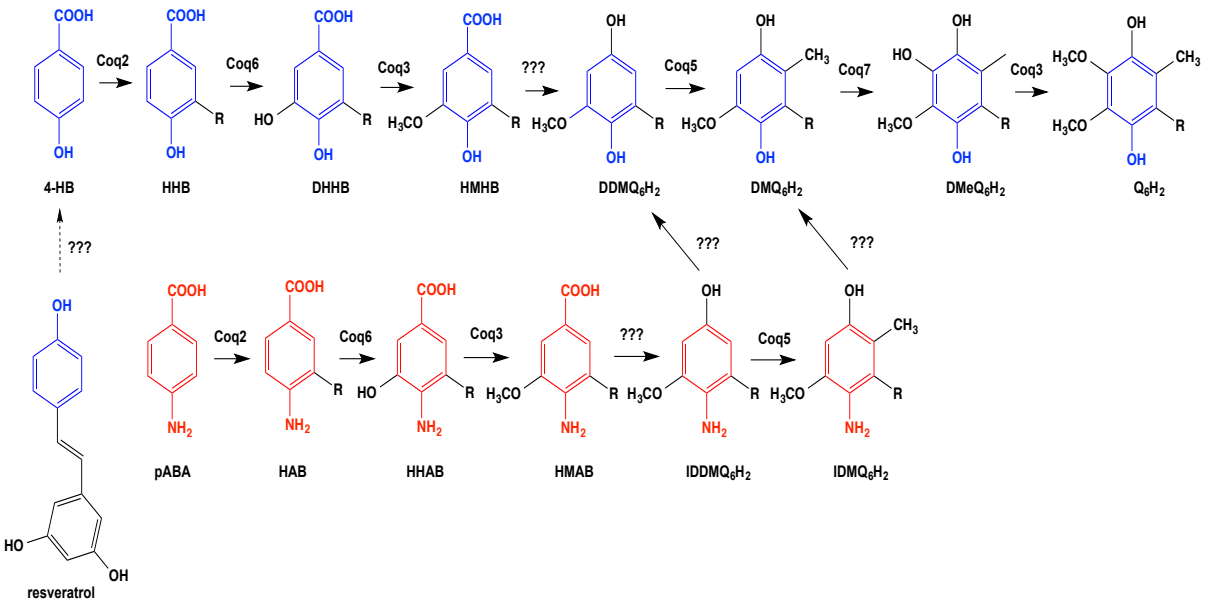



**Figure 1A. Q biosynthesis in yeast *S. cerevisiae.*** Most recent Q biosynthesis pathway reported in *S. cerevisiae*. Coq2 adds the hexaprenyl tail to either 4-hydroxy benzoic acid and *para*-aminobenzoic acid, forming 3-hexaprenyl-4-hydroxybenzoic acid (HHB) or 3-hexaprenyl 4-aminobenzoic acid (HAB). Coq6 adds the first hydroxyl group to the C5 position of the aromatic ring, forming either 3-hexaprenyl-4, 5-dihydroxybenzoic acid(DHHB) or 3-hexaprenyl-5-hydroxy-4-aminobenzoic acid (HHAB). An undetermined enzyme catalyzes the decarboxylation step, forming demethyl-demtheoxy $Q_6$ (DDMQ6) and immino-demethyl-demethoxy $Q_6$(IDDMQ$_6$). Coq5 catalyzes the *C-methylation* at C2 position of the aromatic ring, producing either demethoxy $Q_6$(DMQ$_6$) or immino-demethoxy $Q_6$(IDMQ$_6$). The 4HB and pABA branches convert at this step. Coq7 adds the second OH group to the C6 position, generating demethyl $Q_6$(DmeQ$_6$), followed by the second *O-methylation* catalyzed by Coq3 to synthesize $Q_6$. R denotes hexaprenyl tail.

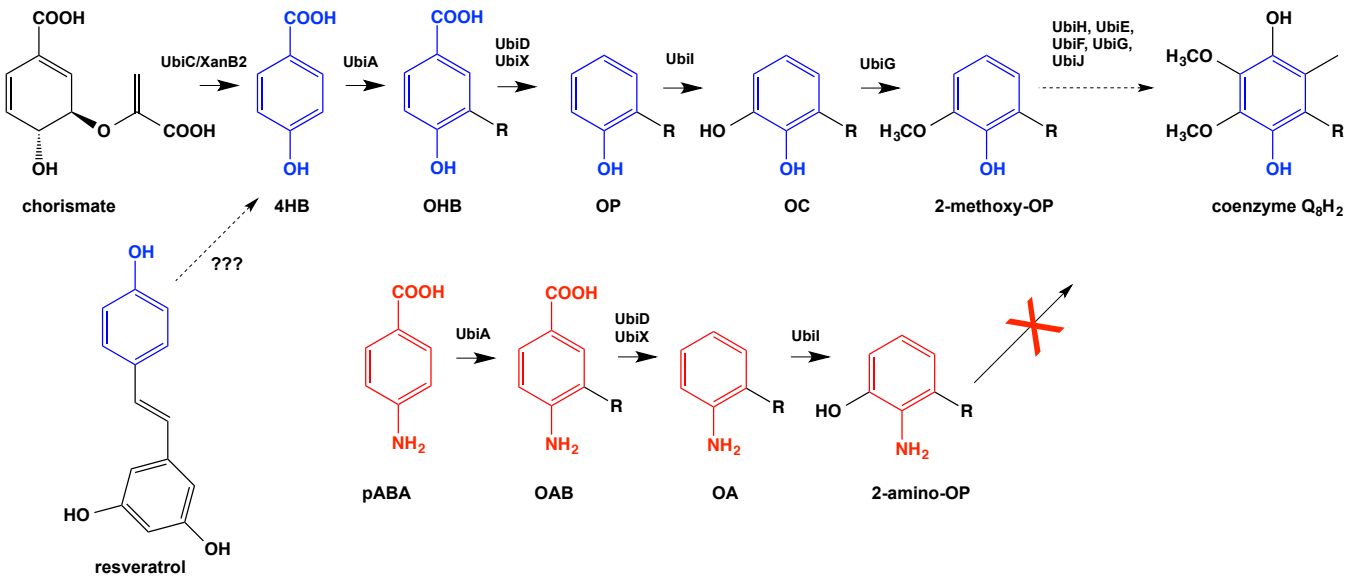



**Figure 1B. Q biosynthesis in *E. coli.*** UbiC converts chorismate to 4HB. UbiA then adds the octaprenyl tail (denoted with R) to the 4HB or pABA to form 3-octaprenyl-4-hydroxybenzoic acid (OHB) or 3-octaprenyl-4-aminobenzoic acid (OAB). UbiD and UbiX catalyzes the decarboxylation of the aromatic ring, forming 2-octaprenyl phenol or 2-octaprenyl aniline. UbiI adds the first hydroxyl to the ring to form OC or 2-amino-octaprenyl phenol. The pABA branch of the pathway stops at this step, while UbiG *O-methylates* OC to form 2-methoxy-OP. Additional ring modifications catalyzed by UbiH, UbiE, UbiF, UbiG and UbiJ form the final product $Q_8H_2$.

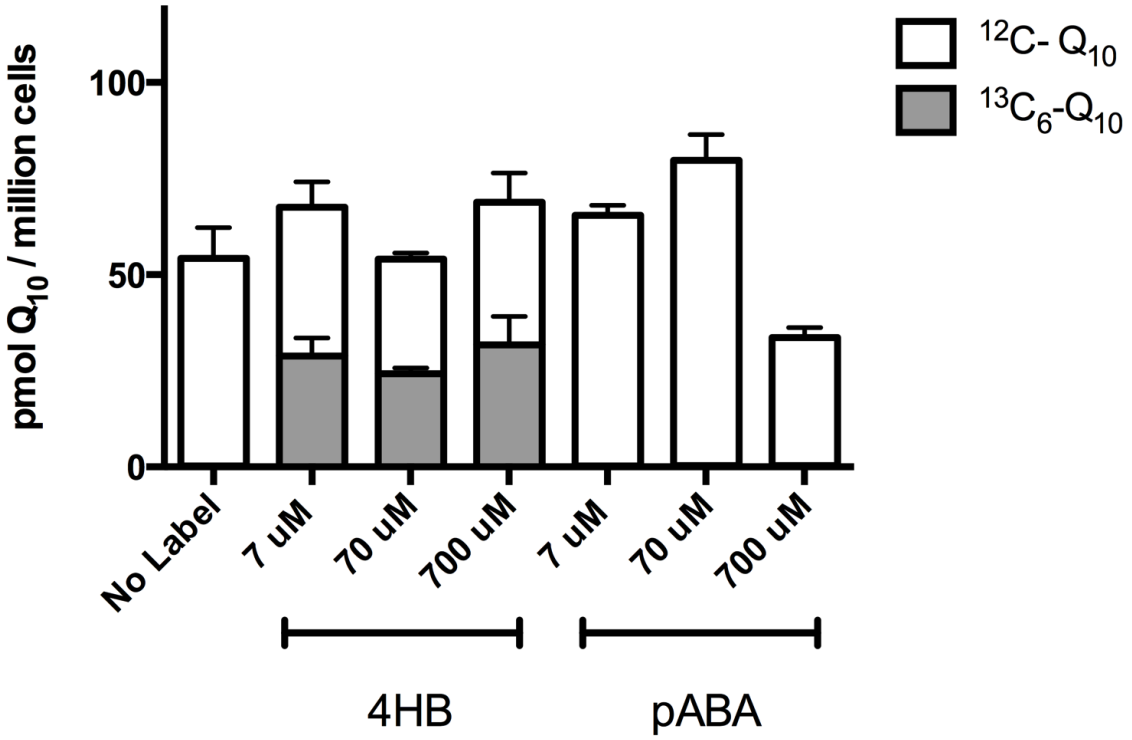



**Figure 2. pABA is not a precursor to $Q_{10}$ in mammalian cells.** U251 cells were cultured and processed as described in methods. Bar plot showing the total $Q_{10}$ content detected by LC/MS/MS under designated precursor conditions. The dark fraction of each bar represents $^{13}C_6$-$Q_{10}$, while the white fraction of each column represents $^{12}C$-$Q_{10}$. Error bars represent standard deviation with n=4. Cells treated with 7uM, 70uM, and 700uM of $^{13}C_6$-4HB contained significant amount of $^{13}C_6$-$Q_{10}$, while none of the $^{13}C_6$-pABA conditions yielded detectable $^{13}C_6$-$Q_{10}$. Cells incubated with 700 uM of $^{13}C_6$-pABA had significantly lower amount of total Q ($p<0.05$, One Way ANOVA).

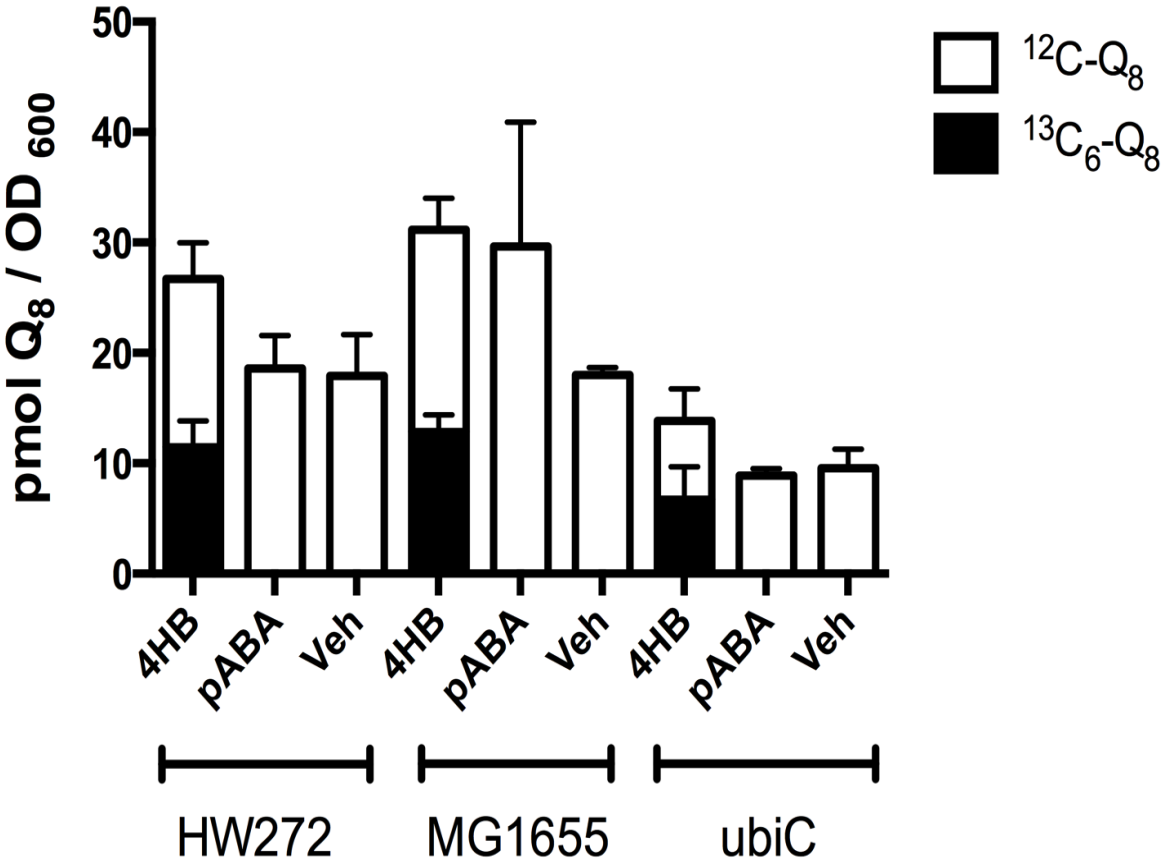



**Figure 3. pABA is not a precursor to $Q_8$ in *E. coli.*** HW272, MG1655 and *ubiC* cells were cultured and processed as described in the methods section. Plots showing total $Q_8$ content detected by LC/MS/MS under designated conditions. The dark fraction of each bar represents $^{13}C_6$-$Q_8$, while the white fraction of each column represents $^{12}C$-$Q_8$. Error bars represent standard deviation with n=4. Only cells from each background treated with $^{13}C_6$-4HB had $^{13}C_6$-$Q_8$. Ethanol was used as vehicle control here.

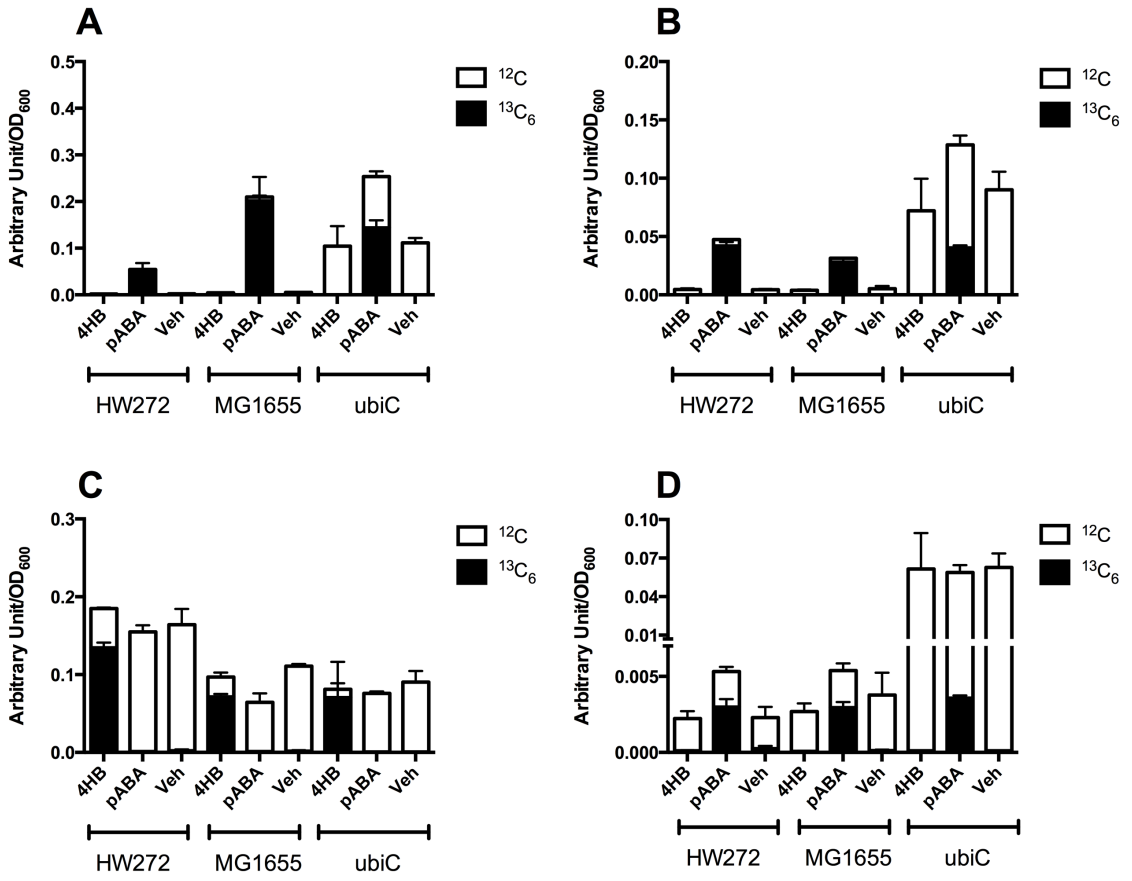
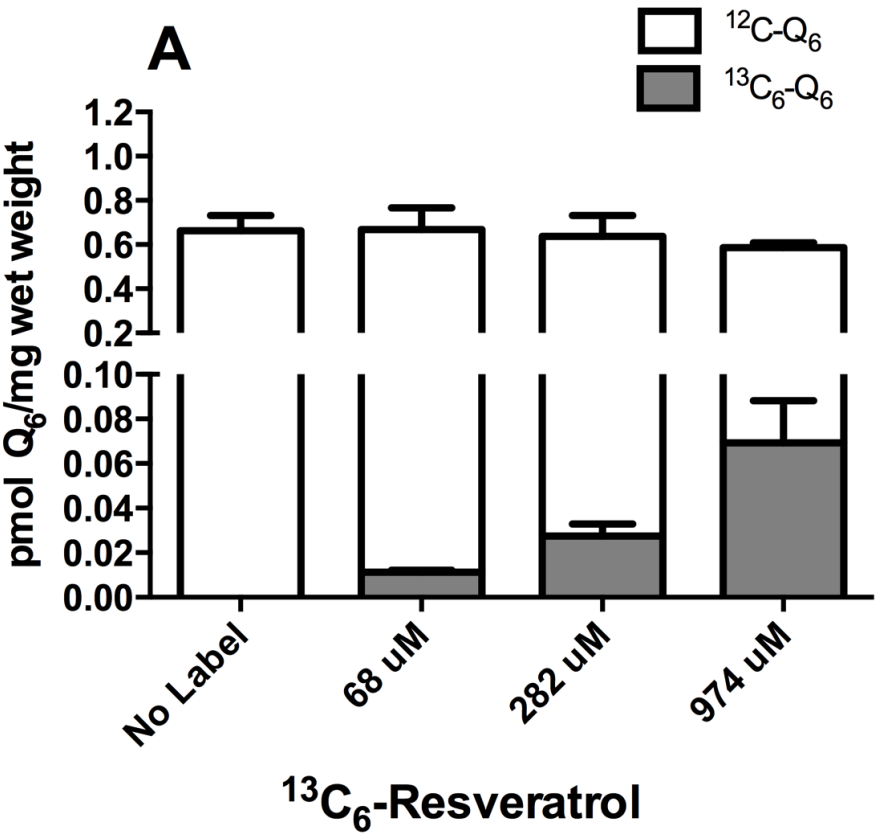



**Figure 4. pABA related intermediates in *E. coli.* Q biosynthesis.** HW272, MG1655 and *ubiC* cells were cultured and processed as described in the methods section. Bar plots showing total content of **a)** Octaprenyl amino benzoic acid (OABA), **b)** Octaprenyl Aniline(OA), **c)** Octaprenyl phenol (OP), and **d)** Octaprenyl amino phenol (OAP). Each bar represents mean ± SD. The dark fraction represents $^{13}C_6$ containing intermediates, while the white fraction of each column represents $^{12}C$ intermedaites. Y-axis represents area under the peak of interest first normalized by internal standard (Diethoxy $Q_{10}$), and then by $OD_{600}$.


A
$^{12}C$-$Q_6$
$^{13}C_6$-$Q_6$
pmol $Q_6$/mg wet weight
1.2
1.0
0.8
0.6
0.4
0.2
0.10
0.08
0.06
0.04
0.02
0.00
No Label
68 uM
282 uM
974 uM
$^{13}C_6$-Resveratrol

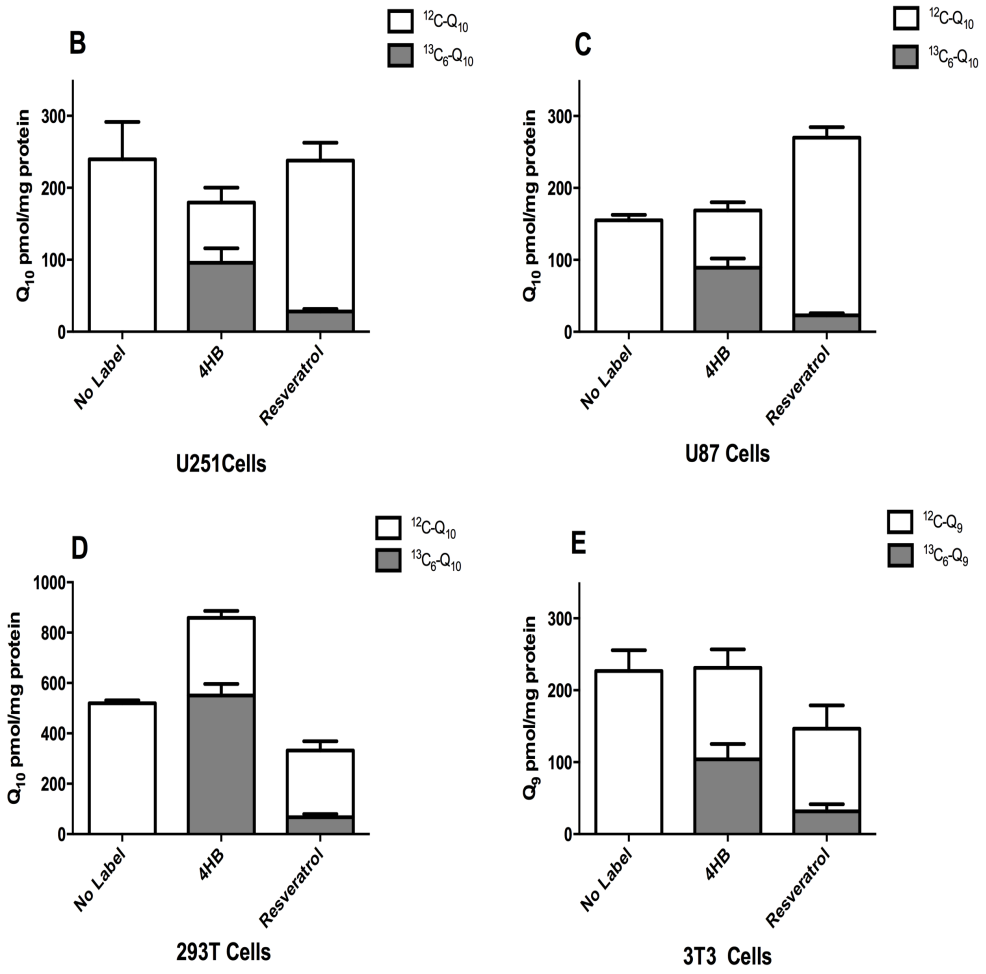



**Figure 5. Resveratrol is a ring precursor to Q biosynthesis in yeast *S. cerevisiae* and mammalian cells. A)**Yeast W303 wild type cells incubated with 0, 68uM, 282uM, and 975uM of $^{13}C_6$-resveratrol were cultured and analyzed as described in the methods section. The grey fraction represents $^{13}C_6$-$Q_6$ and the white fraction indicates $^{12}$C-$Q_6$. $Q_4$ was used as the internal standard. **b)** U251 cells, **c)** U87 cells, **d)** 293T cells, **e)** 3T3 cells were cultured in 0.1 % FBS in the presence of either $^{13}C_6$-4HB, $^{13}C_6$-resveratrol, or ethanol for 24 hours prior to collections. Collected cells were extracted and analyzed by LC/MS/MS as described in the methods. Each bar represents mean ± SD (n=4). The dark fraction represents $^{13}C_6$-$Q_{10}$ (b,c,d) or $^{13}C_6$-$Q_9$ (e), while the white fraction of each column represents $^{12}$C-Q.

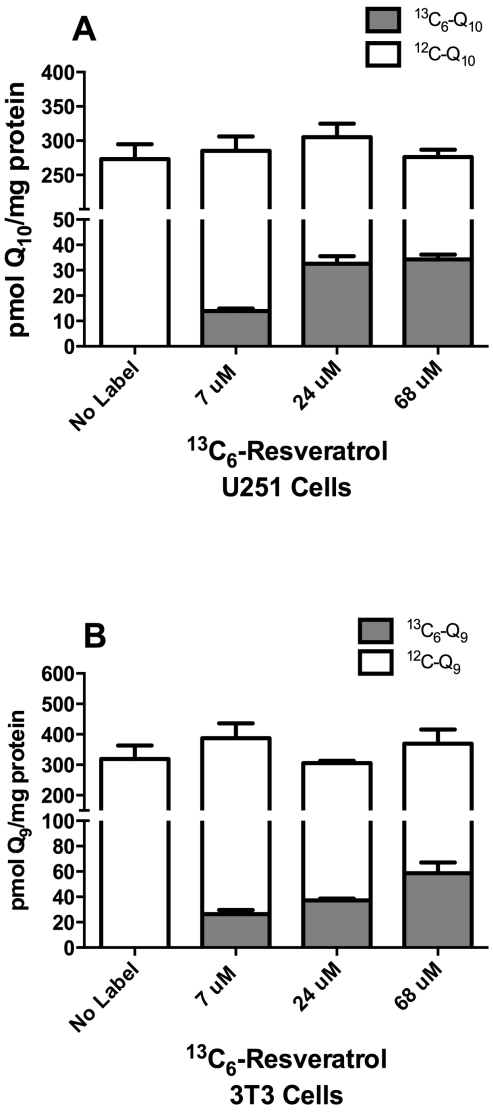



**Figure 6. Increase concentration of resveratrol did not alter total Q levels in mammalian cells. A)** U251 and **B)** 3T3 cells cultured in the presence of 0 uM, 7 uM, 24 uM, or 68 uM $^{13}C_6$-resveratrol were processed and analyzed by LC/MS/MS as described. The gray fractions represent $^{13}C_6$-containing Q, the white fractions represent Q derived from natural carbon precursors. The height of each bar indicates total Q content under each condition. Error bars represent SD (n=4). Diethoxy $Q_{10}$ was used as internal standard.

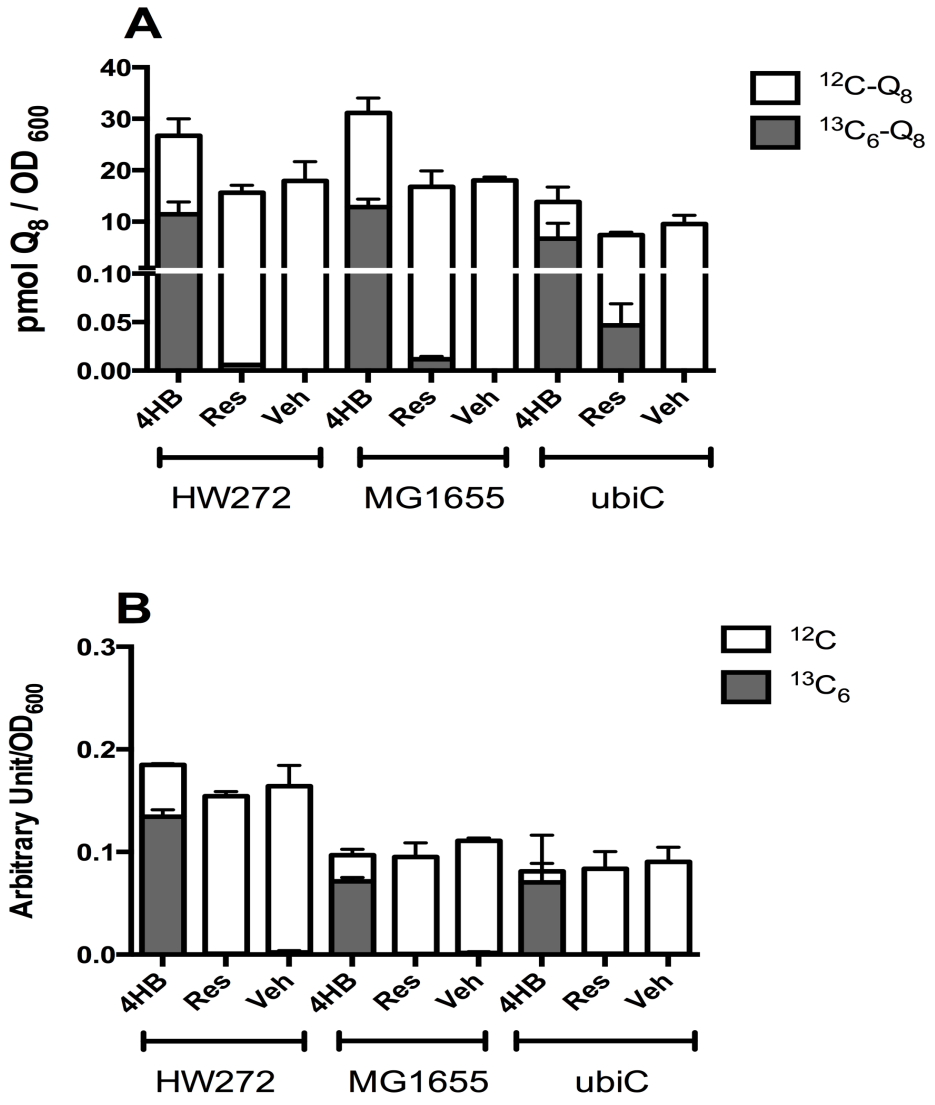



**Figure 7.** ***E. coli*** **ubiC mutant utilizes resveratrol better as a ring precursor to Q biosynthesis.** Wild type HW272, GM1655 cells and mutant *ubiC* cells were cultured in LB medium in the presence of 10ug/ml of $^{13}C_6$-4HB, $^{13}C_6$-resveratrol or plain ethanol. Collected cells were extracted and analyzed by LC/MS/MS as described. Each bar represents mean ± SD (n=4). The dark fraction represents (**A**) $^{13}C_6$-$Q_8$ or (**B**) $^{13}C_6$-octaprenyl-phenol, while the white fraction of each column represents (**A**) $^{12}$C-$Q_8$ or (**B**)$^{12}C_6$-octaprenyl-phenol.

# Chapter 5

# Perspectives

This work describes progress made in characterization of Coq8 and potential alternate ring precursors in Coenzyme Q biosynthesis. In Chapter 2, the enzymatic function of Coq8 was investigated. Seven distinct Q-less *coq8* point mutants that maintained steady-state levels of the Coq8 polypeptide were characterized. Over-expression of Coq8 human homolog ADCK3 harboring an amino-terminal yeast mitochondrial leader sequence successfully rescued growth of *coq8* mutants on non-fermentable carbon source and partially restored Q biosynthesis. The phosphorylation states of Coq3, Coq5, and Coq7 were detected with 2D-IEF gel electrophoresis and immune-blotting; the phosphorylated forms of these polypeptides were dependent on Coq8.A point mutation either before the conserved N-terminus motif or within the conserved kinase motif I abolished the phosphorylated states of Coq3, Coq5, and Coq7. Overexpression of human ADCK3 in *coq8* mutants was able to restore the phosphorylation states of Coq3, Coq5, and Coq7 similar to those in wild type.

Two dimensional iso-electric focusing followed by Western analysis results demonstrated indirectly that Coq8 was a protein kinase and the phosphorylation states of Coq3, Coq5, and Coq7 were Coq8 dependent. In order to test whether Coq8 directly phosphorylates Coq3, Coq5, and Coq7, an *in vitro* kinase assay is essential. I attempted to express and purify His-tagged yeast Coq8 in the *E. coli* system but failed to obtain enough amount of purified soluble Coq8 for the kinase assay. Thus, optimal purification conditions for Coq8 and its potential substrates Coq3, Coq5, and Coq7 need to be determined so that an *in vitro* kinase assay with $^{32}$P-ATP can be attempted again.

A recent study reported that phosphatase Ptc7 induced Q biosynthesis by activating Coq7 hydroxylase in yeast (6). This finding contrasts our findings that phosphorylation of Coq3, Coq5, and Coq7 in a Coq8 dependent manner stabilizes the Coq protein complex and induces Q biosynthesis. Thus, the rate of Q biosynthesis in wild type over-expressing *COQ8* with and without phosphatase should be closely studied. It will be interesting to find out the exact phosphorylation sites of Coq3, Coq5, and Coq7 and investigate the outcomes of mutating those phosphorylation sites. One strategy is to perform an affinity pull down experiment with tagged Coq polypeptide followed by proteomic analysis. Once enough protein is collected, the proteomic analyses should be able to reveal phosphorylation sites of Coq3, Coq5, and Coq7, and may also reveal sites in Coq polypeptides that were not resolved by 2D-IEF.

It was previously discovered that deletion of any one of the yeast *COQ* genes would result in the collapse of the high holecular mass Coq complex, which in turn destabilized the rest of the Coq polypeptides except Coq1, Coq2, Coq3, and Coq5(1). In Chapter 3, I discovered that over-expression of *COQ8* in certain yeast *coq3, coq4, coq5, coq6, coq7, coq9* null mutants restored the steady state levels of Coq3, Coq4, Coq6, Coq7 and Coq9. This finding created the possibility to employ Coq8 as a molecular tool to explore the yeast Q biosynthesis pathway. Indeed, over-expression of *COQ8* in *coq5, coq6, coq7,* and *coq9 null* mutants led to the accumulation of several novel and diagnostic Q biosynthetic intermediates. Yeast *coq5* null mutants harboring multi-copy *COQ8* accumulated demethyl-demethoxy-$Q_6$, *coq6* null and *coq9* null bearing multi-copy *COQ8* accumulated 3-hexaprenyl-4-hydroxyphenol and 3-hexaprenyl-4-aminophenol. Demethoxy-$Q_6$ and imino-demethoxy $Q_6$ were detected in *coq7 null* and *coq9* null

harboring multi-copy *COQ8.* The discovery of these novel Q intermediates provided key information in the Q biosynthesis pathway and suggested functional roles for Coq4 and Coq9.

In Chapter 4, I evaluated possible alternate aromatic ring precursors in Q biosynthesis in *E. coli, S. cerevisiae,* mouse and human cells. Marbois *et. al.* reported in 2010 that *para*-aminobenzoic was a precursor in Coenzyme $Q_6$ biosynthesis in yeast *S. cerevisiae*(2). This was a rather surprising finding since pABA was a precursor for folate biosynthesis and the addition of pABA to *E. coli* and human cells significantly inhibited Q biosynthesis(3,4). Thus, *E. coli,* mouse, and human cells were cultured in the presence of $^{13}C_6$-pABA to investigate whether pABA lowered the total Q content or if it indeed inhibited *de novo* Q biosynthesis. As a result, neither *E. coli* cells nor mammalian cells cultured with $^{13}C_6$-pABA synthesized detectable amounts of $^{13}C_6$-Q, indicating that pABA is not an alternative ring precursor in Q biosynthesis in *E. coli,* mouse, or human cells. Block *et. al* recently reported that Arabidopsis could use para-coumarate for Q biosynthesis (5). Because of the similarity in structure, I tested if resveratrol could be utilized for Q biosynthesis. Surprisingly, *E. coli,* yeast *S. cerevisiae,* and mammalian cells were all able to use resveratrol as a precursor to synthesize Q.

Overexpression of *COQ8* in *coq null* mutants stabilized other Coq polypeptides and resulted the accumulation of novel intermediates. This finding led us to postulate whether the stabilization of Coq polypeptide was achieved through the stabilization of the HMW Coq complex. It was later discovered *via* 2D blue native analysis that overexpression of *COQ8* indeed restored the HMW Coq complex in *coq3, coq5, coq6, coq7, coq9 null* mutants(7). Our collaborator Pierrel *et. al* utilized 2,4-dihydroxy benzoic acid to bypass the *coq6* mutation and

restored Q biosynthesis in *coq6 null*. This approach, together with the overexpression of *COQ8* created a new set of tools that now allow researchers to further investigate the yeast Q biosynthesis pathway. Furthermore, an array of small molecules, such as vanillic acid, 2,3-dihydroxy benzoic acid, 4-aminosalicylic acid and others can now be employed to characterize Coq polypeptides with undetermined functions. As we postulated that Coq9 might involve with the removal of nitrogen from N-containing intermediates, it will be interesting to apply 2,4-dihydroxybenzoic acid and 4-aminosalicylic acid, together with *COQ8* overexpression to *coq9* null mutants to test this hypothesis.

In Chapter 4, LC/MS/MS analyses detected no $^{13}C_6$-Q derived from $^{13}C_6$-pABA in *E. coli*, mouse or human cells. However, multiple $^{13}C_6$-pABA derived intermediates were detected in both wild type *E. coli* and *ubiC* mutants. Non-targeted LC/MS/MS approach should be employed to detect whether there's more N-containing intermediates derived from pABA further downstream. In mammalian cells, I failed to detect any N-containing intermediates; even decaprenyl *para*-aminobenzoic acid was not detectable. Thus uptake of pABA by mammalian cells was not directly verified. Therefore, optimal LC/MS/MS conditions for the detection of N-containing intermediates in mammalian cells need to be developed.

Of the more than one hundred clinical trials testing the efficacy of resveratrol or other polyphenols, few determine the metabolic fate of the administered supplement. When metabolism of resveratrol is studied, the focus is on aqueous soluble polar metabolites of resveratrol, including sulfated and glucuronidated conjugation products (8). The new finding that

resveratrol can convert into Q pose an interesting question regarding the molecular mechanism of such conversion.

**References**


1. Hsieh, E. J., Gin, P., Gulmezian, M., Tran, U. C., Saiki, R., Marbois, B. N., and Clarke, C. F. (2007) Saccharomyces cerevisiae Coq9 polypeptide is a subunit of the mitochondrial coenzyme Q biosynthetic complex. *Arch Biochem Biophys* **463**, 19-26
2. Marbois, B., Xie, L. X., Choi, S., Hirano, K., Hyman, K., and Clarke, C. F. (2010) para-Aminobenzoic acid is a precursor in coenzyme Q6 biosynthesis in Saccharomyces cerevisiae. *J Biol Chem* **285**, 27827-27838
3. Hamilton, J. A., and Cox, G. B. (1971) Ubiquinone biosynthesis in Escherichia coli K-12. Accumulation of an octaprenol, farnesylfarnesylgeraniol, by a multiple aromatic auxotroph. *Biochem J* **123**, 435-443
4. Turunen, M., Olsson, J., and Dallner, G. (2004) Metabolism and function of coenzyme Q. *Biochim Biophys Acta* **1660**, 171-199
5. Block, A., Widhalm, J. R., Fatihi, A., Cahoon, R. E., Wamboldt, Y., Elowsky, C., Mackenzie, S. A., Cahoon, E. B., Chapple, C., Dudareva, N., and Basset, G. J. (2014) The Origin and Biosynthesis of the Benzenoid Moiety of Ubiquinone (Coenzyme Q) in Arabidopsis. *The Plant cell*
6. Martin-Montalvo, A., Gonzalez-Mariscal, I., Pomares-Viciana, T., Padilla-Lopez, S., Ballesteros, M., Vazquez-Fonseca, L., Gandolfo, P., Brautigan, D. L., Navas, P., and Santos-Ocana, C. (2013) The phosphatase Ptc7 induces coenzyme Q biosynthesis by activating the hydroxylase Coq7 in yeast. *J Biol Chem* **288**, 28126-28137
7. He, C. H., Xie, L. X., Allan, C. M., Tran, U. C., and Clarke, C. F. (2014) Coenzyme Q supplementation or over-expression of the yeast Coq8 putative kinase stabilizes multi-

subunit Coq polypeptide complexes in yeast coq null mutants. *Biochim Biophys Acta* **1841**, 630-644

8. Walle, T. (2011) Bioavailability of resveratrol. *Ann N Y Acad Sci* **1215**, 9-15

# Appendix I

THE JOURNAL OF BIOLOGICAL CHEMISTRY VOL. 285, NO. 36, pp. 27827–27838, September 3, 2010
© 2010 by The American Society for Biochemistry and Molecular Biology, Inc. Printed in the U.S.A.

# *para*-Aminobenzoic Acid Is a Precursor in Coenzyme $Q_6$ Biosynthesis in *Saccharomyces cerevisiae*[*]

Received for publication, June 5, 2010, and in revised form, June 30, 2010 Published, JBC Papers in Press, June 30, 2010, DOI 10.1074/jbc.M110.151894

**Beth Marbois[‡§], Letian X. Xie[‡], Samuel Choi[‡], Kathleen Hirano[‡], Kyle Hyman[‡], and Catherine F. Clarke[‡§1]**

*From the [‡]Department of Chemistry and Biochemistry and the [§]Molecular Biology Institute, University of California, Los Angeles, California 90095-1569*

**Coenzyme Q (ubiquinone or Q) is a crucial mitochondrial lipid required for respiratory electron transport in eukaryotes. 4-Hydroxybenzoate (4HB) is an aromatic ring precursor that forms the benzoquinone ring of Q and is used extensively to examine Q biosynthesis. However, the direct precursor compounds and enzymatic steps for synthesis of 4HB in yeast are unknown. Here we show that *para*-aminobenzoic acid (*p*ABA), a well known precursor of folate, also functions as a precursor for Q biosynthesis. A hexaprenylated form of *p*ABA (prenyl-*p*ABA) is normally present in wild-type yeast crude lipid extracts but is absent in yeast *abz1* mutants starved for *p*ABA. A stable $^{13}C_6$-isotope of *p*ABA (*p*-amino[*aromatic*-$^{13}C_6$]benzoic acid ([$^{13}C_6$]*p*ABA)), is prenylated in either wild-type or *abz1* mutant yeast to form prenyl-[$^{13}C_6$]*p*ABA. We demonstrate by HPLC and mass spectrometry that yeast incubated with either [$^{13}C_6$]*p*ABA or [$^{13}C_6$]4HB generate both $^{13}C_6$-demethoxy-Q (DMQ), a late stage Q biosynthetic intermediate, as well as the final product $^{13}C_6$-coenzyme Q. Pulse-labeling analyses show that formation of prenyl-*p*ABA occurs within minutes and precedes the synthesis of Q. Yeast utilizing *p*ABA as a ring precursor produce another nitrogen containing intermediate, 4-imino-$DMQ_6$. This intermediate is produced in small quantities in wild-type yeast cultured in standard media and in *abz1* mutants supplemented with *p*ABA. We suggest a mechanism where Schiff base-mediated deimination forms $DMQ_6$ quinone, thereby eliminating the nitrogen contributed by *p*ABA. This scheme results in the convergence of the 4HB and *p*ABA pathways in eukaryotic Q biosynthesis and has implications regarding the action of *p*ABA-based antifolates.**

Coenzyme Q (Q)[2] is an essential polyprenylated benzoquinone lipid in cellular energy metabolism. The prenyl tail anchors Q in cellular membranes, whereas the redox chemistry of the benzoquinone ring plays a crucial role in respiratory electron transport, in catabolic and biosynthetic metabolism (1), as a co-antioxidant able to recycle vitamin E, and as a chain-terminating antioxidant (2). In these reactions the quinone ring of Q thus cycles between oxidized and reduced ($QH_2$, or hydroquinone) states.

Cells rely on *de novo* synthesis for an adequate supply of Q. Studies in *Escherichia coli*, *Schizosaccharomyces pombe*, and *Saccharomyces cerevisiae* have made use of Q-deficient mutants to elucidate the biosynthetic pathway (3–5). In *S. cerevisiae*, nine *COQ* genes are required, and each of the yeast *coq* mutants (*coq1* through *coq9*) lack $Q_6$ and are unable to grow on media containing non-fermentable carbon sources such as glycerol or ethanol. The dedicated precursors in the biosynthesis of Q are polyisoprene diphosphate, which provides the tail (*S. cerevisiae* synthesizes $Q_6$, with a tail containing six isoprene units), and 4-hydroxybenzoic acid (4HB) (6, 7). Studies in animal cells and in *E. coli* indicate that different metabolic pathways are used to produce 4HB. Animals (*e.g.* rats and humans) generate 4HB from the essential dietary amino acid tyrosine (6–8). Phenylalanine also acts as a precursor for 4HB, however, the incorporation is thought to proceed primarily following its conversion to tyrosine via phenylalanine hydroxylase (8). The biosynthetic steps leading from 4-hydroxyphenylpyruvate to 4HB in animal cells are not yet characterized (see Fig. 1). *E. coli* relies on shikimate biosynthesis, the formation of chorismate, and chorismate pyruvate lyase (encoded by the *ubiC* gene) to synthesize 4HB (9, 10). *E. coli ubiC* mutants lack Q unless 4HB is provided in the growth media (9). *E. coli* mutants lacking shikimate or chorismate also require exogenous 4HB to synthesize Q (11). Thus, *E. coli* cells are unable to convert tyrosine or phenylalanine to Q and rely exclusively on the *de novo* synthesis of 4HB from chorismate.

In contrast, *S. cerevisiae* may utilize either shikimate or tyrosine to synthesize the aromatic ring precursor of Q (6, 12). Yeast preferentially utilize shikimate to produce Q, and tyrosine is utilized only when the synthesis of shikimate is blocked (12). Thus, yeast *aro1C* mutants (unable to synthesize shikimate), and yeast *aro2* mutants (unable to synthesize chorismate) still synthesize Q *de novo*, because they are able to utilize exogenously added tyrosine (Fig. 1). The steps producing 4HB from tyrosine have not been identified, although the pathway may be similar to that described for the catabolism of *p*-coumarate to 4HB in *Acinetobacter bayli* (13). Although it has been assumed that yeast may generate 4HB via chorismate pyruvate lyase activity, *S. cerevisiae* lack a homolog of UbiC. This raises the

* This work was supported, in whole or in part, by National Institutes of Health Grant GM4592 (to C. F. C.). This work was also supported by National Science Foundation Grant 0919609 (to C. F. C. and B. M.). UCLA mass spectrometry resources were funded by a NIH grant 4000QT for mass spectrometry resources and Grant S10RR024605 from the National Center For Research Resources.

[1] To whom correspondence should be addressed: Dept. of Chemistry and Biochemistry, University of California, Los Angeles, 607 Charles E. Young Drive East, Los Angeles, CA 90095-1569. Tel.: 310-825-0771; Fax: 310-206-5213; E-mail: cathy@chem.ucla.edu.

[2] The abbreviations used are: Q, coenzyme Q; [$^{13}C_6$]4HB, *p*-hydroxy[*aromatic*-$^{13}C_6$]benzoic acid; [$^{13}C_6$]*p*ABA, *p*-amino[*aromatic*-$^{13}C_6$]benzoic acid; DMQ, demethoxy-Q; ESI-MS/MS, electrospray ionization mass spectrometry; HHB, 3-hexaprenyl-4-hydroxybenzoic acid; 4HB, 4-hydroxybenzoic acid; 4-imino-$DMQ_6$, 3-hexaprenyl-4-imino-5-methoxy-2-methylcyclohexa-2,5-dienone; *p*ABA, 4-aminobenzoic acid; prenyl-*p*ABA, 3-hexaprenyl-4-aminobenzoic acid; psig, pound-force per square inch gauge; $Q_6$, coenzyme $Q_6$ with a tail of 6 isoprene units; $Q_6H_2$, reduced or hydroquinone form of $Q_6$; RP, reverse phase.



Downloaded from http://www.jbc.org/ at UCLA-Louise Darling Biomed. Lib. on July 2, 2014

question: how do yeast utilize chorismate to produce a ring precursor of Q?

Here we describe our surprising findings that *para*-aminobenzoic acid (*p*ABA), a known precursor of folates, is also an aromatic precursor for Q biosynthesis, via the synthesis of 3-hexaprenyl-4-aminobenzoic acid (prenyl-*p*ABA). These pathways are described in Fig. 1. The biosynthetic steps in yeast necessary for the production of *p*ABA are catalyzed by the *ABZ1* and *ABZ2* gene products. Abz1 amidates chorismate to make the 4-aminodeoxychorismate intermediate (14, 15), and the Abz2 lyase forms free *p*ABA (16). Import of *p*ABA into the mitochondria is necessary for further folate synthesis; the *FOL1* gene product is required for this import and also performs multiple enzymatic functions in pteroglutamoyl synthesis (17). Immunogold particle labeling and a Fol1-GFP fusion localized the tri-functional polypeptide Fol1p in yeast to mitochondrial membranes (17).

We recently became aware of similar work identifying *p*ABA and prenyl-*p*ABA as Q biosynthetic precursors (18). These authors identified *p*ABA as a Q precursor in their search for iron-mediated effects on the function of the Coq7 monooxygenase in Q biosynthesis. Our studies independently determined that *p*ABA is a novel coenzyme Q precursor, and we show prenyl-*p*ABA is an endogenously synthesized intermediate in the Q biosynthetic pathway. We further demonstrate the relative contributions of the $^{13}C_6$-isotope of 4HB and *p*ABA under competition conditions with the alternative unlabeled ring precursor. In addition we identify 4-imino-$DMQ_6$ in wild-type yeast and in *p*ABA-supplemented *abz1* null mutants. Based on our identification of this intermediate, we suggest a possible mechanism for the removal of the nitrogen donated by *p*ABA, and its replacement with an oxygen atom to form the 1,4-quinone moiety in DMQ via Schiff base chemistry.

## EXPERIMENTAL PROCEDURES

*Yeast Growth Analysis*—Yeast strains used in this work are described in Table 1. The *abz1* null mutant (W303Δ*abz1*) was generated as described (19). Yeast colonies from YPD (2% glucose, 1% yeast extract, 2% peptone, 2% agar) plates were inoculated into 18- × 100-mm culture tubes containing 5 ml of *D*rop *O*ut *Gal*actose (Dogal media): 2% galactose, 0.1% dextrose, and 6.8 g/liter Bio101 yeast nitrogen base minus *p*ABA minus folate with ammonium sulfate (MP Biomedicals) and 5.83 mM sodium monophosphate (pH adjusted to 6.0 with NaOH). Amino acids and nucleotides were included at the following final concentrations (milligrams/liter): adenine hemisulfate, 80; arginine hydrochloride, 40; aspartic acid, 100; cysteine hydrochloride, 80; glutamic acid, 100; histidine hydrochloride, 80; isoleucine, 60; leucine, 120; lysine hydrochloride, 60; methionine, 80; phenylalanine, 80; serine, 60; threonine, 400; tryptophan, 200; tyrosine, 40; uracil, 80; and valine, 150. Following overnight incubation, yeast cultures were diluted 1:100 into fresh Dogal minimal media to deplete intrinsic stores of *p*ABA and folate. Alternatively, cultures were diluted into *D*rop *O*ut *G*lycerol *E*thanol media (Doge; made as above, except galactose was

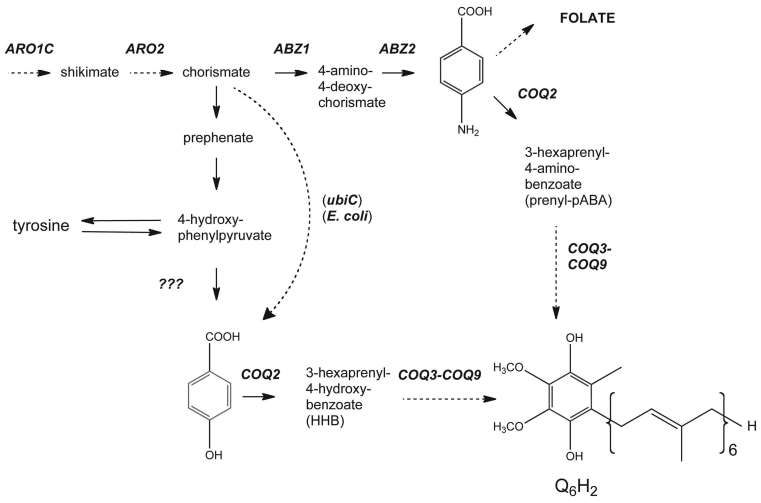



FIGURE 1. **Yeast aromatic ring precursors involved in Q biosynthesis.** We propose that yeast generate aromatic precursors for Q biosynthesis by at least two pathways. One branches from chorismate to produce *p*ABA, a new aromatic ring precursor in Q biosynthesis. The other pathway also branches from chorismate to produce the typical aromatic ring precursor 4HB, via unknown gene products from tyrosine or 4-hydroxyphenylpyruvate. Both 4HB and *p*ABA are prenylated by Coq2. Yeast lack a homolog of *E. coli* UbiC (chorismate pyruvate lyase), which directly forms 4HB from chorismate (*dotted line*). Animals lack the ability to produce shikimate, and rely on Tyr (or Phe) for production of 4HB. The steps involved in converting 4-hdroxyphenylpyruvate to 4HB are not known in yeast or animal cells.

**TABLE 1**
**Genotypes and sources of *S. cerevisiae* strains**

| Strain | Genotype | Source |
|---|---|---|
| W303-1A | MATa *ade2-1 his3-1,15 leu2-3,112 trp1-1 ura3-1* | R. Rothstein[a] |
| W303ΔCOQ2 | MATa *ade2-1 his3-1,15 leu2-3,112 trp 1-1 ura3-1 coq2::HIS3* | (49) |
| W303ΔABZ1 | MATa *ade2-1 his3-1,15 leu2-3,112 trp1-1 ura3-1 abz1::KANMX4* | This work |
| NM101 | MATa *leu2-3,112, ura3-52, coq7-1* | (29) |
| E2–249 | MATa *met6, coq3* | (50) |
| BY4741 | MATa *his3Δ1 leu2Δ0 met15Δ0 ura3Δ0* | (51)[b] |
| BY4741Δabz1 | MATa *abz1Δ::kanMX4 his3Δ1 leu2Δ0 met15Δ0 ura3Δ0* | (52)[b] |

[a] Dept. of Human Genetics, Columbia University, New York, NY.
[b] European *Saccharomyces cerevisiae* Archive for Functional Analysis (EUROSCARF), available on-line.

Downloaded from http://www.jbc.org/ at UCLA-Louise Darling Biomed. Lib. on July 2, 2014

replaced with 3% glycerol, 2% ethanol). Solid plate media were made by adding 2.5 g/liter Gelrite (Sigma). When noted media were supplemented with folinic acid, 0.4 $\mu$g/ml; 4HB, 2 $\mu$g/ml; or *p*ABA (Sigma) 2 $\mu$g/ml.

*Radioactive and Stable Isotope Labeling*—Radioactive compounds included *p*-hydroxy[U-$^{14}$C]benzoic acid (450 mCi/mmol, 0.1 mCi/ml, American Radiolabeled Chemicals, Inc., St. Louis, MO), and *p*-amino[*aromatic*-$^{14}$C]benzoic acid (57 mCi/mmol, 0.1 mCi/ml, Moravek Biochemicals, Brea CA). *p*-Amino[*aromatic*-$^{13}C_6$]benzoic acid ([$^{13}C_6$]*p*ABA) or *p*-hydroxy-[*aromatic*-$^{13}C_6$]benzoic acid ([$^{13}C_6$]4HB) were obtained from Cambridge Isotope Laboratories (Andover, MA). The manufacturers' analyses of the pure $^{13}$C-labeled aromatic ring compounds by GC-MS and NMR verified a better than 98% chemical purity with 99% isotopic enrichment. $^{13}C_6$- and $^{14}$C-labeled aromatic ring precursors were also examined for purity by HPLC. Yeast cells were grown as described to deplete *p*ABA and folate. Optical density (*A*) measurements (600 nm) were recorded for each sample at time of harvest, and the total $A_{600\ nm}$ values were used to normalize lipid content. For radioactive labeling studies, the cells were suspended in 300–600 ml of fresh media as above (Dogal or Doge) and grown to an $A_{600\ nm}$ of 0.6, then collected by centrifugation (1000 $\times$ *g*, 5 min) and resuspended in small volumes of fresh media (~2 ml), containing 4 $\mu$Ci, of the designated $^{14}$C-labeled ring precursor. Cells were collected by centrifugation as before, and pellets were stored at −20 °C. Stable isotopic labeling was essentially as above except that individual amounts of [$^{13}C_6$]*p*ABA or [$^{13}C_6$]4HB were weighed and dissolved in DMSO (Sigma), and then added to a final concentration of 2–10 $\mu$g/ml.

*Competition and Pulse Experiments*—Time course and competition experiments with normal and stable isotope forms of precursors were conducted in 18- $\times$ 100-mm culture tubes. Cells were collected from a larger volume culture, and equivalent optical density amounts of yeast cells (between 20 and 100 $A_{600\ nm}$) were re-suspended in 5 ml of fresh media as described, which contained either the DMSO (vehicle control), [$^{13}C_6$]*p*ABA, or [$^{13}C_6$]4HB at 10 $\mu$g/ml, or each of these plus an additional 10 $\mu$g/ml of the competing unlabeled precursor 4HB or *p*ABA. These samples were prepared in duplicate or triplicate, and analyzed via mass spectrometry two or three times ($n$ = 4–9). For pulse analyses cells were grown in large volume as described above, re-suspended in pre-warmed media (30 °C) to a total volume of 16 ml in a 125-ml flask, and incubated with shaking (250 rpm, 30 °C). Prior to addition of labeled ring precursors, two (1 ml) aliquots were removed, to represent a "no-label" control. [$^{13}C_6$]*p*ABA was added (final concentration, 10 $\mu$g/ml), and further 1-ml aliquots were collected in duplicate at the time points as described. The time zero point was defined by removing two aliquots prior to addition of labeled precursors. The first time point (termed 2 min) represented the addition of label with mixing and immediate removal of two sequential samples, effectively allowing the label to be present for ~1 min and 3 min, respectively.

*Lipid Extraction*—Yeast cell pellets were thawed on ice, and solvents were added as follows: 100 $\mu$l of $H_2O$, 1 ml of methanol, and 2 ml of petroleum ether. Samples were vortexed for 30 s each. This was repeated, and then samples were centrifuged at 1000 $\times$ *g* to separate layers. The upper layer was moved to a new tube, 2 ml of petroleum ether was added to the lower phase, and the sample was vortexed. This upper phase was added to the previous upper organic phase, and the solvent was evaporated under $N_2$ gas. Samples were routinely analyzed immediately after extraction. When Q or other intermediates were quantified, $Q_4$ (Sigma) was added in a known amount (expected final concentration, 1 pmol/$\mu$l upon analysis) as internal standard to all samples, and to a simultaneously prepared and extracted calibration curve. Typical standard curve final concentrations were 0.2 fmol/$\mu$l, 1 fmol/$\mu$l, 25 fmol/$\mu$l, 200 fmol/$\mu$l, 1 pmol/$\mu$l, and 5 pmol/$\mu$l. The petroleum ether extracts were dried under nitrogen gas and resuspended in 200 $\mu$l of ethanol (USP, Aaper Alcohol and Chemical Co., Shelbyville, KY), in sample vials compatible for use with HPLC. Lipid extractions for the pulse experiments were similar, except that the cells were collected onto glass microfiber filter disks (Whatman) placed on a vacuum apparatus, and the collected cells and disks were immersed in ice-cold methanol (2 ml), containing 125 $\mu$l of 0.1% bromcresol green. Samples were stored in methanol at −20 °C. $Q_4$ was added as an internal standard as described above, and samples were kept on ice during the extraction. Re-extraction with petroleum ether (3 ml) was repeated two times. For all quantitative analyses, the standard curve was prepared and analyzed along side the samples, with freshly prepared internal standard and analytes. Routinely, the low end of the standard curve was monitored for recovery of the analyte by comparison of these concentrations a non-extracted standard curve. To ensure that analytes in low concentration gave a reproducible response, a signal to noise threshold ratio was set at 5. If measured analytes did not meet these criteria, or if the standard integrations did not identify the peak of interest accurately, the data were not used.

*RP-HPLC and Detection by Scintillation Counting*—Detection of radioactive coenzyme Q and intermediates used a B-ram model 2 (IN/US Systems, Inc., Tampa, FL) with a 500-$\mu$l flow cell. The column eluate was combined with Safety Solve (Research Products International Corp., Mount Prospect, IL) at a 2:1 ratio with a dwell setting of 1. Data from the device were collected into the Chem Station software supplied with the Agilent 1090 HPLC system. Simultaneous UV data were collected from the intrinsic diode array detector, 274 ± 4 nm, and 250 ± 4 nm. The system contained a Peltier cooled sample chamber maintained at 4 °C and a column oven set to 40 °C. A binary HPLC solvent delivery system was used with a phenyl-hexyl column (Luna 5$\mu$, 100 $\times$ 4.60 mm, 5 $\mu$m, Phenomenex). The mobile phase consisted of Solvent A (methanol:isopropanol, 95:5, with 2.5 mM ammonium formate) to Solvent B (isopropanol, 2.5 mM ammonium formate) beginning at 100% Solvent A and over 8 min decreasing to 95%. The total run time was 11 min. Sample volumes for injection ranged from 40 to 70 $\mu$l, and the software was set to respond at 1 mV = 1 cpm.

*RP-HPLC with Detection by MS*—A 4000 QTRAP linear MS/MS spectrometer from Applied Biosystems (Foster City, CA) was used in combination with an Agilent Technologies 1200 HPLC system consisting of a PAL autosampler with thermostatted tray holders and Stack (LEAP Technologies, Carrboro, NC). Nitrogen was used for all gases in the mass

Downloaded from http://www.jbc.org/ at UCLA-Louise Darling Biomed. Lib. on July 2, 2014

spectrometer; the nitrogen gas was provided as boil-off from a bulk liquid nitrogen storage tank. Applied Biosystems software, Analyst version 1.4.2, was used for data acquisition and processing. Infusion experiments for tuning and optimization were performed with a model 11 plus syringe infusion pump (Harvard Apparatus, Inc., South Natick, MA). RP-HPLC separation was performed as described above. The 4000QT spectrometer was operated in Turbo electrospray positive mode. Q1 and Q3 were operated in unit resolution. For multiple reaction monitoring detection, the precursor-to-product ion transitions in multiple reaction monitoring mode were used to quantify Q and intermediates (*m/z*): 591.4/197 ($Q_6$), 455.2/197 ($Q_4$), 561.4/167.0 ($DMQ_6$), and 546.4/150 (prenyl-*p*ABA). Optimum positive turbospray conditions for coenzyme Q compounds: nebulizer gas, 50 psig; turbo gas, 60 psig; curtain gas, 20 psig; collision gas set to "medium"; nebulizer current, 20; and temperature, 450 °C. Optimal settings for compound-dependent parameters are in volts, and dwell is in milliseconds (data are declustering potential, entrance potential, collision energy, collision cell exit potential, and dwell): $Q_4$ (75, 10, 29, 12, and 125), $Q_6$ (111, 10, 37, 10, and 125), $DMQ_6$ (96, 9, 37, 11, and 125), and prenyl-*p*ABA (96, 9, 33, 11, and 125). The same settings were used for $^{13}C$-labeled forms. Settings as described are theoretical and based on differences required for the analyses of farnesylated standards (20), with a compensation for increased isoprene length. For ion trap detection, similar gases as above were used for Q and Q intermediates: nebulizer gas, 45 psig; turbo gas, 55 psig; curtain gas, 25 psig; collision gas, high; nebulizer current, 35; and temperature, 450 °C. The enhanced product ion scan used default dynamic settings for trap filling and other parameters. The mass spectrometer detection conditions also included an enhanced resolution scan with standard parameters, between *m/z* 520 and *m/z* 620. The injection volume was 10 or 20 μl. Stock solutions of the $Q_4$ and $Q_6$ (Sigma) were prepared in hexanes and stored under argon gas at −20 °C. Aliquots added to ethanol and the concentrations were then determined spectrophotometrically with a molar extinction coefficient of $E$ = 14,900 at 275 nm (21). Integration of peak areas was performed with Analyst software, with a bunching factor of 1 and 3 smoothing events. Area ratios were constructed in Microsoft Excel for the calibration curve and experimental samples. The slope was calculated with a linear curve forced through zero. Standard deviations represent duplicate/triplicate samples, independently extracted with duplicate/triplicate injections ($n$ = 4–6).

## RESULTS

*Prenyl-pABA Is a Naturally Occurring Lipid Component of Yeast Cells*—Neutral lipid extracts prepared from wild-type yeast cells cultured in standard rich media contain a lipid that we have identified as prenyl-*p*ABA. The identification of prenyl-*p*ABA was based on the presence of an HPLC peak with an elution similar to that for HHB, a previously characterized yeast Q intermediate (22). The precursor ion $[M+H]^+$ of 546, and predominant tropylium [*m/z* = 150] and chromenylium [*m/z* = 190] product ions, detected in ion-trap analyses, were consistent with a ring amino replacing the ring hydroxyl present in HHB (Fig. 2*A*). The tropylium-like ion is a transition ion generated from prenylated aromatic and benzoquinone rings and is formed under dissociation conditions by incorporation of a methylene remnant (produced by fragmentation of the prenyl tail after the first carbon) to form a 7-membered ring (23). The chromenylium-like ion is larger in mass by +40 ($C_3H_4$) under these electrospray ionization conditions and is derived by fragmentation and cyclization to include the first four prenyl tail carbons (23).

To confirm the identity of prenyl-*p*ABA, wild-type yeast (W303-1A) were pre-cultured in Dogal media (minus *p*ABA and folate) to deplete cellular stores of *p*ABA (16). Either dextrose or galactose can be used as a fermentable carbon source in minimal media; galactose is used because it is non-repressing to aerobic respiration (24). Yeast cells were transferred to fresh Dogal medium plus folate, and then cultured in the presence of [$^{13}C_6$]*p*ABA as described under "Experimental Procedures." Product ion analyses from the crude lipids of yeast grown in the presence of [$^{13}C_6$]*p*ABA show that yeast incorporate the ring carbons into prenyl-*p*ABA to generate prenyl-[$^{13}C_6$]*p*ABA ($^{13}C_6{}^{12}C_{31}H_{55}NO_2$) (Fig. 2*B*). Although prenyl-*p*ABA is readily detectable in lipid extracts of wild-type yeast (W303-1A harvested at 1.8 *A* in YPGal media contain 89.0 ± 5.6 fmol/*A*), it is much less abundant than $Q_6$ (84.6 ± 4.3 pmol) under standard log phase growth conditions in rich media.

*Yeast coq3 Mutants Cultured with $^{13}C_6$-4HB Produce $^{13}C_6$-labeled HHB*—Previous work has shown that yeast *coq* mutants grown in the presence of 4HB produce HHB (25). However, this intermediate is unstable and difficult to detect without derivatization (22). For purposes of comparison, we wished to generate both the normal and $^{13}C$-labeled form of HHB. To do this, a *coq3* yeast mutant was cultured in the presence of [$^{13}C_6$]4HB. The E2–249 *coq3* mutant is Q-deficient and is a member of the G31 complementation group defined by Dieckmann and Tzagoloff (26, 27). As shown in Fig. 3 both the normal isotopic form of HHB and [$^{13}C_6$]HHB are detected in lipid extracts prepared from the *coq3* mutant. Our product ion spectra match that described previously (28); of particular note is the fragmentation pattern showing the shift in mass from the precursor molecule (Fig. 3*A*) with an analogous series of fragments from the same compound in the separated crude lipids of [$^{13}C_6$]4HB-labeled *coq3* point mutant (Fig. 3*B*). Both HHB compounds elute with exactly the same retention time. These results demonstrate that the precursor and product ions of prenyl-*p*ABA are each one mass unit less than for HHB, the intermediate formed via the 4HB pathway; HHB $[M+H]^+$ of 547; tropylium ion [*m/z* = 151] (compare Figs. 2*A* and 2*B* with 3*A* and 3*B*).

*Yeast Cultured with [U-$^{14}C$]pABA Produce $^{14}C$-Labeled $Q_6$ and $DMQ_6$*—The identification of prenyl-*p*ABA in yeast neutral lipid extracts led us to investigate whether *p*ABA might serve as a ring precursor in yeast Q biosynthesis. We obtained [$^{14}C$]4HB and [$^{14}C$]*p*ABA and determined that [*ring*-$^{14}C$]*p*ABA is free of detectable 4HB and *vice versa* ("Experimental Procedures"). *S. cerevisiae* wild-type cells (W303-1A), *coq7-1* mutants (NM101), or *coq2* mutants (W303ΔCOQ2), were pre-cultured in Dogal media (minus *p*ABA and folate) to deplete cellular stores of *p*ABA (16). Yeast cells were transferred to fresh Dogal medium plus folate, with the addition of either [$^{14}C$]4HB or [$^{14}C$]*p*ABA (in each case the specific activity was

Downloaded from http://www.jbc.org/ at UCLA-Louise Darling Biomed. Lib. on July 2, 2014

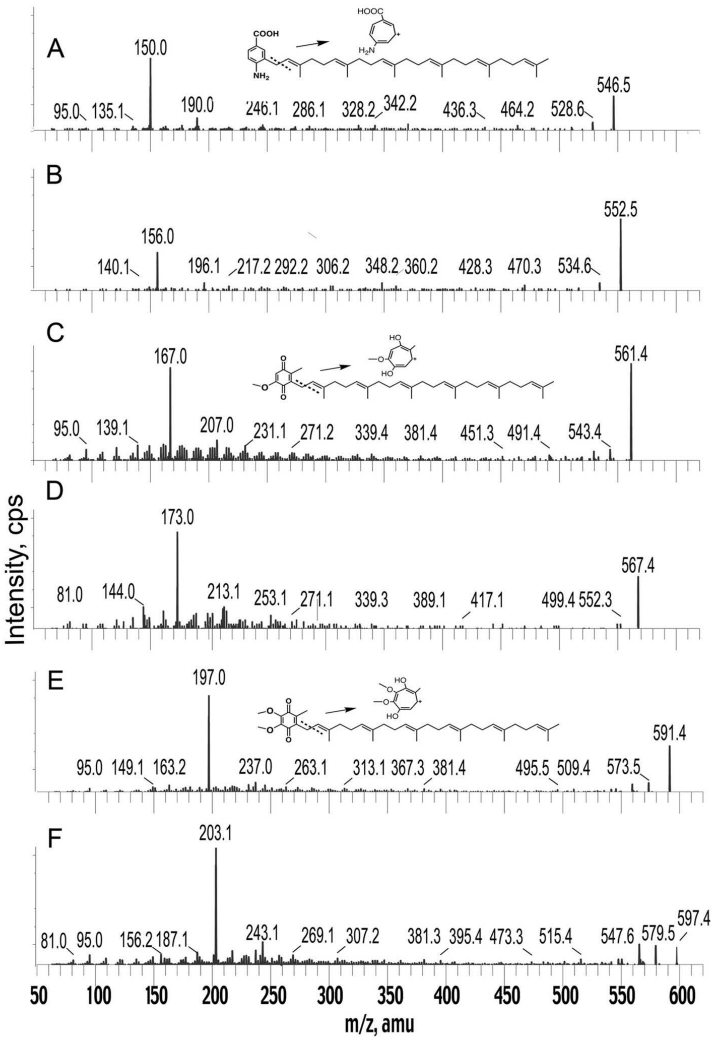



FIGURE 2. **Detection of prenyl-*p*ABA, $DMQ_6$, and $Q_6$ in lipid extracts of wild-type yeast cultured in the absence or presence of $^{13}C_6$-*p*ABA.** Wild-type yeast (W303-1A) were pre-cultured in Dogal media (minus *p*ABA and folate) as described under "Experimental Procedures." Cells were harvested during mid-log from large cultures (300–600 ml of media; $A_{600\,nm}$ = 0.6), resuspended in 2 ml of fresh media or fresh media containing 2–10 $\mu$g/ml [$^{13}C_6$]*p*ABA (final concentration), incubated at 30 °C and harvested after 16 h. Lipid extracts were prepared and quinones and prenylated intermediates were subjected to RP-HPLC-ESI-MS/MS as described. *A–F* show product ion spectra: *A*, prenyl-*p*ABA $[M+H]^+$ precursor ion ($C_{37}H_{55}NO_2^+$; exact mass, 546.4) and the prenyl-*p*ABA tropylium ion $[M]^+$ ($C_8H_8N_1O_2^+$; exact mass, 150.0); *B*, prenyl-[$^{13}C_6$]*p*ABA $[M+H]^+$ precursor ion ($^{13}C_6{}^{12}C_{31}H_{55}NO_2^+$; exact mass, 552.4) and the $^{13}C_6$-prenyl-*p*ABA tropylium ion $[M]^+$ ($^{13}C_6{}^{12}C_2H_8NO_2^+$; exact mass, 156.0); *C*, $DMQ_6$ $[M+H]^+$ precursor ion ($C_{38}H_{56}O_3^+$; exact mass, 561.4) and the $DMQ_6$ tropylium ion $[M]^+$ ($C_9H_{11}O_3^+$; exact mass, 167.1); *D*, [$^{13}C_6$]$DMQ_6$ $[M+H]^+$ precursor ion ($^{13}C_6{}^{12}C_{32}H_{56}O_3^+$; exact mass, 567.4) and the [$^{13}C_6$]$DMQ_6$ tropylium ion $[M]^+$ ($^{13}C_6{}^{12}C_3H_{11}O_3^+$; exact mass, 173.1); *E*, $Q_6$ $[M+H]^+$ precursor ion ($C_{39}H_{58}O_4^+$; exact mass, 591.4) and the $Q_6$ tropylium ion $[M]^+$ ($C_{10}H_{13}O_4^+$; exact mass, 197.1); *F*, [$^{13}C_6$]$Q_6$ $[M+H]^+$ precursor ion ($^{13}C_6{}^{12}C_{33}H_{58}O_4^+$; exact mass, 597.4) and the [$^{13}C_6$]$Q_6$ tropylium ion $[M]^+$ ($^{13}C_6{}^{12}C_4H_{13}O_4^+$; exact mass, 203.1). $Q_6$ (Sigma) and the lipid extract prepared from NM101 (*coq7-1*) yeast strains were used to establish the retention times of $Q_6$ and $DMQ_6$, respectively (29). *A*, *C*, and *E* show the structures of the compounds detected and indicate the identity of the predicted tropylium-like ion of the base peak (tallest peak) formed under collision associated dissociative conditions.

adjusted to 50 Ci/mmol; 800 nM final concentration). Cells were incubated 24 h, lipid extracts were prepared and subjected to RP-HPLC, and the radioactivity was detected as described under "Experimental Procedures." Yeast lipid extracts prepared from wild-type cells contained two peaks of $^{14}$C-radiolabeled material, consistent with the elution of $Q_6$ and $Q_6H_2$ (the hydroquinone) (Fig. 4). Similarly, the yeast *coq7-1* mutant NM101, when incubated with either [$^{14}$C]4HB or [$^{14}$C]*p*ABA, produced radiolabeled material slightly more polar than $Q_6$, previously identified as $DMQ_6$ (29). The synthesis of [$^{14}$C]$Q_6$ under both experimental conditions requires the yeast *COQ2* gene product (Fig. 4). These results indicate that $DMQ_6$ and $Q_6$ may be synthesized in yeast from either *p*ABA or 4HB aromatic ring precursors, and both ring precursors require Coq2p for prenyl tail attachment.

*Yeast Cultured with [$^{13}C_6$]pABA produce $^{13}C_6$-labeled Prenyl-pABA, $DMQ_6$, and $Q_6$*—The results obtained with the $^{14}$C-labeled precursors strongly suggest that *p*ABA functions as a ring precursor in yeast $Q_6$ biosynthesis. Metabolic labeling studies with stable isotopes provide a definitive test, because the ring carbons can be detected in both precursor and product ions by mass spectrometry. Wild-type yeast were first depleted of *p*ABA and folate as described above and then cultured in the presence of [$^{13}C_6$]*p*ABA as described under "Experimental Procedures." The identification of hexaprenylated compounds in the crude lipids of wild-type yeast is represented by the spectra in Fig. 2. The normal (unlabeled) precursor ions monitored included: prenyl-*p*ABA (Fig. 2*A*), demethoxy-$Q_6$ (Fig. 2*C*), and $Q_6$ (Fig. 2*E*). Product ion analyses from the crude lipids of yeast grown in the presence of [$^{13}C_6$]*p*ABA show that the ring carbons of this compound are incorporated into demethoxy-$Q_6$ and $Q_6$ and alter the average isotopic masses of the tro-

Downloaded from http://www.jbc.org/ at UCLA-Louise Darling Biomed. Lib. on July 2, 2014

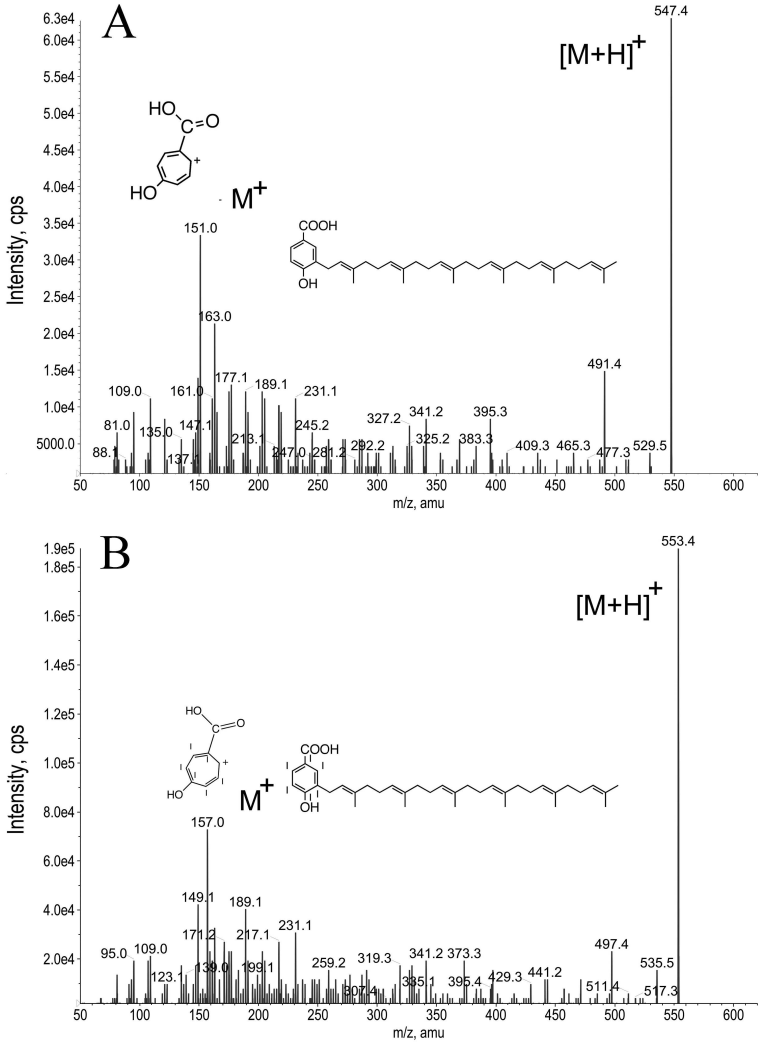



FIGURE 3. **Detection of HHB in lipid extracts of a yeast *coq3* mutant cultured in the absence (*A*) or presence (*B*) of $^{13}C_6$-4HB.** The yeast *coq3* mutant E2-249 was pre-cultured in Dogal media as described previously, harvested, and incubated in fresh media or fresh media with 10 $\mu$g/ml [$^{13}C_6$]4HB as described in Fig. 2. Lipid extracts were prepared and subjected to RP-HPLC-ESI-MS/MS as described. Product ion spectra are shown: *A*, HHB [M+ H]$^+$ precursor ion ($C_{37}H_{54}O_3^+$; exact mass, 547.4) and the HHB tropylium ion [M]$^+$ ($C_8H_7O_3^+$; exact mass, 151.0); *B*, [$^{13}C_6$]HHB [M+H]$^+$ precursor ion ($^{13}C_6{}^{12}C_{31}H_{54}O_3^+$; exact mass, 553.4) and the [$^{13}C_6$]HHB tropylium ion ($^{13}C_6{}^{12}C_2H_7O_3^+$; exact mass, 157.0).

pylium-like ion and molecular ion by 6 mass units. This results in the following $^{13}C_6$-labeled compounds in Fig. 2: prenyl-[$^{13}C_6$]*p*ABA ($^{13}C_6{}^{12}C_{31}H_{55}NO_2$) (Fig. 2*B*); $^{13}C_6$-demethoxy-$Q_6$ ($^{13}C_6{}^{12}C_{32}H_{56}O_3$) (Fig. 2*D*); and [$^{13}C_6$]$Q_6$ ($^{13}C_6{}^{12}C_{33}H_{58}O_4$) (Fig. 2*F*). The incorporation of [$^{13}C_6$]*p*ABA into the penultimate Q intermediate, $DMQ_6$, was readily detected in wild-type yeast cell lipid extracts (Fig. 2*D*). Wild-type yeast cultured in the presence of [$^{13}C_6$]4HB also generate the expected +6 isotopically labeled forms of $Q_6$ and $DMQ_6$, however, under these labeling conditions, it was difficult to detect the +6 form of HHB (data not shown).

*Prenyl-pABA Is Absent in Yeast abz1 Mutants Starved for pABA, Yet Content of Q Is Similar to That of Wild-type Yeast*—Yeast produce *p*ABA from chorismate by a two-step process that requires the *ABZ1* and *ABZ2* gene products (14, 16). Thus, it seemed likely that the production of prenyl-*p*ABA would depend on the supply of *p*ABA from this biosynthetic pathway, or from the *p*ABA supplied in the media. To test this idea, wild-type yeast, or *abz1* yeast mutants were serially cultured under conditions where the exogenous supply of *p*ABA was eliminated (16). As shown in Fig. 5, *abz1* mutants starved for *p*ABA show dramatic decline in the content of prenyl-*p*ABA, whereas the content of prenyl-*p*ABA in wild-type cells remains unchanged or increased. These results indicate that a combination of the *abz1* deletion and nutritional depletion of *p*ABA results in the depletion of prenyl-*p*ABA. Under these *p*ABA-depleted conditions, the *abz1* mutants are still able to produce $DMQ_6$ and $Q_6$. This is consistent with the presence of at least two pathways in yeast able to supply aromatic ring precursors for Q biosynthesis (Fig. 1).

*What Are the Relative Contributions of the pABA and 4HB Ring Precursors to Q Biosynthesis?*—Once we recognized that [$^{13}C_6$]*p*ABA could serve as a precursor to [$^{13}C_6$]$Q_6$, we decided to investigate whether cells demonstrated a preference for *p*ABA or 4HB as an aromatic ring precursor for Q. As expected, incubation of wild-type or *abz1* mutant cells labeled for 3.5 h with a single designated precursor show that either [$^{13}C_6$]*p*ABA or [$^{13}C_6$]4HB serve as ring precursors in biosynthesis of $DMQ_6$ (Fig. 6*A*) and $Q_6$ (Fig. 6*B*); the *darkly shaded* lower section of each column designates the amount of the [$^{12}$C]quinone, and the *upper light gray bar* shows the amount of [$^{13}C_6$]quinone. We then performed competition experiments to examine the ability of the normal isotopic $^{12}$C form of the alternative precursor to diminish the incorporation of the $^{13}$C-form into [$^{13}C_6$]$DMQ_6$ or [$^{13}C_6$]$Q_6$ (Fig. 6). For these competitor experi-

Downloaded from http://www.jbc.org/ at UCLA-Louise Darling Biomed. Lib. on July 2, 2014

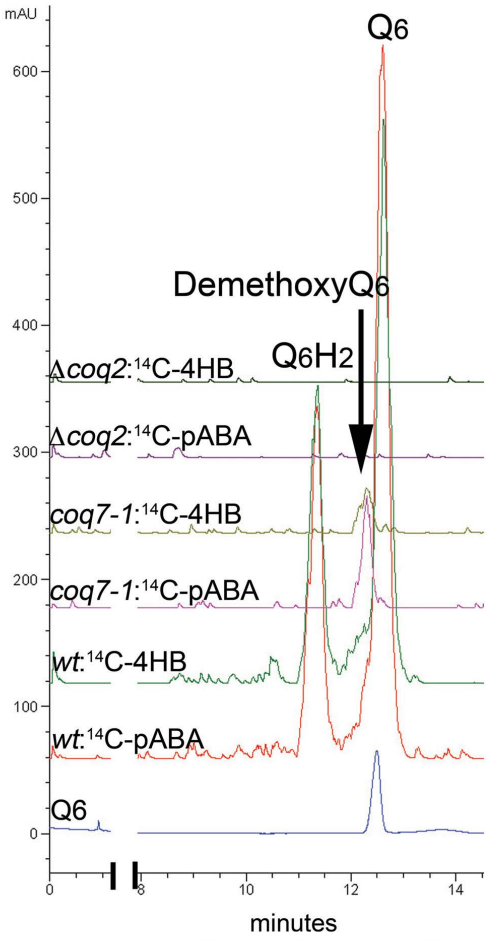



FIGURE 4. **Yeast cultured with $^{14}$C-*p*ABA or $^{14}$C-4HB produce $^{14}$C-labeled $Q_6$ and $DMQ_6$.** Wild-type yeast (W303-1A), *coq7-1* mutants (NM101), or *coq2* mutants (W303ΔCOQ2), were pre-cultured in Dogal media (minus *p*ABA, minus folate) to deplete cellular stores of *p*ABA (16). Yeast cells were transferred to fresh Dogal medium plus folate, with the addition of either [$^{14}$C]4HB or [$^{14}$C]*p*ABA (in each case specific activity was adjusted to 50 Ci/mmol; 800 nM final concentration). Cells were incubated 24 h, and lipid extracts were prepared and subjected to RP-HPLC and the radioactivity detected as described under "Experimental Procedures." The *bottom blue* trace indicates the $Q_6$ standard (12.2 min, 274 nm). *Green* and *red* traces show elution of $^{14}$C-radiolabeled material present in lipid extracts of wild-type yeast cultured (24 h) with either [$^{14}$C]4HB or [$^{14}$C]*p*ABA, as indicated. The elution of [$^{14}$C]$Q_6$ at 12.35 min includes a time delay of 0.15 min between the UV detector and the BetaRam (Model 2 in-line scintillation) detector. Reduced [$^{14}$C]$Q_6H_2$ eluted 2 min earlier at 11.3 min. *Olive* and *Pink* traces identify $^{14}$C-radiolabeled material eluting at 12.1 min as $DMQ_6$, because the *coq7-1* yeast mutant lacks $Q_6$ and contains $DMQ_6$ (29). The *top two traces* (*dark green* and *purple*) indicate the lack of incorporation of $^{14}$C precursors into *coq2* null cells. The *arrow* designates the $^{14}$C-material co-migrating with $DMQ_6$, present in the NM101 extracts. Chromatograms are not normalized; the amounts of [$^{14}$C]$DMQ_6$ produced in NM101 is 5- to 20-fold lower than the amount of [$^{14}$C]$Q_6$ present in wild-type cells.

ments, cells were incubated (3.5 h) in the presence of equivalent concentrations of the alternative ring precursor (10 $\mu$g/ml). In wild-type cells, the presence of the competitor did not substantially affect the amount of [$^{13}C_6$]$Q_6$ content. Indeed, total levels of $Q_6$ were slightly higher in wild-type cells incubated with both aromatic ring precursors concurrently. In *abz1* mutant cells, the total content of $Q_6$ was increased (relative to the no-addition control) by addition of any combination of aromatic ring precursors, and the presence of added $^{12}$C competitor significantly decreased the amount of [$^{13}C_6$]$Q_6$ produced from the $^{13}$C-aromatic ring precursor. It seems likely that the presence of both ring precursors better satisfies the requirement for both folate and Q.

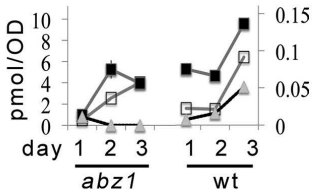



FIGURE 5. **Nutritional and genetic depletion of *p*ABA eliminate the formation of prenyl-*p*ABA.** BY4741 wild-type yeast and BY4741Δ*abz1* yeast mutants were grown overnight in YPD, and then diluted 1:100 (v/v) into fresh Dogal media minus *p*ABA and folate and incubated for 1 day. The *day 1* culture was used to inoculate fresh Dogal media (minus *p*ABA and folate), and the process was repeated to generate the *day2* and *day 3* cultures. The serial dilution into *p*ABA minus media exhausts endogenous stores of *p*ABA (16). Cells were harvested, and lipid extracts were examined for content of $Q_6$ (*filled squares*; *left y axis*), $DMQ_6$ (*open squares*; *right y axis*), and prenyl-*p*ABA (*triangles*; *right y axis*).

Although the different ring precursors had only modest effects on the amount of $Q_6$ formed, they had dramatic effects on the content of $DMQ_6$. For example, both wild-type yeast and *abz1* mutants had increased content of $DMQ_6$ when incubated with *p*ABA as compared with 4HB. In fact *abz1* mutants incubated with [$^{13}C_6$]*p*ABA produced a high content of $DMQ_6$ of which almost all is [$^{13}C_6$]$DMQ_6$ (Fig. 6*A*). We speculate that prenyl-*p*ABA, or more likely a subsequent intermediate derived from prenyl-*p*ABA, might act to inhibit the hydroxylation of DMQ.

*Prenylation of pABA Precedes Biosynthesis of DMQ and Q from pABA*—A pulse-labeling experiment was conducted to determine whether the incorporation of $^{13}C_6$-ring carbons into $^{13}C_6$-prenyl-*p*ABA preceded the formation of [$^{13}C_6$]$DMQ_6$ and [$^{13}C_6$]$Q_6$. Wild-type cells and *abz1* yeast mutants were pre-cultured as described in Fig. 6 and incubated with [$^{13}C_6$]*p*ABA over a time course from 0 to 30 min, as described in Fig. 7 and "Experimental Procedures." Samples were removed from the incubation at stated times, collected by filtration, and quenched, and lipid extracts were analyzed to determine the amounts of prenyl-*p*ABA, $DMQ_6$, and $Q_6$ by HPLC-MS/MS and multiple reaction monitoring. In both wild-type and *abz1* mutant yeast, prenyl-[$^{13}C_6$]*p*ABA is detectable within a minute of label addition (see *inset*, Fig. 7), and its *de novo* synthesis precedes that of [$^{13}C_6$]$DMQ_6$ and [$^{13}C_6$]$Q_6$, consistent with the notion of a precursor-product relationship.

*pABA-replete Yeast Produce 4-Imino-$DMQ_6$*—In the crude lipid extracts of wild-type cells grown in media supplemented with [$^{13}C_6$]*p*ABA, we identify what appears to be a nitrogen containing form of 4-imino-$DMQ_6$ (Fig. 8). The tropylium, chromenylium, and molecular ion are all shifted in accordance with M+6 (*m*/*z*), as is detected for $DMQ_6$ (Fig. 2*D*);

Downloaded from http://www.jbc.org/ at UCLA-Louise Darling Biomed. Lib. on July 2, 2014

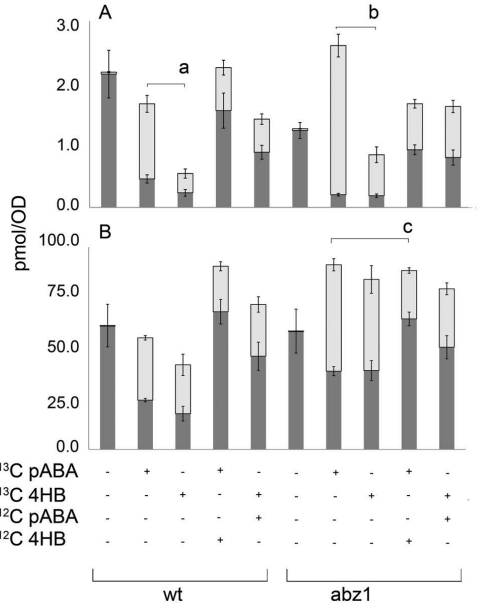



FIGURE 6. **4HB and *p*ABA are mutually incorporated into $Q_6$, but differentially incorporated into $DMQ_6$.** Wild-type (W303-1A) or *abz1* null (W303ΔABZ1) cells were serially cultured to deplete them of *p*ABA and folinic acid as described. The depleted cells were harvested and used to inoculate a 4-ml culture. This was divided to supply duplicate samples of cells to five different media conditions. The media contained either no addition or 10 $\mu$g/ml of the following: [$^{13}C_6$]*p*ABA, [$^{13}C_6$]4HB, or similar cultures in the presence of equivalent concentrations of the alternative unlabeled ($^{12}$C) ring precursor (10 $\mu$g/ml). Independent replicates were made of each condition. The amount of the competing $^{12}$C form of precursor (ratio of $^{13}$C:$^{12}$C) was 1:1. After incubation for 3.5 h, cells were harvested, and lipid extracts were subjected to analyses by RP-HPLC-ESI/MS-MS. *A*, $DMQ_6$ content; *B*, $Q_6$ content. The content of [$^{12}$C]$DMQ_6$ or [$^{12}$C]$Q_6$ is designated by the *darkly shaded lower section* of each *bar* (in *A* and *B*, respectively), and [$^{13}C_6$]$DMQ_6$ and [$^{13}C_6$]$Q_6$ by the *upper light gray bar* (in *A* and *B*, respectively). Each condition was cultured as an independent replicate, and each lipid extract was injected twice ($n = 4$). This experiment is representative of three others, conducted independently. The *brackets* with *letters* denote the values being compared: Content of [$^{13}C_6$]$DMQ_6$ is significantly different in wild-type cells cultured in [$^{13}$C]*p*ABA as compared with [$^{13}$C]4HB (*a*, $p = 0.0002$); content of [$^{13}C_6$]$DMQ_6$ is significantly different in *abz1* mutant cells cultured in [$^{13}$C]*p*ABA as compared with [$^{13}$C]4HB (*b*, $p = 0.0002$); and content of [$^{13}C_6$]$Q_6$ is significantly different in in *abz1* mutant cells cultured in [$^{13}$C]*p*ABA as compared with [$^{13}$C]*p*ABA plus unlabeled 4HB (*c*, $p = 0.0001$).

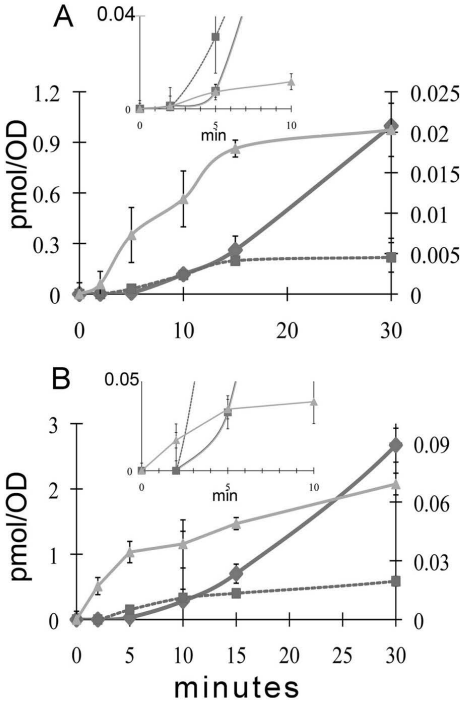



FIGURE 7. **Time course assays with $^{13}C_6$-*p*ABA.** *A*, wild-type (W303-1A) or *B*, *abz1* null (W303ΔABZ1) cells were pre-cultured as described to deplete endogenous *p*ABA, resuspended in pre-warmed Dogal media (30 °C) to a total volume of 16 ml in a 125-ml flask, and incubated with shaking (250 rpm, 30 °C). Prior to addition of ring precursors, two (1 ml) aliquots were removed, to represent a "no-label or zero time" control. [$^{13}C_6$]*p*ABA was added (final concentration, 10 $\mu$g/ml), and further 1-ml aliquots were collected in duplicate at the time points indicated on the glass filter disks for lipid extraction: no label control (defines the "zero" time point), 2, 5, 10, 15, or 30 min. Lipid extracts were subjected to analyses by RP-HPLC-ESI/MS-MS as described, and the amount of *de novo* prenyl-[$^{13}C_6$]*p*ABA (*triangles*), [$^{13}C_6$]$DMQ_6$ (*squares*), and [$^{13}C_6$]$Q_6$ (*diamonds*) is depicted. The *left y axis* represents the picomoles/*A* (for plots of [$^{13}C_6$]$DMQ_6$ and [$^{13}C_6$]$Q_6$), whereas the *right y axis* shows the content in picomoles/*A* for prenyl-[$^{13}C_6$]*p*ABA. Values are plotted as average ± S.D. ($n = 4$, wild type; $n = 6$ *abz1* null). The *insets* in *each panel* depict early time points (in minutes) for all three components plotted on the same scale (pmol/*A*).

however, the masses of these ions are reduced by 1 Da relative to the fragment ion masses of $DMQ_6$, consistent with an imino nitrogen rather than a quinone oxygen atom in the *para* ring position. The chromenylium ion fragment of 4-imino-$DMQ_6$ is abundant, because it is likely to be more stable to dissociative conditions due to the interaction of the first four carbons of the prenyl tail with the imino nitrogen forming a second ring (23). The normal isotopic form of 4-imino-$DMQ_6$ is present in crude lipid extracts of strains grown in YPD (data not shown).

The detection of 4-imino-$DMQ_6$ led us to test whether it might function as an intermediate in $Q_6$ biosynthesis. To simplify the precursor-product relationship between 4-imino-$DMQ_6$ and $DMQ_6$, we examined the synthesis of both as a function of time in NM101 yeast, a strain known to be blocked in Q biosynthesis and to produce $DMQ_6$ due to a mutation in *COQ7* (29). The pulse labeling with [$^{13}C_6$]*p*ABA was performed over a time course of 0 to 60 min, and the content of $^{13}$C-labeled intermediates (prenyl-[$^{13}C_6$]*p*ABA, [$^{13}C_6$]imino-$DMQ_6$, and [$^{13}C_6$]$DMQ_6$) were determined (Fig. 9). The rate of formation of prenyl-[$^{13}C_6$]*p*ABA and [$^{13}C_6$]imino-$DMQ_6$ were very similar, suggesting that both serve as biosynthetic precursors in the synthesis of $DMQ_6$. We note that $DMQ_6$ is relatively unstable in the *coq7-1* mutant, as is evident from the rate of loss of the [$^{12}$C]$DMQ_6$. This rate of loss seems to be compensated by the formation of [$^{13}C_6$]$DMQ_6$. These results suggest that the nitrogen substituent of *p*ABA may be retained up to the step generating 4-imino-$DMQ_6$, and are consistent with a possible mechanism where oxygen from a water-based hydroxyl could replace the nitrogen imino via Schiff base chemistry (Fig. 10).

Downloaded from http://www.jbc.org/ at UCLA-Louise Darling Biomed. Lib. on July 2, 2014

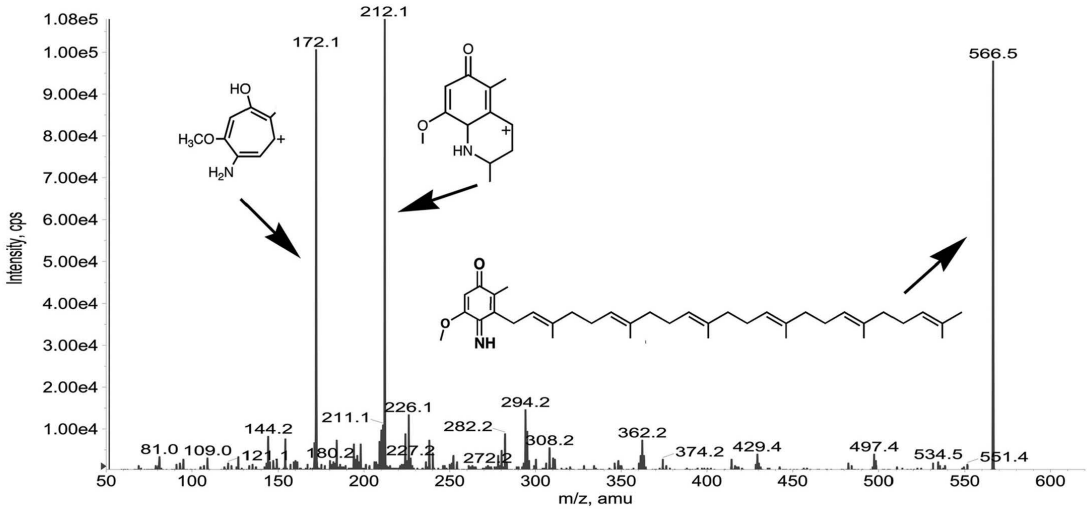



FIGURE 8. **Identification of 4-imino-DMQ$_6$ in lipid extracts of wild-type cells.** An imino form of [$^{13}C_6$]DMQ$_6$ is present in wild-type yeast cultured in the presence of [$^{13}C_6$]*p*ABA and is consistent with the structures as shown. The imino substituent forms a more stable interaction with isoprene proximal to the ring, creating more stable and abundant chromenylium ion upon collision associated dissociation: *m/z* 212. Masses detected at *m/z* 497.4, 429.4, 362.2 and 294.2 are characteristic of the loss of successive isoprene units (*m/z* 68). This compound can be detected in wild-type strains grown in rich media and appears to be a normally accumulating form of demethoxy-Q$_6$ (see Fig. 9). [$^{13}C_6$]imino-DMQ$_6$ [M+H]$^+$ precursor ion ($^{13}C_6{}^{12}C_{32}H_{56}NO_2$+; exact mass, 566.4), the [$^{13}C_6$]imino-DMQ$_6$ tropylium ion [M]$^+$ ($^{13}C_6{}^{12}C_3H_{11}NO_2{}^+$; exact mass, 172.2), and the [$^{13}C_6$]imino-DMQ$_6$ chromenylium ion [M]$^+$ ($^{13}C_6{}^{12}C_6H_{16}NO_2{}^+$; exact mass, 212.3).

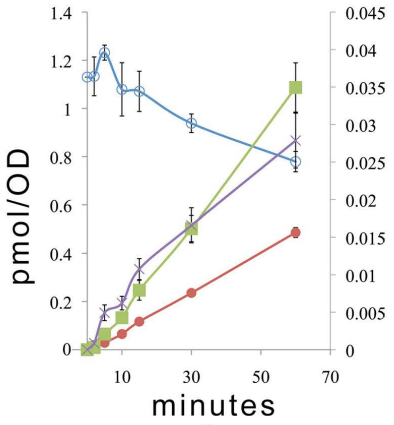



FIGURE 9. **Time course assays with $^{13}C_6$-*pABA* examine the formation novel Q intermediates in NM101 (*coq7-1*) yeast.** NM101 yeast cells were pre-cultured and analyzed by pulse-labeling with [$^{13}C_6$]*p*ABA as described in Fig. 7. Lipid extracts were subjected to analyses by RP-HPLC-ESI/MS-MS as described, and the amount of *de novo* prenyl-[$^{13}C_6$]*p*ABA (*green squares*), [$^{13}C_6$]DMQ$_6$ (*red circles*), and [$^{13}C_6$]imino-DMQ$_6$ (*purple cross*) is depicted. Also depicted is the decay of non-isotopically labeled DMQ$_6$ (*blue open circles*). The *right y axis* represents the pmol/*A* (for plots of prenyl-[$^{13}C_6$]*p*ABA and [$^{13}C_6$]imino-DMQ$_6$), whereas the *left y axis* shows the content in pmol/*A* for DMQ$_6$ and [$^{13}C_6$]DMQ$_6$. Values are plotted as average ± standard deviations ($n$ = 4).

## DISCUSSION

Schemes of Q biosynthesis in *E. coli*, yeast, and animals universally depict 4HB as the aromatic ring precursor. In each of these species, isoprenylation of 4HB is thought to represent a committed step in Q biosynthesis. Here we show that *S. cerevisiae* can also utilize *p*ABA as a ring precursor in Q biosynthesis. This is a surprising finding, because *p*ABA is a crucial intermediate in folate biosynthesis. It is also surprising because the addition of *p*ABA to either *E. coli* or human cells causes a concentration-dependent inhibition of Q biosynthesis (30–33). In *E. coli*, rat, and human cells, the *p*ABA ring competes with 4HB at the ring:polyprenyltransferase step (catalyzed by Coq2), and the product prenyl-*p*ABA appears to be a dead-end product. Recently another aromatic ring inhibitor, 4-nitrobenzoic acid, was shown to inhibit Q biosynthesis in mammalian cells through its competition with 4HB for Coq2 (34). Thus it appears that several benzoic acid ring analogs function as competitive inhibitors of Q biosynthesis in mammalian cells (33, 34).

In contrast, our studies identify prenyl-*p*ABA, a normal metabolite present in lipid extracts of wild-type yeast, as a Q intermediate. The synthesis of prenyl-*p*ABA depends on Coq2 (Fig. 4), and we show that prenyl-*p*ABA is a normal metabolite present in lipid extracts of wild-type yeast cultured in standard yeast media (Fig. 2). An interesting independent confirmation of prenyl-*p*ABA in yeast neutral lipid extracts was recently published, found in lipid extracts of yeast with defects in ferredoxin (*YAH1*) and ferredoxin reductase (*ARH1*) (18). These authors discovered the role of *p*ABA in Q biosynthesis through their analyses of iron chaperones required for the activity of Coq7, the Coq diiron enzyme required for the last ring hydroxylation in Q biosynthesis (29, 35).

Our work clearly explores the biochemical relationship of prenyl-*p*ABA in yeast Q biosynthesis, demonstrating prenyl-*p*ABA is a *bona fide* biosynthetic precursor. *p*ABA can be prenylated immediately following its addition to cells. Pulse label-

Downloaded from http://www.jbc.org/ at UCLA-Louise Darling Biomed. Lib. on July 2, 2014

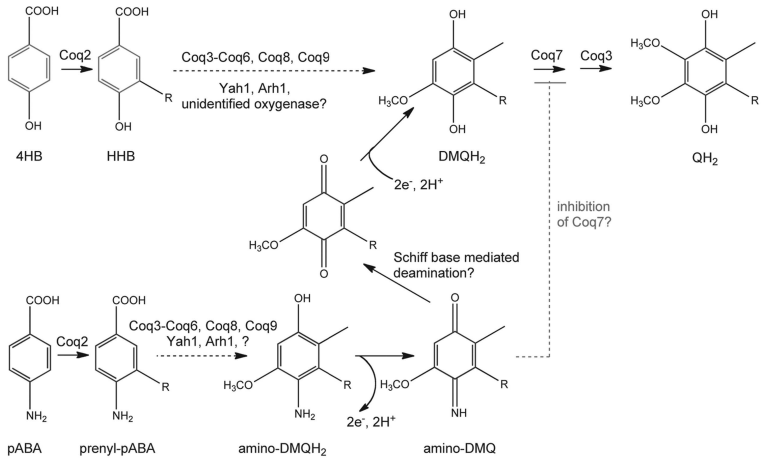



FIGURE 10. **Scheme for generation of 4-imino-$DMQ_6$ and loss of nitrogen generating $DMQ_6$.** The pulse-labeling studies in Figs. 7 and 9 suggest that prenyl-*p*ABA and 4-imino-$DMQ_6$ are *bona fide* precursors in yeast Q synthesis from *p*ABA. A possible mechanism for replacement of the imino nitrogen with a hydroxy substituent via Schiff base chemistry is proposed. The new steps of oxidation, de-imination, and reduction allow the two pathways to converge at formation of $DMQ_6H_2$.

ing studies with [$^{13}C_6$]*p*ABA show that *p*ABA-deficient *abz1* null yeast mutants synthesize prenyl-[$^{13}C_6$]*p*ABA within 1 min of incubation (Fig. 7). This rapid incorporation of the isotope into prenyl-*p*ABA precedes the formation of [$^{13}C_6$]$DMQ_6$ and [$^{13}C_6$]$Q_6$ and is consistent with a precursor-product relationship. Yeast *abz1* mutants, known to be defective in *p*ABA biosynthesis (15, 16), become depleted in prenyl-*p*ABA when cultured in *p*ABA-free media (Fig. 5). However, under these culture conditions Q is still produced, reflecting use of an alternate ring precursor, 4HB (Fig. 1). Prenylation of 4HB by Coq2 is the "classic" arm of the pathway. We also identify for the first time the underivatized forms of HHB, detected in a *coq3* yeast mutant.

*Identification of 4-Imino-$DMQ_6$ and a Model for Nitrogen Loss*—Both wild-type and *abz1* yeast null mutants when precultured under conditions to deplete *p*ABA, followed by growth with *p*ABA supplementation, have a higher $DMQ_6$ content as compared with wild-type yeast or *abz1* mutants supplemented with 4HB (Fig. 6). In isotopic labeling studies with the *abz1* mutant >90% of the $DMQ_6$ detected contains the $^{13}C_6$-aromatic ring from *p*ABA. The preferential incorporation of *p*ABA into $DMQ_6$ is particularly intriguing in light of our finding that 4-imino-$DMQ_6$, a lipid derived from prenyl-*p*ABA, is present in the *p*ABA-supplemented *abz1* mutant and in normally cultured wild-type cells (Fig. 8). The rate of formation of 4-imino-$DMQ_6$ is similar to that of prenyl-*p*ABA (Fig. 9), identifying it as a new Q intermediate and indicating that the nitrogen of *p*ABA can potentially be retained up to the step preceding $DMQ_6$.

If this is the case, what is the fate of 4-imino-$DMQ_6$? We speculate 4-imino-$DMQ_6$ is produced from the two-electron oxidation of 4-amino-$DMQ_6H_2$ (Fig. 10). Once the imino-quinone is formed, the potential for loss of the ring nitrogen as ammonia and its replacement by oxygen from a water or hydroxide ion to form the quinone could reasonably occur by Schiff base chemistry. Although we designate the ring nitrogen loss step as immediately preceding $DMQ_6$, it is possible the loss could occur earlier. However, we favor the depiction in Fig. 10, because $DMQ_6$ is a relatively abundant Q intermediate, detected even in wild-type cells (36, 37), and is also a component of a Q biosynthetic complex (38). It seems possible that the enhanced accumulation of $DMQ_6$ in cells first starved for and then supplemented with *p*ABA may be due to inhibition of the Coq7 monooxygenase step (Fig. 10). However, the effect may also be indirect, as the influx of *p*ABA would also replete folate synthesis. We note that the redox state of mitochondria might very well affect the relative rates of oxidation and reduction of amino-$DMQ_6H_2$ to imino-$DMQ_6$, and $DMQ_6$ to $DMQ_6H_2$.

*Which Ring Precursor, 4HB or p*ABA, *Is Normally Preferred?*—Our labeling with $^{13}$C-aromatic ring precursors is accomplished by lowering the supply of *p*ABA and folate to cells with deficient media prior to isotopic incorporation. Thus, at present we cannot differentiate the relative importance of each ring precursor (4HB or *p*ABA) for $Q_6$ production in wild-type cells, under physiological conditions. It remains possible that *p*ABA could be converted to 4HB prior to lipidation in mitochondria. However, the competition experiments (Fig. 6) suggest that, when one $^{13}$C-ring precursor is provided to yeast cells in a one to one molar ratio with the other unlabeled ring, *p*ABA and 4HB are indistinguishable for [$^{13}$C]Q synthesis. In addition, if [$^{13}C_6$]*p*ABA was converted into [$^{13}C_6$]4HB prior to its prenylation by mitochondrial Coq2, then the enhanced accumulation of [$^{13}C_6$]$DMQ_6$ from the [$^{13}C_6$]*p*ABA labeling relative to that of [$^{13}C_6$]4HB (Fig. 6*A*) would be unlikely. Although the *abz1* null avidly incorporates and synthesizes [$^{13}$C]demethoxy from [$^{13}$C]*p*ABA, our data do not suggest that *p*ABA is a better source for demethoxy $Q_6$ in normal yeast. Media conditions, for example carbon source and nitrogen source(s), may radically alter ring precursor preference. Finally, we note that our conclusions regarding the incorporation of 4HB and *p*ABA into $Q_6$ are valid only if the uptake of 4HB and *p*ABA are identical.

It is likely but uncertain that 4HB and *p*ABA may share some mechanisms of uptake and transport of the free form into mitochondria. *p*ABA and 4HB are weakly ionic compounds (*p*ABA: p$K_a$ 4.9; 4HB: p$K_a$ 4.67 (39)), and their uptake and retention has a pH-dependent component. Uptake is favored at low pH, and the formation of the carboxylate anion once imported into the cell favors retention. Although the pH of our media is 6.0, which has been shown to relieve *p*ABA growth inhibition in *S. cerevisiae* (40), other work has shown *p*ABA uptake cannot be saturated (41). The studies of inhibition of yeast growth by *p*ABA are intriguing (40), and are different from *E. coli* growth inhibi-

Downloaded from http://www.jbc.org/ at UCLA-Louise Darling Biomed. Lib. on July 2, 2014

tion by *p*ABA. *E. coli* have *ubiC* encoded chorismate lyase, which directly converts chorismate to 4HB (9) (Fig. 1), whereas yeast lack this homolog. *E. coli* can be growth inhibited by excess *p*ABA, and relief is accomplished by large concentrations of 4HB (31). However, rescue of growth inhibition by *p*ABA in *S. cerevisiae* requires aromatic amino acids, with phenylalanine and tyrosine in combination to best resume growth (40).

*What Are the Pathway(s) to 4HB Production?*—Radiolabeled cinnamic and coumaroyl acids produce radiolabeled Q when fed to bakers' yeast (42), with coumarate being the best precursor, and both these compounds are shown to precede 4HB. Other work describes the ability of radiolabeled aromatic amino acids to donate their carbons to Q in yeast (43), however the intermediary compounds have not been described. In other microorganisms the direct precursors for 4HB have been examined more recently and thoroughly. An alternative is described in plants (44), where phenylalanine is a probable precursor, although *S. cerevisiae* lacks an identifiable phenylalanine ammonia lyase homolog. The *Acinetobactor baylyi* system describes the production of 4HB precursors from the catabolism of primarily plant cell wall components into hydroxycinnamate precursors (13).

*Do Anti-folates Target Both Folate and Q?*—Studies of chorismate synthesis have been stimulated by investigations of drug resistance in microorganisms and *p*ABA metabolism. Depletion of folate is difficult, because it is recycled as a cofactor and yeast carry reserves of both folate and *p*ABA. Yeast cells must be serially cultured in media depleted of these nutrients to elicit a *p*ABA or folate growth deficiency (16). A *p*ABA deficiency is also accomplished by inclusion of sulfanilamide in the media, because sulfanilamide acts as a competitive *p*ABA analog (14). The discovery of sulfanilamide antibiotics hinges on the ability of this class of compound to interfere with the condensation of *p*ABA to pteroglutamoyl for the synthesis of folate (19). The enzyme dihydropteroate synthase is the target of the *p*ABA analog sulfamethoxazole, within the "sulfa" drug class. Previous work by Macreadie's group on resistance to this drug showed resistance depended on expression of the dihydropteroate synthase homolog in yeast (*FOL1*), as long as *p*ABA was supplied in the media (45).

This report describes a novel and physiologically relevant, lipidated form of *p*ABA in yeast, establishing a possible linkage between Q biosynthesis and folate metabolism. Although direct relationships between coenzyme Q biosynthesis and folate metabolism have not been characterized until now, relationships are known to exist between folate synthesis and sulfa drug resistance. A storage form of *p*ABA in microorganisms satisfies the logistics for folate synthesis, just as a glucosylated form of *p*ABA functions in plants (41, 45, 46). It would be undesirable for a crucial metabolic intermediate such as *p*ABA to fall into low supply, but large quantities of the free acid may act as uncouplers to the electrochemical gradient (47). Larger amounts of *p*ABA may also act as a substrate inhibitor of dihydropteroate synthase, the enzyme that couples *p*ABA to a pterin moiety during folate synthesis. Although inhibition occurs at micromolar levels of *p*ABA for the bacterial dihydropteroate synthase homolog (48), its inhibition by high amounts is not complete and it retains much lower but steady activity.

In summary, our analyses document *p*ABA and 4HB as two aromatic rings that serve as precursors for $DMQ_6$ and $Q_6$. The observation of a normally produced imino form of DMQ found in the crude lipid extract of wild-type cells (Fig. 8), and its similar rate of formation as compared with prenyl-*p*ABA in a *coq7-1* point mutant (Fig. 9), suggest that both are novel Q intermediates. Based on the 4-imino-$DMQ_6$ intermediate, we suggest a mechanism for the loss of the *p*ABA-derived nitrogen. Finally the findings presented here suggest an intimate relationship may exist between synthesis of folic acid, necessary for many cellular essential functions and cellular respiration in *S. cerevisiae*, coordinated through the overlapping substrate prenyl-*p*ABA.

*Acknowledgments—We thank John Greaves, University of California, Irvine, for his insight and advice about the presence of nitrogen in our unknown that was 1 Da less than HHB. We also thank Jennifer Shepherd, Gonzaga University, for discussions regarding aromatic compounds containing nitrogen substituents, and Jane Strouse, Chemistry and Biochemistry at UCLA, for assistance with mass spectrometry. We thank the C.F. Clarke laboratory group members for discussions and input.*

## REFERENCES

1. Lenaz, G., and De Santis, A. (1985) in *Coenzyme Q* (Lenaz, G., ed) pp. 165–199, Wiley & Sons, Chichester, UK
2. Bentinger, M., Brismar, K., and Dallner, G. (2007) *Mitochondrion* **7,** (suppl.) S41–S50
3. Meganathan, R. (2001) *FEMS Microbiol. Lett.* **203,** 131–139
4. Kawamukai, M. (2009) *Biotechnol. Appl. Biochem.* **53,** 217–226
5. Tran, U. C., and Clarke, C. F. (2007) *Mitochondrion* **7,** (suppl.) S62–S71
6. Olson, R. E., and Rudney, H. (1983) *Vitam. Horm.* **40,** 1–43
7. Pennock, J. F., and Threlfall, D. R. (1983) in *Biosynthesis of Isoprenoid Compounds* (Porter, J. W., and Spurgeon, S. L., eds) pp. 191–302, John Wiley and Sons, New York
8. Olson, R. E. (1966) *Vitam. Horm.* **24,** 551–574
9. Siebert, M., Severin, K., and Heide, L. (1994) *Microbiology* **140,** 897–904
10. Dosselaere, F., and Vanderleyden, J. (2001) *Crit. Rev. Microbiol.* **27,** 75–131
11. Cox, G. B., Gibson, F., and Pittard, J. (1968) *J. Bacteriol.* **95,** 1591–1598
12. Goewert, R. R. (1981) PhD thesis, *Studies on the Biosynthesis of Ubiquinone: The Identification of 3,4-Dihydroxy-5-hexaprenylbenzoic Acid, 3-Methoxy-4-hydroxy-5-hexaprenylbenzoic Acid and the Regulation of the Conversion of Tyrosine and Chorismic Acid to Ubiquinone in* Saccharomyces cerevisiae, University of St. Louis, St. Louis, MO
13. Young, D. M., Parke, D., and Ornston, L. N. (2005) *Annu. Rev. Microbiol.* **59,** 519–551
14. Edman, J. C., Goldstein, A. L., and Erbe, J. G. (1993) *Yeast* **9,** 669–675
15. Castelli, L. A., Nguyen, N. P., and Macreadie, I. G. (2001) *FEMS Microbiol. Lett.* **199,** 181–184
16. Botet, J., Mateos, L., Revuelta, J. L., and Santos, M. A. (2007) *Eukaryot. Cell* **6,** 2102–2111
17. Güldener, U., Koehler, G. J., Haussmann, C., Bacher, A., Kricke, J., Becher, D., and Hegemann, J. H. (2004) *Mol. Biol. Cell* **15,** 3811–3828
18. Pierrel, F., Hamelin, O., Douki, T., Kieffer-Jaquinod, S., Mühlenhoff, U., Ozeir, M., Lill, R., and Fontecave, M. (2010) *Chem. Biol.* **17,** 449–459
19. Güldener, U., Heck, S., Fielder, T., Beinhauer, J., and Hegemann, J. H. (1996) *Nucleic Acids Res.* **24,** 2519–2524
20. Brajcich, B. C., Iarocci, A. L., Johnstone, L. A., Morgan, R. K., Lonjers, Z. T., Hotchko, M. J., Muhs, J. D., Kieffer, A., Reynolds, B. J., Mandel, S. M., Marbois, B. N., Clarke, C. F., and Shepherd, J. N. (2010) *J. Bacteriol.* **192,**

Downloaded from http://www.jbc.org/ at UCLA-Louise Darling Biomed. Lib. on July 2, 2014

436–445
21. Lester, R. L., and Crane, F. L. (1959) *J. Biol. Chem.* **234,** 2169–2175
22. Poon, W. W., Marbois, B. N., Faull, K. F., and Clarke, C. F. (1995) *Arch. Biochem. Biophys.* **320,** 305–314
23. Elliot, W. H., and Waller, G. R. (1972) in *Biochemical Applications of Mass Spectrometry* (Waller, G. R., ed) pp. 499–536, Wiley-Interscience, New York
24. Carlson, M. (1999) *Curr. Opin. Microbiol.* **2,** 202–207
25. Poon, W. W., Do, T. Q., Marbois, B. N., and Clarke, C. F. (1997) *Mol. Aspects Med.* **18,** (suppl.) S121–S127
26. Tzagoloff, A., and Dieckmann, C. L. (1990) *Microbiol. Rev.* **54,** 211–225
27. Ashby, M. N., and Edwards, P. A. (1990) *J. Biol. Chem.* **265,** 13157–13164
28. Young, I. G., Stroobant, P., Macdonald, C. G., and Gibson, F. (1973) *J. Bacteriol.* **114,** 42–52
29. Marbois, B. N., and Clarke, C. F. (1996) *J. Biol. Chem.* **271,** 2995–3004
30. Alam, S. S., Nambudiri, A. M., and Rudney, H. (1975) *Arch. Biochem. Biophys.* **171,** 183–190
31. Davis, B. D. (1951) *J. Exp. Med.* **94,** 243–254
32. Hamilton, J. A., and Cox, G. B. (1971) *Biochem. J.* **123,** 435–443
33. Turunen, M., Olsson, J., and Dallner, G. (2004) *Biochim. Biophys. Acta* **1660,** 171–199
34. Forsman, U., Sjöberg, M., Turunen, M., and Sindelar, P. J. (2010) *Nat. Chem. Biol.* **6,** 515–517
35. Stenmark, P., Grünler, J., Mattsson, J., Sindelar, P. J., Nordlund, P., and Berthold, D. A. (2001) *J. Biol. Chem.* **276,** 33297–33300
36. Trumpower, B. L., Aiyar, A. S., Opliger, C. E., and Olson, R. E. (1972) *J. Biol. Chem.* **247,** 2499–2511
37. Padilla, S., Tran, U. C., Jiménez-Hidalgo, M., López-Martín, J. M., Martín-Montalvo, A., Clarke, C. F., Navas, P., and Santos-Ocaña, C. (2009) *Cell Mol. Life Sci.* **66,** 173–186
38. Marbois, B., Gin, P., Faull, K. F., Poon, W. W., Lee, P. T., Strahan, J., Shepherd, J. N., and Clarke, C. F. (2005) *J. Biol. Chem.* **280,** 20231–20238
39. Dawson, R. M. (1986) *Data for Biochemical Research*, 3rd ed., pp. 42 and 116, Clarendon Press, Oxford
40. Reed, L. J., Schram, A. C., and Loveless, L. E. (1959) *J. Biol. Chem.* **234,** 904–908
41. Quinlivan, E. P., Roje, S., Basset, G., Shachar-Hill, Y., Gregory, J. F., 3rd, and Hanson, A. D. (2003) *J. Biol. Chem.* **278,** 20731–20737
42. Threlfall, D. R., Law, A., and Whistance, G. R. (1970) *Biochem. J.* **118,** 55P
43. Parson, W. W., and Rudney, H. (1964) *Proc. Natl. Acad. Sci. U.S.A.* **51,** 444–450
44. Sircar, D., and Mitra, A. (2009) *J. Plant Physiol.* **166,** 1370–1380
45. Iliades, P., Berglez, J., Meshnick, S., and Macreadie, I. (2003) *Microb. Drug Resist.* **9,** 249–255
46. Eudes, A., Bozzo, G. G., Waller, J. C., Naponelli, V., Lim, E. K., Bowles, D. J., Gregory, J. F., 3rd, and Hanson, A. D. (2008) *J. Biol. Chem.* **283,** 15451–15459
47. Cohen, F. S., Eisenberg, M., and McLaughlin, S. (1977) *J. Membr. Biol.* **37,** 361–396
48. Hampele, I. C., D'Arcy, A., Dale, G. E., Kostrewa, D., Nielsen, J., Oefner, C., Page, M. G., Schonfeld, H. J., Stüber, D., and Then, R. L. (1997) *J. Mol. Biol.* **268,** 21–30
49. Ashby, M. N., Kutsunai, S. Y., Ackerman, S., Tzagoloff, A., and Edwards, P. A. (1992) *J. Biol. Chem.* **267,** 4128–4136
50. Tzagoloff, A., Akai, A., and Needleman, R. B. (1975) *J. Biol. Chem.* **250,** 8228–8235
51. Brachmann, C. B., Davies, A., Cost, G. J., Caputo, E., Li, J., Hieter, P., and Boeke, J. D. (1998) *Yeast* **14,** 115–132
52. Winzeler, E. A., Shoemaker, D. D., Astromoff, A., Liang, H., Anderson, K., Andre, B., Bangham, R., Benito, R., Boeke, J. D., Bussey, H., Chu, A. M., Connelly, C., Davis, K., Dietrich, F., Dow, S. W., El Bakkoury, M., Foury, F., Friend, S. H., Gentalen, E., Giaever, G., Hegemann, J. H., Jones, T., Laub, M., Liao, H., Liebundguth, N., Lockhart, D. J., Lucau-Danila, A., Lussier, M., M'Rabet, N., Menard, P., Mittmann, M., Pai, C., Rebischung, C., Revuelta, J. L., Riles, L., Roberts, C. J., Ross-MacDonald, P., Scherens, B., Snyder, M., Sookhai-Mahadeo, S., Storms, R. K., Véronneau, S., Voet, M., Volckaert, G., Ward, T. R., Wysocki, R., Yen, G. S., Yu, K., Zimmermann, K., Philippsen, P., Johnston, M., and Davis, R. W. (1999) *Science* **285,** 901–906

Downloaded from http://www.jbc.org/ at UCLA-Louise Darling Biomed. Lib. on July 2, 2014

Downloaded on July 3, 2014. The Journal of Clinical Investigation. More information at www.jci.org/articles/view/45693



Research article

# *COQ6* mutations in human patients produce nephrotic syndrome with sensorineural deafness

Saskia F. Heeringa,[1] Gil Chernin,[1] Moumita Chaki,[1] Weibin Zhou,[1] Alexis J. Sloan,[2] Ziming Ji,[3] Letian X. Xie,[3] Leonardo Salviati,[4] Toby W. Hurd,[1] Virginia Vega-Warner,[1] Paul D. Killen,[5] Yehoash Raphael,[5] Shazia Ashraf,[1] Bugsu Ovunc,[1] Dominik S. Schoeb,[1] Heather M. McLaughlin,[1,6] Rannar Airik,[1] Christopher N. Vlangos,[1] Rasheed Gbadegesin,[1] Bernward Hinkes,[1,7] Pawaree Saisawat,[1] Eva Trevisson,[4] Mara Doimo,[4] Alberto Casarin,[4] Vanessa Pertegato,[4] Gianpietro Giorgi,[4] Holger Prokisch,[8,9] Agnès Rötig,[10] Gudrun Nürnberg,[11,12,13] Christian Becker,[11] Su Wang,[5] Fatih Ozaltin,[14] Rezan Topaloglu,[14] Aysin Bakkaloglu,[14] Sevcan A. Bakkaloglu,[15] Dominik Müller,[16] Antje Beissert,[17] Sevgi Mir,[18] Afig Berdeli,[18] Seza Özen,[14] Martin Zenker,[19] Verena Matejas,[7] Carlos Santos-Ocaña,[20] Placido Navas,[20] Takehiro Kusakabe,[21] Andreas Kispert,[22] Sema Akman,[23] Neveen A. Soliman,[24] Stefanie Krick,[2] Peter Mundel,[2] Jochen Reiser,[2] Peter Nürnberg,[11,12,13] Catherine F. Clarke,[3] Roger C. Wiggins,[5] Christian Faul,[2] and Friedhelm Hildebrandt[1,6,25]

[1]Department of Pediatrics, University of Michigan, Ann Arbor, Michigan, USA. [2]Department of Medicine, University of Miami Miller School of Medicine, Miami, Florida, USA. [3]Department of Chemistry and Biochemistry and Molecular Biology Institute, UCLA, Los Angeles, California, USA. [4]Department of Pediatrics, University of Padua, Padua, Italy. [5]Department of Internal Medicine, Department of Pathology, and Department of Otolaryngology and [6]Department of Human Genetics, University of Michigan, Ann Arbor, Michigan, USA. [7]Institute of Human Genetics, University Hospital of Erlangen, Erlangen, Germany. [8]Institute of Human Genetics, Helmholtz Zentrum Munich, German Research Center for Environmental Health, Neuherberg, Germany. [9]Institute of Human Genetics, Klinikum rechts der Isar, Technical University Munich, Munich, Germany. [10]INSERM U781, Hôpital Necker-Enfants Malade, Université René Descartes, Paris, France. [11]Cologne Center for Genomics, [12]Center for Molecular Medicine Cologne (CMMC), and [13]Cologne Excellence Cluster on Cellular Stress Responses in Aging-Associated Diseases (CECAD), University of Cologne, Cologne, Germany. [14]Department of Pediatric Nephrology, Hacettepe University, Ankara, Turkey. [15]Department of Pediatric Nephrology, Gazi University Faculty of Medicine, Ankara, Turkey. [16]Department of Pediatric Nephrology, Charité, Berlin, Germany. [17]University Children's Hospital, Würzburg, Germany. [18]Department of Pediatrics, Ege University, Izmir, Turkey. [19]Institute of Human Genetics, University Hospital of Magdeburg, Magdeburg, Germany. [20]Centro Andaluz de Biología del Desarrollo, Universidad Pablo de Olavide-CSIC and CIBERER, ISCIII, Seville, Spain. [21]Department of Biology, Faculty of Science and Engineering, Konan University, Kobe, Japan. [22]Institut für Molekularbiologie, Medizinische Hochschule Hannover, Hannover, Germany. [23]Department of Pediatric Nephrology, Akdeniz University, School of Medicine, Antalya, Turkey. [24]Department of Pediatrics, Kasr Alainy School of Medicine, Cairo University, Cairo, Egypt. [25]Howard Hughes Medical Institute, University of Michigan, Ann Arbor, Michigan, USA.

**Steroid-resistant nephrotic syndrome (SRNS) is a frequent cause of end-stage renal failure. Identification of single-gene causes of SRNS has generated some insights into its pathogenesis; however, additional genes and disease mechanisms remain obscure, and SRNS continues to be treatment refractory. Here we have identified 6 different mutations in coenzyme $Q_{10}$ biosynthesis monooxygenase 6 (*COQ6*) in 13 individuals from 7 families by homozygosity mapping. Each mutation was linked to early-onset SRNS with sensorineural deafness. The deleterious effects of these human *COQ6* mutations were validated by their lack of complementation in *coq6*-deficient yeast. Furthermore, knockdown of *Coq6* in podocyte cell lines and *coq6* in zebrafish embryos caused apoptosis that was partially reversed by coenzyme $Q_{10}$ treatment. In rats, COQ6 was located within cell processes and the Golgi apparatus of renal glomerular podocytes and in stria vascularis cells of the inner ear, consistent with an oto-renal disease phenotype. These data suggest that coenzyme $Q_{10}$–related forms of SRNS and hearing loss can be molecularly identified and potentially treated.**

## Introduction

Nephrotic syndrome (NS), a malfunction of the kidney glomerular filter, leads to proteinuria, hypoalbuminemia, and edema. Steroid-resistant NS (SRNS) represents a frequent cause of end-stage renal failure (ESRF), which requires renal replacement therapy for survival. Identification of single-gene causes of NS (1–7) has generated the first insights (8, 9) into its pathogenesis: (a) that single-gene causes of NS result in SRNS (10, 11) with very few exceptional cases that respond to treatment (3, 12); (b) that SRNS-causing genes are expressed in a specialized cell type, the glomerular podocyte (13); and (c) that the pathohistology ranges from the intrauterine-onset severe developmental phenotype of diffuse mesangial sclerosis (DMS) to the childhood-onset phenotype of focal segmental glomerulosclerosis (FSGS). Two-thirds of all SRNS cases with onset in the first year of life (14) and 10%–28% of all childhood cases (15) are caused by single-gene mutations in 1 of only 4 genes, *NPHS1* (1), *NPHS2* (2), *LAMB2* (16), and *WT1* (17). However, the molecular cause of more than 80% of all cases of SRNS is unknown, and treatment options have yet to be discovered. We therefore performed total genome search for linkage to identify further causative recessive genes.

**Authorship note:** Saskia F. Heeringa and Gil Chernin contributed equally to this work.

**Conflict of interest:** The authors have declared that no conflict of interest exists.

**Citation for this article:** *J Clin Invest.* 2011;121(5):2013–2024. doi:10.1172/JCI45693.

Downloaded on July 3, 2014. The Journal of Clinical Investigation. More information at www.jci.org/articles/view/45693



## Results

*COQ6 mutations cause SRNS with sensorineural deafness (SND).* To identify further single-gene causes for SRNS, we performed a genome-wide search for linkage in 14 different consanguineous families with SRNS. Calculating lod under the hypothesis of locus heterogeneity yielded a significant maximum heterogeneity lod score of 4.9 ($\alpha = 52\%$) on human chromosome 14q24.3, covering a region of 6.4 Mb (Figure 1A). Of 7 families homozygous at this locus (*SRNS2*), families A1072 and F1082 from Turkey revealed haplotype sharing (Figure 1B), restricting the critical genetic region to 2.1 Mb under the hypothesis that an ancestor common to both families introduced the disease allele (i.e., homozygosity by descent). This interval contained 32 positional candidate genes (Figure 1C).

Exon sequencing of *COQ6* yielded homozygous mutations in 3 of the 7 families homozygous at the *SRNS2* locus (Table 1). In both affected individuals of family A1072, we detected a homozygous A353D substitution (Figure 1G and Table 1) that was also found in family F1082, as predicted from haplotype sharing at *SRNS2* (Figure 1B). All 3 affected individuals that were examined in the northern Lebanese family F252 exhibited the homozygous change G255R (Figure 1G and Table 1). This mutation was shared by 3 affected individuals of family A234 from southern Turkey (Table 1), most likely as a founder effect. Both missense mutations altered amino acid residues that are uniformly conserved from *E. coli* to humans (Figure 1G). Another individual with SRNS from Turkey revealed 2 compound heterozygous truncating mutations, W447X and Q461fsX478 (Figure 1G and Table 1). All mutations were absent from more than 90 healthy control subjects from central Europe and 60 healthy control subjects from Turkey. Segregation of mutations was consistent with recessive inheritance (Table 1). In all 9 individuals with SRNS that were examined for hearing loss, there was SND (Table 1). Exon sequencing of all other 31 genes at the *SRNS2* locus did not yield any mutations in the families F252, F1082, and A1072. We thus identified mutations in *COQ6* as a cause of recessive early-onset SRNS with SND (NPHS type 5), which we believe to be novel.

We then performed exon PCR of *COQ6* in another 530 families: 70 with SRNS, 35 that were homozygous for 3 markers at the *COQ6* locus, 55 with a neurologic phenotype, and 370 with a mitochondriopathy. We identified a single heterozygous nonsense mutation, R162X, in A988-21, an individual with cyclosporine A–dependent (CsA-dependent) NS, and a single heterozygous nonsense mutation, W188X, in A1904-21, an individual with DMS (Figure 1G). As NPHS type 5 appears recessive, the second mutation most likely escaped identification in these 2 families.

All 11 affected individuals of the 5 families with 2 recessive *COQ6* mutations had SRNS. They manifested with proteinuria at a median age of 1.2 years (range, 0.2–6.4 years) and progressed to ESRF by a median age of 1.7 years (range, 0.4–9.3 years); 5 individuals died in early childhood (median age, 5.0 years). Renal biopsy revealed FSGS in 7 cases (Table 1 and Figure 2, A–C) and DMS in 1 case. Subject A234-21 presented with seizures, and subject F1082-21 had white matter abnormalities and seizures and died of multiorgan failure in sepsis; 2 other individuals had ataxia and facial dysmorphism (individuals F252-51 and A234-26, respectively; Table 1).

*COQ6 function.* The *COQ6* gene extends over 13.2 kb and contains 12 exons (Figure 1, D and E). There are 18 putative isoforms resulting from alternative splicing (www.aceview.org). Full-length isoforms a and b contain 12 exons, but use alternative exons 1a and 1b (Supplemental Figure 1, A and B; supplemental material available online with this article; doi:10.1172/JCI45693DS1). Full-length isoforms were expressed in multiple tissues, including the kidney (Supplemental Figure 1, C–F). Using in situ hybridization analysis, we demonstrated *Coq6* mRNA expression in the metanephric mesenchyme and forming nephrons of mouse kidney (Supplemental Figure 1, G–L). Isoform a (encoding a 54-kDa protein) is predicted to be expressed in mitochondria with a Predotar score of 0.81 (http://urgi.versailles.inra.fr/predotar) because of a mitochondrial leader peptide, whereas isoform b (encoding a 51-kDa protein), which uses an alternative exon 1, is considered only possibly mitochondrial, with a Predotar score of 0.45. Both isoforms encode a flavin-dependent monooxygenase with 3 flavin adenine dinucleotide–binding motifs (18). The amino acid sequence is highly conserved throughout evolution, with identity to the human COQ6 protein sequence of 66% for *Danio rerio* and 33% for the *E. coli* ortholog *UbiH*. The enzyme coenzyme $Q_{10}$ monooxygenase 6 (COQ6) is required for biosynthesis of coenzyme $Q_{10}$ ($CoQ_{10}$; also referred to as ubiquinone) and is thought to catalyze one or more ring hydroxylation steps. Humans synthesize $CoQ_{10}$, and yeast synthesizes $CoQ_6$ (where $CoQ_n$ designates a polyisoprene residue with *n* isoprene units). $CoQ_{10}$ operates as a redox carrier in the mitochondrial respiratory chain shuttling electrons from respiratory chain complexes RCCI and RCCII to complex RCCIII (19). $CoQ_{10}$ also serves as a lipid-soluble antioxidant and has previously been implicated in protection from cell damage by ROS (20).

Because rare recessive mutations have been described in syndromic and nonsyndromic forms of NS (21, 22) in other genes involved in $CoQ_{10}$ biosynthesis (23–25), we performed sequencing of all exons of the following 11 candidate genes: *PDSS1*, *PDSS2*, *COQ2*, *COQ3*, *COQ4*, *COQ5*, *COQ7*, *COQ8*, *COQ9*, *COQ10a*, and *COQ10b*. We examined 42 individuals with SRNS who had extrarenal symptoms suggestive of mitochondrial disease or in whom only 1 heterozygous *COQ6* mutation was found. However, we did not detect any further mutations. The 4 protein-truncating mutations in *COQ6* that we detected in subjects A988, A1904, and A3331-21 (Figure 1G and Table 1) may be considered null alleles. Similarly, the fully conserved homozygous missense mutations G225R and A353D that we observed in 4 families with SRNS and SND may also represent loss-of-function mutations (Figure 1G and Table 1). To test this hypothesis, we examined all 6 *COQ6* mutations for potential deleterious effects by complementation in *coq6*-deficient yeast strains. Yeast cells harboring a deletion mutation in the *coq6* gene were unable to grow on yeast extract/peptone/glycerol media (YPG; in which glycerol acts as a nonfermentable carbon source) and were deficient in $CoQ_6$ (Figure 2, D and E, and ref. 18). Expression of human WT *COQ6* with an aminoterminal yeast mitochondrial leader sequence rescued both YPG growth and $CoQ_6$ content (Figure 2, D and E), although not as robustly as did yeast harboring the WT *COQ6* gene (pSR1-1; Figure 2, D and E). Rescue of growth on YPG was observed with either low-copy number (pQM; Figure 2D) or high-copy number (pRCM; data not shown) expression constructs. Both constructs also rescued the deficiency in $CoQ_6$ content (Figure 2E). In contrast, none of the *Coq6* constructs harboring the human mutations (Figure 1G and Table 1) were able to rescue the growth deficiency phenotype or $CoQ_6$ content phenotypes (Figure 2, D and E), thereby demonstrating the deleterious effects of these mutations.

*Response to $CoQ_{10}$ treatment.* Monogenic variants of childhood NS are characterized by a lack of response to therapy (26). Because successful $CoQ_{10}$ treatment had been described previously in an

Downloaded on July 3, 2014. The Journal of Clinical Investigation. More information at www.jci.org/articles/view/45693



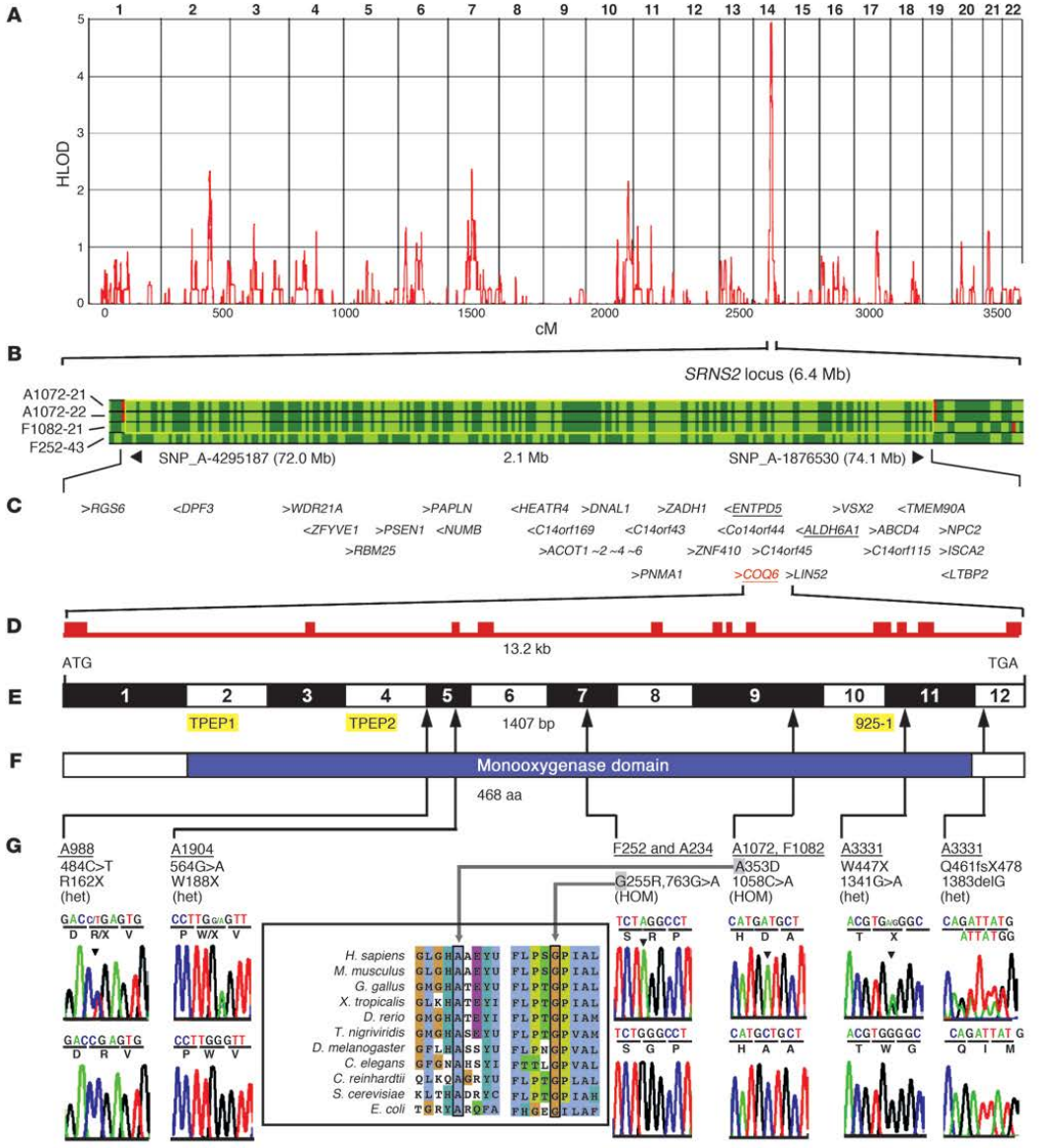



**Figure 1**

Positional cloning of *COQ6* mutations in individuals with NS and SND. (**A**) lod score profile across the human genome in affected children from 14 consanguineous kindred with SRNS. Parametric heterogeneity lod (HLOD) scores are plotted against human chromosomal mapping positions, concatenated from p-ter (left) to q-ter (right). (**B**) Within the *SRNS2* locus, haplotypes from 250k SNP analysis are shown for 3 of the 7 families with homozygosity at the *SRNS2* locus. Alleles are colored light green (AA), dark green (BB), and red (AB). (**C**) The 32 genes within the *SRNS2* locus; 3 genes preferentially expressed in kidney podocytes are underlined. Mutations were found in *COQ6*. Transcriptional direction is indicated by < or >. (**D**) *COQ6* extends over 13.2 kb and contains 12 exons (boxes). (**E**) Exon structure of COQ6 cDNA. Arrows indicate relative positions of mutations (see **G**). Positions of peptides for antibody generation are shown in yellow. (**F**) Domain structure of COQ6 protein. Extent of the monooxygenase domain is shown in relation to encoding exon position (**E**). (**G**) 6 different *COQ6* mutations in 7 families with SRNS. Family number and amino acid change (see Table 1) are given above sequence traces. Arrows denote positions of mutations in relation to exons and protein domains. For the 2 missense mutations, G255R and A363D, full conservation across evolution of altered amino acid residues is illustrated.

Downloaded on July 3, 2014. The Journal of Clinical Investigation. More information at www.jci.org/articles/view/45693



**Table 1**
Recessive *COQ6* mutations detected in 5 families with NS and deafness

| Patient ID | Origin | Consang | Nucleotide mutation | Protein sequence change[A] | Exon (segregation)[B] | Age at onset (yr) | Age at ESRF (yr) | Kidney disease/ treatment[C] | Histology (at yr of age) | Extrarenal manifestations |
|---|---|---|---|---|---|---|---|---|---|---|
| F252-43 | Lebanon | Y | 763G>A | G255R | 7 (hom,M,P) | 6.4 | 9.3 | SRNS | FSGS (6.8) | Congenital SND |
| F252-46 | Lebanon | Y | 763G>A | G255R | 7 (hom,M,P) | 0.3 | 1.7 | SRNS | ND | Congenital SND (died 17.5 yr) |
| F252-51 | Lebanon | Y | 763G>A | G255R | 7 (hom,M,P) | 1.2 | 1.4 | SRNS | FSGS (1.2) | SND, ataxia (died 6.5 yr) |
| F252-42 | Lebanon | Y | ND | ND | 7 (hom,M,P) | <1.0 | 3.0 | SRNS, CP-R | FSGS (1.1) | Congenital SND (died 5.0 yr) |
| A234-21 | Turkey | Y | 763G>A | G255R | 7 (hom,M,P) | 0.3 | 0.4 | SRNS | DMS | Seizures (died) |
| A234-26 | Turkey | Y | 763G>A | G255R | 7 (hom,M,P) | 0.3 | 0.4 | SRNS, $CoQ_{10}$[D] | ND | SND, facial dysmorphism |
| A234-27 | Turkey | Y | 763G>A | G255R | 7 (hom,M,P) | 0.2 | (none at 15 mo) | $CoQ_{10}$, ACE-I[D] | ND | SND (10 mo), bilateral nephrolithiasis (5 mo), GR |
| A1072-21 | Turkey | Y | 1058C>A | A353D | 9 (hom,M,P) | 6.0 | 6.5 | SRNS, CP-R | FSGS (6) | SND (6 yr) |
| A1072-22 | Turkey | Y | 1058C>A | A353D | 9 (hom,M,P) | 2.5 | NA | SRNS, CsA-S, $CoQ_{10}$[D] | FSGS (2.5) | SND (4 yr) |
| F1082-21 | Turkey | Y | 1058C>A | A353D | 9 (hom,M,ND) | 2.5 | 3.4 | SRNS | FSGS (3) | Seizures, white matter abnormalities (died, sepsis) |
| A3331-21 | Turkey | N | 1341G>A | W447X | 11 (het,P) | 3.0 | NA | SRNS, CP-R, ACE-I, levamizole | FSGS (3) | SND (40% of normal) |
| A3331-21 | Turkey | N | 1383delG[E] | Q461fsX478[E] | 12 (het,M) | 3.0 | NA | SRNS, CP-R, ACE-I, levamizole | FSGS (3) | SND (40% of normal) |

2 additional mutations (heterozygous only) were detected in families A998 (R162X) and A1904 (W188X) (see Figure 1G). ND, no data or DNA available. Consang, Consanguinity. [A]All mutations were absent from more than 90 healthy control subjects from Central Europe and from 60 healthy control subjects from Turkey. All missense mutations were conserved down to *E. coli*. [B]hom, homozygous in affected individual; het, heterozygous in affected individual; M, heterozygous mutation identified in mother; P, heterozygous mutation identified in father. [C]ACE-I, ACE inhibitor; CsA-S, CsA sensitive; CP-R, cyclophosphamide resistant; GR, growth retardation; $CoQ_{10}$, treatment with $CoQ_{10}$. [D]Treatment-sensitive case (renal replacement therapy not listed). [E]Isoform a.

individual with *COQ2* mutations (12), we administered $CoQ_{10}$ in 2 children whose parents consented. Treatment was administered orally, giving 1 Softgel $CoQ_{10}$ capsule (50 mg; GNC Preventive Nutrition) twice per day. Individual A234-27 presented with proteinuria without edema at 2 months of age, when the *COQ6* mutation was detected in his sister (A234-26) and cousin (A234-21). Urine protein/creatinine ratio was 40 mg/mg initially (normal, <0.2 mg/mg). Treatment was commenced at 2 months of age, giving $CoQ_{10}$ orally at 15 mg/kg/d divided in 3 doses over 2 months together with enalapril (1.25 mg/d orally). $CoQ_{10}$ treatment was then increased to 30 mg/kg/d, and urine protein/creatinine ratio decreased to 8 mg/mg within 2 months. Proteinuria decreased further to 5.8 mg/mg and remained stable at 4.8 mg/mg during the last follow-up at 15 months of age. Renal function was normal throughout. Bilateral severe SND and severe growth retardation were noted at 10 months. After treatment with 50 mg $CoQ_{10}$ orally twice per day, SND substantially improved in A234-26. Individual A1072-22 manifested with NS at age 2.5 years. $CoQ_{10}$ treatment was started at 5.5 years of age, when the subject was in partial remission from CsA treatment, which was discontinued at 5.8 years. At the beginning of $CoQ_{10}$ treatment, 24-hour protein excretion was 7 mg/m$^2$/h (117 mg/d); 2 months into treatment, it decreased to 3.7 mg/m$^2$/h (76 mg/d), and remission was maintained at the end of the study period. Hearing was not improved after $CoQ_{10}$ treatment. When $CoQ_{10}$ treatment was inadvertently interrupted, proteinuria reappeared at a level of 57 mg/m$^2$/h (1,100 mg/d). Following reinstitution of $CoQ_{10}$ treatment, proteinuria decreased again to 9 mg/m$^2$/h (188 mg/d).

*Exogenous Coq6 localizes to mitochondria.* To study the subcellular localization of COQ6, we generated GFP-labeled clones of human full-length isoforms a, b, and c (Supplemental Figure 1, A and B). We also generated anti-COQ6 antibodies directed against the synthetic peptides, whose positions in relation to exons and protein domains are shown in Figure 1E. Following affinity purification, antibody α-COQ6-TPEP2 detected a major band at the expected size of 50.8 kDa for full-length human COQ6 (Supplemental Figure 2). Because human full-length *COQ6* isoform a contains a putative mitochondrial leader sequence, we predicted that exogenous expression would result in mitochondrial localization. Indeed, after transient exogenous transfection into Cos-7 or HeLa cells or into murine podocyte cell lines, exogenous *COQ6* isoform a colocalized quantitatively in mitochondria with mitochondrial markers cytochrome *c* and cytochrome *c* oxidase (COXIV; Figure 3, A and B). Surprisingly, whereas α-COQ6-TPEP2 clearly detected exogenously expressed COQ isoform a, thereby confirming specificity of the antibody, it detected an additional endogenous signal that appeared to be localized in Golgi apparatus (Figure 3C). In fact, this endogenous signal detected by α-COQ6-TPEP2 was located in Golgi, as confirmed by double labeling with the Golgi marker Golgin 97 (Figure 3D). Interestingly, α-COQ6-TPEP2 did not reveal any endogenous COQ6 expression in mitochondria (Figure 3, D and E). Furthermore, exogenously

Downloaded on July 3, 2014. The Journal of Clinical Investigation. More information at www.jci.org/articles/view/45693



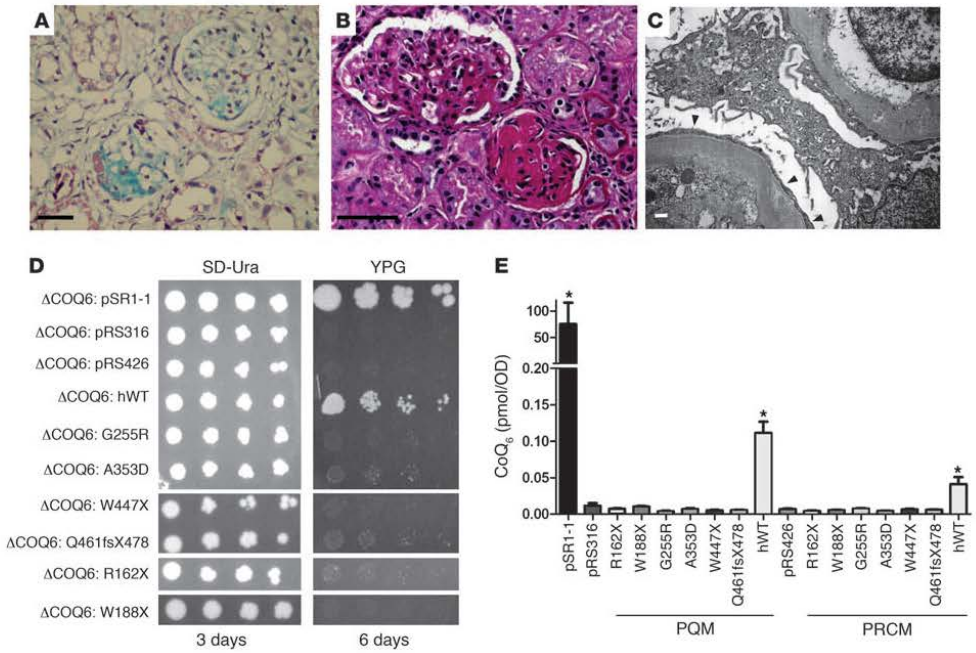



**Figure 2**

*COQ6* loss-of-function causes glomerular damage in human kidney and growth defects in yeast. (**A**–**C**) Renal histology in individuals revealed homozygous *COQ6* mutation in A3331-21 FSGS, demonstrated by increased fibrosis (blue) in Trichrome-Masson staining (**A**), and in F1082-21, demonstrated by excess PAS staining (red) (**B**). (**C**) Transmission electron microscopy for F1082 showed effacement of podocyte foot processes, resulting in a continuous electron-dense layer (arrowheads). Scale bars: 50 μm (**A** and **B**); 250 nm (**C**). (**D** and **E**) Functional test of human *COQ6* mutations in yeast *coq6*-null mutants. (**D**) WT human *COQ6* (hWT), but not mutations, rescued growth in yeast *coq6*-null mutants plated on a nonfermentable carbon source. Yeast cells harboring the indicated low-copy plasmids were cultured in SD-Ura, seeded to both SD-Ura and YPG plate media, and incubated at 30°C for the times indicated. pSR1-1 contains the yeast *COQ6* gene (18) and served as positive control. Empty vectors pRS316 and pRS426 served as negative controls. (**E**) WT human *COQ6*, but not mutations, rescued $CoQ_6$ synthesis in yeast *coq6*-null mutants. $CoQ_6$ content of each yeast *coq6*-null mutant harboring 1 of the designated plasmids was determined as described in Methods. Each $CoQ_6$ measurement represents mean ± SD of 4 measurements from 2 independent samples. *$P < 0.0005$ versus negative control (99% confidence level). PQM and PRCM indicate low– and high–copy number plasmids, respectively.

expressed full-length *COQ6* isoform a spared Golgi expression, as demonstrated with Giantin as a Golgi marker (Figure 3F). Likewise, in podocyte cell lines, the cell type central to the disease mechanism of SRNS, α–COQ6-TPEP2 detected endogenous COQ6 in Golgi, but not in mitochondria (Figure 3G). The endogenous COQ6 expression pattern was confirmed with the antibody α–COQ6–925-1 (Supplemental Figure 3, A and B), which was derived from a different peptide (Figure 1E).

*Endogenous COQ6, COQ7, and COQ9 colocalize to cell processes and Golgi in rat podocytes.* Monogenic forms of SRNS are caused by dysfunction of the glomerular podocyte, a terminally differentiated cell critical for the filtering function of the kidney glomerulus. (13, 26). We therefore examined expression of the COQ6 protein in kidney. COQ6 was seen almost exclusively in glomeruli, rather than in tubules (Figure 4A). As predicted, within glomeruli, COQ6 was expressed specifically in podocytes, as marked by WT1 labeling (Figure 4A). Within podocytes, COQ6 was absent from mitochondria (labeled with COXIV; Figure 4A); conversely, it was expressed within cellular processes and within Golgi apparatus (Figure 4, B and C), which confirmed the results obtained in cell lines (Figure 3). Because nonmitochondrial localization and function has been previously described for $CoQ_6$ (27), we hypothesized that nonmitochondrial expression would also apply to COQ7 and COQ9, which are known as mitochondrial proteins but share a multienzyme complex together with COQ6 for the biosynthesis of $CoQ_{10}$ and $CoQ_6$ (21). Indeed, upon immunofluorescence, both COQ6 and COQ7 fully colocalized to cellular processes and Golgi of rat glomerular podocytes (Figure 4, B and C), as did COQ7 and COQ9 (Supplemental Figure 3C). We demonstrated specificity of this signal for α–COQ6-TPEP2 by showing the absence of the podocyte signal after preabsorption with the cognate peptide TPEP2, in contrast to its presence after preabsorption with the noncognate peptide TPEP1 (Supplemental Figure 3D). In addition, COQ6 colocalized to podocyte cellular processes with podocin (Figure 4E), another gene product that, if mutated, causes a Mendelian form of SRNS (2). These findings demonstrate that COQ6, COQ7, and COQ9 are all 3 expressed in cellular processes and Golgi apparatus of podocytes rather than in mitochondria.

Downloaded on July 3, 2014. The Journal of Clinical Investigation. More information at www.jci.org/articles/view/45693



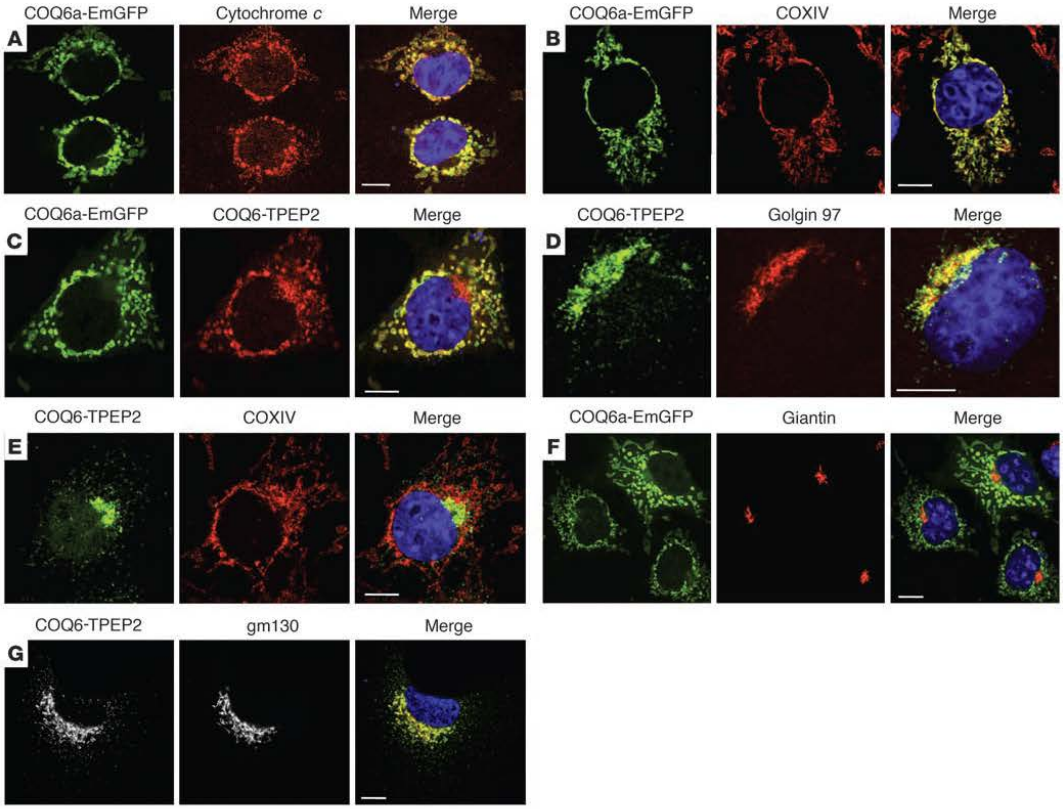



**Figure 3**

Transient exogenous expression of full-length human *COQ6* isoform a into Cos-7 cells, HeLa cells, or murine podocyte cell lines. (**A** and **B**) GFP-labeled full-length human *COQ6* isoform a (COQ6a-EmGFP) exogenously expressed in Cos-7 cells colocalized quantitatively with mitochondrial markers cytochrome *c* (**A**) and COXIV (**B**). (**C**–**E**) GFP-labeled full-length human *COQ6* isoform a expressed exogenously in HeLa cells was detected by α–COQ6-TPEP2 upon immunofluorescence, thereby confirming specificity of the antibody (**C**). α–COQ6-TPEP2 detected an additional endogenous signal, which appeared to be localized in Golgi apparatus (**C**), as confirmed by double labeling with Golgi marker Golgin 97 (**D**). α–COQ6-TPEP2 did not reveal any endogenous COQ6 expression in mitochondria (**D** and **E**). (**F**) GFP-labeled full-length human *COQ6* isoform a expressed exogenously in HeLa cells spared Golgi expression, as demonstrated with Giantin as a Golgi marker. (**G**) α–COQ6-TPEP2 detected endogenous COQ6 in Golgi of a podocyte cell line, as marked by gm130, but not in mitochondria. Scale bars: 5 μm.

We then investigated expression of COQ6 in the inner ear, because hearing loss is the other phenotype in this oto-renal syndrome. Immunofluorescence studies using α–COQ6-TPEP2 revealed COQ6 expression in the spiral ganglion as well as in cells of stria vascularis and spiral ligament (Figure 4, F and G), which are involved in maintaining the high potassium concentration in the cochlear duct necessary for sound transduction of the hair cells of Corti organ.

*Coq6 knockdown in cultured podocytes induces apoptosis that is reversed by $CoQ_{10}$ treatment.* In order to study *COQ6* function in glomerular podocytes, the cell type involved in the disease phenotype, we performed knockdown of *Coq6* expression in vitro using a vector-based siRNA approach (28). Murine podocytes (29) were stably transfected with *COQ6* siRNA constructs, and clones were analyzed by RT-PCR for *Coq6* expression levels. We compared clones transfected using a scrambled siRNA oligonucleotide with non-transfected WT podocytes. The 3 clones that showed the highest degree of *Coq6* downregulation (clones 1, 2, and 5) were selected for functional studies (Supplemental Figure 1M). First, we analyzed the growth behavior of *Coq6* knockdown clones when kept in an undifferentiated and proliferative state (Figure 5A). When we seeded a defined number of cells and counted them after 24, 48, and 72 hours of cultivation, we found that the growth rate of the 3 *Coq6* knockdown clones was strongly decreased, while the scrambled siRNA clone C proliferated at the same rate as WT cells (Figure 5A). This difference reached statistical significance after 24 hours for clones 2 and 5 ($P < 0.05$) and after 72 hours for clone 1 ($P < 0.005$; Figure 5A). As the scrambled siRNA clone C did not

Downloaded on July 3, 2014. The Journal of Clinical Investigation. More information at www.jci.org/articles/view/45693



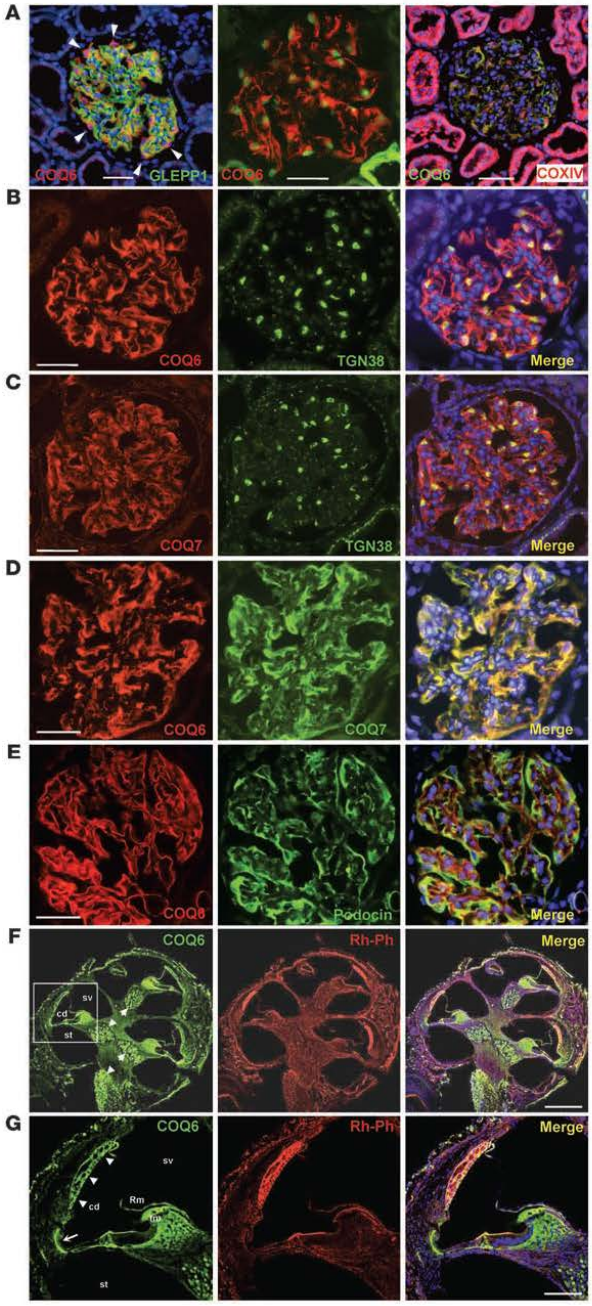



**Figure 4**
COQ6 and COQ7 colocalize in rat podocytes to cell processes and Golgi and in the inner ear to stria vascularis and spiral ligament cells. (**A**) In rat renal glomeruli (marked with an α-GLEPP1 antibody), α–COQ6-TPEP2 labeled podocyte cytoplasm and cell processes (left). COQ6 was expressed in podocytes, whose nuclei were marked with α-WT1 (middle), but not in mitochondria, marked with α-COXIV (right). (**B**) COQ6 (red) was located in podocyte cellular processes and in Golgi (marked with the trans-Golgi antibody TGN38), demonstrating colocalization (yellow). (**C**) COQ7 exhibited an expression pattern identical to that of COQ6 (see **B**). (**D**) There was full colocalization of COQ6 and COQ7 in podocyte cytoplasm, cell processes, and (by inference from **B** and **C**) Golgi. (**E**) COQ6 colocalized in podocyte cellular processes with podocin, another protein that, if mutated, causes SRNS. COQ6 showed additional expression more centrally in cell processes. (**F**) In cochlea (counterstained with rhodamin-phalloidin [Rh-Ph] for F-actin), COQ6 was expressed in spiral ganglion neurons in Rosenthal canal (arrowheads). (**G**) Higher-magnification view of boxed region in **F** showing COQ6 expression in stria vascularis cells (arrowheads) and the spiral ligament (arrow). Signal in tectorial membrane (tm) and adjacent structures most likely represents background staining. Rm, Reissner membrane; cd, cochlear duct; st, scala tympani; sv, scala vestibuli. In merged images, nuclei are stained blue with DAPI. Scale bars: 50 μm (**A**–**E**); 300 μm (**F**); 100 μm (**G**).

show any difference in growth behavior compared with WT podocytes, the scrambled clone was used as negative control for further experiments. To analyze whether the diminished overall growth rate in podocytes after *Coq6* knockdown is associated with activation of the intrinsic apoptotic pathway, we next determined the inner mitochondrial membrane potential ($\Delta\Psi m$) in these podocyte clones by using the fluorescent dye tetramethylrhodamine ethylester (TMRE). Compared with control cells, all 3 knockdown clones showed a substantial drop in TMRE fluorescence (data not shown), indicative of an increased percentage of podocytes with depolarized $\Delta\Psi m$.

We then analyzed activity of caspase-9 (Figure 5B), the major caspase downstream of mitochondria-mediated apoptosis (30). Using fluorometric immunosorbent enzyme assay (FIENA), we detected a more than 2-fold increase of caspase-9 activity in all 3 knockdown clones compared with control podocytes ($P < 0.005$; Figure 5B). Moreover, caspase-3, the final downstream executioner caspase of different apoptotic signaling pathways (31), showed significant elevation of activity for all 3 siRNA clones ($P < 0.05$; Figure 5C), consistent with the effect seen in zebrafish (see below). These data suggest that the observed decline in podocyte growth after *Coq6* knockdown is caused, at least in part, by increased apoptosis. Since mitochondria-induced apoptosis is associated with depolarization of the inner mitochondrial membrane (32) as well as caspase-9 activation (30), it is likely that lack of growth upon *Coq6* knockdown is caused by activation of the intrinsic apoptotic pathway. Because some of the SRNS patients in our study that carry *COQ6* mutations responded partially to $CoQ_{10}$ treatment, we then analyzed whether $CoQ_{10}$ has a beneficial effect on the phenotype caused by knockdown

Downloaded on July 3, 2014. The Journal of Clinical Investigation. More information at www.jci.org/articles/view/45693



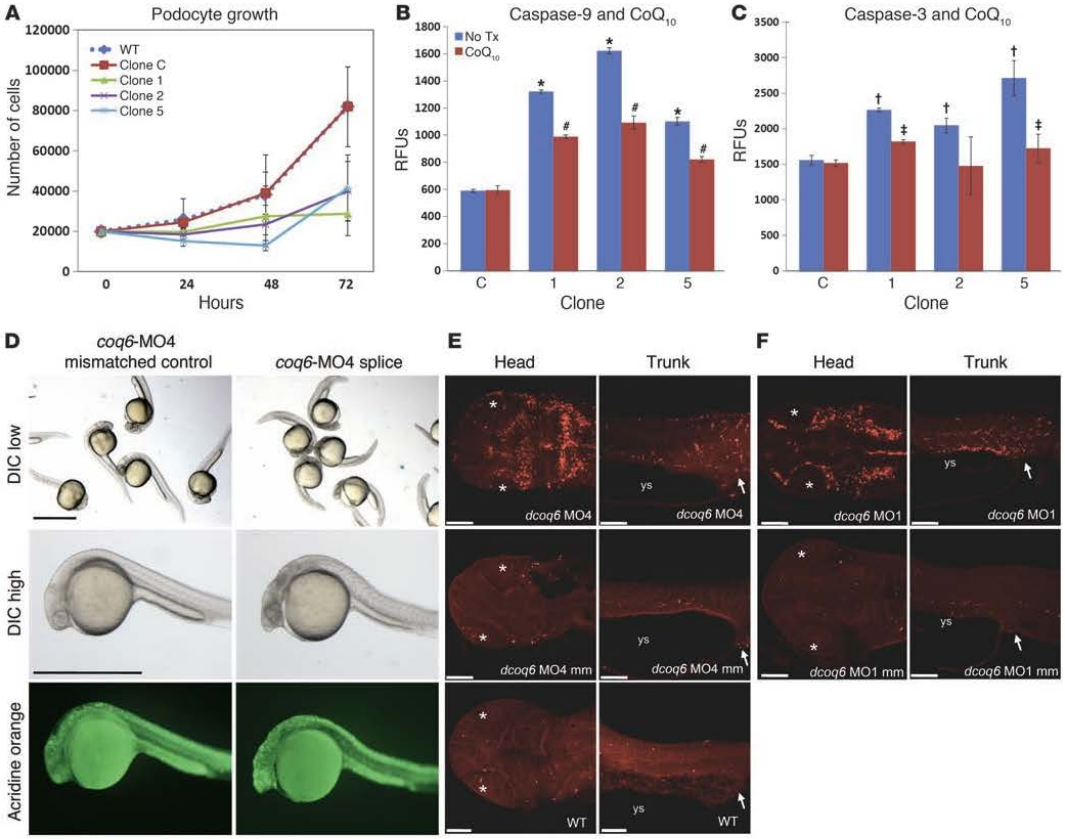



**Figure 5**

*COQ6* knockdown causes apoptosis in podocytes and zebrafish embryos. (**A**–**C**) *Coq6* downregulation in cultured mouse podocytes induced apoptosis that was diminished by $CoQ_{10}$ treatment. Data are mean ± SEM. (**A**) Growth curve analysis of *Coq6* knockdown clones. 20,000 podocytes were seeded per 24-well plate, plated, detached, and counted ($n = 4$). (**B** and **C**) Caspase-9 (**B**) and caspase-3 (**C**) activity in undifferentiated *Coq6* knockdown clones by FIENA before and after $CoQ_{10}$ treatment. RFUs derived from cleaved capase-9 or caspase-3 substrate peptide were measured in lysates from $1 \times 10^6$ cells ($n = 3$). C, control clone; No Tx, no treatment. $^*P < 0.001$, $^\dagger P < 0.05$ versus control; $^\#P < 0.005$, $^\ddagger P < 0.05$ versus untreated. (**D**–**F**) *coq6* knockdown in zebrafish embryos 28 hours after fertilization increases apoptosis. (**D**) *coq6*-MO4 directed against zebrafish *coq6* intron 7 splice donor blocked proper splicing of *coq6* mRNA (see Supplemental Figure 1N). Negative controls were injected with 0.1 mM *coq6* mismatch MO. Note the gray appearance of zebrafish heads upon differential interference contrast (DIC) microscopy as a sign of increased cell death. (**E** and **F**) Zebrafish dorsal head and lateral trunk views. Embryos were injected as indicated with 0.1 mM *coq6*-MO4 splice targeting MO (**E**), MO targeting the AUG translation start site (*dcoq6* MO1; **F**), *coq6* mismatch (mm) MO negative controls, or left uninjected (WT). Cells were stained by an antibody against cleaved caspase-3, a specific marker for apoptotic cells. Lens (asterisk), yolk sac (ys), and cloaca (arrow) are indicated. Scale bars: 1 mm (**D**); 100 μm (**E** and **F**).

of *Coq6* expression in podocytes in vitro. When culturing podocyte clones 1, 2, and 5 in the presence of $CoQ_{10}$ at a concentration of 50 μM for 48 hours, we observed a decrease in caspase-9 and caspase-3 activities (Figure 5, B and C). Compared with clones cultured in the absence of $CoQ_{10}$, this decrease was statistically significant ($P < 0.05$), whereas we did not detect any changes in caspase activities of negative control clones (Figure 5, B and C).

To examine *COQ6* loss of function in a vertebrate organism rather than cell lines, we performed morpholino oligonucleotide (MO) knockdown of *coq6* in zebrafish. We demonstrate that *coq6*-MO4 MOs directed against the zebrafish *coq6* intron 7 splice donor site (Supplemental Figure 1N) and the AUG translation start site induced apoptosis preferentially in heads and trunks of zebrafish embryos 28 hours after fertilization (Figure 5, D–F).

Because *COQ6* mutations cause SND, it is interesting to note that treatment with water-soluble $CoQ_{10}$ decreased apoptosis and activated caspase-3 and improved hearing in a guinea pig model of noise-induced hearing loss (33). The kidney phenotype

Downloaded on July 3, 2014. The Journal of Clinical Investigation. More information at www.jci.org/articles/view/45693





of *COQ6* mutations is remarkably similar to that of mutations in *COQ2* (23) and *PDSS2* in humans (34) and *Pdss2* in mice (24), all of which respond to $CoQ_{10}$ treatment (12, 35). Patients with defects in genes required for $CoQ_{10}$ biosynthesis — *PDSS2*, *COQ2*, and *COQ9* — exhibit renal disease, and in some cases there is a dramatic response to $CoQ_{10}$ therapy, but this is quite variable (36).

## Discussion

In this study, we report what we believe to be a novel cause of SRNS that appears to respond to oral $CoQ_{10}$ supplementation. $CoQ_{10}$, an essential component of the mitochondrial electron transport chain and one of the most potent lipophilic antioxidants (37), is also required for pyrimidine nucleoside biosynthesis and has been implicated in the inhibition of apoptosis by its prevention of inner mitochondrial membrane collapse (38). In multiple studies, the deleterious effect of $CoQ_{10}$ deficiency to mitochondria has been shown. $CoQ_{10}$ deficiency can lead to the opening of the mitochondrial permeability transition pore (MPTP) directly, but an increased amount of ROS caused by $CoQ_{10}$ deficiency can also induce the MPTP by opening of nonspecific high-conductance permeability transition pores in the mitochondrial inner membrane (39). Experiments in HEK293 cells recently showed that $CoQ_{10}$ inhibits Bax-induced mitochondrial dysfunction and protects mitochondria from permeability transition pore opening (9). Here, we confirmed that *COQ6* mutations that cause $CoQ_{10}$ deficiency led to the upregulation of proapoptotic factors. Interestingly, CsA inhibits the MPTP through interaction with cyclophilin D, an essential component of the MPTP (40). We showed that incubation of *COQ6* knockdown podocytes with CsA had a mild rescue effect and decreased activity of caspase-3. Patient A1072-22, who had been treated with CsA in the past, also showed partial remission of proteinuria after treatment with CsA.

Mutations in 5 other $CoQ_{10}$ biosynthesis enzymes leading to $CoQ_{10}$ deficiency have been recently implicated in other monogenic mitochondriopathies, generally characterized by central nervous system signs and myopathy (22, 34, 41–43); 1 patient with mutations in *PDSS2* and 5 patients with mutations in *COQ2* also presented with SRNS (22, 34, 43). So far, the exact pathogenic mechanism has remained unclear. Interestingly, 1 patient with mutations in *COQ2* was successfully treated with oral $CoQ_{10}$ supplementation, showing progressive recovery of renal function and a reduced level of proteinuria until 5 years after completion of treatment (22). The podocyte-specific phenotype caused by *PDSS2* mutations leading to primary $CoQ_{10}$ deficiency was demonstrated in the *Pdss2* knockout mouse (24). Conditional knockouts targeted to renal tubular epithelium, monocytes, or hepatocytes did not show disease manifestation. It remains unclear why the podocyte in particular is affected by *PDSS2*-dependent $CoQ_{10}$ deficiency.

Interestingly, the presentation of primary $CoQ_{10}$ deficiency caused by genetic mutations is very heterogeneous. It seems that the mutations in *PDSS2* and *COQ2* are partial loss-of-function mutations. Therefore, the phenotypes (ATP synthesis, ROS production) may depend on the content of Q in the cell, which is determined by the severity of the mutation. Mutations in *PDSS2*, for example, cause reduced ATP synthesis in cultured fibroblasts, but no increase in ROS production, whereas mutations in *COQ2* cause no difference in ATP synthesis in cultured fibroblasts, but increase ROS production (36). One could speculate that different cell types and/or tissues react differently to ROS and ATP synthesis defects according to their antioxidant defense mechanisms or the level of respiratory activity, explaining the wide spectrum of clinical features. Based on the surprising Golgi localization of COQ6, COQ7, and COQ9, we speculate that the antioxidant function of Q/QH2 in certain cells, such as podocytes, may depend on targeted synthesis of CoQ in the Golgi for delivery to the plasma membrane, which in the podocyte constitutes an enormous surface area that must contain vulnerable lipid components. Whereas most other forms of monogenic childhood NS are characterized by a lack of response to therapy (10, 16, 17, 44), the identification by mutation analysis of individuals with NS caused by $CoQ_{10}$ biosynthesis defects, as described here, is important because those individuals may respond to treatment with $CoQ_{10}$.

## Methods

### *Subjects*

We obtained blood, tissue samples, and pedigrees following informed consent from individuals with NS and/or from their parents. Human subject research was approved by the University of Michigan Institutional Review Board. The diagnosis of NS was made by a pediatric nephrologist based on either chronic or recurrent high-grade proteinuria (>40 $mg/m^2/h$) or persistent low-grade proteinuria (>4 $mg/m^2/h$) (45). Steroid-sensitive NS and SRNS were defined according to standard criteria (45, 46). Renal biopsies were evaluated by a reference renal pathologist. Age at onset of ESRF was defined as age at first renal replacement therapy, i.e., dialysis or renal transplantation. Clinical data were obtained using a standardized questionnaire (www.renalgenes.org).

### *Genetic mapping and exon sequencing*

We performed a genome-wide search for linkage by homozygosity mapping using the 250k Affymetrix SNP microarray (47). Data were evaluated by calculating nonparametric lod scores and scoring for homozygosity ($Z_{hom}$) across the whole genome in order to identify regions of homozygosity. The GENEHUNTER-MODSCORE program (48) was used to calculate multipoint lod scores assuming recessive inheritance with complete penetrance, a disease allele frequency of 0.001, and the marker allele frequencies for individuals of mixed European descent specified by Affymetrix. Parametric and nonparametric lod scores were plotted over genetic distance across the entire human genome using GNUPLOT software (http://www.gnuplot.info/). See Supplemental Table 2 for exon sequencing primers.

### *COQ6 mRNA expression*

The probe for human Northern blot analysis was obtained by digesting the *COQ6* isoform a coding region cloned into pCRIITOPO with *EcoRI* and was radiolabeled with $\alpha$-$^{32}$P dCTP (Amersham Biosciences) using the Random Primers DNA Labeling System kit (Invitrogen) and successively purified with Quick-Spin columns (Roche) according to the manufacturer's protocol. Radiolabeled probes were hybridized to a commercial preblotted membrane (FirstChoice Human Blot 1 membrane; Ambion) containing 2 μg/lane poly(A)$^+$ RNA from 10 human tissues. Prehybridization and hybridization were both performed in a 50% formamide buffer at 42 °C, with a working concentration of $1.5 \times 10^6$ cpm and 0.1 mg salmon sperm DNA per milliliter. The excess probe was removed by washing at 65 °C for 15 minutes using a 0.1% SDS, 0.1× sodium chloride–sodium citrate buffer solution. Radioactivity was detected with a Storm PhosphoImager (Molecular Dynamics) after overnight exposure. Selective amplification of *COQ6* isoform b was carried out using primers in exon 1b and in exon 4. Simultaneous amplification of isoform a and isoform b was carried out using primers on exon 2 and on exon 4. PCR conditions were 94°C for 3 minutes followed by 35 cycles of 94°C for 30 seconds,

Downloaded on July 3, 2014. The Journal of Clinical Investigation. More information at www.jci.org/articles/view/45693



55°C for 30 seconds, and 72°C for 30 seconds and a final extension step of 72°C for 7 minutes. Amplified fragments were also purified from agarose gel and sequenced. Primer sequences were as follows: exon 1b forward, 5′-TCTAGCTTTGGCGTCTGGTT-3′; exon 2 forward, 5′-CTTCTAAGCTTGATATGATATTCACTTTCATGACAAG-3′; exon 4 reverse, 5′-CTTCTGGATCCATGATGACATCATTCTCCAC-3′.

### *Generation of plasmids*

Yeast *COQ6* was amplified from genomic DNA extracted from a WT BY4741 strain and cloned in pCM189 vector. Site-specific mutagenesis was performed using the QuickChange kit (Stratagene) according to the manufacturer's protocol. To generate constructs that expressed the gene under the control of the endogenous yeast *coq6* promoter, the different pCM189-yeast COQ6 constructs were digested with *SacI* and *MscI* (to eliminate the CYC1 promoter and control elements); religated with a fragment encompassing the yeast COQ6 promoter, the 5′ end of the gene, and the *MscI* site; amplified from genomic DNA; and cut accordingly. Plasmid maps were described previously (49). Yeast growth and transformation were performed as described below.

### *COQ6-GFP expression studies*

The complete coding region of full-length human *COQ6* isoform a, lacking termination codon but including the Kozak sequence, was PCR amplified from pCRIITOPO-COQ6 and subcloned into the *HindIII* and *BamHI* sites of pEGFP-N1 (BD Biosciences – Clontech). The correctness of the construct was verified by direct sequencing. HeLa cells stably expressing mitochondrially targeted red fluorescent protein (50) were grown on coverslips in complete DMEM (Sigma-Aldrich) containing 10% fetal bovine serum until 70% confluent, then transfected with the purified plasmid using Effectene Transfection Reagent (Qiagen) according to the manufacturer's instructions. Cells were visualized after 48 hours using a Nikon Video Confocal microscope.

### *In situ hybridization analysis in mice*

Whole-mount in situ hybridization was performed following a standard procedure with digoxigenin-labeled antisense riboprobes (51). Stained specimens were transferred in 80% glycerol prior to documentation. In situ hybridization on 10-μm paraffin sections was done as described previously (52).

### *Immunofluorescence*

Rat kidneys were perfusion-fixed with paraformaldehyde/lysine/periodate and processed as previously described (3). For absorption experiments, the immunopurified α–COQ6-TPEP2, COQ7, and COQ9 antibodies were preabsorbed with an equal weight of cognate or noncognate peptide overnight at 4°C. The following antibodies were used: WT1 mouse monoclonal antibody (catalog no. sc-7385; Santa Cruz Biotechnology Inc.); PLCe1 goat polyclonal antibody (catalog no. sc-28404; Santa Cruz Biotechnology Inc.); α–COQ6-TPEP2 immunopurified rabbit antipeptide antibody (against peptide sequence N-DKDNLDDMGYIVEND-C; anti-rat Glepp1 mouse monoclonal antibody (1B4; ref. 53), CoQ7 goat polyclonal antibody (catalog no. sc-66353; Santa Cruz Biotechnology Inc.); CoQ9 rabbit polyclonal antibody (catalog no. 14874-1-AP; Protein Tech); TGN38 monoclonal mouse antibody (catalog no. 610898; BD Biosciences); and GM130 mouse monoclonal antibody (catalog no. 610823; BD Biosciences).

### *Yeast studies*

*Yeast growth.* The *S. cerevisiae coq6*-null mutants W303ΔG63 (Mat α ade2-1 his 3-1,15 leu2-3,112 trp1-1 ura3-1 ΔCOQ6:HIS3; ref. 18) and W303ΔCOQ8 (Mat α ade2-1 his 3-1,15 leu2-3,112 trp1-1 ura3-1 ΔABC1/COQ8:HIS3; ref. 54) were used in this study. Yeast growth media were prepared as described previously (55): YPD, containing 1% yeast extract, 2% peptone, and 2% dextrose; YPGal, containing 1% yeast extract, 2% peptone, 2% galactose, and 0.1% dextrose; YPG, containing 1% yeast extract, 2% peptone, and 3% glycerol; and SD-Ura, containing 0.18% nitrogen base without amino acids, 2% dextrose, 0.14% $NaH_2PO_4$, 0.5% $(NH_4)_2SO_4$, and a complete amino acid supplement (56), minus uracil. Solid plate media contained 2% agar.

*Yeast transformation.* Yeast was subjected to transformation as described previously (57), with either a low-copy number (pQM; ref. 58) or a high-copy number (pRCM; ref. 59) yeast expression plasmid. These vectors were used to prepare plasmids containing the human *COQ6* open reading frame with an in-frame aminoterminal yeast mitochondrial leader sequence (pQM_hCOQ6-MLS and pRCM_hCOQ6-MLS). Each of the following mutations in human *COQ6* were introduced by site-directed mutagenesis (Stratagene): R162X, W188X, G255R, A353D, W447X, and Q461fsX478. See Supplemental Table 1 for a complete list of plasmids used in yeast transformation experiments.

*Lipid extraction and analysis.* Yeast cells were grown in YPGal and harvested during log phase growth (1.0 $OD_{600nm}$). Lipid extracts were prepared from yeast whole cells as described previously (60). Lipids were separated by reverse-phase high-performance liquid chromatography with a Phenylhexyl column (Phenomenex 5-μm, 100 × 4.6 mm). The column was equilibrated with a mobile phase consisting of 95:5 methanol/2-propanol with 2.5 mM ammonium formate as solvent A and a flow rate of 650 μl/min. Upon sample injection, the percentage of solvent B (2-propanol with 2.5 mM ammonium formate) was increased linearly from 0% to 5% over 6 minutes, and the flow rate was also increased linearly to 800 μl/min. The flow rate and mobile phase were linearly changed back to initial conditions by 8 minutes. Q was quantified with an Applied Biosystems-MDS Sciex 4000 Q Trap (hybrid triple-quad linear ion trap analyzer with autosampler and a Turbo-V source equipped with ESI and APCI sources) as described previously (35). The samples were analyzed in multiple reaction monitoring (MRM) mode; MRM transitions were as follows: *m/z* 591.6/197.1 for $Q_6$; *m/z* 610.6/197.1 for $Q_6H_2$ with ammonium adduct; *m/z* 455.6/197.1 for $Q_4$ (Sigma-Aldrich), used as internal standard.

### *Podocyte expression studies*

*Preparation of $CoQ_{10}$ solution for use in cell culture.* Pure $CoQ_{10}$ in powder form (Kaneka Corp.) was dissolved in 1 ml of molecular biology–grade isopropanol at a concentration of 10 mM by heating it briefly in a 95°C water bath. Thereafter, the $CoQ_{10}$ solution was diluted 1:10 in podocyte culture media to a final stock concentration of 1 mM and reheated for an additional 5 minutes at 95°C with gentle shaking. This $CoQ_{10}$ stock solution was stored at 4°C, protected from light for up to 4 weeks, and diluted immediately before use at 1:20 in cell culture medium to a final working concentration of 50 μM.

*Podocyte culture.* Immortalized murine podocytes were cultured as described previously (29). For treatment studies of undifferentiated podocytes, cells were incubated in the presence of 50 μM $CoQ_{10}$, 1 μM dexamethasone (Sigma-Aldrich), or 1 μM CsA (Sigma-Aldrich) for 48 hours. For analysis of differentiated podocytes, undifferentiated podocytes were cultured under nonpermissive conditions in the presence of 1 μM dexamethasone for 14 days. Cultivation was then continued in the absence of dexamethasone for an additional 48 hours. For determination of cell number and growth curve analysis, cells were seeded in 24-well plates at 20,000 cells/well. After 24, 48, or 72 hours, cells were trypsinized and counted using a hemocytometer. Experiments were done 4 times with at least 3 internal replicates.

### *COQ6 RNAi*

For the targeted downregulation of protein expression in podocytes, we used the pSuper RNAi System (OligoEngine) (28) following the manufacturer's instructions and as done previously (61). Briefly, we cloned a 60-nt oligo including a 19-nt *COQ6* target sequence and a hairpin (5′-TTCAAGA-

Downloaded on July 3, 2014. The Journal of Clinical Investigation. More information at www.jci.org/articles/view/45693



GA-3′) into a modified pSuper vector, which also encoded for a zeocin selection marker (61). After transfection of undifferentiated podocytes using FuGene 6 (Roche) followed by zeocin selection at 500 μg/ml for 7–10 days, appearing podocyte clones were covered by cloning chambers, trypsinized, and expanded separately from each other in culture medium containing 100 μg/ml zeocin. In total, 5 different *COQ6* targeting sequences were used (clone 1, AACAGAGTCAGCTCCATAT; clone 2, AATGACGTCATCATGTATG; clone 3, CTGTGGCAGATCGAGTGAA; clone 4, AACTGTTGATTGGTGCTGA; clone 5, AAGGACTTAGGCTCCATGA) as well as 1 scrambled control sequence (5′-CCGCGACTCGCCGTCTGCG-3′). Stable transfected clones were expanded and used for RNA isolation and functional studies.

### *RNA isolation and RT-PCR*

RNA was isolated from 2 × $10^6$ undifferentiated podocytes using the RNeasy kit (Qiagen) following the manufacturer's protocol. Prior to RT-PCR, total RNA samples were digested with DNase I (Roche) and RNA was transcribed into cDNA using Superscript II (Invitrogen). For RT-PCR, 100 ng cDNA, AmpliTaq Gold DNA polymerase (Applied Biosystems), and sequence-specific, intron-spanning primers were used (COQ6 forward, CAGACACCGTGTACGACGTG; COQ6 reverse, CCAACAGCTTTGCTCTCATAGAG; GAPDH forward, TATGTCGTGGAGTCTACTGG; GAPDH reverse, AGTGATGGCATGGACTGTGG). 30 PCR cycles (5 minutes at 95°C, 30 seconds at 53°C, and 30 seconds at 72°C) were run on a GeneAmp PCR System 9700 (Applied Biosystems). PCR reactions were analyzed on a 2% agarose gel, and ethidium bromide signals were captured with a Bio-Rad Gel Doc XR system.

### *Inner ΔΨm*

To analyze changes in the ΔΨm of undifferentiated podocytes, we used TMRE (Invitrogen) as described previously (62). Briefly, 3 × $10^5$ cells were trypsinized and incubated in 25 nM TMRE for 30 minutes at 37°C. With this concentration (nonquenching mode), depolarization causes a drop in TMRE fluorescence. Cells were washed with PBS and analyzed by flow cytometry (FACSCalibur; BD), measuring TMRE fluorescence in FL-2. The relative fluorescence of TMRE was compared with that of the respective untreated control cells in each experiment. 3 replicates were analyzed per treatment group.

### *FIENA*

To determine caspase-3 and -9 activities in podocyte extracts, we used the Fluorometric Assay Kits from BioVision according to the manufacturer's protocol. In brief, podocytes were cultured in 6- or 12-well plates, trypsinized, and counted using a hemocytometer. 1 × $10^5$ to 1 × $10^6$ cells were lysed on ice for 10 minutes, and the derivatized peptide DEVD-7-amino-4-trifluoromethyl coumarin (DEVD-AFC) caspase-3 or -9 cleavage substrate was added at a final concentration of 50 μM in 2× reaction buffer containing 10 mM dithiothreitol. The reaction was incubated at 37°C for 1–24 hours, and green fluorescence ($\lambda_{max}$, 505 nm) of free AFC after caspase-3– or caspase-9–mediated cleavage was measured in relative fluorescence units (RFU) using a fluorometer (SpectraMax M5; Molecular Devices) at different time points. Values were normalized to cell lysates without substrate and to substrate in reaction buffer in the absence of cell lysate. Experiments were done 3 times with at least 3 internal replicates.

### *Zebrafish MO-mediated knockdown*

MOs were obtained from Gene Tools. The nucleotide sequences of the translation-blocking (coq6-MO1) and splice-blocking (coq6-MO4) MOs against *D. rerio coq6* were 5′-GCTTAGCTTTAGCCAGAGACAGCAT-3′ and 5′-ACACATAAGGTCAGCTCACGGGAAG-3′, respectively. The 5-bp mismatch controls for the MOs were as follows: coq6-MO1mm, 5′-GGTTACCTTTACCCAGACACACCAT-3′; coq6-MO4mm, 5′-ACAGATAACGTCACCTCAGGGCAAG-3′. Fertilized eggs were microinjected with the specified amount of MO dissolved in 0.1M KCl. For immunohistochemical labeling, embryos were fixed with 4% PFA in PBS (pH 7.4) and stained with antibody against activated caspase-3 (1:200; BD Biosciences) following standard protocols (63).

### *Statistics*

To evaluate caspase-3 and -9 activity in cell lines, Pearson $\chi^2$ test was used with a critical *P* value of 0.05 (Figure 5).

### *Databases*

Genetic mapping was performed using http://genome.ucsc.edu (May 2004 freeze).

### *Accession numbers*

Accession numbers of *COQ6* orthologs were NP_872282 for *Homo sapiens*, NP_001038869 for *D. rerio*, and ZP_00723222 *E. coli*.

## Acknowledgments

We thank the affected individuals and their families for participation. We thank Corina Nailescu for contribution of clinical data. This research was supported by grants from the NIH to F. Hildebrandt (DK076683 and DK086542), C.F. Clarke (GM45952), and R.C. Wiggins (DK46073 and P30 DK081943) and by a grant from the KMD Foundation and the Thrasher Research Fund to F. Hildebrandt. F. Hildebrandt is an Investigator of the Howard Hughes Medical Institute, a Doris Duke Distinguished Clinical Scientist, and the Frederick G.L. Huetwell Professor. H. Prokisch was supported by the Impulse and Networking Fund of the Helmholtz Association in the framework of the Helmholtz Alliance for Mental Health in an Ageing Society (HA-215), by the German Network for Mitochondrial Disorders (mitoNET 01GM0862 and 01GM0867), and by Systems Biology of Metabotypes (SysMBo 0315494A). The work was further supported by a grant from the German Research Foundation (DFG, SFB 423, TP B19) to M. Zenker, by the German Federal Ministry of Science and Education through the National Genome Research Network to G. Nürnberg and P. Nürnberg, by the European Community FP7 program (EUNEFRON 201590) to D. Müller, by Fondazione CARIPARO Telethon Italy (GGP09207) to L. Salviati, by a Spanish FIS grant (PI080500) to P. Navas, and by the Young Investigator Career Development Grant from the NephCure Foundation and the National Scientist Development Grant from the American Heart Association to C. Faul.

Received for publication November 6, 2010, and accepted in revised form February 9, 2011.

Address correspondence to: Friedhelm Hildebrandt, Howard Hughes Medical Institute, Departments of Pediatrics and Human Genetics, University of Michigan Health System, 8220C MSRB III, 1150 West Medical Center Drive, Ann Arbor, Michigan 48109-5646, USA. Phone: 734.615.7285; Fax: 734.615.1386; E-mail: fhilde@umich.edu.

1. Kestila M, et al. Positionally cloned gene for a novel glomerular protein–nephrin–is mutated in congenital nephrotic syndrome. *Mol Cell.* 1998;1(4):575–582.
2. Boute N, et al. NPHS2, encoding the glomerular protein podocin, is mutated in autosomal recessive steroid-resistant nephrotic syndrome. *Nat Genet.* 2000;24(4):349–354.
3. Hinkes B, et al. Positional cloning uncovers mutations in PLCE1 responsible for a nephrotic syndrome variant that may be reversible. *Nat Genet.* 2006; 38(12):1397–1405.
4. Kaplan JM, et al. Mutations in ACTN4, encoding

Downloaded on July 3, 2014. The Journal of Clinical Investigation. More information at www.jci.org/articles/view/45693



alpha-actinin-4, cause familial focal segmental glomerulosclerosis. *Nat Genet.* 2000;24(3):251–256.
5. Reiser J, et al. TRPC6 is a glomerular slit diaphragm-associated channel required for normal renal function. *Nat Genet.* 2005;37(7):739–744.
6. Winn MP, et al. A mutation in the TRPC6 cation channel causes familial focal segmental glomerulosclerosis. *Science.* 2005;308(5729):1801–1804.
7. Brown EJ, et al. Mutations in the formin gene INF2 cause focal segmental glomerulosclerosis. *Nat Genet.* 2010;42(1):72–76.
8. Somlo S, Mundel P. Getting a foothold in nephrotic syndrome. *Nat Genet.* 2000;24(4):333–335.
9. Machuca E, Benoit G, Antignac C. Genetics of nephrotic syndrome: connecting molecular genetics to podocyte physiology. *Hum Mol Genet.* 2009; 18(R2):R185–R194.
10. Ruf RG, et al. Patients with mutations in NPHS2 (podocin) do not respond to standard steroid treatment of nephrotic syndrome. *J Am Soc Nephrol.* 2004; 15(3):722–732.
11. Weber S, et al. NPHS2 mutation analysis shows genetic heterogeneity of steroid-resistant nephrotic syndrome and low post-transplant recurrence. *Kidney Int.* 2004;66(2):571–579.
12. Montini G, Malaventura C, Salviati L. Early coenzyme Q10 supplementation in primary coenzyme Q10 deficiency. *N Engl J Med.* 2008;358(26):2849–2850.
13. Wiggins RC. The spectrum of podocytopathies: a unifying view of glomerular diseases. *Kidney Int.* 2007;71(12):1205–1214.
14. Hinkes BG, et al. Nephrotic syndrome in the first year of life: two thirds of cases are caused by mutations in 4 genes (NPHS1, NPHS2, WT1, and LAMB2). *Pediatrics.* 2007;119(4):e907–e919.
15. Karle SM, Uetz B, Ronner V, Glaeser L, Hildebrandt F, Fuchshuber A. Novel mutations in NPHS2 detected in both familial and sporadic steroid-resistant nephrotic syndrome. *J Am Soc Nephrol.* 2002;13(2):388–393.
16. Hasselbacher K, et al. Recessive missense mutations in LAMB2 expand the clinical spectrum of LAMB2-associated disorders. *Kidney Int.* 2006;70(6):1008–1012.
17. Mucha B, et al. Mutations in the Wilms' tumor 1 gene cause isolated steroid resistant nephrotic syndrome and occur in exons 8 and 9. *Pediatr Res.* 2006; 59(2):325–331.
18. Gin P, et al. The Saccharomyces cerevisiae COQ6 gene encodes a mitochondrial flavin-dependent monooxygenase required for coenzyme Q biosynthesis. *J Biol Chem.* 2003;278(28):25308–25316.
19. DiMauro S, Mancuso M. Mitochondrial diseases: therapeutic approaches. *Biosci Rep.* 2007;27(1–3):125–137.
20. Hyun DH, Hernandez JO, Mattson MP, de Cabo R. The plasma membrane redox system in aging. *Ageing Res Rev.* 2006;5(2):209–220.
21. DiMauro S, Quinzii CM, Hirano M. Mutations in coenzyme Q10 biosynthetic genes. *J Clin Invest.* 2007; 117(3):587–589.
22. Diomedi-Camassei F, et al. COQ2 nephropathy: a newly described inherited mitochondriopathy with primary renal involvement. *J Am Soc Nephrol.* 2007; 18(10):2773–2780.
23. Lopez-Martin JM, et al. Missense mutation of the COQ2 gene causes defects of bioenergetics and de novo pyrimidine synthesis. *Hum Mol Genet.* 2007; 16(9):1091–1097.
24. Peng M, et al. Primary coenzyme Q deficiency in Pdss2 mutant mice causes isolated renal disease. *PLoS Genet.* 2008;4(4):e1000061.
25. Salviati L, et al. Infantile encephalomyopathy and nephropathy with CoQ10 deficiency: a CoQ10-responsive condition. *Neurology.* 2005;65(4):606–608.
26. Tryggvason K, Patrakka J, Wartiovaara J. Hereditary proteinuria syndromes and mechanisms of proteinuria. *N Engl J Med.* 2006;354(13):1387–1401.
27. Padilla-Lopez S, Jimenez-Hidalgo M, Martin-Montalvo A, Clarke CF, Navas P, Santos-Ocana C. Genetic evidence for the requirement of the endocytic pathway in the uptake of coenzyme Q6 in Saccharomyces cerevisiae. *Biochim Biophys Acta.* 2009; 1788(6):1238–1248.
28. Brummelkamp TR, Bernards R, Agami R. A system for stable expression of short interfering RNAs in mammalian cells. *Science.* 2002;296(5567):550–553.
29. Mundel P, et al. Rearrangements of the cytoskeleton and cell contacts induce process formation during differentiation of conditionally immortalized mouse podocyte cell lines. *Exp Cell Res.* 1997; 236(1):248–258.
30. Green DR. Apoptotic pathways: ten minutes to dead. *Cell.* 2005;121(5):671–674.
31. Wilson MR. Apoptosis: unmasking the executioner. *Cell Death Differ.* 1998;5(8):646–652.
32. Green DR, Kroemer G. The pathophysiology of mitochondrial cell death. *Science.* 2004; 305(5684):626–629.
33. Fetoni AR, Piacentini R, Fiorita A, Paludetti G, Troiani D. Water-soluble Coenzyme Q10 formulation (Q-ter) promotes outer hair cell survival in a guinea pig model of noise induced hearing loss (NIHL). *Brain Res.* 2009;1257:108–116.
34. Lopez LC, et al. Leigh syndrome with nephropathy and CoQ10 deficiency due to decaprenyl diphosphate synthase subunit 2 (PDSS2) mutations. *Am J Hum Genet.* 2006;79(6):1125–1129.
35. Saiki R, et al. Coenzyme Q10 supplementation rescues renal disease in Pdss2kd/kd mice with mutations in prenyl diphosphate synthase subunit 2. *Am J Physiol Renal Physiol.* 2008;295(5):F1535–F1544.
36. Quinzii CM, et al. Respiratory chain dysfunction and oxidative stress correlate with severity of primary CoQ10 deficiency. *FASEB J.* 2008;22(6):1874–1885.
37. Bentinger M, Brismar K, Dallner G. The antioxidant role of coenzyme Q. *Mitochondrion.* 2007; 7(suppl):S41–S50.
38. Turunen M, Olsson J, Dallner G. Metabolism and function of coenzyme Q. *Biochim Biophys Acta.* 2004; 1660(1–2):171–199.
39. Kim I, Rodriguez-Enriquez S, Lemasters JJ. Selective degradation of mitochondria by mitophagy. *Arch Biochem Biophys.* 2007;462(2):245–253.
40. Waldmeier PC, Zimmermann K, Qian T, Tintelnot-Blomley M, Lemasters JJ. Cyclophilin D as a drug target. *Curr Med Chem.* 2003;10(16):1485–1506.
41. Lagier-Tourenne C, et al. ADCK3, an ancestral kinase, is mutated in a form of recessive ataxia associated with coenzyme Q10 deficiency. *Am J Hum Genet.* 2008; 82(3):661–672.
42. Duncan AJ, et al. A nonsense mutation in COQ9 causes autosomal-recessive neonatal-onset primary coenzyme Q10 deficiency: a potentially treatable form of mitochondrial disease. *Am J Hum Genet.* 2009; 84(5):558–566.
43. Mollet J, et al. Prenyldiphosphate synthase, subunit 1 (PDSS1) and OH-benzoate polyprenyltransferase (COQ2) mutations in ubiquinone deficiency and oxidative phosphorylation disorders. *J Clin Invest.* 2007;117(3):765–772.
44. Antignac C. Molecular basis of steroid-resistant nephrotic syndrome. *Nefrologia.* 2005; 25(suppl 2):25–28.
45. [No authors listed]. Short versus standard prednisone therapy for initial treatment of idiopathic nephrotic syndrome in children. *Lancet.* 1988;1(8582):380–383.
46. ISKDC. Primary nephrotic syndrome in children: Clinical significance of histopathologic variants of minimal change and of diffuse mesangial hypercellularity. A Report of the International Study of Kidney Disease in Children. *Kidney Int.* 1981;20(6):765–771.
47. Hildebrandt F, et al. A systematic approach to mapping recessive disease genes in individuals from outbred populations. *PloS Genet.* 2009;5(1):e1000353.
48. Strauch K. Parametric linkage analysis with automatic optimization of the disease model parameters. *Am J Hum Genet.* 2003;73(suppl 1):A2624.
49. Gari E, Piedrafita L, Aldea M, Herrero E. A set of vectors with a tetracycline-regulatable promoter system for modulated gene expression in *Saccharomyces cerevisiae*. *Yeast.* 1997;13(9):837–848.
50. Casarin A, et al. Functional characterization of human COQ4, a gene required for Coenzyme Q10 biosynthesis. *Biochem Biophys Res Commun.* 2008;372(1):35–39.
51. Wilkinson DG. Whole mount in situ hybridization of vertebrate embryos. In: Wilkinson DG, ed. *In Situ Hybridization: A Practical Approach.* Oxford, United Kingdom: IRL Press; 1992:75–83.
52. Franco D, de Boer PA, de Gier-de Vries C, Lamers WH, Moorman AF. Methods on in situ hybridization, immunohistochemistry and beta-galactosidase reporter gene detection. *Eur J Morphol.* 2001; 39(3):169–191.
53. Yang DH, et al. Glomerular epithelial protein 1 and podocalyxin-like protein 1 in inflammatory glomerular disease (crescentic nephritis) in rabbit and man. *Lab Invest.* 1996;74(3):571–584.
54. Do TQ, Hsu AY, Jonassen T, Lee PT, Clarke CF. A defect in coenzyme Q biosynthesis is responsible for the respiratory deficiency in *Saccharomyces cerevisiae abc1* mutants. *J Biol Chem.* 2001;276(21):18161–18168.
55. Burke D, Dawson D, Stearns T. *Methods in Yeast Genetics.* Plainview, New York, USA: Cold Spring Harbor Laboratory Press; 2000.
56. Poon WW, et al. Yeast and rat Coq3 and *Escherichia coli* UbiG polypeptides catalyze both O-methyltransferase steps in coenzyme Q biosynthesis. *J Biol Chem.* 1999;274(31):21665–21672.
57. Elble R. A simple and efficient procedure for transformation of yeasts. *Biotechniques.* 1992;13(1):18–20.
58. Hsu AY, Poon WW, Shepherd JA, Myles DC, Clarke CF. Complementation of *coq3* mutant yeast by mitochondrial targeting of the *Escherichia coli* UbiG polypeptide: evidence that UbiG catalyzes both O-methylation steps in ubiquinone biosynthesis. *Biochemistry.* 1996;35(30):9797–9806.
59. Xie LX, et al. Expression of the human atypical kinase *ADCK3* rescues coenzyme Q biosynthesis and phosphorylation of Coq polypeptide in yeast *coq8* mutants [published online ahead of print February 3, 2011]. *Biochim Biophys.* doi:10.1016/j.bbalip.2011.01.009.
60. Jonassen T, Clarke CF. Isolation and functional expression of human *COQ3*, a gene encoding a methyltransferase required for ubiquinone biosynthesis. *J Biol Chem.* 2000;275(17):12381–12387.
61. Asanuma K, et al. Synaptopodin regulates the actin-bundling activity of alpha-actinin in an isoform-specific manner. *J Clin Invest.* 2005;115(5):1188–1198.
62. Krick S, et al. Mpv17l protects against mitochondrial oxidative stress and apoptosis by activation of Omi/HtrA2 protease. *Proc Natl Acad Sci U S A.* 2008; 105(37):14106–14111.
63. Zhou W, Dai J, Attanasio M, Hildebrandt F. Nephrocystin-3 is required for ciliary function in zebrafish embryos. *Am J Physiol Renal Physiol.* 2010; 299(1):F55–F62.

EMBO
Molecular Medicine



# Probucol ameliorates renal and metabolic sequelae of primary CoQ deficiency in *Pdss2* mutant mice

*Marni J. Falk[1,2]*, Erzsebet Polyak[1], Zhe Zhang[3], Min Peng[4], Rhonda King[5], Jonathan S. Maltzman[5], Ezinne Okwuego[1], Oksana Horyn[2], Eiko Nakamaru-Ogiso[6], Julian Ostrovsky[1], Letian X. Xie[7], Jia Yan Chen[7], Beth Marbois[7], Itzhak Nissim[2,6], Catherine F. Clarke[7], David L. Gasser[4]*

Keywords: coenzyme Q; kidney; mitochondria; mouse; probucol

DOI 10.1002/emmm.201100149

Received January 14, 2011
Revised April 27, 2011
Accepted April 28, 2011

Therapy of mitochondrial respiratory chain diseases is complicated by limited understanding of cellular mechanisms that cause the widely variable clinical findings. Here, we show that focal segmental glomerulopathy-like kidney disease in *Pdss2* mutant animals with primary coenzyme Q (CoQ) deficiency is significantly ameliorated by oral treatment with probucol (1% w/w). Preventative effects in missense mutant mice are similar whether fed probucol from weaning or for 3 weeks prior to typical nephritis onset. Furthermore, treating symptomatic animals for 2 weeks with probucol significantly reduces albuminuria. Probucol has a more pronounced health benefit than high-dose $CoQ_{10}$ supplementation and uniquely restores $CoQ_9$ content in mutant kidney. Probucol substantially mitigates transcriptional alterations across many intermediary metabolic domains, including peroxisome proliferator-activated receptor (*PPAR*) pathway signaling. Probucol's beneficial effects on the renal and metabolic manifestations of *Pdss2* disease occur despite modest induction of oxidant stress and appear independent of its hypolipidemic effects. Rather, decreased $CoQ_9$ content and altered *PPAR* pathway signaling appear, respectively, to orchestrate the glomerular and global metabolic consequences of primary CoQ deficiency, which are both preventable and treatable with oral probucol therapy.

## INTRODUCTION

Primary mitochondrial respiratory chain (RC) disease represents a complex compilation of multi-systemic disorders caused by pathogenic mutations in more than 60 nuclear and all 37 mitochondrial DNA-encoded genes (Haas et al, 2008). Therapy for this heterogeneous group of often devastating diseases is largely relegated to vitamin and supplement cocktails of theoretical utility whose objective efficacy is difficult to monitor but which commonly appear to have minimal clinical benefit (Parikh et al, 2009). A translational mouse model of primary mitochondrial RC disease caused by a homozygous amino acid substitution affecting the nuclear-encoded prenyl diphosphate synthase subunit 2 (Pdss2) enzyme required for coenzyme Q (CoQ) biosynthesis (Dell et al, 2000; Peng et al, 2004) develops a lethal kidney disease by 4 months of life (Lyon & Hulse, 1971).

(1) Division of Human Genetics, Department of Pediatrics, The Children's Hospital of Philadelphia, Philadelphia, PA, USA
(2) Division of Metabolic Disease, Department of Pediatrics, The Children's Hospital of Philadelphia, Philadelphia, PA, USA
(3) Division of Biomedical Informatics, Department of Pediatrics, The Children's Hospital of Philadelphia, Philadelphia, PA, USA
(4) Department of Genetics, University of Pennsylvania School of Medicine, Philadelphia, PA, USA
(5) Department of Medicine, University of Pennsylvania School of Medicine, Philadelphia, PA, USA
(6) Department of Biochemistry and Biophysics, University of Pennsylvania School of Medicine, Philadelphia, PA, USA
(7) Department of Chemistry and Biochemistry, University of California Los Angeles, Los Angeles, CA, USA
***Corresponding author:** Tel: +1-215-590-4564, Fax: +1-267-426-2876; E-mail: falkm@email.chop.edu

 © 2011 EMBO Molecular Medicine 

CoQ is a highly lipophilic molecule that consists of a benzoquinone ring joined to a polyisoprenoid side chain that is comprised predominantly of 9 or 10 isoprenoid groups in mouse and humans, respectively. The isoprenyl side chain is synthesized by a heterotetramer of two subunits (Saiki et al, 2005), Pdss1 and Pdss2. In addition to serving an essential role in electron shuttling within the mitochondrial RC, CoQ has both antioxidant and oxidant functions (Linnane et al, 2007). Severe, collapsing glomerulopathy variant, focal segmental glomerulosclerosis (FSGS)-like renal disease in B6.*Pdss2*$^{kd/kd}$ missense mutant mice results from CoQ deficiency within glomerular podocytes (Peng et al, 2008). High-dose $CoQ_{10}$ supplementation mitigates renal disease in B6.*Pdss2*$^{kd/kd}$ mice through approximately 140 days of life, but does not normalize albuminuria to control levels, prevent nephritis, nor restore $CoQ_9$ or $CoQ_{10}$ content in renal tissue (Saiki et al, 2008).

Here, we report the efficacy and results of detailed mechanistic investigations for both preventative and therapeutic trials in *Pdss2* mutant mice with the oral lipophilic drug probucol.

## RESULTS

### Probucol therapy prevents renal disease in *Pdss2*$^{kd/kd}$ missense mutant mice

As probucol was previously reported to be beneficial in a mouse model of mitochondrial-based glomerular disease caused by mutations in *Mpv17* (Binder et al, 1999), we added 1% probucol to standard mouse chow (TestDiet) fed to B6.*Pdss2*$^{kd/kd}$ missense mutant mice. Probucol effects were compared to those of long-term $CoQ_{10}$ supplementation, since high-dose $CoQ_{10}$ was previously observed to delay manifestations of renal disease in young B6.*Pdss2*$^{kd/kd}$ mice (Saiki et al, 2008). Urine albumin immediately preceding, and histological nephritis score immediately following sacrifice were determined in 4–5-month-old missense mutant littermates placed on standard unsupplemented diet (controls), probucol supplementation from birth, weaning or day 100 of life, high-dose $CoQ_{10}$ supplementation from birth, weaning or day 100 of life, or vitamin E from weaning (Table 1). Probucol therapy significantly prevented renal disease whether administered from the time of weaning through at least 6 months of age or for only approximately 3 weeks prior to sacrifice. While all of the probucol-treated missense mutant groups showed significantly higher urine albumin than gender-matched healthy B6 controls ($p < 0.01$ in each case), no significant differences were seen in their mean nephritis score relative to gender-matched healthy B6 controls ($p > 0.05$). Representative examples of normal renal histology seen in probucol-treated missense mutant animals are illustrated in Fig 1. Vitamin E long-term administration from weaning had modest beneficial effect in female B6.*Pdss2*$^{kd/kd}$ mice but no significant effect in males (Table 1). Long-term $CoQ_{10}$ therapy also significantly prevented renal disease manifestations when provided from weaning through 6 months of age. However, significantly improved renal histology and

**Table 1. Effects of probucol or $CoQ_{10}$ supplementation on renal disease manifestations of B6.*Pdss2*$^{kd/kd}$ missense mutant mice**

| Strain | Gender | Treatment group | Treatment duration | N | Age at sacrifice (Days) | Nephritis score | Urine albumin (mg/24 h) | Albumin comparison group | Albumin *p*-value |
|---|---|---|---|---|---|---|---|---|---|
| B6 | M | No treatment | n/a | 14 | 156 ± 48.58 | 0.43 ± 0.46 | 0.46 ± 0.61 | | |
| B6 | F | No treatment | n/a | 12 | 156 ± 59.57 | 0.63 ± 0.62 | 0.22 ± 0.12 | | |
| B6.*Pdss2*$^{kd/kd}$ | M | No treatment | n/a | 24 | 135 ± 18.37 | 1.61 ± 0.93 | 10.60 ± 9.12 | | |
| B6.*Pdss2*$^{kd/kd}$ | F | No treatment | n/a | 20 | 136 ± 20.49 | 2.69 ± 0.99 | 31.47 ± 30.12 | B6.*Pdss2*$^{kd/kd}$ males | $p < 0.001$ |
| B6.*Pdss2*$^{kd/kd}$ | M | CoQ10 | Birth to sacrifice | 7 | 145 ± 8.29 | 0.69 ± 0.43 | 3.64 ± 4.85 | B6.*Pdss2*$^{kd/kd}$ untreated males | $p < 0.05$ |
| B6.*Pdss2*$^{kd/kd}$ | F | CoQ10 | Birth to sacrifice | 13 | 144 ± 16.29 | 0.71 ± 0.70 | 2.24 ± 1.79 | B6.*Pdss2*$^{kd/kd}$ untreated females | $p < 0.001$ |
| B6.*Pdss2*$^{kd/kd}$ | M | CoQ10 | Weaning to sacrifice | 6 | 125 ± 4.5 | 1.67 ± 0.75 | 4.11 ± 2.04 | B6.*Pdss2*$^{kd/kd}$ untreated males | $p < 0.01$ |
| B6.*Pdss2*$^{kd/kd}$ | F | CoQ10 | Weaning to sacrifice | 4 | 124 ± 3.19 | 2.26 ± 0.92 | 1.75 ± 0.43 | B6.*Pdss2*$^{kd/kd}$ untreated females | $p < 0.001$ |
| B6.*Pdss2*$^{kd/kd}$ | M | CoQ10 | Day 100 to sacrifice | 6 | 121 ± 0.94 | 1.42 ± 0.45 | 10.47 ± 3.47 | B6.*Pdss2*$^{kd/kd}$ untreated males | $p > 0.05$ |
| B6.*Pdss2*$^{kd/kd}$ | F | CoQ10 | Day 100 to sacrifice | 5 | 121 ± 0 | 1.30 ± 0.40 | 4.08 ± 1.15 | B6.*Pdss2*$^{kd/kd}$ untreated females | $p < 0.001$ |
| B6.*Pdss2*$^{kd/kd}$ | M | Probucol | Birth to sacrifice[a] | 5 | 206 ± 0 | 0.6 ± 0.49 | 0.76 ± 0.14 | B6.*Pdss2*$^{kd/kd}$ untreated males | $p < 0.001$ |
| B6.*Pdss2*$^{kd/kd}$ | F | Probucol | Birth to sacrifice | 3 | 206 ± 0 | 1.67 ± 0.47 | 19.01 ± 9.50 | B6.*Pdss2*$^{kd/kd}$ untreated females | $p > 0.05$ |
| B6.*Pdss2*$^{kd/kd}$ | M | Probucol | Weaning to sacrifice | 14 | 156 ± 30.36 | 0.57 ± 0.82 | 1.15 ± 1.12 | B6.*Pdss2*$^{kd/kd}$ untreated males | $p < 0.001$ |
| B6.*Pdss2*$^{kd/kd}$ | F | Probucol | Weaning to sacrifice | 11 | 136 ± 9.43 | 0.55 ± 0.99 | 1.42 ± 0.91 | B6.*Pdss2*$^{kd/kd}$ untreated females | $p < 0.001$ |
| B6.*Pdss2*$^{kd/kd}$ | M | Probucol | Day 100 to sacrifice | 5 | 122 ± 0 | 1.40 ± 0.37 | 0.64 ± 0.17 | B6.*Pdss2*$^{kd/kd}$ untreated males | $p < 0.001$ |
| B6.*Pdss2*$^{kd/kd}$ | F | Probucol | Day 100 to sacrifice | 4 | 122 ± 0 | 0.88 ± 0.55 | 1.53 ± 0.36 | B6.*Pdss2*$^{kd/kd}$ untreated females | $p < 0.001$ |
| B6.*Pdss2*$^{kd/kd}$ | M | Vitamin E | Weaning to sacrifice | 9 | 122 ± 2.85 | 1.56 ± 0.50 | 11.58 ± 4.23 | B6.*Pdss2*$^{kd/kd}$ untreated males | $p > 0.05$ |
| B6.*Pdss2*$^{kd/kd}$ | F | Vitamin E | Weaning to sacrifice | 10 | 120 ± 2.20 | 1.20 ± 0.40 | 11.38 ± 4.72 | B6.*Pdss2*$^{kd/kd}$ untreated females | $p < 0.01$ |

Probucol therapy significantly prevented renal sequelae that are typically manifest by 4 months of age whether administered either from the time of weaning or for only 3 weeks prior to sacrifice, with significant disease prevention still evident through approximately 6 months of age. $CoQ_{10}$ therapy significantly prevented renal manifestations only when provided from weaning through 4 months of age, although significantly greater effects were seen with probucol than $CoQ_{10}$ at all treatment durations tested ($p < 0.01$ at younger age when treated from weaning; $p < 0.001$ at younger age when treated for 3 weeks prior to sacrifice; and $p < 0.001$ at older age). All values are reported as mean ± standard deviation. *p*-Values were calculated based on urine albumin by Mann–Whitney *U*-test relative to designated (male or female) age-matched untreated B6.*Pdss2*$^{kd/kd}$ animals.

[a]Probucol treated missense mutant males showed the greatest therapeutic response in urine albumin at all ages examined, from the earliest age (122 days) through the oldest (206 days).

 © 2011 EMBO Molecular Medicine 

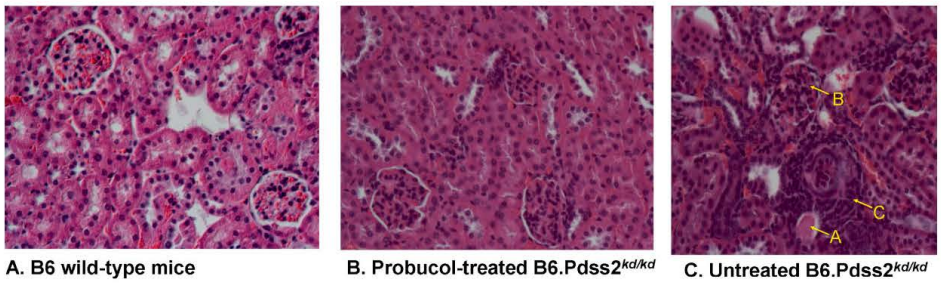



**Figure 1. Comparison of probucol-treated and untreated B6.*Pdss2*$^{kd/kd}$ mouse kidney pathology.** Near-normal glomerular histology is evident upon haematoxylin and eosin staining of renal sections from male probucol-treated missense mutant mice shown at 100X magnification.

**A.** Wild-type B6 control.

**B.** Probucol-treated B6.*Pdss2*$^{kd/kd}$ missense mutant mouse; 128-day old; 0.77 mg urine albumin.

**C.** Untreated B6.*Pdss2*$^{kd/kd}$ missense mutant mouse; 132-day old; 7.3 mg urine albumin. Note tubular dilatation (**arrow A**), glomerular crescents (**arrow B**) and severe interstitial inflammation (**arrow C**) evident in kidney from untreated missense mutant mouse.

function was seen when $CoQ_{10}$ treatment was initiated at birth rather than upon weaning (Table 1 and Supporting information File 1). The most dramatic rescue of the renal phenotype occurred in B6.*Pdss* $^{kd/kd}$ males that were treated with probucol from birth to 206 days of age (Table 1). Overall, probucol provided more long-lasting and effective prevention of renal disease than did supplemental $CoQ_{10}$.

Data analysis suggested gender may influence drug treatment response. A gender effect was seen in response to *short-term* and *long-term* probucol treatments, as male B6.*Pdss2*$^{kd/kd}$ missense mutant mice had a significantly greater response in both cases than did females ($p < 0.05$). In contrast, short-term $CoQ_{10}$ therapy for approximately 3 weeks prior to sacrifice had a significant effect in female B6.*Pdss2*$^{kd/kd}$ mice but no effect in males. When directly comparing probucol and $CoQ_{10}$ treatment responses, significantly greater improvement following *long-term* treatment from weaning with probucol than $CoQ_{10}$ was seen among male mice for albuminuria ($p = 0.001$ males and $p = 0.1$ females) and among both genders for nephritis score ($p = 0.03$ males and $p = 0.06$ females). *Short-term* treatment from day 100 to sacrifice resulted in significantly greater improvement in both genders treated with probucol relative to $CoQ_{10}$ only in albuminuria ($p = 0.002$ males and $p = 0.008$ females) with equivalent effects on the more subjective nephritis score. Overall, male missense mutant mice tended to respond similarly or better to probucol therapy, whereas, females tended to respond similarly or better to $CoQ_{10}$ supplementation.

### Probucol therapy reverses renal disease manifestations in symptomatic *Pdss2*$^{kd/kd}$ missense mutant mice

A second cohort of B6.*Pdss2*$^{kd/kd}$ mice was maintained on normal chow until approximately 100 days of age and then tested in metabolic cages for urine albumin. Animals with urine albumin >1 mg in 24 h were placed on probucol-supplemented chow for approximately 2 weeks, retested in metabolic cages, and then sacrificed. As shown in Table 2, 24 h urine albumin in this cohort decreased from 11.46 +/− 12.3 mg before to 4.07 +/− 4.22 mg after probucol treatment ($p < 0.01$). A highly significant reduction occurred in both genders, with a greater reduction in albuminuria seen in males. Although considerable variation was present between animals especially prior to treatment, albuminuria was reduced by probucol treatment in every instance.

### Probucol treatment lowers plasma cholesterol and hepatic phospholipid levels in B6.*Pdss2*$^{kd/kd}$ missense mutant and B6.*Podocin/cre,Pdss2*$^{loxP/loxP}$ glomerular-conditional knockout mice

We previously reported that *Pdss2* missense mutants develop hypercholesterolemia that is partly attributable to nephritis and partly a direct consequence of primary CoQ deficiency, since blood cholesterol is also significantly increased in B6.*Alb/cre,Pdss2*$^{loxP/loxP}$ liver-conditional *Pdss2* knockout mice that have normal renal function (Peng et al, 2008). Probucol has been previously reported to have potent lipid-lowering properties, which remain of uncertain mechanism (Stocker, 2009). To determine whether renal disease resolution on probucol therapy correlated with its lipoprotein effects, blood cholesterol and triglyceride levels were determined in both missense and glomerular podocyte-conditional knockout *Pdss2* mutant mice following long-term probucol treatment (Table 3). We previously observed that, whereas, B6.*Pdss2*$^{kd/kd}$ mice with more advanced stage disease (152 +/− 16 days of age) had significantly elevated blood cholesterol, mutant mice up to 133 days of age did not (Madaio et al, 2005). Similarly, plasma lipids were not significantly elevated in 4-month-old (mean: 133-day old) B6.*Pdss2*$^{kd/kd}$ missense mutant mice that had clear evidence of renal disease (Table 3). Nonetheless, probucol treatment significantly decreased plasma cholesterol and triglyceride levels, as well as renal disease manifestations of albuminuria and nephritis relative to untreated B6.*Pdss2*$^{kd/kd}$ missense mutant littermates (consistent with data presented in Table 1). Although probucol treatment did normalize the significantly

 © 2011 EMBO Molecular Medicine 

**Table 2. Renal disease phenotypes following short-term treatment of B6.*Pdss2*$^{kd/kd}$ missense mutant mice with probucol**

| | | | | Urine albumin (mg/24 h) | | |
|---|---|---|---|---|---|---|
| **Group** | **N** | **Age at first test** | **Probucol treatment duration** | **Pre-treatment test** | **Post-treatment test** | ***p*-Value** |
| Males | 7 | 102 ± 0.49 | 14.6 ± 1.40 days | 14.40 ± 19.1 | 2.32 ± 1.73 | $p < 0.05$ |
| Females | 12 | 106 ± 1.37 | 13.4 ± 2.36 days | 10.30 ± 7.59 | 5.09 ± 5.10 | $p < 0.05$ |
| ALL | 19 | 104 ± 2.52 | 13.8 ± 2.13 days | 11.46 ± 12.3 | 4.07 ± 4.22 | $p < 0.01$ |

Elevated 24 h urine albumin levels suggestive of renal glomerular disease in 100-day-old untreated missense mutants (pre-treatment test) were significantly reduced in both males and females following approximately 2 weeks of oral probucol treatment (post-treatment test). Histological nephritis score was also lower following probucol treatment than typical of untreated age-matched missense mutants (Table 1). Non-parametric statistical analysis (Mann–Whitney *U*-test) of mean urine albumin in treated *versus* untreated missense mutant groups showed short-term probucol treatment significantly reduced albuminuria ($p - 0.01$). A trend towards greater reduction in urine albumin was seen in males, with a mean reduction by 71.1% +/− 14.1% in males and 47.1% +/− 27.6% in females ($p - 0.07$).

**Table 3. Probucol effects on plasma lipids in B6.*Pdss2*$^{kd/kd}$ missense and B6.*Podocin/cre,Pdss2*$^{loxP/loxP}$ conditional knockout mice**

| **Mouse strain** | **N** | **Age (days)** | **Treatment** | **Cholesterol (mg/dl)** | **Triglycerides (mg/dl)** | **Urine albumin (mg/24 h)** | **Nephritis score (0–4)** |
|---|---|---|---|---|---|---|---|
| B6 | 8 | 160 ± 13 | Control | 85.96 ± 17.0 | 75.94 ± 24.5 | 0.5 ± 0.1 | 0.07 ± 0.17 |
| B6.*Pdss2*$^{kd/kd}$ | 16 | 133 ± 7.2 | Control | 97.1 ± 24.8 | 67.0 ± 22.3 | 24.3 ± 17.2 | 3.4 ± 0.5 |
| B6.*Pdss2*$^{kd/kd}$ | 12 | 169 ± 23.4 | Probucol | < 12.5[a] | 42.7 ± 19.7 | 1.6 ± 1.0 | 1.0 ± 1.3 |
| | | | | **($p < 0.001$)** | **($p < 0.01$)** | **($p < 0.001$)** | **($p < 0.01$)** |
| *Pod/cre* | 14 | 150 ± 9.8 | Control | 369.1 ± 168.4 | 114.5 ± 51.0 | 96.6 ± 31.1 | 3.7 ± 0.5 |
| *Pod/cre* | 11 | 164 ± 3.5 | Probucol | <63.2 ± 68.9[b] | 168.3 ± 77.4 | 45.6 ± 33.4 | 3.4 ± 0.7 |
| | | | | **($p < 0.001$)** | ($p - 0.069$) | **($p < 0.01$)** | ($p - 0.178$) |

Probucol therapy significantly lowered plasma cholesterol and triglycerides in B6.*Pdss2*$^{kd/kd}$ missense mutants, as well as plasma cholesterol in renal podocyte-conditional *Pdss2* knockout mutants ('*pod/cre*'). While renal disease manifestations of albuminuria and nephritis were prevented by probucol in missense mutants (consistent with data presented in Table 1), renal disease manifestations were largely unabated by probucol therapy in *pod/cre* conditional knockouts.
[a]Cholesterol levels in all samples from this group were below the level of detection.
[b]Cholesterol levels in four of the samples from this group were below the level of detection. All values are reported as mean ± standard deviation. *p*-Values were calculated by student's *t*-test for each mutation type relative to untreated mutant animals.

elevated blood cholesterol that was seen in B6.*Podocin/cre,Pdss2*$^{loxP/loxP}$ podocyte-conditional knockout animals, this lipid-lowering effect was insufficient to prevent or mitigate severe renal disease in these animals. To determine whether the hypolipidemic effects of probucol observed in plasma also extend to the cardiolipin-rich lipid milieu of the inner mitochondrial membrane in which the RC is located (Schlame & Ren, 2009), $^{31}$P-NMR analysis was performed on combined liver extracts from two animals per strain and treatment group (to provide sufficient tissue for analysis). Probucol significantly reduced liver membrane phospholipids in *Pdss2* mice, including cardiolipin, sphingomyelin and phospholipids (Supporting information File 2). Thus, while probucol is clearly an effective anti-hyperlipidemic agent, this property was insufficient to rescue the renal sequelae of severe CoQ deficiency in mice without Pdss2 activity within renal glomerular podocytes. Interestingly, prophylactic therapy from birth with Simvastatin, an anti-hyperlipidemic agent that inhibits HMG-CoA reductase, neither prevented renal disease nor dramatically lowered blood cholesterol in *Pdss2* missense mutant mice (data not shown), as was similarly observed following Simvastatin administration to apolipoprotein E-deficient mice (Ivanovski et al, 2008). Overall, the mechanism by which probucol prevents renal disease in missense mutant mice with some residual Pdss2 activity within podocytes (Peng et al, 2008) appears to be independent of its hypolipidemic effects.

### Resistance to oxidative stress is increased in *Pdss2* mutant mice when treated long-term with $CoQ_{10}$ but not when treated with probucol

Although CoQ has both antioxidant and oxidant roles (Linnane & Eastwood, 2004), we observed no evidence of increased reactive species damage attributable to primary CoQ deficiency in either *Pdss2* missense (*kd/kd*) or liver-conditional (*Alb/cre*) knockout mutants. Specifically, total lipid peroxidation of isolated liver mitochondria appeared unchanged in either mutant type relative to wild-type (WT) healthy controls both at baseline (Supporting information File 3A and B) and following long-term supplementation with either $CoQ_{10}$ or probucol (Supporting information File 3C). To further evaluate oxidant stress in *Pdss2* mice, aconitase activity was assayed in freeze-thawed liver mitochondria. Whereas, no significant difference was observed in *Pdss2* mutants at baseline or following long-term $CoQ_{10}$ therapy relative to B6 controls, aconitase activity was significantly increased by 15% in probucol-treated compared to untreated *Pdss2* missense mutants ($p < 0.05$, Fig 2A).

Antioxidant defenses can be assessed by monitoring induction of manganese superoxide dismutase (MnSOD), the primary mitochondrial enzyme to scavenge matrix superoxide (Macmillan-Crow & Cruthirds, 2001). MnSOD activity in isolated kidney mitochondria was significantly increased only in missense mutant or renal podocyte-conditional (*pod/cre*)

 © 2011 EMBO Molecular Medicine 

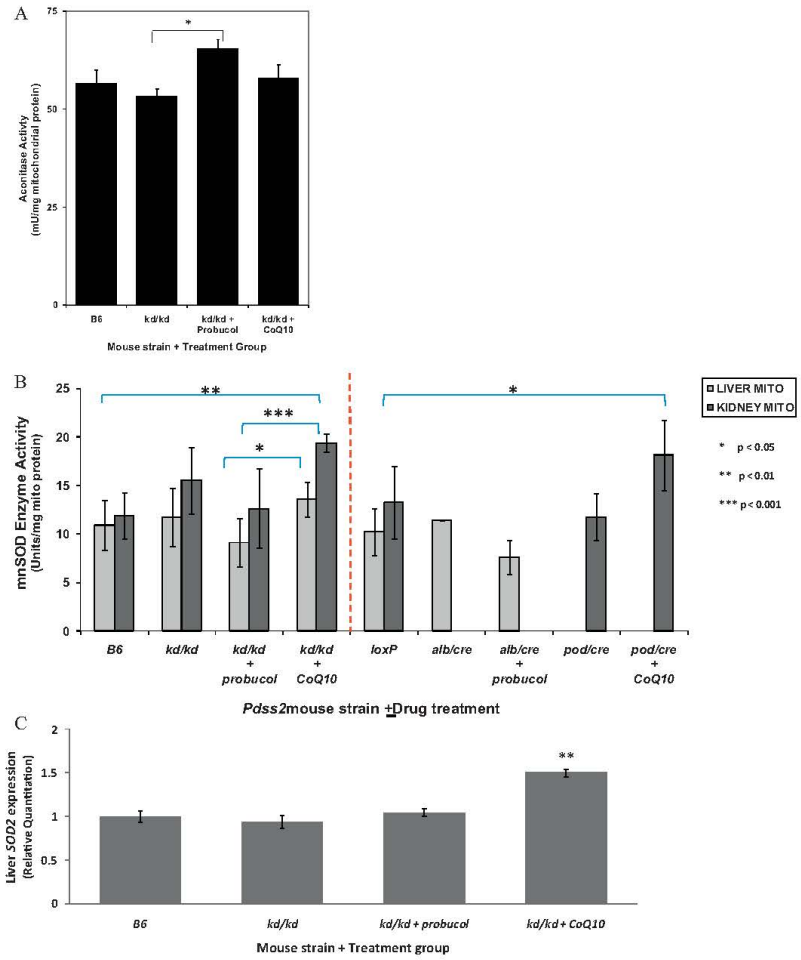



**Figure 2. Assessment of mitochondrial oxidant stress and scavenging defenses in *Pdss2* mutants following supplementation with probucol or $CoQ_{10}$.**

**A.** Aconitase activity in isolated liver mitochondria is significantly increased in *kd/kd* mutants treated with probucol relative to untreated littermates ($p < 0.05$ relative to untreated *kd/kd* mutants). No significant increase in aconitase activity was seen in *kd/kd* mutants at baseline or upon $CoQ_{10}$ supplementation. Results are the average ± standard error of five measurements per mitochondrial preparation from $n = 3$–5 female mice. Ages of mice ranged from 140 to 154 days for *kd/kd* and 215–216 days for B6.

**B.** MnSOD enzyme activity is significantly increased in kidney mitochondria isolated from missense mutants (*kd/kd*) and podocyte-conditional knockouts (*pod/cre*) treated with $CoQ_{10}$ relative to respective healthy controls. In contrast, a trend towards decreased mean MnSOD enzyme activity is observed in liver mitochondria from missense (*kd/kd*) and liver-conditional knockout (*Alb/cre*) mutant animals treated with probucol relative to respective healthy controls. Further, $CoQ_{10}$-treated missense mutant (*kd/kd*) animals have significantly greater MnSOD enzyme activity in both liver and kidney relative to probucol-treated missense (*kd/kd*) animals. Brackets highlight statistically significant comparisons relative to either untreated controls or between treatment groups, as indicated. Column height and error bars indicate activity mean and standard deviation (SD), respectively. Dashed red line distinguishes missense mutant (*kd/kd*) animals (compared to WT B6 controls) from two different tissue-specific conditional knockout mutants (compared to LoxP controls). *kd/kd*, missense mutant; *Alb/cre*, liver-conditional knockout mutant; *pod/cre*, renal glomerular podocyte-conditional knockout mutant.

**C.** *SOD2* (mitochondrial MnSOD) hepatic gene expression is significantly increased in *kd/kd* mutants treated with $CoQ_{10}$ relative to untreated littermates. In contrast, *SOD2* expression is unchanged relative to B6 WT controls in *kd/kd* mutants on standard chow with or without probucol supplementation. Values are reported as mean ± standard error. Mean age of each group was B6, 216 days; *kd/kd*, 137 days; probucol-treated *kd/kd*, 144 days; and $CoQ_{10}$-treated *kd/kd* 154 days. $n = 5$ for each group, except $CoQ_{10}$-treated animals where $n = 3$. All animals were female and the same individuals in which global microarray expression profiling was performed.

knockout mice following long-term treatment with $CoQ_{10}$ relative to respective healthy controls (Fig 2B). In contrast, a trend towards decreased MnSOD enzyme activity in isolated liver mitochondria was seen in missense mutant or liver-conditional knockout mice treated long-term with probucol. Significantly greater MnSOD enzyme activity was seen following $CoQ_{10}$ compared to probucol treatment in both liver and kidney mitochondria from missense mutant mice. Similarly, hepatic expression of *SOD2* (mitochondrial MnSOD) was significantly increased only in $CoQ_{10}$-treated missense mutants (Fig 2C), but unchanged in missense mutants on standard chow with or without probucol. These data suggest that, while long-term, high-dose $CoQ_{10}$ supplementation induces mitochondrial oxidant scavenging capacity and oxidative stress resistance, long-term probucol supplementation does not.

#### Probucol reverses hyperglycemia in B6.*Alb/cre*,*Pdss2*$^{loxP/loxP}$ liver-conditional knockout mice

Given the central role of the liver in intermediary metabolism, we assessed major blood metabolites indicative of hepatic function and metabolic control in alb/cre liver-conditional knockout mice. B6.*Alb/cre*,*Pdss2*$^{loxP/loxP}$ mice exhibited no evidence of liver damage based on histologic (data not shown) or plasma ALT levels (Supporting information File 4), either at baseline or following long-term probucol therapy. Blood glucose was significantly elevated in *Alb/cre* liver-conditional knockout mutants ($p < 0.05$) and significantly decreased by feeding mice probucol from weaning. No significant difference due to either *Pdss2* knockout in liver or long-term probucol therapy was observed in blood urea, which is exclusively synthesized in liver. Although blood ammonia was not increased in *Alb/cre* liver-conditional knockout mice relative to B6.*Pdss2*$^{loxP/loxP}$ ('LoxP') controls, probucol did significantly decrease blood ammonia relative to both untreated *Alb/cre* mutants and age-matched healthy controls (Supporting information File 4). Thus, probucol appears to have no adverse effect on hepatic function or biosynthetic capacity and actually appears to have potentially beneficial systemic metabolic effects by lowering blood levels of glucose and ammonia.

#### Probucol therapy reverses global transcriptional alterations across intermediary metabolic pathways in *Pdss2* mice

To discern whether the same transcriptional signature of mitochondrial dysfunction previously reported in B6.*Alb/cre*,*Pdss2*$^{loxP/loxP}$ liver-conditional knockout mice (Peng et al, 2008) was present regardless of mutation type, as well as to assess whether pharmacologic therapies modulate expression of particular pathways, genome-wide transcriptional profiling was performed in livers from B6.*Pdss2*$^{kd/kd}$ missense mutant mice on standard chow or supplemented long-term with either probucol or $CoQ_{10}$. The influence of long-term probucol treatment on pathway-level expression alterations was also assessed in liver-conditional *Pdss2* knockout mice. Significantly altered KEGG pathways as determined using Gene Set Enrichment Analysis (GSEA) to analyse relative genome-wide expression changes in both mutant types on standard chow and following supplementation with probucol or $CoQ_{10}$ are visually represented by heatmap in Fig 3. Full details of all pathways analysed are provided in excel format in Supporting information File 5. Upregulated expression of oxidative phosphorylation (OXPHOS), the tricarboxylic acid cycle, directly interacting pathways involved in amino acid metabolism, and cell defense pathways was previously observed in liver-conditional *Pdss2* knockout mice (Peng et al, 2008), as well as in several mitochondrial RC subunit missense mutant *Caenorhabditis elegans* strains (Falk et al, 2008). We now conclude that upregulation of OXPHOS, protein processing pathways, multiple immune pathways, and nucleotide metabolism occurs in both missense and liver-conditional knockout *Pdss2* mice. However, *Pdss2* missense mutants uniquely upregulate lipid biosynthesis and downregulate fatty acid metabolism, amino acid metabolism, glycolysis, cell defenses and peroxisome proliferator-activated receptor (*PPAR*) transcriptional signaling pathway expression. Regardless of the direction of transcriptional changes in either *Pdss2* mutant type, probucol largely (but not completely, as detailed in Supporting information File 5) reversed the global pattern of metabolic pathway alterations (Fig 4). Indeed, long-term probucol therapy in both mutant types reversed expression alterations within the *PPAR* signalling pathway, fatty acid metabolism and glycolysis, despite these having been concordantly upregulated in knockouts and downregulated in missense *Pdss2* mutants.

Probucol had no significant effect on OXPHOS pathway upregulation that occurs in these primary mitochondrial RC mutants, consistent with its apparent inability to serve as an electron acceptor to replace deficient CoQ in the RC. Further support for this finding is provided by polarographic RC analysis of permeabilized skeletal muscle fibres (Oroboros), which showed no significant difference in RC capacity of probucol treated B6.*Pdss2*$^{kd/kd}$ missense mutants relative to untreated B6.*Pdss2*$^{kd/kd}$ controls (Supporting information File 6). Furthermore, probucol had no significant effect on gene expression of major pathways previously linked to its apparent mechanistic effects in other models, including antioxidant genes (Supporting information File 7) or heme oxygenase (*HMOX1* and *HMOX2*; Supporting information File 8).

Branched-chain amino acid catabolism was the most upregulated KEGG metabolic pathway by either therapy in *Pdss2* missense mutants (Fig 4B and Supporting information File 5). Steroid biosynthesis and the complement and coagulation cascade were the most downregulated pathways in missense mutants by $CoQ_{10}$ and probucol therapy, respectively (Fig 4A and Supporting information File 5). Steroid biosynthesis was also the most down-regulated pathway in liver-conditional knockout mutants on probucol therapy (Supporting information File 5), a result technically validated on three additional microarray platforms (Zhang et al, 2010). $CoQ_{10}$ supplementation in missense mutants caused a less global and pronounced 'reversal' of metabolic alterations than did probucol (Fig 4). Gene-level heatmap analysis among the most significantly altered KEGG pathways illustrates that a particular subset of a given pathway's genes may drive overall pathway significance (Supporting information File 9; Zhang et al, 2010). Overall, the KEGG Atlas overview of intermediary metabolism provides an

 © 2011 EMBO Molecular Medicine 

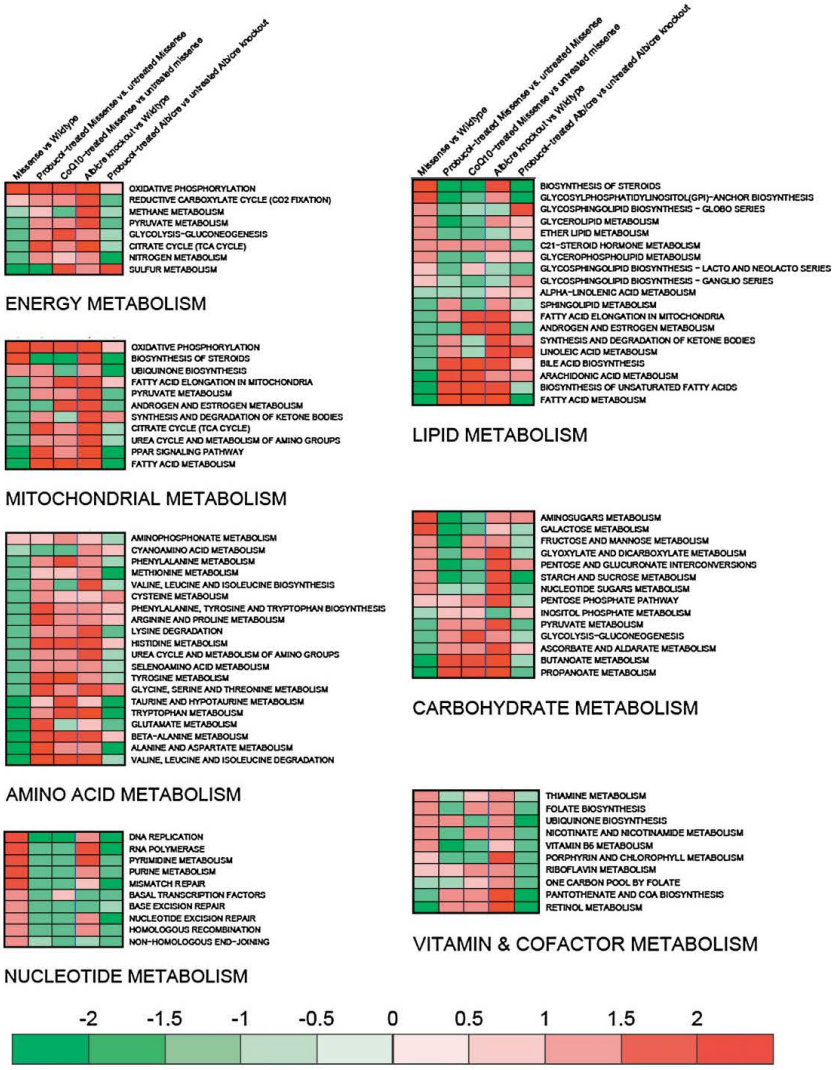



**Figure 3. Pathway-level heatmap depicts metabolic pathways whose expression was significantly altered following chronic probucol or $CoQ_{10}$ supplementation in missense and liver-conditional knockout *Pdss2* mutants.** Heatmaps clustered by primary metabolic functions are provided for all KEGG-defined pathways in both mutant types on standard chow alone or with chronic supplementation of either probucol (both mutant types) or $CoQ_{10}$ (missense mutants only). This view illustrates that the most significantly altered KEGG-defined pathways fall into several key areas of intermediary metabolism. Probucol therapy has a dramatic effect in normalizing observed expression alterations across many metabolic domains in both mutant types. Rows represent overall expression alterations among individual KEGG-defined pathways. Columns represent pair-wise comparisons, from left to right: (1) B6.*Pdss2*$^{kd/kd}$ *versus* B6 WT control; (2) probucol-treated B6.*Pdss2*$^{kd/kd}$ *versus* untreated B6.*Pdss2*$^{kd/kd}$; (3) $CoQ_{10}$-treated B6.*Pdss2*$^{kd/kd}$ *versus* untreated B6.*Pdss2*$^{kd/kd}$; (4) B6.*Alb/CrePdss2*$^{loxP/loxP}$ *versus* LoxP WT control; and (5) probucol-treated B6.*Alb/CrePdss2*$^{loxP/loxP}$ *versus* untreated B6.*Alb/CrePdss2*$^{loxP/loxP}$. Red or green colour indicates pathway up- or down-regulation in the first group relative to the second, where intensity conveys significance of overall pathway alterations for each pair-wise comparison. Illumina and Affymetrix 3′ expression microarrays were used for analysis of B6.*Pdss2*$^{kd/kd}$ and B6.*Alb/CrePdss2*$^{loxP/loxP}$ experiments, respectively. Cross-platform validation of probucol-treated B6.*Alb/CrePdss2*$^{loxP/loxP}$ *versus* untreated B6.*Alb/CrePdss2*$^{loxP/loxP}$ results was performed by replicate analysis of the same samples on three additional expression microarray platforms, including Illumina (Zhang et al, 2010). Complete GSEA data output including statistical significance for KEGG pathways analysed in all comparisons are provided in Supporting information File 5.

 © 2011 EMBO Molecular Medicine 

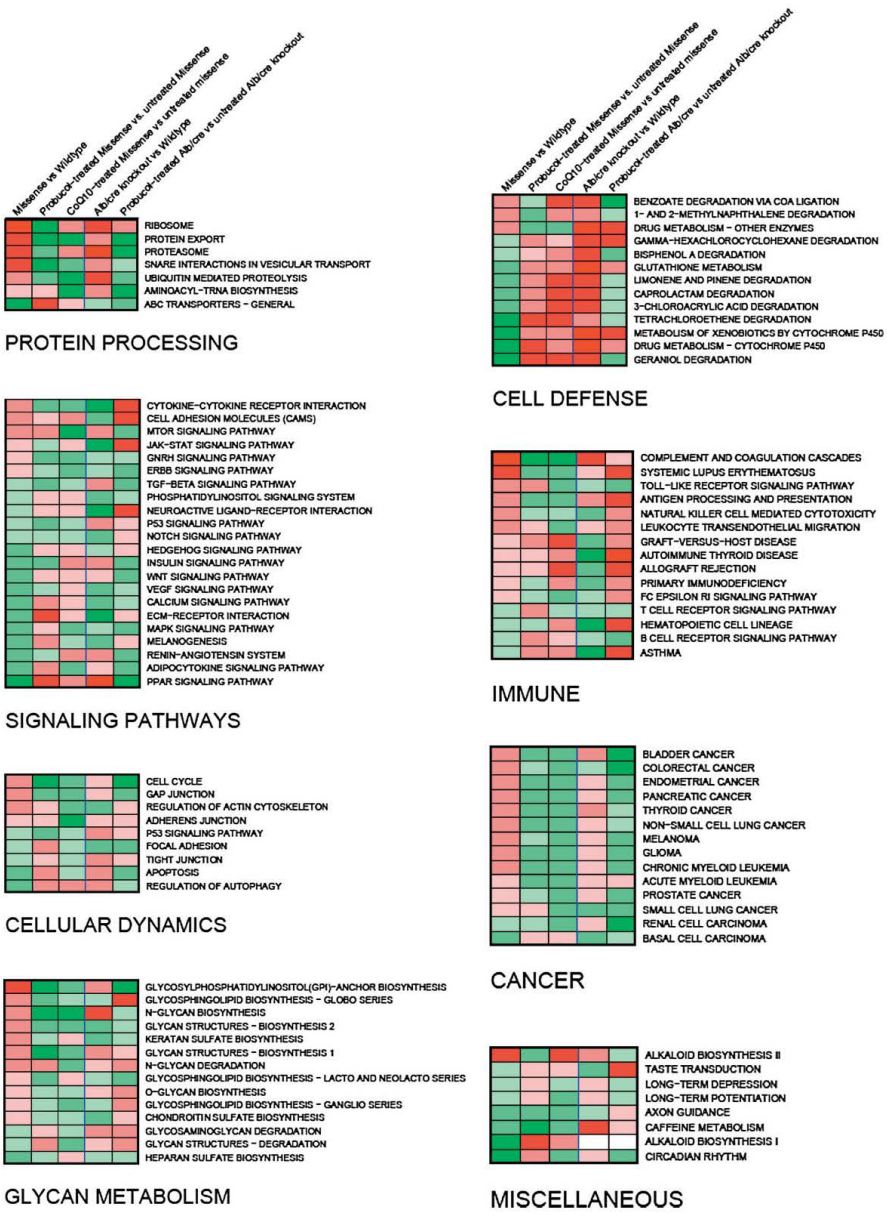



**Figure 3.** Continued

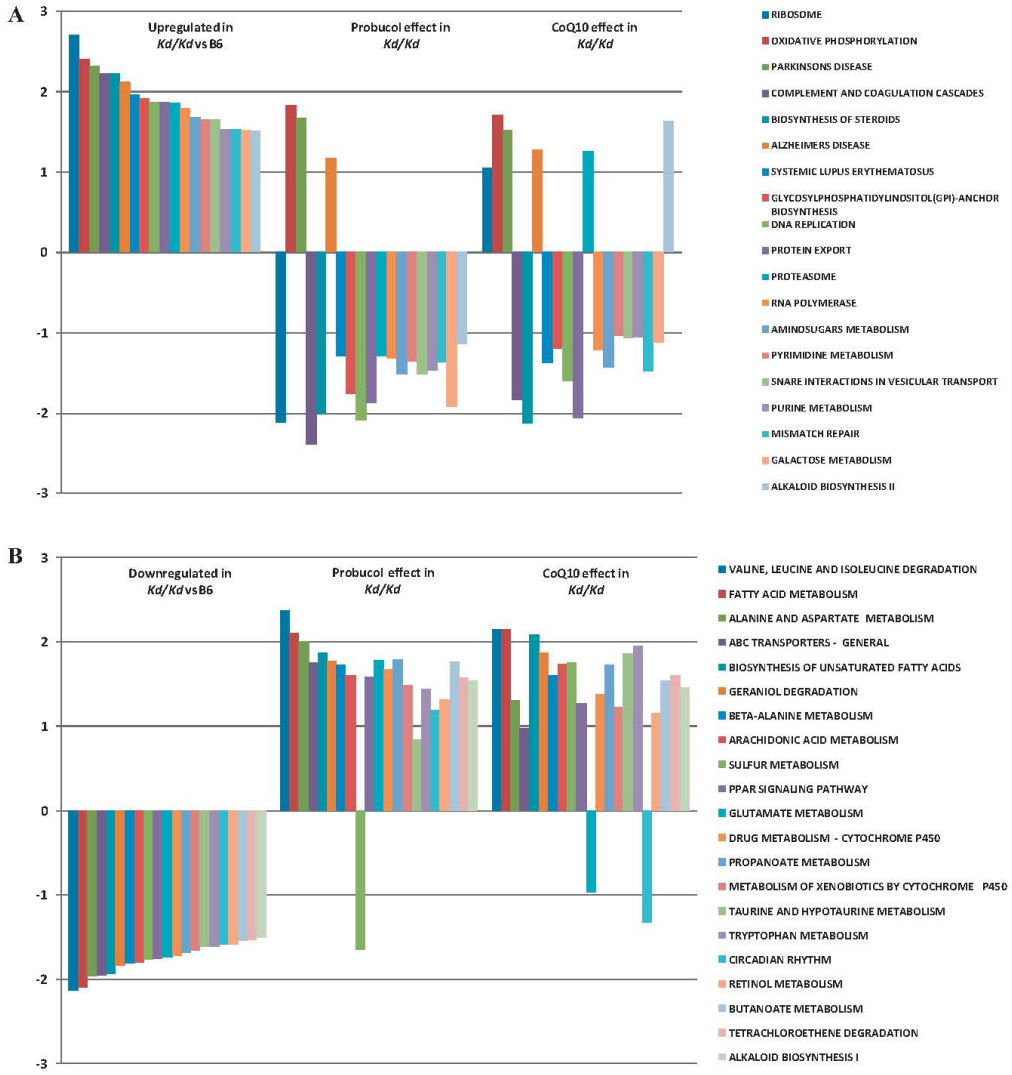



**Figure 4. Probucol has a greater effect than $CoQ_{10}$ supplementation in normalizing alterations among the most differentially expressed metabolic pathways in *Pdss2* missense mutant mouse liver.** The most differentially regulated KEGG-defined pathways as determined in GSEA to have normalized enrichment score (NES) >1.5 are shown for B6.*Pdss2*$^{kd/kd}$ missense mutants relative to B6 healthy controls. Probucol has a more widespread and substantial effect than does $CoQ_{10}$ in 'reversing', or preventing, expression alterations among pathway that are both upregulated (**Panel A**) and downregulated (**Panel B**) in missense mutants. Bar length represents NES for each pathway as determined in GSEA v2.0. Complete GSEA data output including statistical analyses of all KEGG-defined pathways analysed in missense animals, as well as in liver-conditional knockout mutants treated with probucol, are provided in Supporting information File 5.

integrated gestalt of the global metabolic expression alterations caused by both mutation types and their substantial normalization with probucol therapy (Supporting information File 10).

### PPAR signaling mediates metabolic consequences of primary $CoQ_{10}$ deficiency in *Pdss2* mutant mice

The *PPAR* family of nuclear transcription factors transcriptionally controls many aspects of metabolism through modulation of

 © 2011 EMBO Molecular Medicine 

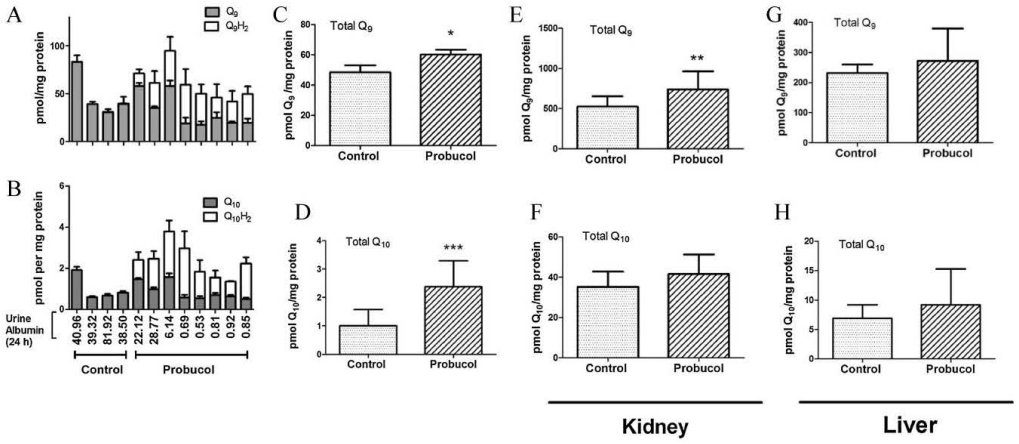



**Figure 6. Probucol supplementation increases content of $CoQ_9$ and $CoQ_{10}$ in kidney and liver of *Pdss2*$^{hd/hd}$ missense mutant mice.**

**Long-term probucol supplementation**

**A–D.** *Pdss2*$^{hd/hd}$ mice (3 females and 5 males) were fed diets supplemented with probucol (1% w/w) from birth and killed at 205–207 days of age. Control B6.*Pdss2*$^{hd/hd}$ mice (2 females and 2 males) were fed unsupplemented standard chow diet and sacrificed at 205–215 days of age. Each bar represents the average content of (**A**) $CoQ_9$ and $CoQ_9H_2$ and (**B**) $CoQ_{10}$ and $CoQ_{10}H_2$ measured in three aliquots of liver homogenates prepared from each mouse, calculated as the average of six measurements from three independent sample aliquots. Error bars indicate SD. Twenty-four hour urine albumin levels collected immediately prior to liver dissection are indicated for each animal. (**C**) Total $CoQ_9$ content represents the average ± SD of the sum of $CoQ_9$ plus $CoQ_9H_2$ (determined from panel A). (**D**) Total $CoQ_{10}$ content represents the average ± SD of the sum of $CoQ_{10}$ and $CoQ_{10}H_2$ (determined from panel B) $^*p < 0.05$ and $^{***}p < 0.001$.

**Short-term probucol supplementation**

**E–H.** Female *Pdss2*$^{hd/hd}$ mice (100-day old) were fed standard diets plus ($n-3$) or minus ($n-2$) probucol for 15 days. Aliquots of kidney (**E** and **F**) and liver (**G** and **H**) homogenates were measured for content of total $CoQ_9$ (**E** and **G**) or total $CoQ_{10}$ (**F** and **H**). $^{**}p < 0.01$. Both $CoQ_9$ and $CoQ_9H_2$ and $CoQ_{10}$ and $CoQ_{10}H_2$ were present in all extracts, with no differences between them as was observed in extracts prepared from the older mice (205–207 days of age) following long-term probucol treatment.

ted animals contained 20–80% of total CoQ content in the reduced or hydroquinone state ($CoQH_2$). Although no precautions were taken to prevent auto-oxidation of $CoQH_2$, liver extracts from the un-supplemented and probucol-supplemented animals were prepared and analysed at the same time. Thus, the lack of $CoQ_9H_2$ and $CoQ_{10}H_2$ is a unique characteristic of samples prepared from the un-supplemented B6.*Pdss2*$^{kd/kd}$ mice. Summation of the hydroquinone and quinone content for $CoQ_9$ (Fig 6C) and $CoQ_{10}$ (Fig 6D) indicated that chronic probucol supplementation significantly elevated total CoQ content, which correlated with a dramatic rescue of kidney disease as evidenced by significantly decreased urine albumin [Fig 6B; average urine albumin in un-supplemented = 50.18 *vs.* probucol-treated = 7.6 ($p < 0.01$) and nephritis score (average nephritis score in un-supplemented = 3.0 *vs.* probucol-treated = 1.0, $p < 0.01$)]. Unfortunately, kidneys from these animals were used for histological purposes and were not available for CoQ content analysis. Similarly as observed when comparing renal disease severity, a gender effect was evident when comparing $CoQ_9$ and $CoQ_{10}$ liver levels (Supporting information File 12). Both CoQ species were approximately two-fold greater in females than males at baseline and increased following long-term probucol treatment in both genders.

Given the ability of long-term probucol supplementation to increase tissue CoQ content, the effect of short-term (15 day) probucol treatment on tissue CoQ content was investigated in liver and kidney from female B6.*Pdss2*$^{kd/kd}$ mice already showing albuminuria (24 h albumin > 1 mg) when treatment was begun. Total $CoQ_9$ content in kidney homogenates was significantly increased by short-term probucol supplementation (Fig 6E, $p < 0.01$). Total $CoQ_{10}$ content in kidney was also marginally increased (Fig 6F; $p = 0.0689$). However, no significant differences in $CoQ_9$ or $CoQ_{10}$ levels were observed in liver (Fig 6G and H). Short-term probucol treatment also did not alter the proportion of hydroquinone in either tissue (data not shown). Thus, probucol supplementation throughout life increased hydroquinone and total quinone levels in liver even at advanced age, whereas, short-term treatment of symptomatic B6.*Pdss2*$^{kd/kd}$ mice significantly increased only the kidney total $CoQ_9$ content.

## DISCUSSION

### Biological significance

This translational investigation of a potential oral therapy for a genetic-based mitochondrial RC disorder revealed that endo-

 © 2011 EMBO Molecular Medicine 

more than 50 target genes involved in lipid, glucose and amino acid homeostasis, as well as inflammation, cell proliferation and cell division (Feldman et al, 2008). Expression of *PPAR* pathway transcription factors and target genes was significantly altered as judged by global microarray-based transcriptional profiling analysis in liver from both missense and liver-conditional knockout mutants, and largely normalized with probucol therapy (Supporting information File 11). Quantitative Polymerase Chain Reaction (after reverse transcription) (RT-PCR) analysis confirmed that expression of the *PPAR-γ* and *PPAR-α* transcription factors were decreased in *Pdss2* missense mutants and fully normalized following probucol treatment, but were unaltered by $CoQ_{10}$ supplementation (Fig 5A and B). Interestingly, *PPAR-γ* expression was significantly increased in *Pdss2* knockout mice but also normalized with probucol therapy (Fig 5C). *PPAR-α* expression was unchanged in *Pdss2* knockout mice (Fig 5D). Overall, these data confirm that *PPAR* expression alterations occur in primary mitochondrial dysfunction caused by CoQ deficiency and normalize with probucol therapy.

### Probucol therapy increases tissue CoQ content in *Pdss2*$^{kd/kd}$ mice

Peroxisomal inducers and *PPAR-α* signaling agonists are known to induce CoQ synthesis in mice (Turunen et al, 2004). The enhanced rescue of kidney disease in B6.*Pdss2*$^{kd/kd}$ mice achieved by both long- and short-term supplementation with probucol relative to $CoQ_{10}$, and the restoration of *PPAR-γ* and *PPAR-α* expression in response to probucol treatment, raised the question of whether probucol alters CoQ tissue levels. To investigate this possibility, B6.*Pdss2*$^{kd/kd}$ mice were fed standard chow alone or supplemented with probucol from birth to age 207 days, when renal disease severity was assessed by measuring 24 h urine albumin levels and determining histological nephritis score (Supporting information File 12). Liver homogenates were analysed to quantify $CoQ_9$, $CoQ_9H_2$, $CoQ_{10}$ and $CoQ_{10}H_2$ levels (Fig 6A and B). $CoQ_9$ and $CoQ_{10}$ in lipid extracts prepared from the liver of un-supplemented mice were present exclusively in the oxidized quinone state. In contrast, lipid extracts from the liver of probucol-supplemen-

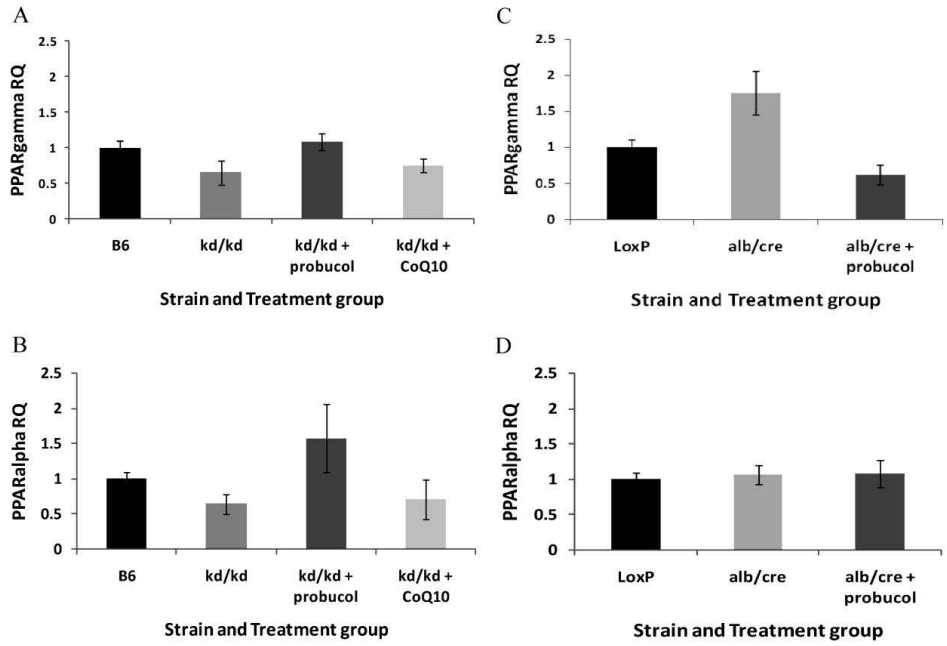



**Figure 5. *PPAR* transcription factor expression normalizes with probucol therapy in *Pdss2* mutant mice.**

**A.** Hepatic expression of *PPAR-γ* and

**B.** *PPAR-α* in *Pdss2* missense mice is decreased by quantitative RT-PCR validation, but increased by long-term probucol supplementation either to (*PPAR-γ*) or exceeding (*PPAR-α*) expression levels seen in B6 WT controls. $CoQ_{10}$ supplementation does not significantly alter expression of either *PPAR* transcription factor in missense mutants. $n = 4$ female mice per strain and treatment group aged 129–156 days.

**C.** Hepatic expression of *PPAR-γ* is increased by quantitative RT-PCR validation in liver-conditional *Pdss2* knockout mice relative to LoxP WT controls, but clearly decreased by long-term probucol therapy below expression levels seen in WT controls.

**D.** In contrast, hepatic *PPAR-α* expression is unchanged in male liver-conditional *Pdss2* knockout mice either on standard chow or supplemented long-term with probucol relative to LoxP WT controls. $n = 3$ male mice per strain and treatment group aged 120–141 days.

 © 2011 EMBO Molecular Medicine 

genous upregulation of CoQ content by probucol treatment is far more effective than attempts to replace the deficient metabolite (CoQ) by exogenous $CoQ_{10}$ supplementation. Probucol treatment successfully improved disease manifestations whether initiated at birth, at weaning, for a short time (3 weeks) prior to onset of typical disease manifestations, or even for just 2 weeks after the onset of the pathophysiologic disease process in untreated *Pdss2* mutant animals. Indeed, the mitochondria defects that are characteristic of this phenotype can be observed in most B6.*Pdss2*$^{kd/kd}$ mice before 100-days old by electron microscopy (Hallman et al, 2006), and B6.*Pdss2*$^{kd/kd}$ mice may manifest significant albuminuria as early as 96-days old (Madaio et al, 2005). Deficiencies in tissue CoQ content can be observed even earlier: the average $CoQ_9$ concentration in kidney extracts from 40-day-old B6 control mice was $1,088 \pm 59$ pmol/mg protein, as compared to $292 \pm 15$ pmol/mg protein in 37-day-old B6.*Pdss2*$^{kd/kd}$ missense mutant mice (Saiki et al, 2008). Therefore, not only does probucol have preventative effects (Table 1), but it successfully treats mice after onset of the disease process, as evidenced by albuminuria (Table 2).

Prophylactic probucol supplementation long-term from birth to pre-symptomatic animals clearly increased $CoQ_9$ and $CoQ_{10}$ levels in liver (Fig 6) and prevented nephritis (Table 1). It is interesting that total CoQ content, particularly $CoQ_9$, was also modestly but significantly increased in kidney (Fig 6) and all markers of nephritis (Table 2) were significantly decreased following only 2 weeks of probucol treatment to B6.*Pdss2*$^{kd/kd}$ mice already showing albuminuria (Fig 6). Strong correlation was similarly observed previously between high-kidney $CoQ_9$ content and low urine albumin in B6.*Pdss2*$^{kd/kd}$ line G mice: two line G mice that had high-urine albumin also had low renal $CoQ_9$ content, whereas six line G mice that did not manifest evidence of nephritis all had high-renal $CoQ_9$ content (Saiki et al, 2008). The gene cluster, 'ubiquinone biosynthesis' was not, however, differentially expressed in liver following long-term probucol therapy (Fig 3). In particular, expression of *ADCK3*, the homologue of yeast *COQ8* that appears to regulate Q content (Barros et al, 2005; Zampol et al, 2010), was not significantly different by microarray profiling in liver from B6.*Pdss2*$^{kd/kd}$ mutants either at baseline or following probucol treatment. It remains possible that CoQ content could be affected by the rate of turnover, or it may be that the ADCK3 polypeptide is regulated by either translational control or post-translational modifications. Further, while hepatic expression offers the benefit of assaying a homogenous tissue, it may not be reflective of CoQ pathway expression changes in renal podocytes. Although the mechanism by which short-term probucol treatment increases renal $CoQ_9$ content in symptomatic B6.*Pdss2*$^{kd/kd}$ mice remains uncertain, it seems likely that this effect is important for kidney disease rescue. The increases detected in *de novo* content of CoQ (whether due to increased synthesis or stability) arising from probucol supplementation are more efficacious than can be attained with $CoQ_{10}$ supplementation (Saiki et al, 2008). To this end, we have previously shown that although long-term $CoQ_{10}$ treatment partially mitigates albuminuria and nephritis, it does not correct the $CoQ_9$ or $CoQ_{10}$ deficiency in B6.*Pdss2*$^{kd/kd}$ mouse kidney (Saiki et al, 2008). Similarly, defects in the *de novo* synthesis of lipoic acid in yeast cannot be corrected by simply providing lipoic acid exogenously (Hiltunen et al, 2010).

Beneficial effects of probucol administered before the onset of overt disease manifestations suggests that an effective application of this lipophilic agent may be as a prophylactic agent to prevent systemic sequelae of mitochondrial disease. In addition, significantly reduced albuminuria following onset of overt disease manifestations suggests that probucol therapy may also have value as a treatment modality for mitochondrial disease. Future studies of probucol are needed to discern whether similar benefit occurs in human subjects, whether its efficacy is multi-systemic or limited to the kidney, whether therapeutic effects are detectable if administered to individuals already manifesting severe disease sequelae, and whether it has a tolerable safety profile in human patients afflicted with the heterogeneous class of mitochondrial diseases. No evidence of overt liver disease (Supporting information File 4) was observed following long-term probucol administration to *Pdss2* mutant mice, although a significant reduction was seen in blood cholesterol, glucose, and ammonia as well as in hepatic phospholipid content (Supporting information File 2). Patients with a multi-systemic infantile form of $CoQ_{10}$ deficiency who harbour mutations in *PDSS1*, *PDSS2*, *COQ2* or *COQ9* may also exhibit renal disease, which in some cases has been reported to respond to treatment with $CoQ_{10}$ (Quinzii & Hirano, 2010). It will be important to evaluate the efficacy of probucol therapy in these patients.

#### Investigation of additional possible mechanisms underlying probucol efficacy in *Pdss2* mutants

Probucol is structurally comprised of two phenol rings joined by a disulfide bridge. It represents a chemical prototype from which newer generation analogues have since been generated that lack some potentially deleterious effects of probucol (Stocker, 2009), including lowering HDL cholesterol and prolonging cardiac repolarization (QTc interval). While neither of these parameters was specifically assessed in probucol-treated *Pdss2* mice, we observed no incidence of sudden or unexplained death as might be seen with prolonged QTc in treated animals up to 8-months old. The mechanisms by which probucol lowers plasma lipid levels, acts as an antioxidant, and fights inflammation remain active areas of investigation (Stocker, 2009). Probucol has recently been reported to have renal protective effects during the administration of nephrotoxic agents (Yin et al, 2009), as well as beneficial effects on cardiac and neurologic function in the face of oxidative stress (Farina et al, 2009; Wu et al, 2006; Zhou et al, 2009). It has successfully been used to prevent restenosis after coronary angioplasty (Tardif et al, 1997) and also prevents atherosclerosis and related cardiovascular diseases associated with increased oxidative stress and inflammation in several animal models, where its efficacy has been attributed to induction of heme oxygenase (Wu et al, 2006). However, heme oxygenase gene expression was not significantly altered by probucol treatment in either missense or liver-conditional *Pdss2* knockout mice when analysed by expression microarray profiling of liver (Supporting information File 8).

 © 2011 EMBO Molecular Medicine 

Probucol's ability to prevent renal disease in this model highlights the question of what aspect of CoQ function underlies the etiology of glomerular disease in *Pdss2* mutants having primary CoQ deficiency. It does not appear likely that their renal disease results solely from decreased electron transport capacity in kidney (Peng et al, 2008). Although probucol supplementation clearly increased tissue CoQ content (Fig 6), it did not appear to improve mitochondrial respiratory capacity (Supporting information File 6). Nor does severely diminished RC capacity necessarily cause renal disease in many forms of primary mitochondrial disease.

Antioxidant properties attributed to probucol appear related to its sulfur atoms more so than its phenol rings (Wu et al, 2006). Resolution of renal disease with probucol, therefore, makes increased oxidative stress in the setting of primary CoQ deficiency an attractive candidate to explain the pathophysiologic mechanism of *Pdss2*-related renal disease. Oxidative stress has also been linked to other forms of primary renal glomerular disease that have diverse etiologies including infection, altered immune responses and altered lipid metabolism (Mayrhofer et al, 2009). However, we were unable to demonstrate evidence of increased oxidative stress, oxidative damage or major oxidant scavenging response in either liver or kidney mitochondria isolated from *Pdss2* mutant animals. Rather, aconitase activity was significantly increased by 15% only following probucol treatment (Fig 3A). In addition, long-term treatment with only vitamin E, another lipophilic antioxidant, did not substantially ameliorate renal disease in B6.*Pdss2*$^{kd/kd}$ mutant mice. Finally, no significant expression alterations were seen in either individual antioxidant scavenging genes or at the level of concordant antioxidant pathways in *Pdss2* missense or liver-conditional knockout mutants supplemented long-term with probucol (Supporting information File 7). Nonetheless, it is well recognized that gene expression changes are not necessarily indicative of cellular antioxidant response. It remains possible that the endogenous boost in tissue CoQ content elicited by probucol may function as a crucial antioxidant in podocyte cellular membranes. Analysis of a fibroblast cell line from the sole human patient reported to be affected with an autosomal recessive *Pdss2*-based disease (Lopez et al, 2006) identified nearly 90% $CoQ_{10}$ deficiency and impaired ATP synthetic capability, but similarly as observed in the *Pdss2* mutant mice, found no sign of increased oxidant stress as assessed by relative oxidant species production and antioxidant defense markers (Quinzii et al, 2008).

Inflammation may play a pathogenic role in *Pdss2*-related nephritis, as probucol has been previously shown to reduce mononuclear cell adhesion to endothelium *in vivo* as well as to inhibit macrophage infiltration. Indeed, we have previously observed substantial inflammatory infiltrates in kidneys of *B6.Pdss2*$^{kd/kd}$ mutants and rearing animals in germ-free conditions substantially mitigates renal disease (Hallman et al, 2006). We also found many immune pathways to have significantly upregulated expression in livers of *Pdss2* mutant mice, alterations that were largely reversed with probucol therapy (Supporting information File 5).

Probucol's well-described effects on lipid metabolism, which include reduction of LDL and HDL levels (Stocker, 2009), prompted us to investigate whether altered lipid metabolism that occurs in the setting of *Pdss2*-related CoQ deficiency correlates with their renal disease. Expression profiling in *Pdss2* missense mutant liver demonstrates these animals do have aberrant lipid metabolism, involving upregulation of lipid biosynthesis and downregulation of fatty acid oxidation (Fig 3 and Supporting information File 10). Plasma lipid abnormalities have also been previously observed to develop with age in both missense and liver-conditional knockout *Pdss2* mutants (Peng et al, 2008), and here we report that significant hypercholesterolemia occurs in podocyte-conditional *Pdss2* knockouts (Table 3). Our data show that both plasma lipids (Table 3) and membrane phosphoplipids in liver (Supporting information File 2) are significantly decreased by probucol therapy. Thus, it is possible that the dramatic prevention of renal disease by probucol supplementation may relate to its role in reversing the lipid abnormalities caused by *Pdss2* deficiency. Indeed, a combination of altered lipid metabolism and oxidative stress was recently shown to underlie puromysin aminonucleoside nephrosis. Downregulation of enzymes involved in antioxidant pathways and fatty acid oxidation was detected at the protein level in cultured podocytes from puromycin aminonucleoside-treated animals (Mayrhofer et al, 2009), similar to what we observed at the expression level for fatty acid oxidation in *Pdss2* mutant mice. However, we found renal disease and cholesterol levels were both unaltered when *Pdss2* mutants were treated long-term with a classic anti-hyperlipidemic agent that inhibits HMG-CoA reductase, Simvastatin. Furthermore, efficient anti-hyperlipidemic activity of probucol in mice without Pdss2 activity within renal glomerular podocytes was insufficient to rescue their severe nephritis. Thus, the mechanism(s) by which probucol prevents renal disease in missense mutants with reduced or no Pdss2 activity within podocytes (Peng et al, 2008) are likely not fully dependent on the drug's hypolipidemic effects.

Finally, we show here that the redox state of CoQ is altered in liver of older *Pdss2*$^{kd/kd}$ mice (Fig 6). Several reports have indicated that $CoQH_2$/CoQ redox status may decrease in various disease states (Kontush et al, 1997; Lim et al, 2006; Mabuchi et al, 2005; Vasta et al, 2011; Wada et al, 2007). Such differences were not noted in our prior analyses of tissue CoQ levels in 180-day-old *Pdss2*$^{kd/kd}$ mice, as we had previously utilized an oxidizing pre-column electrode to oxidize hydroquinones and generate just the quinone species (Peng et al, 2008; Saiki et al, 2008). Thus, it will be important to monitor $CoQH_2$/CoQ ratios as a function of disease progression and response to probucol in future studies of this model of FSGS-like renal disease.

It is interesting to compare *Pdss2* mutants with the other mouse mutant whose kidney disease is ameliorated by probucol, the *Mpv17* knockout mouse. Both models involve primary mitochondrial defects and have severe proteinuria caused by a kidney disease similar to FSGS. Kidney disease occurred before 6 months of age in *Mpv17*$^{-/-}$ mice that were initially identified as a result of insertional inactivation (Weiher et al, 1990). Subsequently, no trace of proteinuria or renal pathology could be observed through at least 12 months of age after backcrossing the transgene to C57BL/6 (Spinazzola et al, 2006), although the renal pathology was again observed when

 © 2011 EMBO Molecular Medicine 

the observation period was extended to 2 years of age (Viscomi et al, 2009). Apparently, the original mixed CFW background enhanced the renal phenotype to a greater extent than did the inbred C57BL/6 background. The *Pdss2*$^{kd/kd}$ genotype has so far been studied only two backgrounds, CBA/CaJ and C57BL/6 (B6), which have appeared equivalent in their effects on the renal phenotype (unpublished observations). The fact that kidney disease in both *Mpv17*$^{-/-}$ and *Pdss2*$^{kd/kd}$ mice can be ameliorated by probucol is puzzling, but may relate to an exquisite sensitivity of glomerular podocytes to mitochondrial dysfunction. Precisely how probucol may remedy the effects of primary mitochondrial deficiency in renal podocytes remains to be determined.

#### Effects of chronic $CoQ_{10}$ supplementation in primary CoQ deficiency

Primary CoQ deficiency in humans has been shown to represent a rare form of mitochondrial RC disease that has four major clinical presentations, which are often but not universally ameliorated by $CoQ_{10}$ supplementation (Quinzii et al, 2007). As mice and humans differ in their major CoQ isoform ($CoQ_9$ and $CoQ_{10}$, respectively), it remains possible that the failure of high-dose $CoQ_{10}$ supplementation to prevent or cause sustained improvement of disease manifestations in *Pdss2* mutant mice may relate to the minor $CoQ_{10}$ isoform we supplied. It may also relate to relatively low tissue bioavailability of the formulation used. While $CoQ_{10}$ is generally a first-line supplement for all forms of human RC disease (Parikh et al, 2009), little *in vivo* evidence either supports or refutes its use despite concerns that $CoQ_{10}$ plays an important role as both an antioxidant and pro-oxidant (Haas, 2007; Linnane et al, 2007). This study provides evidence that chronic high-dose $CoQ_{10}$ supplementation of *Pdss2* mutant mice in equivalent doses to that provided to many human patients does induce antioxidant defenses, as assessed by both activity and relative expression assays of the prime mitochondrial antioxidant defense enzyme, MnSOD (Fig 2). Aconitase activity as a marker of oxidative stress (Fig 2) and qualitative analysis of 4-HNE-based mitochondrial lipid peroxidation (Supporting information File 3) were unchanged in both untreated and $CoQ_{10}$-treated mutant mice relative to age-matched controls. Future study will be required to determine whether increased oxidant scavenging capacity ultimately represents a pro-oxidant or antioxidant effect.

#### Metabolic pathway expression profiling as a tool to survey cellular consequences and treatment response in mitochondrial disease

Applying metabolic pathway clustering to global transcriptional profiling presents a powerful opportunity to reduce the complexity of describing metabolic regulation in mitochondrial disease. We previously reported that mice harbouring conditional homozygous hepatic deletion of *Pdss2* have altered intermediary metabolism characterized by amino acid abnormalities and upregulated expression of 15 basic intermediary metabolic and cellular defense pathways (Peng et al, 2008). Here, we show that while these mice manifest mild but significant hyperglycemia, they do not have obvious abnormalities of liver transaminase (ALT) or synthetic function (urea; Supporting information File 4). We further now report that significantly altered hepatic expression of many metabolic pathways also occurs in spontaneous *Pdss2* missense mutants (Fig 3). We conclude that while the transcriptional signatures of these two mutant types are in many ways distinct, several metabolic pathways are similarly upregulated in both missense and knockout *Pdss2* mutants, including OXPHOS, protein processing, immune pathways and nucleotide metabolism. Future study of intermediary metabolic flux alterations by isotopic profiling in both mutant types will be necessary to dissect whether the direction, rather than mere occurrence, of transcriptional alterations in multiple metabolic pathways is indicative of a specific adaptive response to primary mitochondrial dysfunction. Interestingly, the direction of altered expression for multiple intermediary metabolic pathways directly correlated in both mutant types with the direction of altered *PPAR* pathway signaling, and in particular, with *PPAR-γ* expression (Figs 3 and 5).

Probucol supplementation largely reversed transcriptional alterations not only globally across many aspects of intermediary metabolism but also in *PPAR* pathway signaling (Fig 4 and Supporting information Files 5 and 11). Altered expression of key *PPAR* pathway transcription factors expressed in liver was confirmed by quantitative RT-PCR, showing that *PPAR-γ* was upregulated in the liver-conditional knockout mice while both *PPAR-α* and *PPAR-γ* were downregulated in missense mutants, all of which normalized on probucol therapy (Fig 5). While high-dose supplemental $CoQ_{10}$ therapy normalized expression of several pathways in *Pdss2* missense mutants, its effect was less pronounced than that of probucol (Fig 4). Furthermore, $CoQ_{10}$ supplementation neither normalized *PPAR* signalling (Fig 5) nor prevented kidney disease (Table 1). *PPAR* pathway activation by oral bezafibrate therapy has also been demonstrated to improve a myopathy caused by mitochondrial complex IV dysfunction in a *COX10* mutant mouse (Wenz et al, 2008). Our findings suggest that *PPAR* pathway signaling alterations may orchestrate the global metabolic consequences of primary mitochondrial RC dysfunction. It is possible that probucol enhances *PPAR* signaling in *Pdss2* missense mice, which then induces CoQ content. Indeed, there is considerable evidence for *PPAR*-induction of CoQ biosynthesis in response to peroxisome proliferators (Turunen et al, 2004). Alternatively, the increase in CoQ (and $CoQH_2$) levels in response to probucol may be the switch that elicits *PPAR* signalling. *PPAR* induction in response to $CoQ_{10}H_2$ supplementation has been reported in *SAMP1* mice (Schmelzer et al, 2010).

Metabolic pathway profiling thus appears to offer a sensitive means to elucidate mechanisms and to monitor treatment effects in primary mitochondrial disease. Pathway expression profiling in individual human mitochondrial disease patients who have widely different genetic causes for their disease may offer a route to effectively tailor clinical treatment regimens. In particular, it would be of interest to discern whether the global metabolic and transcriptional sequelae of RC dysfunction we observed in the mouse model of *Pdss2* deficiency (Peng et al, 2008) are evident in the sole reported *Pdss2* patient cell line, and whether probucol

 © 2011 EMBO Molecular Medicine 

## The paper explained

### PROBLEM:

Mitochondrial RC defects are inherited diseases for which effective therapy has remained elusive. Simply providing a missing metabolite frequently has no clinical efficacy even when the specific enzymatic defect is well defined. For example, while some children born with defective CoQ biosynthesis respond to $CoQ_{10}$ supplementation, many do not. We study a mouse model of a fatal renal glomerular disease caused by primary CoQ deficiency. These *Pdss2* mutant mice show only limited therapeutic response to lifelong $CoQ_{10}$ supplementation. During our investigation of other potential therapeutic agents, we have discovered that probuocol, a lipid-soluble antioxidant drug with lipid-lowering and anti-inflammatory activities of uncertain mechanism previously used to treat hyperlipidemia, has considerably greater therapeutic efficacy for the renal and metabolic disease sequelae in these mice than $CoQ_{10}$ supplementation. Understanding the basis for the effectiveness of this drug could provide a valuable lead towards designing novel therapies for human mitochondrial diseases.

### RESULTS:

We demonstrate that long-term oral administration of probucol prevented an otherwise lethal glomerulopathy in B6.*Pdss2*$^{kd/kd}$ mice through at least 6 months of life. By contrast, long-term prophylactic $CoQ_{10}$ supplementation was comparatively less effective for renal disease prevention, despite its induction of mitochondrial oxidant scavenging capacity. Short-term administration of probucol limited to just 2–3 weeks before the onset of nephritis also prevented renal disease, whereas, short-term supplementation with $CoQ_{10}$ had no effect in males and only a modest therapeutic effect in female mutant mice. Remarkably, probucol treatment also significantly mitigated renal disease when fed for only 2 weeks to already symptomatic B6.*Pdss2*$^{kd/kd}$ animals. Mechanistic investigations demonstrated that despite a modest induction of oxidative stress, probucol administration substantially prevented renal disease and largely reversed global metabolic pathway transcriptional abnormalities. Probucol's beneficial effects on the renal and metabolic manifestations of *Pdss2* disease appeared to be independent of its hypolipidemic properties. However, when administered from birth through 6 months of life, probucol significantly increased both the hydroquinone ($CoQ_9H_2$ and $CoQ_{10}H_2$) and total $CoQ_9$ and $CoQ_{10}$ content in liver. Furthermore, treating symptomatic animals with probucol for only 2 weeks beginning at day of life 100 significantly increased $CoQ_9$ levels in mutant kidney. Finally, we observed that the mitochondrial RC dysfunction caused by primary CoQ deficiency in *Pdss2* mutant mice elicited aberrant expression of many intermediary metabolic pathways and *PPAR* transcription factor pathway signaling, which were all significantly rescued by probucol treatment.

### IMPACT:

These data suggest that decreased $CoQ_9$ content and altered *PPAR* pathway signaling may orchestrate the glomerular and global metabolic consequences of primary CoQ deficiency, respectively. Remarkably, these renal and metabolic sequelae of primary mitochondrial RC dysfunction were both preventable and treatable with oral probucol therapy. Thus, targeting the *de novo* supply of CoQ may be a more effective therapeutic strategy than supplementing the missing co-factor.

has any discernible modifying effect. Furthermore, elucidation of common pathway alterations across different classes of RC dysfunction may permit the development of pathway-targeted therapies for the difficult to treat class of primary mitochondrial disorders (Parikh et al, 2009).

Probucol is a lipophilic agent with previously reported antioxidant, anti-inflammatory and lipid-lowering properties (Stocker, 2009) that we found to prevent an otherwise lethal renal glomerular disease as well as expression alterations across many domains of intermediary metabolism in a *Pdss2* mutant mouse model of mitochondrial RC disease caused by primary CoQ deficiency. The beneficial effects of probucol exceeded those of supplemental $CoQ_{10}$, both in terms of ameliorating renal disease and increasing tissue CoQ content. Furthermore, probucol treatment reversed albuminuria in B6.*Pdss2*$^{kd/kd}$ missense mutant animals that already manifested renal disease. The renal efficacy of probucol appears to lie in its ability to increase tissue CoQ content, although it is not yet known whether this phenomenon is mediated through enhanced *de novo* synthesis or decreased degradation. Probucol's beneficial effects on the renal and metabolic manifestations of *Pdss2* disease occur despite its modest induction of oxidant stress and appear to be independent of its hypolipidemic effects.

In summary, the data suggest that decreased $CoQ_9$ content and altered *PPAR* pathway signaling orchestrate the glomerular and global metabolic consequences of primary CoQ deficiency, respectively, which are both preventable and treatable with oral probucol therapy. Thus, we conclude that it is more important to induce the *de novo* supply of CoQ in the *Pdss2*$^{kd/kd}$ CoQ deficient animals, than to directly supplement the missing co-factor ($CoQ_{10}$).

## MATERIALS AND METHODS

### B6.*Pdss2*$^{kd/kd}$ missense mutant mice treatment groups

B6.*Pdss2*$^{kd/kd}$ mice were derived by backcrossing a recombinant chromosome derived by positional cloning onto the B6 background (Dell et al, 2000). B6.*Pdss2*$^{kd/kd}$ mice in this report were in the 13th backcross generation. Untreated mice were fed a standard *LabDiet*

 © 2011 EMBO Molecular Medicine 

rodent chow obtained from PMI Nutrition International (Brentwood, MO). Probucol-treated mice were either given the same diet to which 1% w/w probucol was added (Animal Specialties and Provisions, Quakertown, PA), which we estimate resulted in a final daily dosage of approximately 95 mg per kg body weight. The gender, ages and lengths of time that different groups of mice were treated with probucol are shown in Tables 1 and 2, and Supporting information File 12. For the mice in Table 2, urine albumin was measured at 100 days of age and only those with significant albuminuria (>1 mg in 24 h) were treated with probucol. Mice fed diets supplemented with probucol from birth (Fig 6) were raised by mothers fed probucol supplemented diets 1% w/w until weaning, and, thereafter, fed a probucol supplemented 1% w/w chow diet. $CoQ_{10}$-treated mice received a standard chow with $CoQ_{10}$ (LiQsorb; Tishcon Corp., Westbury, NY) added to their drinking water from either birth, weaning or day of life 100, as specified in Table 1. The amount of $CoQ_{10}$ added was 1 mg/ml, which we estimate resulted in a final daily dosage of approximately 400 mg $CoQ_{10}$ per kg body weight. Vitamin E was provided from weaning in standard chow at a dose of 300 IU per kg chow (Animal Specialties and Provisions), which we estimate resulted in a final daily dosage of approximately 29 IU per kg body weight. Simvastatin treatment consisted of feeding mice chow with 0.1% w/w Simvastatin from weaning, which we estimate resulted in a final daily dosage of approximately 100 mg per kg body weight. All studies were carried out in accordance with NIH guidelines and approved by the Institutional Animal Care and Use Committees of The University of Pennsylvania and The Children's Hospital of Philadelphia.

#### Tissue-specific conditional *Pdss2* knockout mice treatment groups

Liver-conditional and podocyte-conditional *Pdss2* knockout mice were generated as previously described (Peng et al, 2008). Briefly, for liver-conditional knockout the mutation was targeted to hepatocytes utilizing mice homozygous for the floxed gene (B6.*Pdss2*$^{lox P/lox P}$) crossed with partners that expressed cre under the control of an *albumin/cre* promoter (B6.Cg-Tg(*Alb-cre*)21 Mgn/J (*Alb/cre*)) obtained from The Jackson Laboratory. Two B6.*Alb/cre,Pdss2*$^{lox P/lox P}$ mice (one male and one female) were fed standard mouse chow supplemented with probucol (1% w/w) from weaning beginning on day of life 44 (Zhang et al, 2010). Untreated controls consisted of two B6.*Alb/cre,Pdss2*$^{lox P/lox}$ mice (one male and one female) fed standard mouse chow. Animals were sacrificed and liver specimens flash frozen for RNA extraction at 140–169-day old. Podocyte-specific knockouts (B6.*Podocin/cre,Pdss2*$^{lox P/lox P}$) were obtained by crossing mice homozygous for the floxed gene with partners that expressed *cre* under the control of the *Podocin* promoter (Moeller et al, 2000). Probucol and $CoQ_{10}$ supplementation were provided to podocyte-conditional knockouts from birth in the same fashion as described above for missense mutants. All procedures were carried out in accordance with NIH guidelines were approved by the Institutional Animal Care and Use Committee of both The University of Pennsylvania and The Children's Hospital of Philadelphia.

#### Kidney disease evaluation

B6.*Pdss2*$^{kd/kd}$ mice were placed in metabolic cages without food for 24 h with 0.45% NaCl and 2.5% sucrose in the drinking water. Total urine volumes were measured and aliquots of urine were tested for albumin concentration by enzyme-linked immunosorbent assay (ELISA). Upon termination of each experiment, mice were euthanized and their kidneys were fixed and stained with haematoxylin and eosin. Histologic sections were scored blindly according to the following scale: 0 = no tubular dilatation and no mononuclear cell infiltrates; 1 = small focal areas of cellular infiltration and tubular dilatation involving less than 10% of the cortex; 2 = involvement of up to 25% of the cortex; 3 = involvement of up to 50% of the cortex; and 4 = extensive damage involving more than 75% of the cortex.

#### Mechanistic investigations in *Pdss2* mouse tissues

Detailed methods of all biochemical and genomic assays reported in this manuscript are described in Supporting information File 13.

## Author contributions

MJF and DLG conceived the study design; MP conducted genotyping and urine albumin assays; RK and JSM assisted with histologic analyses; LXX, JYC and BM wrote methods for and performed and analysed tissue CoQ levels; EP wrote methods for and performed qRT-PCR analyses, along with EO and MPEP wrote the methods for, and along with MP performed the MnSOD enzyme activity assay; EP wrote the methods for and performed both 4-HNE Western blot analysis and high-resolution polarography; ENO wrote the methods for and performed aconitase enzyme activity analysis; JO wrote the methods for and prepared liver specimens for $^{31}$P-NMR analysis; ZZ performed and assisted MJF in writing methods for and interpretation of microarray expression pathway analyses; OH and IN wrote the methods for and performed plasma glucose, ammonia and urea analyses; IN assisted with interpretation of lipid NMR data; MJF, DLG, BM and CFC wrote the manuscript.

## Acknowledgements

We are grateful to Meera Rao, MS and Stephen Dingley, BA, for their assistance with RNA isolation and specimen handling; to Eric Rappaport, PhD, Stephen G. Mahoney, BS and Kristen Hunter, BS, for microarray hybridization; to Roger C. Helgeson, PhD, for synthesis of diethoxy-Q10; to Suzanne Wherli, PhD, for performance of $^{31}$P-NMR analysis; to Harry Ischiropoulos, PhD, for providing generous access to imaging and spectrofluorimetry equipment; and to our Anonymous Reviewers for their helpful suggestions. We thank the members of the Morphology Core for Molecular Studies in Digestive and Liver Diseases at The University of Pennsylvania for histologic preparations. This work was supported by the National Institutes of Health [R01-DK55852 to DLG, K08-DK073545 to MJF, R01-DK53761 to IN, GM45952 to CFC, and DK050306]. The content is solely the responsibility of the authors and does not necessarily represent the official views of the National Institutes of Health.

Supporting information is available at EMBO Molecular Medicine online.

The authors declare that they have no conflict of interest.

 © 2011 EMBO Molecular Medicine 

## For more information

Online Mendelian Inheritance in Man (OMIM)

Prenyl Diphosphate Synthase, Subunit 2
http://www.ncbi.nlm.nih.gov/omim/610564

Mitochondrial Medicine Society
http://www.mitosoc.org/

Mitochondria Research Society
http://www.mitoresearch.org/

The United Mitochondrial Disease Foundation
http://www.umdf.org/

## References

Barros MH, Johnson A, Gin P, Marbois BN, Clarke CF, Tzagoloff A (2005) The *Saccharomyces cerevisiae* COQ10 gene encodes a START domain protein required for function of coenzyme Q in respiration. J Biol Chem 280: 42627-42635

Bergmeyer HU, Bernt E, Schidt F, Stork H (1974) D-Glucose. In: *Methods of Enzymatic Analysis*, Bergmeyer HU, (ed), New York, Academic Press: pp 1198-1201.

Binder CJ, Weiher H, Exner M, Kerjaschki D (1999) Glomerular overproduction of oxygen radicals in Mpv17 gene-inactivated mice causes podocyte foot process flattening and proteinuria: a model of steroid-resistant nephrosis sensitive to radical scavenger therapy. Am J Pathol 154: 1067-1075

Catala A (2009) Lipid peroxidation of membrane phospholipids generates hydroxy-alkenals and oxidized phospholipids active in physiological and/or pathological conditions. Chem Phys Lipids 157: 1-11

Dai M, Wang P, Boyd AD, Kostov G, Athey B, Jones EG, Bunney WE, Myers RM, Speed TP, Akil H, *et al* (2005) Evolving gene/transcript definitions significantly alter the interpretation of GeneChip data. Nucleic Acids Res 33: e175

Dell KM, Li YX, Peng M, Neilson EG, Gasser DL (2000) Localization of the mouse kidney disease (kd) gene to a YAC/BAC contig on Chromosome 10. Mamm Genome 11: 967-971

Dingley S, Polyak E, Lightfoot R, Ostrovsky J, Rao M, Greco T, Ischiropoulos H, Falk MJ (2009) Mitochondrial respiratory chain dysfunction variably increases oxidant stress in *Caenorhabditis elegans*. Mitochondrion 10: 125-136

Edlund PO (1988) Determination of coenzyme Q10, alpha-tocopherol and cholesterol in biological samples by coupled-column liquid chromatography with coulometric and ultraviolet detection. J Chromatogr 425: 87-97

Falk MJ, Zhang Z, Rosenjack JR, Nissim I, Daikhin E, Sedensky MM, Yudkoff M, Morgan PG (2008) Metabolic pathway profiling of mitochondrial respiratory chain mutants in *C. elegans*. Mol Genet Metab 93: 388-397

Farina M, Campos F, Vendrell I, Berenguer J, Barzi M, Pons S, Sunol C (2009) Probucol increases glutathione peroxidase-1 activity and displays long-lasting protection against methylmercury toxicity in cerebellar granule cells. Toxicol Sci 112: 416-426

Feldman PL, Lambert MH, Henke BR (2008) PPAR modulators and PPAR pan agonists for metabolic diseases: The next generation of drugs targeting peroxisome proliferator-activated receptors? Curr Top Med Chem 8: 728-749

Gardner PR (2002) Aconitase: sensitive target and measure of superoxide. Methods Enzymol 349: 9-23

Geyer JW, Dabich D (1971) Rapid method for determination of arginase activity in tissue homogenates. Anal Biochem 39: 412-417

Haas RH (2007) The evidence basis for coenzyme Q therapy in oxidative phosphorylation disease. Mitochondrion 7: S136-S145

Haas RH, Parikh S, Falk MJ, Saneto RP, Wolf NI, Darin N, Wong LJ, Cohen BH, Naviaux RK (2008) The in-depth evaluation of suspected mitochondrial disease. Mol Genet Metab 94: 16-37

Hallman TM, Peng M, Meade R, Hancock WW, Madaio MP, Gasser DL (2006) The mitochondrial and kidney disease phenotypes of *kd/kd* mice under germfree conditions. J Autoimmun 26: 1-6

Hiltunen JK, Autio KJ, Schonauer MS, Kursu VA, Dieckmann CL, Kastaniotis AJ (2010) Mitochondrial fatty acid synthesis and respiration. Biochim Biophys Acta 1797: 1195-1202

Irizarry RA, Bolstad BM, Collin F, Cope LM, Hobbs B, Speed TP (2003) Summaries of Affymetrix GeneChip probe level data. Nucleic Acids Res 31: e15

Ivanovski O, Szumilak D, Nguyen-Khoa T, Nikolov IG, Joki N, Mothu N, Maizel J, Westenfeld R, Ketteler M, Lacour B, *et al* (2008) Effect of simvastatin in apolipoprotein E deficient mice with surgically induced chronic renal failure. J Urol 179: 1631-1636

Kontush A, Reich A, Baum K, Spranger T, Finckh B, Kohlschutter A, Beisiegel U (1997) Plasma ubiquinol-10 is decreased in patients with hyperlipidaemia. Atherosclerosis 129: 119-126

Lemieux H, Gneiger E (2008) Preparation of permeabilized muscle fibers for diagnosis of mitochondrial respiratory function. Mitochondrial Physiol Netw 12.22: 1-4

Lemieux H, Votion M.-D, Gneiger E (2009) Mitochondrial respiration in permeabilized fibers: needle Biopsies from horse skeletal muscle. Mitochondrial Physiol Netw 12.23: 1-4

Lim SC, Tan HH, Goh SK, Subramaniam T, Sum CF, Tan IK, Lee BL, Ong CN (2006) Oxidative burden in prediabetic and diabetic individuals: evidence from plasma coenzyme Q(10). Diabet Med 23: 1344-1349

Linnane AW, Eastwood H (2004) Cellular redox poise modulation; the role of coenzyme Q10, gene and metabolic regulation. Mitochondrion 4: 779-789

Linnane AW, Kios M, Vitetta L (2007) Coenzyme Q(10)—its role as a prooxidant in the formation of superoxide anion/hydrogen peroxide and the regulation of the metabolome. Mitochondrion 7: S51-S61

Lopez LC, Schuelke M, Quinzii CM, Kanki T, Rodenburg RJ, Naini A, Dimauro S, Hirano M (2006) Leigh syndrome with nephropathy and CoQ10 deficiency due to decaprenyl diphosphate synthase subunit 2 (PDSS2) mutations. Am J Hum Genet 79: 1125-1129

Lyon MF, Hulse EV (1971) An inherited kidney disease of mice resembling human nephronophthisis. J Med Genet 8: 41-48

Mabuchi H, Higashikata T, Kawashiri M, Katsuda S, Mizuno M, Nohara A, Inazu A, Koizumi J, Kobayashi J (2005) Reduction of serum ubiquinol-10 and ubiquinone-10 levels by atorvastatin in hypercholesterolemic patients. J Atheroscler Thromb 12: 111-119

Macmillan-Crow LA, Cruthirds DL (2001) Invited review: manganese superoxide dismutase in disease. Free Radic Res 34: 325-336

Madaio MP, Ahima RS, Meade R, Rader DJ, Mendoza A, Peng M, Tomaszewski JE, Hancock WW, Gasser DL (2005) Glomerular and tubular epithelial defects in *kd/kd* mice lead to progressive renal failure. Am J Nephrol 25: 604-610

Marbois B, Xie LX, Choi S, Hirano K, Hyman K, Clarke CF (2010) Para-aminobenzoic acid is a precursor in coenzyme Q6 biosynthesis in *Saccharomyces cerevisiae*. J Biol Chem 285: 27827-27838

Mayrhofer C, Krieger S, Huttary N, Chang MW, Grillari J, Allmaier G, Kerjaschki D (2009) Alterations in fatty acid utilization and an impaired antioxidant defense mechanism are early events in podocyte injury: a proteomic analysis. Am J Pathol 174: 1191-1202

McCord JM, Fridovich I (1969) Superoxide dismutase. An enzymic function for erythrocuprein (hemocuprein). J Biol Chem 244: 6049-6055

Moeller MJ, Kovari IA, Holzman LB (2000) Evaluation of a new tool for exploring podocyte biology: mouse Nphs1 5′ flanking region drives LacZ expression in podocytes. J Am Soc Nephrol 11: 2306-2314

Nissim I, Weinberg JM (1996) Glycine attenuates Fanconi syndrome induced by maleate or ifosfamide in rats. Kidney Int 49: 684-695

Nissim I, Luhovyy B, Horyn O, Daikhin Y, Yudkoff M (2005) The role of mitochondrially bound arginase in the regulation of urea synthesis: studies with [U-15N4]arginine, isolated mitochondria, and perfused rat liver. J Biol Chem 280: 17715-17724

Parikh S, Saneto R, Falk MJ, Anselm I, Cohen BH, Haas R, Medicine Society TM (2009) A modern approach to the treatment of mitochondrial disease. Curr Treat Options Neurol 11: 414-430

Paterson JR, Rumley AG, Oldroyd KG, Tait GW, Smellie WS, Packard CJ, Shepherd J, Lorimer AR (1992) Probucol reduces plasma lipid peroxides in man. Atherosclerosis 97: 63-66

Peng M, Jarett L, Meade R, Madaio MP, Hancock WW, George AL, Jr., Neilson EG, Gasser DL (2004) Mutant prenyltransferase-like mitochondrial protein (PLMP) and mitochondrial abnormalities in *kd/kd* mice. Kidney Int 66: 20-28

Peng M, Falk MJ, Haase VH, King R, Polyak E, Selak M, Yudkoff M, Hancock WW, Meade R, Saiki R, *et al* (2008) Primary coenzyme Q deficiency in *Pdss2* mutant mice causes isolated renal disease. PLoS Genet 4: e1000061

Quinzii CM, Hirano M (2010) Coenzyme Q and mitochondrial disease. Dev Disabil Res Rev 16: 183-188

Quinzii CM, DiMauro S, Hirano M (2007) Human coenzyme Q10 deficiency. Neurochem Res 32: 723-727

Quinzii CM, Lopez LC, Von-Moltke J, Naini A, Krishna S, Schuelke M, Salviati L, Navas P, DiMauro S, Hirano M (2008) Respiratory chain dysfunction and oxidative stress correlate with severity of primary CoQ10 deficiency. FASEB J 22: 1874-1885

Rose IA, O'Connell EL (1967) Mechanism of aconitase action. I. The hydrogen transfer reaction. J Biol Chem 242: 1870-1879

Saiki R, Nagata A, Kainou T, Matsuda H, Kawamukai M (2005) Characterization of solanesyl and decaprenyl diphosphate synthases in mice and humans. FEBS J 272: 5606-5622

Saiki R, Lunceford AL, Shi Y, Marbois B, King R, Pachuski J, Kawamukai M, Gasser DL, Clarke CF (2008) Coenzyme Q10 supplementation rescues renal disease in Pdss2*kd/kd* mice with mutations in prenyl diphosphate synthase subunit 2. Am J Physiol Renal Physiol 295: F1535-F1544

Schlame M, Ren M (2009) The role of cardiolipin in the structural organization of mitochondrial membranes. Biochim Biophys Acta 1788: 2080-2083

Schmelzer C, Kubo H, Mori M, Sawashita J, Kitano M, Hosoe K, Boomgaarden I, Doring F, Higuchi K (2010) Supplementation with the reduced form of Coenzyme Q10 decelerates phenotypic characteristics of senescence and induces a peroxisome proliferator-activated receptor-alpha gene expression signature in SAMP1 mice. Mol Nutr Food Res 54: 805-815

Spinazzola A, Viscomi C, Fernandez-Vizarra E, Carrara F, D'Adamo P, Calvo S, Marsano RM, Donnini C, Weiher H, Strisciuglio P, *et al* (2006) MPV17 encodes an inner mitochondrial membrane protein and is mutated in infantile hepatic mitochondrial DNA depletion. Nat Genet 38: 570-575

Stocker R (2009) Molecular mechanisms underlying the antiatherosclerotic and antidiabetic effects of probucol, succinobucol, and other probucol analogues. Curr Opin Lipidol 20: 227-235

Tardif JC, Cote G, Lesperance J, Bourassa M, Lambert J, Doucet S, Bilodeau L, Nattel S, de Guise P (1997) Probucol and multivitamins in the prevention of restenosis after coronary angioplasty. Multivitamins and Probucol Study Group. N Engl J Med 337: 365-372

Turunen M, Olsson J, Dallner G (2004) Metabolism and function of coenzyme Q. Biochim Biophys Acta 1660: 171-199

Vasta V, Sedensky M, Morgan P, Hahn SH (2011) Altered redox status of coenzyme Q9 reflects mitochondrial electron transport chain deficiencies in *Caenorhabditis elegans*. Mitochondrion 11: 136-138

Viscomi C, Spinazzola A, Maggioni M, Fernandez-Vizarra E, Massa V, Pagano C, Vettor R, Mora M, Zeviani M (2009) Early-onset liver mtDNA depletion and late-onset proteinuric nephropathy in Mpv17 knockout mice. Hum Mol Genet 18: 12-26

Wada H, Goto H, Hagiwara S, Yamamoto Y (2007) Redox status of coenzyme Q10 is associated with chronological age. J Am Geriatr Soc 55: 1141-1142

Weiher H, Noda T, Gray DA, Sharpe AH, Jaenisch R (1990) Transgenic mouse model of kidney disease: insertional inactivation of ubiquitously expressed gene leads to nephrotic syndrome. Cell 62: 425-434

Wenz T, Diaz F, Spiegelman BM, Moraes CT (2008) Activation of the PPAR/PGC-1alpha pathway prevents a bioenergetic deficit and effectively improves a mitochondrial myopathy phenotype. Cell Metab 8: 249-256

Wu BJ, Kathir K, Witting PK, Beck K, Choy K, Li C, Croft KD, Mori TA, Tanous D, Adams MR, *et al* (2006) Antioxidants protect from atherosclerosis by a heme oxygenase-1 pathway that is independent of free radical scavenging. J Exp Med 203: 1117-1127.

Yin L, Li GP, Liu T, Liu HM, Chen X, He M, Zheng XT, Liu EZ, Zhou LJ (2009) Role of probucol in preventing contrast induced acute kidney injury after coronary interventional procedure: a randomized trial. Zhonghua Xin Xue Guan Bing Za Zhi 37: 385-388

Zampol MA, Busso C, Gomes F, Ferreira-Junior JR, Tzagoloff A, Barros MH (2010) Over-expression of COQ10 in *Saccharomyces cerevisiae* inhibits mitochondrial respiration. Biochem Biophys Res Commun 402: 82-87

Zhang Z, Gasser DL, Rappaport EF, Falk MJ (2010) Cross-platform expression microarray performance in a mouse model of mitochondrial disease therapy. Mol Genet Metab 99: 309-318

Zhou SX, Zhou Y, Zhang YL, Lei J, Wang JF (2009) Antioxidant probucol attenuates myocardial oxidative stress and collagen expressions in post-myocardial infarction rats. J Cardiovasc Pharmacol 54: 154-162

 © 2011 EMBO Molecular Medicine 

*Am J Physiol Renal Physiol* 305: F1228–F1238, 2013.
First published August 7, 2013; doi:10.1152/ajprenal.00143.2013.

# Focal segmental glomerulosclerosis is associated with a *PDSS2* haplotype and, independently, with a decreased content of coenzyme $Q_{10}$

**David L. Gasser,[1] Cheryl A. Winkler,[2] Min Peng,[1] Ping An,[2] Louise M. McKenzie,[2] Gregory D. Kirk,[3] Yuchen Shi,[4] Letian X. Xie,[4] Beth N. Marbois,[4] Catherine F. Clarke,[4] and Jeffrey B. Kopp[5]**

[1]*Department of Genetics, University of Pennsylvania School of Medicine, Philadelphia, Pennsylvania;* [2]*Basic Research Laboratory, Center for Cancer Research, SAIC-Frederick, Frederick National Laboratory for Cancer Research, Frederick, Maryland;* [3]*Department of Epidemiology, Johns Hopkins School of Public Health, Baltimore, Maryland;* [4]*Department of Chemistry and Biochemistry and Molecular Biology Institute, University of California Los Angeles, Los Angeles, California; and* [5]*Kidney Disease Section, National Institute of Diabetes and Digestive and Kidney Diseases, National Institutes of Health, Bethesda, Maryland*

Submitted 8 March 2013; accepted in final form 5 August 2013

**Gasser DL, Winkler CA, Peng M, An P, McKenzie LM, Kirk GD, Shi Y, Xie LX, Marbois BN, Clarke CF, Kopp JB.** Focal segmental glomerulosclerosis is associated with a *PDSS2* haplotype and, independently, with a decreased content of coenzyme $Q_{10}$. *Am J Physiol Renal Physiol* 305: F1228–F1238, 2013. First published August 7, 2013; doi:10.1152/ajprenal.00143.2013.—Focal segmental glomerulosclerosis (FSGS) and collapsing glomerulopathy are common causes of nephrotic syndrome. Variants in >20 genes, including genes critical for mitochondrial function, have been associated with these podocyte diseases. One such gene, *PDSS2*, is required for synthesis of the decaprenyl tail of coenzyme $Q_{10}$ ($Q_{10}$) in humans. The mouse gene *Pdss2* is mutated in the *kd/kd* mouse model of collapsing glomerulopathy. We examined the hypothesis that human *PDSS2* polymorphisms are associated with podocyte diseases. We genotyped 377 patients with primary FSGS or collapsing glomerulopathy, together with 900 controls, for 9 single-nucleotide polymorphisms in the *PDSS2* gene in a case-control study. Subjects included 247 African American (AA) and 130 European American (EA) patients and 641 AA and 259 EA controls. Among EAs, a pair of proxy SNPs was significantly associated with podocyte disease, and patients homozygous for one *PDSS2* haplotype had a strongly increased risk for podocyte disease. By contrast, the distribution of *PDSS2* genotypes and haplotypes was similar in AA patients and controls. Thus a *PDSS2* haplotype, which has a frequency of 13% in the EA control population and a homozygote frequency of 1.2%, is associated with a significantly increased risk for FSGS and collapsing glomerulopathy in EAs. Lymphoblastoid cell lines from FSGS patients had significantly less $Q_{10}$ than cell lines from controls; contrary to expectation, this finding was independent of *PDSS2* haplotype. These results suggest that FSGS patients have $Q_{10}$ deficiency and that this deficiency is manifested in patient-derived lymphoblastoid cell lines.

nephrotic syndrome; collapsing glomerulopathy; focal segmental glomerulosclerosis; mitochondria; ubiquinone

FOCAL SEGMENTAL GLOMERULOSCLEROSIS (FSGS) comprises several distinct pathological entities that start with injury to the glomerular podocytes and progress to loss of these normally postmitotic cells and, eventually, to focal and segmental glomerular scarring. FSGS has become the leading cause of idiopathic nephrotic syndrome in adults and is responsible for ~6% of cases of end-stage kidney disease in children (24).

Address for reprint requests and other correspondence: D. L. Gasser, Dept. of Genetics, Univ. of Pennsylvania School of Medicine, 415 Curie Blvd., Philadelphia, PA 19104 (e-mail: gasserd@mail.med.upenn.edu).

Approximately 50% of patients with FSGS reach end-stage kidney disease within 10 yr of diagnosis, which represents the worst prognosis among common glomerular diseases. One recent classification recognizes three major variants: genetic FSGS, primary FSGS, and adaptive FSGS (3). Genetic mutations that have been associated with familial FSGS have been identified in the genes encoding nephrin (*NPHS1*), podocin (*NPHS2*), α-actinin-4 (*ACTN4*), CD2-associated protein (*CD2AP*), and the *TRPC6* cation channel (41, 63), as well as numerous other genes. Common variants in the adjacent *WT1* and *WIT1* genes, encoding a transcription factor that, when mutated, can cause Wilms' tumor, were associated with idiopathic FSGS in African Americans (AAs). Coding variants in the *APOL1* gene are strongly associated with risk for FSGS, collapsing glomerulopathy associated with HIV infection, and nondiabetic chronic kidney disease in AAs (16, 25). Collapsing glomerulopathy accounts for ~11% of FSGS cases and is characterized by podocyte proliferation and dedifferentiation, which eventually lead to glomerular scarring (55).

There is reason to believe that additional genes that affect susceptibility to FSGS and collapsing glomerulopathy remain to be identified. The *kd/kd* mouse, which originated as a spontaneous mutant and was initially thought to be similar to nephronophthisis (29), is a promising animal model for these types of syndromes. Mutant homozygotes develop a severe tubulointerstitial nephritis (36), but the same phenotype also develops in *Rag-1*$^{-/-}$*kd/kd* mice in the absence of an adaptive immune response (21). By linkage analysis and positional cloning, the *kd* allele was shown to have a missense mutation in a prenyltransferase-like mitochondrial protein that corresponds to a human gene product originally identified as "candidate tumor suppressor protein" (9, 40). This gene is now known to be an ortholog of polyprenyl diphosphate synthase in *Schizosaccharomyces pombe*; it consists of two subunits (Dlp1 and Dps1) that form a heterotetramer with decaprenyl diphosphate synthase activity (46). This heterotetramer catalyzes the synthesis of a polyisoprenoid chain that forms the tail of ubiquinone, which in mice consists predominantly of coenzyme $Q_9$ ($Q_9$) and in humans consists predominantly of coenzyme $Q_{10}$ ($Q_{10}$) (45).

The mutant *kd/kd* mice have immunohistochemical, ultrastructural, and biochemical features of defects that are similar to those seen in collapsing glomerulopathy (2). When associated with certain other mutations, heterozygotes, as well as homozygotes, may manifest glomerular disease (30), and en-

vironmental conditions such as caloric restriction and a germ-free environment affect disease expression (20). A child with encephalomyopathy and nephrotic syndrome who was a compound heterozygote for mutations at the *PDSS2* locus was recently reported (28), and we subsequently demonstrated that *kd/kd* mice have neuromuscular defects (66). We have therefore examined DNA samples from individuals with or without FSGS with regard to single-nucleotide polymorphisms (SNPs) in the human gene that corresponds to *kd*, designated prenyl (decaprenyl) diphosphate synthase subunit 2 (*PDSS2*) by the Human Gene Nomenclature Committee. We have conducted a case-control study to address the hypothesis that particular haplotypes of the *PDSS2* gene are associated with FSGS. B cell lines derived from FSGS patients and controls were prepared and assayed for $Q_{10}$ content. Surprisingly, FSGS was associated with a decreased content of $Q_{10}$, irrespective of *PDSS2* haplotype.

## MATERIALS AND METHODS

*Clinical ascertainment.* Study inclusion criteria included diagnosis of primary FSGS or collapsing glomerulopathy on the basis of a biopsy of the native kidney or within the 1st yr following renal transplant. Since no approach has been proven to ensure consensus in diagnosis of these two podocyte disorders among pathologists, the distinction between primary FSGS and collapsing glomerulopathy cannot be made reliably in this study population: for simplicity, the diagnostic term FSGS is used for all patients. Study exclusion criteria include a diagnosis of adaptive FSGS or medication-associated FSGS. All patients except two had undergone at least one renal biopsy documenting FSGS. Two patients did not have a native kidney biopsy but had a presentation and course compatible with FSGS and then developed FSGS in the renal transplant.

*Demographics of the study population.* DNA samples were obtained from FSGS patients identified at 21 US-based academic medical centers as part of the National Institutes of Health (NIH) FSGS Genetic Study (26, 38), which was initiated in 1994 and continues to accrue subjects. The study enrolled 377 patients with FSGS and 900 subjects without known kidney disease (controls) (Table 1). Written informed consent was obtained from all participants. Racial classification was based on self-identification. There was no evidence of population substructure among FSGS patients and controls (38). The NIH FSGS Genetic Study has enrolled relatively few Hispanic subjects, Native American subjects, or subjects of Asian descent; therefore, these population groups were not included.

There were 130 European American (EA) FSGS patients. At the time of renal biopsy, 13 EA patients were children (<18 yr of age) and 117 were adults. EAs rarely, if ever, develop HIV-associated collapsing glomerulopathy (here, termed FSGS for simplicity); 94 FSGS patients were found to be HIV-seronegative and 36 were not tested, most or all of whom lacked risk factors for HIV-1 infection; therefore, we consider this group to be HIV-1-uninfected. A family history of biopsy-documented FSGS was present in three patients. Among these families, only one family member was studied, so all patients were unrelated individuals. All three kindreds were studied for *NPHS2*, *ACTN4*, *CD2AP*, and *WT1*, and no disease-associated mutations were found.

Table 1. *Racial background and HIV infection status of FSGS patients and controls*

| | FSGS Patients ($n$ = 377) | | Controls ($n$ = 900) | |
|---|---|---|---|---|
| | HIV-seronegative | HIV-seropositive | HIV-seronegative | HIV-seropositive |
| EA | 130* | 0 | 259 | 0 |
| AA | 195 | 52 | 393 | 248 |
| Total | 325 | 52 | 652 | 248 |

FSGS, focal segmental glomerulosclerosis; EA, European American; AA, African American. *94 FSGS patients were HIV-seronegative and 36 were not tested; most or all of the untested patients lacked risk factors for HIV-1 infection.

There were 195 AA HIV-seronegative patients. At the time of renal biopsy, 22 of the AA patients were children (<18 yr of age) and 173 were adults. Among these, 181 were found to be HIV-seronegative and 14, most or all of whom lacked risk factors for HIV-1 infection, were not tested; therefore, we consider this group to be HIV-1-uninfected patients. A family history of biopsy-proven FSGS was present in 10 patients. Only one member was studied among these families, so all patients were unrelated individuals.

There were 52 HIV-seropositive FSGS patients, and all were AAs. The renal biopsies were consistent with HIV-associated collapsing glomerulopathy, with collapse of glomerular capillaries and podocyte abnormalities. No patient reported a family history of FSGS.

The control groups included 900 adults, 652 of whom were HIV-1-uninfected and 248 of whom were HIV-1-seropositive. The HIV-uninfected controls were recruited at the NIH Clinical Center (Bethesda, MD) and at the Frederick National Laboratory for Cancer Research. All controls were in self-defined good health, none were known to have kidney disease, and all were tested at the time of blood donation and found to be HIV-1-seronegative.

The 248 HIV-1-seropositive controls were enrolled in the Johns Hopkins AIDS Link to the Intravenous Drug Experience (ALIVE) cohort in Baltimore, MD (61). This control group represents a hypernormal population, defined as individuals who do not have FSGS, do have a genetic susceptibility to FSGS (AA descent), and have been exposed to an environmental factor (HIV-1) known to cause FSGS. The controls had been HIV-1-infected for ≥8 yr, had a serum creatinine <1.5 mg/dl, and had a random urine protein-to-creatinine ratio <0.5. These normal tests for renal function strongly suggest that HIV-associated FSGS was absent at the time of recruitment. The duration of HIV infection was determined as the time since recruitment into the study (for seroprevalent individuals) or as the date of HIV seroconversion, imputed as the midpoint between last negative test date and first positive test date (for seroconverting individuals). The duration of HIV infection was a mean and median of 10 yr.

Institutional Review Board approval was obtained at each participating institution, and written informed consent was obtained from all subjects.

*SNP genotyping.* SNPs were selected from the National Center for Biotechnology Information SNP database within the *PDSS2* gene, the human ortholog of the mouse gene that encodes the *kd* allele, considering their map positions within *PDSS2*, minor allele frequency >5% in EAs or AAs, and linkage disequilibrium (LD) among SNPs using HapMap data or based on HapMap data for CEU and YRI. The nine selected SNPs were distributed at approximately equal distances across the *PDSS2* gene, as shown in Fig. 1*A*. Genotypes were determined using TaqMan SNP Genotyping Assays (Applied Biosystems, Foster City, CA) according to the manufacturer's protocols. TaqMan genotypes were automatically called and plotted on the basis of a two-parameter plot using fluorescence intensities of FAM and VIC dye-labeled MGB probes. Eight water controls were included on each 386-well plate to monitor potential PCR contamination, and 10% of the DNA samples were duplicated between plates to control for sampling-handling error or genotyping errors. We observed 100% concordance among duplicate DNA samples. All water controls were negative, indicating no PCR contamination.

*Statistical analysis.* Allele frequencies observed in the patients and the racially matched control population were compared by Fisher's exact test; the odds ratios (ORs) with 95% confidence intervals (CIs) were calculated using SAS software version 9.1 (SAS Institute, Cary, NC).

The SNP alleles were arranged into possible haplotypes by a Bayesian statistical method using PHASE version 2.1 (51, 52). As-

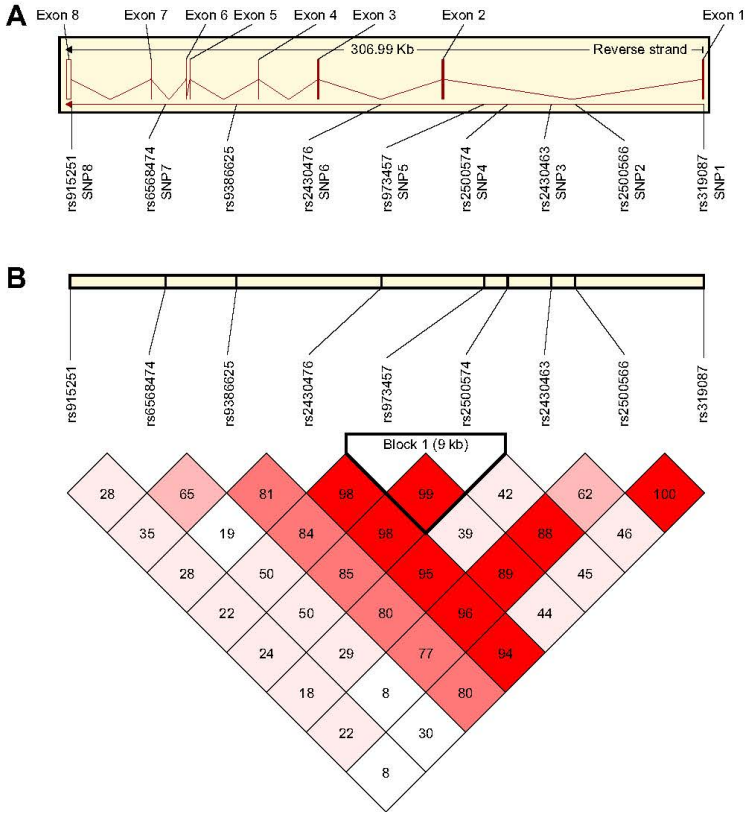



Fig. 1. Organization of the prenyl (decaprenyl) diphosphate synthase subunit 2 (*PDSS2*) locus and haplotype block structure. *A*: exon/intron organization of the *PDSS2* locus showing positions of single-nucleotide polymorphisms (SNPs). Eight exons are designated by vertical bars; lines between bars represent introns. Gene image was obtained from the Ensembl Web site (http://www.ensembl.org/Homo_sapiens/geneview?gene=ENSG00000164494). *B*: haplotype block structure defined by 8 SNPs at the *PDSS2* locus. White blocks indicate low $D'$ [a measure of linkage disequilibrium (LD), where 1.00 = complete LD] and, consequently, high recombination rates, with deepening shades of pink to red indicating increasing $D'$ values. Numbers in boxes represent actual $D'$ values multiplied by 100.

sociations between haplotypes and FSGS were assessed by comparison of frequencies between patients and controls by Fisher's exact test or the $\chi^2$ test; ORs and CIs were also calculated using SAS version 9.1. LD and correlation coefficients ($r^2$) were assessed by the Haploview program (Whitehead Institute, Cambridge, MA) (4).

*Generation and culture of lymphoblastoid cell lines.* Lymphoblastoid cell lines (LCLs) were generated from subjects using Epstein-Barr virus to transform B lymphocytes from peripheral blood mononuclear cells; cells were cultured in 15% fetal calf serum and RPMI culture medium (GIBCO, Life Technologies, Grand Island, NY) (37).

*Determination of $Q_{10}$ content in LCL lipid extracts by HPLC tandem mass spectroscopy.* LCL cell pellets were thawed on ice and then suspended in 3 ml of phosphate-buffered saline (0.14 M NaCl, 1.2 mM $NaH_2PO_4$, and 8.1 mM $Na_2HPO_4$, pH 7.4) and homogenized for 1.5 min with a Polytron (Kinematica PT2000) at maximum speed on ice. Aliquots of the homogenate (50 μl) were removed to determine the protein content [bicinchoninic acid (BCA) kit, Pierce], with bovine serum albumin as standard. Remaining aliquots (300 μl) were transferred to borosilicate tubes and stored at −20°C. Lipid extracts were prepared by addition of 1.2 ml of methanol followed by 1.8 ml of petroleum ether. Diethoxy-$Q_{10}$ (12) was used as an internal standard for determination of $Q_{10}$ in human cell lipid extracts. Samples were vortexed for 45 s. After removal of the organic upper layer, another 1.8 ml of petroleum ether was added, samples were vortexed again, and the combined organic phase was dried under a stream of nitrogen gas and resuspended in 200 μl of ethanol (USP, Aaper Alcohol and Chemical, Shelbyville, KY). A standard curve, composed of tubes containing 3, 15, 72, 204, or 1,021 pmol of $Q_{10}$ and a constant amount of diethoxy-$Q_{10}$, was prepared in duplicate. Lipid extraction and resuspension of each standard in 200 μl of ethanol was performed as described above.

HPLC-tandem mass spectrometry (MS/MS) analyses were performed as previously described for determination of $Q_9$ and $Q_{10}$ in mouse lipid extracts (12). Briefly, a 4000 QTRAP linear MS/MS spectrometer (Applied Biosystems, Foster City, CA) was used. Analyst version 1.4.2 (Applied Biosystems) was used for data acquisition and processing. A binary HPLC solvent delivery system was used with a Luna phenyl-hexyl column (particle size 3 μm, 50 × 2.00 mm; Phenomenex). The mobile phase consisted of *solvent A* (95:5 methanol-isopropanol with 2.5 mM ammonium formate) and *solvent B* (isopropanol and 2.5 mM ammonium formate). The percentage of *solvent B* for the first 1.5 min was 0% and increased linearly to 15% by 2 min. The percentage of *solvent B* remained unchanged for the next minute and decreased linearly to 0% by 4 min. A constant flow rate of 600 μl/min was used. All samples and standards (10 μl injected) were analyzed in multiple reaction monitoring mode (MRM); MRM transitions were as follows: mass-to-charge ratio (*m/z*) 880.7/197.0 ($Q_{10}$ with ammonium adduct), *m/z* 882.7/197.0 ($Q_{10}H_2$ with ammonium adduct), *m/z* 908.7/225.1 (diethoxy-$Q_{10}$ with ammonium adduct), and *m/z* 910.7/225.1 (diethoxy-$Q_{10}H_2$ with ammonium adduct).

Table 2. *Linkage disequilibrium and correlation among eight PDSS2 SNPs in EAs*

| | SNP7 rs6568474 | SNP6 rs2430476 | SNP5 rs973457 | SNP4 rs2500574 | SNP3 rs2430463 | SNP2 rs2500566 | SNP1 rs319087 |
|---|---|---|---|---|---|---|---|
| SNP8 rs915251 | 0.29 (0.03) | 0.29 (0.03) | 0.23 (0.04) | 0.24 (0.05) | 0.19 (0.02) | 0.22 (0.04) | 0.08 (0.00) |
| SNP7 rs6568474 | | 0.19 (0.01) | 0.50 (0.07) | 0.50 (0.07) | 0.29 (0.03) | 0.08 (0.00) | 0.30 (0.02) |
| SNP6 rs2430476 | | | 0.98 (0.28) | 0.99 (0.29) | 0.96 (0.50) | 0.96 (0.45) | 0.95 (0.22) |
| SNP5 rs973457 | | | | 0.99 (0.95) | 0.39 (0.08) | 0.89 (0.47) | 0.44 (0.17) |
| SNP4 rs2500574 | | | | | 0.43 (0.10) | 0.89 (0.48) | 0.46 (0.17) |
| SNP3 rs2430463 | | | | | | 0.63 (0.35) | 0.46 (0.10) |
| SNP2 rs2500566 | | | | | | | 1.00 (0.51) |

Values represent linkage disequilibrium ($D'$), with correlation coefficient ($r^2$) in parentheses. SNP, single-nucleotide polymorphism; *PDSS2*, prenyl (decaprenyl) diphosphate synthase subunit 2.

The standard curve was a simple linear fit forced through the origin. The limit of detection (LOD) and the limit of quantitation (LOQ) of $Q_{10}$ analysis using the 4000 QTRAP were defined as the concentrations that give a peak with signal-to-noise ratio of 3 and 10, respectively. For the assays presented, we determined that the LOD and LOQ of $Q_{10}$ using 4000 QTRAP were 0.02 and 0.05 pmol, respectively. Thus the first point of the standard curve (0.15 pmol of $Q_{10}$) was well above the LOD and LOQ. Each of the samples analyzed (lipid extracts from FSGS patients or controls) contained >0.15 pmol of $Q_{10}$ and, thus, was also well above the established LOQ.

Comparisons of $Q_{10}$ content were restricted to samples that were prepared and treated in the same way and analyzed at the same time. $Q_{10}$ in control and haplotype H2-positive ($H2^+$) FSGS patient LCLs were measured first, and $Q_{10}$ in a new set of control and $H2^-$ LCLs was measured ~2 yr later. During the intervening period, the mass spectrometer went through numerous maintenance procedures and adjustments, and cells cultured during the different times may have been subjected to slight differences in culture conditions. These variables preclude the direct comparison of the two control groups or the $H2^+$ and $H2^-$ patients.

## RESULTS

*Association of SNPs with FSGS. PDSS2* spans ~307 kb on chromosome 6 and has seven introns and eight exons encoding a 399-amino acid protein (Fig. 1*A*). All the SNPs that were genotyped occurred within noncoding regions of the gene: SNP1 (rs319087), SNP2 (rs2500566), SNP3 (rs2430463), SNP4 (rs2500574), and SNP5 (rs973457) were in intron 1; SNP6 (rs2430476) was in intron 2; rs9386625 was in intron 4; SNP7 (rs6568474) was in intron 6; and SNP8 (rs915251) was near the 3′-untranslated region. None of the SNPs are in known splice sites. Genotypic frequencies in rs9386625 did not conform to Hardy-Weinberg equilibrium (HWE) in the control group ($P = 0.01$) because of a deficiency in the observed number of heterozygotes, so the results for rs9386625 were not included in further calculations regarding differences between patients and controls. All exons at ~3 kb upstream were resequenced in eight control cell lines and eight cell lines from FSGS patients. Although additional SNPs were identified and were also resequenced in patients and controls, none could explain the susceptibility differences that were observed (M. Peng, unpublished observations).

The extent of LD and correlation ($r^2$) among the remaining SNPs is shown in Fig. 1*B* and Table 2 for EAs. There was complete LD between the two SNPs near the COOH terminus of the molecule: the SNP1 A allele always occurred with the SNP2 A allele ($D' = 1.00$, $r^2 = 0.507$). SNP4 and SNP5 in a 9-kb block were highly correlated ($r^2 = 0.951$) and showed near-absolute LD ($D' = 0.99$) and are, therefore, proxies (i.e., each SNP conveys equivalent information).

No significant difference in allele frequencies was observed between the affected and unaffected AAs (Table 3; $P \geq 0.06$), but there were significant differences in allele frequencies between the EA patients and controls for the proxy SNPs, SNP4 ($P = 0.001$) and SNP5 ($P = 0.008$; Table 4). We next tested the null hypothesis that genotype frequencies within the patient groups would be in conformance with HWE for a binomial distribution. The observed genotypic frequencies for the minor allele showed significant distortions from expectation for SNP5, SNP4, and SNP1 ($P = 0.03$, 0.004, and 0.04, respectively) and a trend for SNP2 ($P = 0.061$), with heterozygotes being underrepresented and homozygotes overrepresented in FSGS patients, but not in controls ($P \geq 0.13$; Table 4). No distortions in HWE were observed in AAs ($P \geq 0.05$).

*Disease-associated haplotype.* On the basis of the distortions in HWE for the four SNPs, we next tested the hypothesis that homozygosity for SNP5, SNP4, SNP2, or SNP1 minor alleles predicts risk of FSGS in EAs. For each SNP, we tested the recessive genetic model, comparing homozygotes for the minor allele with heterozygotes and homozygotes for the major allele in patients and controls. The strongest associations were observed for the proxy SNP4 and SNP5 (OR = 2.6, 2.2, $P = 0.001$ and 0.008), with weaker associations observed for SNP1 and SNP2 (Table 4). Since risk factors for HIV were self-reported and there remains a possibility that some individuals within the HIV-1-uninfected control group might actually be HIV-1-infected, we reanalyzed the data excluding the 36 FSGS patients who were not tested for HIV-1 sero status. The results of these analyses corroborated the results described above (data not shown).

Six of the eight SNPs were in strong LD, and these were used to infer haplotypes (Fig. 1*B*). The six most frequent

Table 3. *PDSS2 minor allele frequencies for FSGS patients and controls*

| | | AA | | EA | |
|---|---|---|---|---|---|
| | SNP | FSGS patients | Controls | FSGS patients | Controls |
| rs319087 | 1 | 0.457 | 0.459 | 0.349 | 0.324 |
| rs2500566 | 2 | 0.155 | 0.140 | 0.462 | 0.479 |
| rs2430463 | 3 | 0.160 | 0.130 | 0.445 | 0.484 |
| rs2500574 | 4 | 0.277 | 0.241 | 0.417* | 0.355 |
| rs973457 | 5 | 0.383 | 0.362 | 0.406† | 0.351 |
| rs2430476 | 6 | 0.084 | 0.082 | 0.319 | 0.336 |
| rs6568474 | 7 | 0.412 | 0.401 | 0.341 | 0.310 |
| rs915251 | 8 | 0.393 | 0.383 | 0.481 | 0.425 |

*$P = 0.001$, †$P = 0.008$ (by Fisher's exact test).

Table 4. *PDSS2 SNP associations with FSGS in EAs for the recessive genetic model*

| SNP | Group | Number (Frequency) | | | OR | 95% CI | *P* Value | HWE |
|---|---|---|---|---|---|---|---|---|
| | | TT | TA | AA | | | | |
| SNP1 rs319087 | FSGS ($n$ = 130) | 60 (0.465) | 48 (0.372) | 21 (0.163) | 1.9 | 1.0–3.5 | 0.063 | 0.041 |
| | Control (n = 258) | 115 (0.446) | 119 (0.461) | 24 (0.093) | | | | 0.387 |
| | | GG | GT | TT | | | | |
| SNP2 rs2500566 | FSGS ($n$ = 130) | 33 (0.254) | 54 (0.415) | 43 (0.331) | 1.7 | 1.0–2.6 | 0.031 | 0.061 |
| | Control ($n$ = 258) | 70 (0.271) | 129 (0.500) | 59 (0.229) | | | | 0.977 |
| | | GG | GA | AA | | | | |
| SNP4 rs2500574 | FSGS ($n$ = 127) | 51 (0.402) | 46 (0.362) | 30 (0.236) | 2.6 | 1.5–4.7 | 0.001 | 0.004 |
| | Control ($n$ = 258) | 102 (0.395) | 129 (0.500) | 27 (0.105) | | | | 0.135 |
| | | AA | AG | GG | | | | |
| SNP5 rs973457 | FSGS ($n$ = 128) | 51 (0.398) | 50 (0.391) | 27 (0.211) | 2.2 | 1.2–3.9 | 0.008 | 0.03 |
| | Control ($n$ = 258) | 105 (0.407) | 125 (0.484) | 28 (0.108) | | | | 0.304 |

Recessive genetic model compares homozygotes for the minor allele with homozygotes and heterozygotes for the major allele. OR, odds ratio; CI, confidence interval; HWE, Hardy-Weinberg equilibrium. In the FSGS group, SNP4 and SNP5 are in strong linkage disequilibrium; therefore, their associations are not independent. TT, TA, AA, GG, GT, GA, and AG refer to the SNP genotypes.

(>5%) haplotypes and their frequencies are arranged in descending order of frequency in Table 5. Also, in Table 5, using a recessive genetic model comparing homozygotes for each haplotype with all others, we show the frequencies of the three haplotype combinations and the ORs. Haplotype H2 homozygotes were more frequent in the FSGS patients than controls (8 of 130 vs. 3 of 259) and were significantly associated with FSGS (OR = 5.6, 95% CI = 1.5–21.5, $P$ = 0.008). This haplotype contained three of the four SNP alleles that were associated with FSGS patients (Table 5). In the eight patients with the H2/H2 genotype, onset age ranged from 14 to 59 yr, with a median of 40 yr. The ages of the three controls were 47, 54, and 61 yr. The renal biopsies showed primary FSGS without unusual features, and electron microscopy did not demonstrate unusual features of mitochondrial structure. No significant differences in haplotype frequencies were seen in AAs (Table 5).

*Measurement of $Q_{10}$ in LCLs.* We utilized HPLC-MS/MS and MRM to detect and quantify $Q_{10}$ in lipid extracts of LCLs (Fig. 2). Diethoxy-$Q_{10}$ was used as an internal standard in lipid extracts of samples and standards, and a typical standard curve is shown in Fig. 3. As *PDSS2* affects the synthesis of coenzyme Q, we examined the $Q_{10}$ content of LCLs that were derived from the FSGS patients with the H2/H2 homozygous genotype and control individuals. The content of $Q_{10}$ was significantly decreased in the cell lines of the H2/H2 homozygotes (198.8 ± 44.2 pmol $Q_{10}$/mg protein) compared with controls analyzed at the same time (267.7 ± 77.3 pmol $Q_{10}$/mg protein; Fig. 4, *A* and *B*). Cell lines from FSGS patients without the H2/H2 haplotype might be expected to have normal $Q_{10}$ content. However, the content of $Q_{10}$ was also significantly decreased in the FSGS patient non-H2 haplotype cell lines (138.6 ± 53.2 pmol $Q_{10}$/mg protein) compared with control LCLs analyzed at the same time (199.6 ± 31.8 pmol $Q_{10}$/mg protein; Fig. 4, *C* and *D*). FSGS patient-derived LCLs manifest a significant $Q_{10}$ deficiency when analyzed as one group ($n$ = 20, 162.7 ± 57.2 pmol $Q_{10}$/mg protein) compared with controls ($n$ = 18, 229.9 ± 64.9 pmol $Q_{10}$/mg protein, $P$ = 0.0017).

Table 5. *PDSS2 haplotype frequencies for AAs and EAs and associations in EAs for the six most common haplotypes (frequency >5%) in FSGS patients and controls*

| | SNP | | | | | | | Haplotype Frequency | | EA Haplotype Distribution | | | | | |
|---|---|---|---|---|---|---|---|---|---|---|---|---|---|---|---|
| | 1 | 2 | 3 | 4 | 5 | 6 | Group | AA | EA | Number (frequency) | | | OR | 95% CI | *P* value |
| Haplotype 1 | T | G | A | G | A | C | | | | Hx/Hx | Hx/H1 | H1/H1 | | | |
| | | | | | | | FSGS | 0.08 | 0.31 | 65 (0.500) | 48 (0.369) | 17 (0.131) | 1.7 | 0.9–3.4 | 0.15 |
| | | | | | | | Control | 0.07 | 0.31 | 117 (0.452) | 121 (0.467) | 21 (0.081) | | | |
| Haplotype 2 | T | T | G | A | G | T | | | | Hx/Hx | Hx/H2 | H2/H2 | | | |
| | | | | | | | FSGS | 0.25 | 0.16 | 96 (0.738) | 26 (0.200) | 8 (0.061) | 5.6 | 1.5–21.4 | 0.008 |
| | | | | | | | Control | 0.26 | 0.13 | 191 (0.737) | 65 (0.251) | 3 (0.012) | | | |
| Haplotype 3 | T | G | G | G | A | T | | | | Hx/Hx | Hx/H3 | H3/H3 | | | |
| | | | | | | | FSGS | 0.03 | 0.11 | 103 (0.792) | 26 (0.200) | 1 (0.077) | 0.7 | 0.1–6.4 | 1 |
| | | | | | | | Control | 0.02 | 0.13 | 195 (0.753) | 61 (0.235) | 3 (0.012) | | | |
| Haplotype 4 | A | T | G | G | A | T | | | | Hx/Hx | Hx/H4 | H4/H4 | | | |
| | | | | | | | FSGS | 0.08 | 0.11 | 130 (0.792) | 26 (0.200) | 1 (0.077) | 0.5 | 0.1–1.5 | 0.67 |
| | | | | | | | Control | 0.09 | 0.12 | 199 (0.768) | 56 (0.216) | 4 (0.015) | | | |
| Haplotype 5 | A | T | G | A | G | T | | | | Hx/Hx | Hx/H5 | H5/H5 | | | |
| | | | | | | | FSGS | 0.30 | 0.14 | 98 (0.754) | 27 (0.201) | 5 (0.038) | 2 | 0.6–7.1 | 0.31 |
| | | | | | | | Control | 0.29 | 0.09 | 218 (0.842) | 36 (0.139) | 5 (0.019) | | | |
| Haplotype 6 | A | T | A | A | G | T | | | | Hx/Hx | Hx/H6 | H6/H6 | | | |
| | | | | | | | FSGS | 0.03 | 0.08 | 108 (0.831) | 22 (0.169) | 0 | | | 0.31 |
| | | | | | | | Control | 0.04 | 0.10 | 213 (0.822) | 42 (0.162) | 4 (0.015) | | | |

Recessive model compares homozygotes for the haplotype with all others. Hx represents all other haplotypes. $n$ = 130 FSGS patients and 259 controls.

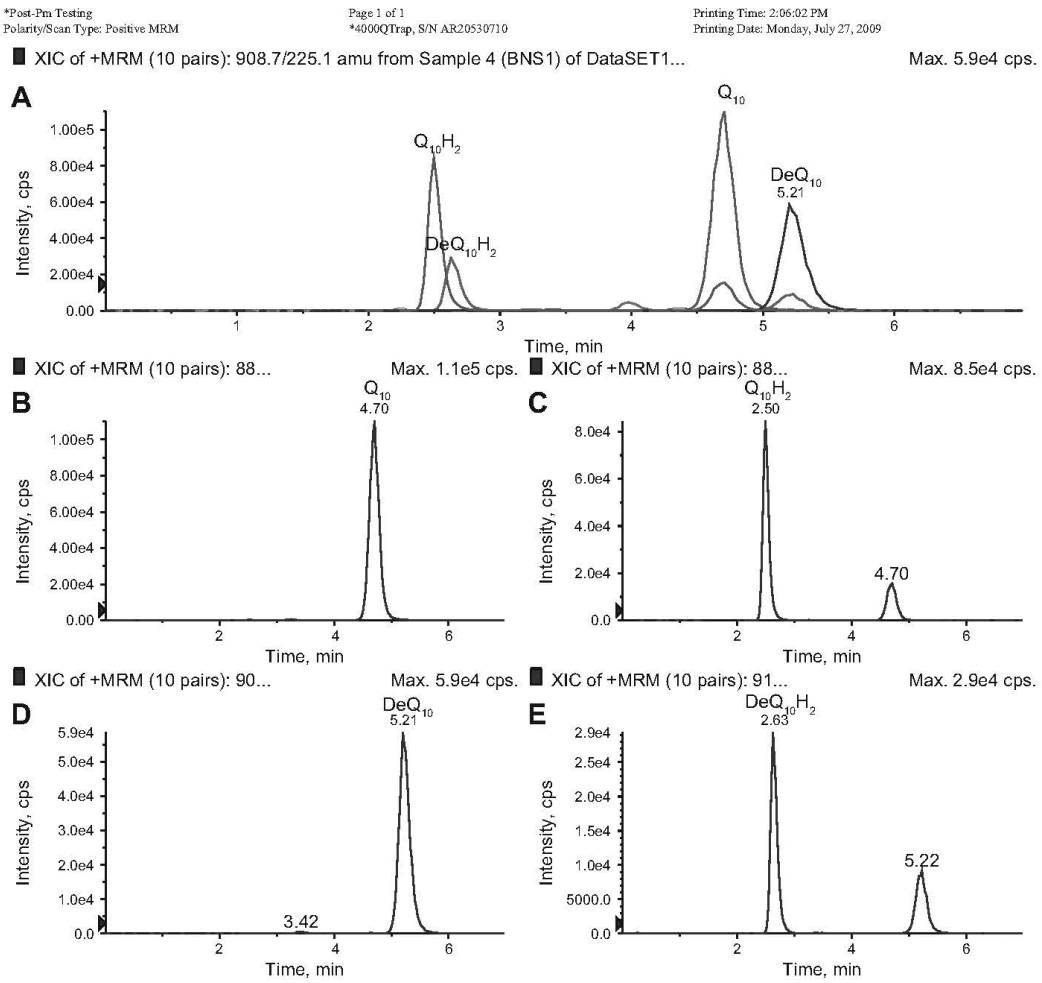



Fig. 2. Sample chromatogram showing detection of reduced and oxidized coenzyme $Q_{10}$ ($Q_{10}$) and diethoxy-$Q_{10}$ ($DeQ_{10}$). Lipid extract from a lymphoblastoid cell line (LCL) pellet was subjected to HPLC-tandem mass spectrometry (MS/MS) multiple-reaction monitoring. *A*: precursor-to-product transitions for ammonium adducts of reduced and oxidized $Q_{10}$ and $DeQ_{10}$. *x*-Axis, retention time (min); *y*-axis, arbitrary units of counts per second (cps). Scale is the same for overlaid traces within *A*. *B–E*: individual transitions. *B*: $Q_{10}$ with ammonium adduct (880.7/197.0). *C*: $Q_{10}H_2$ with ammonium adduct (882.7/197.0). *D*: $DeQ_{10}$ with ammonium adduct (908.7/225.1). *E*: $DeQ_{10}H_2$ with ammonium adduct (910.7/225.1). The sum of peak areas corresponding to $Q_{10}$ and $Q_{10}H_2$ was divided by the sum of peak areas corresponding to $DeQ_{10}$ and $DeQ_{10}H_2$, and the ratio was used to derive total $Q_{10}$ content from a standard curve (see Fig. 3).

## DISCUSSION

This project began as an attempt to determine whether a genetic locus associated with FSGS in mice would also be associated with the corresponding disease in humans. We demonstrated that homozygous genotypes for variant alleles for the *PDSS2* gene were indeed more common in FSGS patients than controls and that a single haplotype containing three of these SNPs was more common in EA, but not AA, FSGS patients, suggesting that *PDSS2* may be an FSGS susceptibility gene. Completely unexpected, however, was our observation that the $Q_{10}$ content of LCLs from FSGS patients was significantly lower than that of LCLs from ethnically matched controls.

With regard to the mode of inheritance, the recessive model is consistent with observations in *kd/kd* mice. None of the results for individual SNPs (OR = 1.7–2.6) were as predictive as haplotype 2 (OR = 5.6), comprising all six SNPs. It should be noted that the SNP associations are not independent, since SNP4 and SNP5 track each other, and the SNP1 A allele always occurs on a haplotype also carrying the SNP2 A allele. The results for SNP5 and haplotype 2 remain significant after correction for multiple comparisons ($P$ = 0.008 and 0.048,

dent effect of *PDSS2* is masked by *APOL1* renal risk alleles, which explain a large fraction of FSGS in the AA population (25). Alternatively, the causal variants tracked by these SNPs in EAs may be less frequent or on different haplotypes in AAs.

Mutations in the mitochondrial genome that are associated with tubulointerstitial nephritis (53, 58, 67), steroid-resistant FSGS (49), and MELAS (mitochondrial encephalomyopathy, lactic acidosis, and strokelike episodes) syndrome have been reported (18, 31). Some patients with MELAS syndrome also have renal lesions such as FSGS or tubulointerstitial nephropathy (18), and other families predominantly express diabetes and deafness (8, 59). The FSGS patients described in this report are also associated with a defective mitochondrial function, but one that is encoded by a nuclear gene. Our findings support the hypothesis recently proposed by Yan and colleagues (65) that emphasizes the importance of energy metabolism for normal podocyte function.

The biochemical function of the gene product suggests that levels of $Q_{10}$ will be affected (45), and this is supported by the data shown in Fig. 4. LCLs from FSGS patients who were homozygous for the H2 haplotype had significantly less $Q_{10}$ than control LCLs (Fig. 4*B*). When 12 additional LCLs from FSGS patients were compared with 10 additional controls, the patients' cell lines again had significantly less $Q_{10}$ than the control cells (Fig. 4*D*). This finding was unexpected and suggests that FSGS patients on average have lower $Q_{10}$ levels than controls, although 12 of the 20 FSGS cell lines examined had an average $Q_{10}$ content within the normal range reported for human white blood cells (159–369 pmol/mg protein) (19). As described in MATERIALS AND METHODS, we have restricted our comparisons of $Q_{10}$ content to samples that were analyzed at the same time. Nevertheless, a significant $Q_{10}$ deficiency was manifested when FSGS patient-derived LCLs were compared as one group ($n$ = 20, 162.7 ± 57.2 pmol $Q_{10}$/mg protein) with the pooled controls ($n$ = 18, 229.9 ± 64.9 pmol $Q_{10}$/mg protein, $P$ = 0.0017).

It may seem counterintuitive that valid information about $Q_{10}$ content relevant to FSGS could be obtained from LCLs. There are several interpretations regarding the finding of decreased $Q_{10}$ content in all cases of FSGS. One possible interpretation is that $Q_{10}$ content is decreased in all cases of FSGS nonspecifically. Perhaps the azotemia in FSGS patients leads to modifications of protein function or gene expression, including epigenetic modifications with the potential to persist through the process of immortalization. If this were the case, the $Q_{10}$ content might be decreased in patients with chronic kidney disease of other causes. In this scenario, the $Q_{10}$ content would be closer to control values in FSGS patients with very early-onset disease than in those with late-stage disease. A second interpretation is that decreased $Q_{10}$ content may be a common pathway of predisposition to FSGS. Previous studies have established the precedence of LCLs for the genetic analysis of gene expression. Cheung and colleagues (6) used cDNA microarrays to measure gene expression among monozygotic twins, siblings, and unrelated individuals and found evidence for a genetic contribution to the polymorphic variation in the level of gene expression. More recently, polymorphic *trans*-regulators were identified by RNA-sequencing analyses of human B cell lines from individuals from large families (7). Ding and colleagues (10) developed a statistical method for measuring the overlap between skin cells and lymphoblastoid cells in levels of gene expression and found that ~70% of the quantitative trait loci detected in lymphoblastoid cells were also observed in skin. Our findings are consistent with the idea that $Q_{10}$ content in cells reflects not only expression of ≥11 genes required for de novo synthesis, but also the assembly of a mitochondrial multisubunit protein-lipid complex known to be modulated by phosphorylation (54, 56, 64). Such multisubunit complexes may be particularly sensitive to polymorphisms. Indeed, patients and diploid yeast with only one copy of the *COQ4* gene show haploinsufficiency of coenzyme Q content (48).

At least 11 genes are known to be involved in the biosynthesis of coenzyme Q in yeast (5, 23, 32, 39, 56). Patients with deficiencies in $Q_{10}$ have been identified with defects in homologs of at least six yeast genes (22, 43). The first to be associated with a human disease was infantile encephalomyopathy and FSGS, which occurred in two patients with $Q_{10}$ deficiency caused by a mutation in *COQ2* (42). The second report was that of Lopez et al. (28), which described severe encephalomyopathy with nephrotic syndrome in a child with mutations in the *PDSS2* gene. Subsequent studies identified mutations in *PDSS1* and *COQ9* in patients with infantile-onset multisystem disorder (11, 34). More recently, mutations in the *COQ6* gene were associated with nephrotic syndrome and sensorineural deafness (22). Our results suggest that a substantial number of FSGS patients have less $Q_{10}$, which could be caused by any one of a number of genes, and this deficiency can be detected in patient-derived LCLs. If it were possible to measure the $Q_{10}$ content of the podocytes, the data might be even more informative.

$Q_{10}$ deficiency has been identified in many other patients with neurological, muscular, and/or renal defects in whom the responsible genes have not been identified, but many of these conditions have proven to be responsive to $Q_{10}$ supplementation (17, 27, 35, 43, 47, 60). This is encouraging with regard to the possibility of treating some FSGS patients with oral supplementation of $Q_{10}$, but there are tissue differences with regard to uptake of $Q_{10}$ from the diet (57), so it remains to be determined whether this approach will be beneficial. In at least one patient, oral $Q_{10}$ improved the neurological symptoms, but not the renal dysfunction. This could have been because renal damage had already occurred before therapy was initiated, which demonstrates the importance of early diagnosis (57). Thus, *PDSS2* joins the list of mitochondrial genes, present in the nuclear or mitochondrial genome, in which mutations or tagging SNPs are associated with FSGS. Podocytes, the target cell in FSGS, are particularly reliant on mitochondrial function for energy generation (1), and thus podocytes may be particularly susceptible to genetic disorders leading to mitochondrial dysfunction.

An association between the *PDSS2* gene and FSGS could be demonstrated in EAs but not AAs in this study. The causal variation in or near the *PDSS2* gene responsible for FSGS has not been identified. The data suggest that such an allele is in significant LD with one or more of the SNP alleles that have been tested and likely to occur on haplotype 2 in EAs, but extensive sequencing studies may be required before the causal allele or alleles associated with FSGS can be identified precisely. We also have no mechanistic information about how allelic differences in the *PDSS2* gene could lead to FSGS. However, the intronic location of the most closely associated

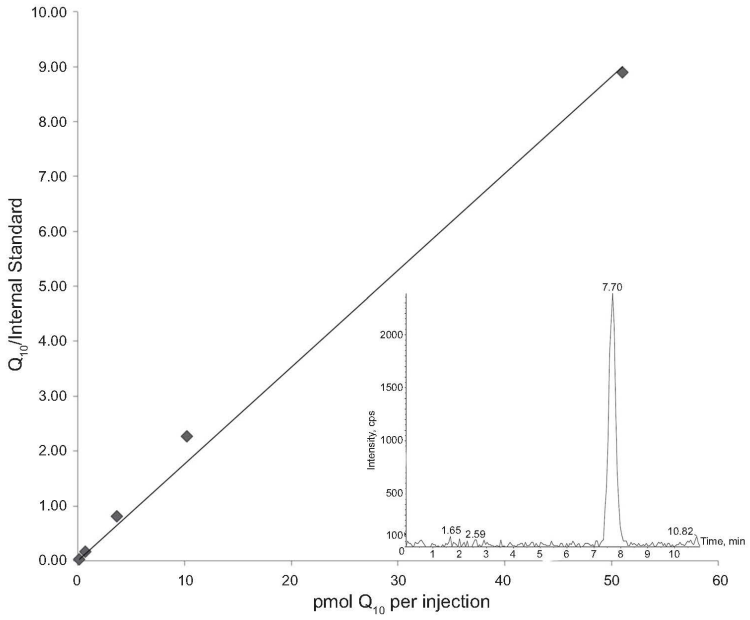



Fig. 3. Determination of $Q_{10}$ content with a standard curve. *x*-Axis, amount of coenzyme $Q_{10}$ contained in each injection (10 μl); *y*-axis, peak area of $Q_{10}$ divided by peak area of the internal standard ($DeQ_{10}$). A line forced through the origin was plotted to generate the standard curve (slope = 0.176, $r^2$ = 0.995). *Inset*: a representative peak for the lowest amount of the $Q_{10}$ standard injected for preparation of the standard curve (0.15 pmol, signal-to-noise ratio = 20:1).

respectively) suggesting that these associations are not due to type 1 error. These data suggest that polymorphism in *PDSS2* may contribute to increased risk of disease and that people of European ancestry homozygous for haplotype 2 may be at increased risk for developing FSGS. The frequency of haplotype 2 homozygotes was 6.1% among EA FSGS patients and 1.2% in the control EA population (Table 5). The lack of association in AAs could have occurred because an indepen-

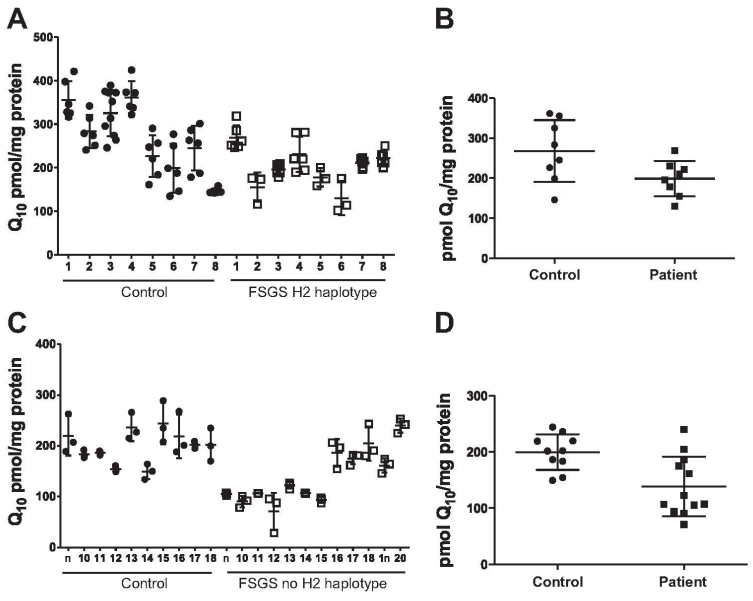



Fig. 4. $Q_{10}$ content in LCLs from focal segmental glomerulosclerosis (FSGS) patients is decreased relative to that of controls. *A*: total $Q_{10}$ content for each LCL derived from control subjects or patients. FSGS patients are the 8 individuals who were homozygous for the H2/H2 haplotype. $Q_{10}$ content is presented as a scatter plot, with average ± SD denoted by 3 horizontal lines ($n$ = 6, except $n$ = 10 for control *sample 3* and $n$ = 3 for FSGS *samples 2, 5*, and *6*). *B*: $Q_{10}$ content of FSGS patients' cell lines ($n$ = 8, 198.8 ± 44.2 pmol/mg protein) is significantly decreased compared with $Q_{10}$ content of control cell lines ($n$ = 8, 267.7 ± 77.3 pmol/mg protein). Each of the average values from *A* is represented as a scatter plot, with average ± SD denoted by 3 horizontal lines. $P < 0.05$ was determined by Student's 2-tailed *t*-test. *C*: total $Q_{10}$ content for each LCL derived from 10 additional control subjects and 12 FSGS patients. FSGS patients did not have the H2/H2 genotype. $Q_{10}$ content is presented as described in *A* ($n$ = 3). *D*: $Q_{10}$ content of FSGS patients' cell lines ($n$ = 10, 138.6 ± 53.2 pmol/mg protein) is significantly decreased compared with $Q_{10}$ content of control cell lines ($n$ = 12, 199.6 ± 31.8 pmol/mg protein). Each of the average values from *C* is represented in a scatter plot, with average ± SD denoted by 3 horizontal lines. $P < 0.005$ was determined by Student's 2-tailed *t*-test.

SNPs is consistent with previous genome-wide association studies. In the majority (~93%) of such studies, the disease-associated variant lies within a noncoding sequence (33).

Furthermore, it is not known to what extent $Q_{10}$ levels might affect disease susceptibility. Although a severely defective allele could possibly behave as a Mendelian factor in the transmission of FSGS, alleles with more moderate effects may only act as contributing factors and only slightly increase the risk of FSGS within the context of other genetic and environmental factors. These findings suggest that *PDSS2* variation and $Q_{10}$ levels may affect respiratory capacity; this pathway warrants further study for its potential role in podocyte injury leading to FSGS and related syndromes. As with any genetic study, the results of this investigation require independent confirmation.

If it is indeed correct that many cases of FSGS involve $Q_{10}$ deficiencies, animal models of these conditions will be useful for studying possible therapies. The *kd/kd* mouse phenotype can be rescued to some extent by $Q_{10}$ supplementation (44) and to an even greater extent by probucol, which has the effect of increasing endogenous $Q_9$ content (12). Diabetic nephropathy in *db/db* mice can also be significantly ameliorated by $Q_{10}$ supplementation (50). It is also well established that mitochondrial deficits are associated with several animal models of hypoxia and acute kidney injury (13–15, 62). Our results suggest that further study of coenzyme Q deficiency in FSGS and its possible treatment may have significant therapeutic benefits.


## ACKNOWLEDGMENTS

We thank Dr. Kathy Ewens, Carl McIntosh, and Randall Johnson for valuable help and advice. We are extremely grateful for the contributions of the following clinical collaborators: Drs. Tejinder S. Ahuja (University of Texas Medical Branch), Diego Aviles (Louisiana State University), Jeffrey S. Berns (University of Pennsylvania), William A. Briggs (Johns Hopkins University School of Medicine), Stephen M. Korbet (Rush University Medical Center), Richard A. Dart (Marshfield Clinic), Dollie Green (University of Miami), Florence Hutchison (University of South Carolina), Paul L. Kimmel (George Washington University Medical Center), Oliver Lenz (University of Miami), Roslyn Mannon (Duke University Medical Center), Donna Michel (West Virgina University), Michele Mokrzycki (Albert Einstein College of Medicine), Patrick Nachman (University of North Carolina), T. K. S. Rao (State University of New York), Elizabeth Ripley (Medical College of Virginia), Jeffrey R. Schelling (Case Western Reserve University), Eric E. Simon (Tulane University School of Medicine), Michael C. Smith (University Hospitals, Cleveland), and Howard Trachtman (Schneider Children's Hospital).

## GRANTS

This project has been funded in whole or in part with federal funds from the National Cancer Institute under Contract HHSN26120080001E. Research was supported in part by the Intramural Research Program of the NIH, National Cancer Institute, Center for Cancer Research, and National Institute of Diabetes and Digestive and Kidney Diseases Intramural Research Programs and was supported by NIH Grants R01 DK-55852 (D. L. Gasser), R01 GM-45952 (C. F. Clarke), and National Cancer Institute Division of Cancer Treatment and Diagnosis under contract N01 CO-12400. L. X. Xie was supported by the Ruth L. Kirschstein National Service Award GM-007185. The HPLC-MS/MS determination of quinones was supported in part by National Center for Research Resources Grant S10 RR-024605. Recruitment of controls through the ALIVE study was supported by National Institute on Drug Abuse Grant R01-DA-04334.

## DISCLAIMER

The content of this publication does not necessarily reflect the views or policies of the US Department of Health and Human Services, nor does mention of trade names, commercial products, or organizations imply endorsement by the US Government.

## DISCLOSURES

No conflicts of interest, financial or otherwise, are declared by the authors.

## AUTHOR CONTRIBUTIONS

D.L.G., C.A.W., L.X.X., C.F.C., and J.B.K. are responsible for conception and design of the research; D.L.G., C.A.W., M.P., P.A., L.A.M., G.D.K., Y.S., L.X.X., B.N.M., C.F.C., and J.B.K. analyzed the data; D.L.G., C.A.W., M.P., P.A., L.A.M., G.D.K., L.X.X., B.N.M., C.F.C., and J.B.K. interpreted the results of the experiments; D.L.G. drafted the manuscript; D.L.G., C.A.W., C.F.C., and J.B.K. edited and revised the manuscript; D.L.G., C.A.W., M.P., P.A., L.A.M., G.D.K., Y.S., L.X.X., B.N.M., C.F.C., and J.B.K. approved the final version of the manuscript; C.A.W., P.A., Y.S., L.X.X., and C.F.C. prepared the figures; M.P., P.A., L.A.M., Y.S., L.X.X., B.N.M., and C.F.C. performed the experiments.


## REFERENCES


1. **Abe Y, Sakairi T, Kajiyama H, Shrivastav S, Beeson C, Kopp JB.** Bioenergetic characterization of mouse podocytes. *Am J Physiol Cell Physiol* 299: C464–C476, 2010.
2. **Barisoni L, Madaio MP, Eraso M, Gasser DL, Nelson PJ.** The *kd/kd* mouse is a model of collapsing glomerulopathy. *J Am Soc Nephrol* 16: 2847–2851, 2005.
3. **Barisoni L, Schnaper HW, Kopp JB.** A proposed taxonomy for the podocytopathies: a reassessment of the primary nephrotic diseases. *Clin J Am Soc Nephrol* 2: 529–542, 2007.
4. **Barrett JC, Fry B, Maller J, Daly MJ.** Haploview: analysis and visualization of LD and haplotype maps. *Bioinformatics* 21: 263–265, 2005.
5. **Belogrudov GI, Lee PT, Jonassen T, Hsu AY, Gin P, Clarke CF.** Yeast COQ4 encodes a mitochondrial protein required for coenzyme Q synthesis. *Arch Biochem Biophys* 392: 48–58, 2001.
6. **Cheung VG, Conlin LK, Weber TM, Arcaro M, Jen KY, Morley M, Spielman RS.** Natural variation in human gene expression assessed in lymphoblastoid cells. *Nat Genet* 33: 422–425, 2003.
7. **Cheung VG, Nayak RR, Wang IX, Elwyn S, Cousins SM, Morley M, Spielman RS.** Polymorphic *cis*- and *trans*-regulation of human gene expression. *PLoS Biol* 8: 2010.
8. **Chinnery PF, Turnbull DM.** Mitochondrial DNA and disease. *Lancet* 354 *Suppl* 1: SI17–SI21, 1999.
9. **Dell KM, Li YX, Peng M, Neilson EG, Gasser DL.** Localization of the mouse kidney disease (*kd*) gene to a YAC/BAC contig on chromosome 10. *Mamm Genome* 11: 967–971, 2000.
10. **Ding J, Gudjonsson JE, Liang L, Stuart PE, Li Y, Chen W, Weichenthal M, Ellinghaus E, Franke A, Cookson W, Nair RP, Elder JT, Abecasis GR.** Gene expression in skin and lymphoblastoid cells: refined statistical method reveals extensive overlap in *cis*-eQTL signals. *Am J Hum Genet* 87: 779–789, 2010.
11. **Duncan AJ, Bitner-Glindzicz M, Meunier B, Costello H, Hargreaves IP, Lopez LC, Hirano M, Quinzii CM, Sadowski MI, Hardy J, Singleton A, Clayton PT, Rahman S.** A nonsense mutation in COQ9 causes autosomal-recessive neonatal-onset primary coenzyme $Q_{10}$ deficiency: a potentially treatable form of mitochondrial disease. *Am J Hum Genet* 84: 558–566, 2009.
12. **Falk MJ, Polyak E, Zhang Z, Peng M, King R, Maltzman JS, Okwuego E, Horyn O, Nakamaru-Ogiso E, Ostrovsky J, Xie LX, Chen JY, Marbois B, Nissim I, Clarke CF, Gasser DL.** Probucol ameliorates renal and metabolic sequelae of primary CoQ deficiency in Pdss2 mutant mice. *EMBO Mol Med* 3: 410–427, 2011.
13. **Feldkamp T, Kribben A, Roeser NF, Senter RA, Kemner S, Venkatachalam MA, Nissim I, Weinberg JM.** Preservation of complex I function during hypoxia-reoxygenation-induced mitochondrial injury in proximal tubules. *Am J Physiol Renal Physiol* 286: F749–F759, 2004.
14. **Feldkamp T, Kribben A, Weinberg JM.** Assessment of mitochondrial membrane potential in proximal tubules after hypoxia-reoxygenation. *Am J Physiol Renal Physiol* 288: F1092–F1102, 2005.
15. **Funk JA, Schnellmann RG.** Persistent disruption of mitochondrial homeostasis after acute kidney injury. *Am J Physiol Renal Physiol* 302: F853–F864, 2012.

16. **Genovese G, Friedman DJ, Ross MD, Lecordier L, Uzureau P, Freedman BI, Bowden DW, Langefeld CD, Oleksyk TK, Uscinski Knob AL, Bernhardy AJ, Hicks PJ, Nelson GW, Vanhollebeke B, Winkler CA, Kopp JB, Pays E, Pollak MR.** Association of trypanolytic ApoL1 variants with kidney disease in African Americans. *Science* 329: 841–845, 2010.
17. **Gironi M, Lamperti C, Nemni R, Moggio M, Comi G, Guerini FR, Ferrante P, Canal N, Naini A, Bresolin N, DiMauro S.** Late-onset cerebellar ataxia with hypogonadism and muscle coenzyme $Q_{10}$ deficiency. *Neurology* 62: 818–820, 2004.
18. **Guery B, Choukroun G, Noel LH, Clavel P, Rotig A, Lebon S, Rustin P, Bellane-Chantelot C, Mougenot B, Grunfeld JP, Chauveau D.** The spectrum of systemic involvement in adults presenting with renal lesion and mitochondrial tRNA(Leu) gene mutation. *J Am Soc Nephrol* 14: 2099–2108, 2003.
19. **Hahn SH, Kerfoot S, Vasta V.** Assay to measure oxidized and reduced forms of CoQ by LC-MS/MS. *Methods Mol Biol* 837: 169–179, 2012.
20. **Hallman TM, Peng M, Meade R, Hancock WW, Madaio MP, Gasser DL.** The mitochondrial and kidney disease phenotypes of *kd/kd* mice under germfree conditions. *J Autoimmun* 26: 1–6, 2006.
21. **Hancock WW, Tsai TL, Madaio MP, Gasser DL.** Multiple autoimmune pathways in *kd/kd* mice. *J Immunol* 171: 2778–2781, 2003.
22. **Heeringa SF, Chernin G, Chaki M, Zhou W, Sloan AJ, Ji Z, Xie LX, Salviati L, Hurd TW, Vega-Warner V, Killen PD, Raphael Y, Ashraf S, Ovunc B, Schoeb DS, McLaughlin HM, Airik R, Vlangos CN, Gbadegesin R, Hinkes B, Saisawat P, Trevisson E, Doimo M, Casarin A, Pertegato V, Giorgi G, Prokisch H, Rotig A, Nurnberg G, Becker C, Wang S, Ozaltin F, Topaloglu R, Bakkaloglu A, Bakkaloglu SA, Muller D, Beissert A, Mir S, Berdeli A, Varpizen S, Zenker M, Matejas V, Santos-Ocana C, Navas P, Kusakabe T, Kispert A, Akman S, Soliman NA, Krick S, Mundel P, Reiser J, Nurnberg P, Clarke CF, Wiggins RC, Faul C, Hildebrandt F.** COQ6 mutations in human patients produce nephrotic syndrome with sensorineural deafness. *J Clin Invest* 121: 2013–2024, 2011.
23. **Johnson A, Gin P, Marbois BN, Hsieh EJ, Wu M, Barros MH, Clarke CF, Tzagoloff A.** COQ9, a new gene required for the biosynthesis of coenzyme Q in *Saccharomyces cerevisiae*. *J Biol Chem* 280: 31397–31404, 2005.
24. **Kitiyakara C, Kopp JB, Eggers P.** Trends in the epidemiology of focal segmental glomerulosclerosis. *Semin Nephrol* 23: 172–182, 2003.
25. **Kopp JB, Nelson GW, Sampath K, Johnson RC, Genovese G, An P, Friedman D, Briggs W, Dart R, Korbet S, Mokrzycki MH, Kimmel PL, Limou S, Ahuja TS, Berns JS, Fryc J, Simon EE, Smith MC, Trachtman H, Michel DM, Schelling JR, Vlahov D, Pollak M, Winkler CA.** APOL1 genetic variants in focal segmental glomerulosclerosis and HIV-associated nephropathy. *J Am Soc Nephrol* 22: 2129–2137, 2011.
26. **Kopp JB, Winkler C.** HIV-associated nephropathy in African Americans. *Kidney Int Suppl* S43–S49, 2003.
27. **Lalani SR, Vladutiu GD, Plunkett K, Lotze TE, Adesina AM, Scaglia F.** Isolated mitochondrial myopathy associated with muscle coenzyme $Q_{10}$ deficiency. *Arch Neurol* 62: 317–320, 2005.
28. **Lopez LC, Schuelke M, Quinzii CM, Kanki T, Rodenburg RJ, Naini A, Dimauro S, Hirano M.** Leigh syndrome with nephropathy and $CoQ_{10}$ deficiency due to decaprenyl diphosphate synthase subunit 2 (PDSS2) mutations. *Am J Hum Genet* 79: 1125–1129, 2006.
29. **Lyon MF, Hulse EV.** An inherited kidney disease of mice resembling human nephronophthisis. *J Med Genet* 8: 41–48, 1971.
30. **Madaio MP, Ahima RS, Meade R, Rader DJ, Mendoza A, Peng M, Tomaszewski JE, Hancock WW, Gasser DL.** Glomerular and tubular epithelial defects in *kd/kd* mice lead to progressive renal failure. *Am J Nephrol* 25: 604–610, 2005.
31. **Majamaa K, Moilanen JS, Uimonen S, Remes AM, Salmela PI, Karppa M, Majamaa-Voltti KA, Rusanen H, Sorri M, Peuhkurinen KJ, Hassinen IE.** Epidemiology of A3243G, the mutation for mitochondrial encephalomyopathy, lactic acidosis, and strokelike episodes: prevalence of the mutation in an adult population. *Am J Hum Genet* 63: 447–454, 1998.
32. **Marbois B, Gin P, Faull KF, Poon WW, Lee PT, Strahan J, Shepherd JN, Clarke CF.** Coq3 and Coq4 define a polypeptide complex in yeast mitochondria for the biosynthesis of coenzyme Q. *J Biol Chem* 280: 20231–20238, 2005.
33. **Maurano MT, Humbert R, Rynes E, Thurman RE, Haugen E, Wang H, Reynolds AP, Sandstrom R, Qu H, Brody J, Shafer A, Neri F, Lee K, Kutyavin T, Stehling-Sun S, Johnson AK, Canfield TK, Giste E, Diegel M, Bates D, Hansen RS, Neph S, Sabo PJ, Heimfeld S, Raubitschek A, Ziegler S, Cotsapas C, Sotoodehnia N, Glass I, Sunyaev SR, Kaul R, Stamatoyannopoulos JA.** Systematic localization of common disease-associated variation in regulatory DNA. *Science* 337: 1190–1195, 2012.
34. **Mollet J, Giurgea I, Schlemmer D, Dallner G, Chretien D, Delahodde A, Bacq D, de Lonlay P, Munnich A, Rotig A.** Prenyldiphosphate synthase, subunit 1 (PDSS1) and OH-benzoate polyprenyltransferase (COQ2) mutations in ubiquinone deficiency and oxidative phosphorylation disorders. *J Clin Invest* 117: 765–772, 2007.
35. **Musumeci O, Naini A, Slonim AE, Skavin N, Hadjigeorgiou GL, Krawiecki N, Weissman BM, Tsao CY, Mendell JR, Shanske S, De Vivo DC, Hirano M, DiMauro S.** Familial cerebellar ataxia with muscle coenzyme $Q_{10}$ deficiency. *Neurology* 56: 849–855, 2001.
36. **Neilson EG, McCafferty E, Feldman A, Clayman MD, Zakheim B, Korngold R.** Spontaneous interstitial nephritis in *kdkd* mice. I. An experimental model of autoimmune renal disease. *J Immunol* 133: 2560–2565, 1984.
37. **Neitzel H.** A routine method for the establishment of permanent growing lymphoblastoid cell lines. *Hum Genet* 73: 320–326, 1986.
38. **Orloff MS, Iyengar SK, Winkler CA, Goddard KA, Dart RA, Ahuja TS, Mokrzycki M, Briggs WA, Korbet SM, Kimmel PL, Simon EE, Trachtman H, Vlahov D, Michel DM, Berns JS, Smith MC, Schelling JR, Sedor JR, Kopp JB.** Variants in the Wilms' tumor gene are associated with focal segmental glomerulosclerosis in the African American population. *Physiol Genomics* 21: 212–221, 2005.
39. **Ozeir M, Muhlenhoff U, Webert H, Lill R, Fontecave M, Pierrel F.** Coenzyme Q biosynthesis: Coq6 is required for the C5-hydroxylation reaction and substrate analogs rescue Coq6 deficiency. *Chem Biol* 18: 1134–1142, 2011.
40. **Peng M, Jarett L, Meade R, Madaio MP, Hancock WW, George AL Jr, Neilson EG, Gasser DL.** Mutant prenyltransferase-like mitochondrial protein (PLMP) and mitochondrial abnormalities in *kd/kd* mice. *Kidney Int* 66: 20–28, 2004.
41. **Pollak MR.** Inherited podocytopathies: FSGS and nephrotic syndrome from a genetic viewpoint. *J Am Soc Nephrol* 13: 3016–3023, 2002.
42. **Quinzii C, Naini A, Salviati L, Trevisson E, Navas P, Dimauro S, Hirano M.** A mutation in para-hydroxybenzoate-polyprenyl transferase (COQ2) causes primary coenzyme $Q_{10}$ deficiency. *Am J Hum Genet* 78: 345–349, 2006.
43. **Rahman S, Clarke CF, Hirano M.** Diagnosis and treatment of coenzyme $Q_{10}$ deficiency. *Neuromuscul Disord* 23: 506–515, 2013.
44. **Saiki R, Lunceford AL, Shi Y, Marbois B, King R, Pachuski J, Kawamukai M, Gasser DL, Clarke CF.** Coenzyme $Q_{10}$ supplementation rescues renal disease in *Pdss2kd/kd* mice with mutations in prenyl diphosphate synthase subunit 2. *Am J Physiol Renal Physiol* 295: F1535–F1544, 2008.
45. **Saiki R, Nagata A, Kainou T, Matsuda H, Kawamukai M.** Characterization of solanesyl and decaprenyl diphosphate synthases in mice and humans. *FEBS J* 272: 5606–5622, 2005.
46. **Saiki R, Nagata A, Uchida N, Kainou T, Matsuda H, Kawamukai M.** Fission yeast decaprenyl diphosphate synthase consists of Dps1 and the newly characterized Dlp1 protein in a novel heterotetrameric structure. *Eur J Biochem* 270: 4113–4121, 2003.
47. **Salviati L, Sacconi S, Murer L, Zacchello G, Franceschini L, Laverda AM, Basso G, Quinzii C, Angelini C, Hirano M, Naini AB, Navas P, DiMauro S, Montini G.** Infantile encephalomyopathy and nephropathy with $CoQ_{10}$ deficiency: a $CoQ_{10}$-responsive condition. *Neurology* 65: 606–608, 2005.
48. **Salviati L, Trevisson E, Rodriguez Hernandez MA, Casarin A, Pertegato V, Doimo M, Cassina M, Agosto C, Desbats MA, Sartori G, Sacconi S, Memo L, Zuffardi O, Artuch R, Quinzii C, Dimauro S, Hirano M, Santos-Ocana C, Navas P.** Haploinsufficiency of COQ4 causes coenzyme $Q_{10}$ deficiency. *J Med Genet* 49: 187–191, 2012.
49. **Scaglia F, Vogel H, Hawkins EP, Vladutiu GD, Liu LL, Wong LJ.** Novel homoplasmic mutation in the mitochondrial tRNATyr gene associated with atypical mitochondrial cytopathy presenting with focal segmental glomerulosclerosis. *Am J Med Genet A* 123A: 172–178, 2003.
50. **Sourris KC, Harcourt BE, Tang PH, Morley AL, Huynh K, Penfold SA, Coughlan MT, Cooper ME, Nguyen TV, Ritchie RH, Forbes JM.** Ubiquinone (coenzyme $Q_{10}$) prevents renal mitochondrial dysfunction in an experimental model of type 2 diabetes. *Free Radic Biol Med* 52: 716–723, 2012.

51. **Stephens M, Donnelly P.** A comparison of Bayesian methods for haplotype reconstruction from population genotype data. *Am J Hum Genet* 73: 1162–1169, 2003.
52. **Stephens M, Smith NJ, Donnelly P.** A new statistical method for haplotype reconstruction from population data. *Am J Hum Genet* 68: 978–989, 2001.
53. **Szabolcs MJ, Seigle R, Shanske S, Bonilla E, DiMauro S, D'Agati V.** Mitochondrial DNA deletion: a cause of chronic tubulointerstitial nephropathy. *Kidney Int* 45: 1388–1396, 1994.
54. **Tauche A, Krause-Buchholz U, Rodel G.** Ubiquinone biosynthesis in *Saccharomyces cerevisiae*: the molecular organization of *O*-methylase Coq3p depends on Abc1p/Coq8p. *FEMS Yeast Res* 8: 1263–1275, 2008.
55. **Thomas DB, Franceschini N, Hogan SL, Ten Holder S, Jennette CE, Falk RJ, Jennette JC.** Clinical and pathologic characteristics of focal segmental glomerulosclerosis pathologic variants. *Kidney Int* 69: 920–926, 2006.
56. **Tran UC, Clarke CF.** Endogenous synthesis of coenzyme Q in eukaryotes. *Mitochondrion* 7 *Suppl*: S62–S71, 2007.
57. **Turunen M, Olsson J, Dallner G.** Metabolism and function of coenzyme Q. *Biochim Biophys Acta* 1660: 171–199, 2004.
58. **Tzen CY, Tsai JD, Wu TY, Chen BF, Chen ML, Lin SP, Chen SC.** Tubulointerstitial nephritis associated with a novel mitochondrial point mutation. *Kidney Int* 59: 846–854, 2001.
59. **van den Ouweland JM, Lemkes HH, Ruitenbeek W, Sandkuijl LA, de Vijlder MF, Struyvenberg PA, van de Kamp JJ, Maassen JA.** Mutation in mitochondrial tRNA(Leu)(UUR) gene in a large pedigree with maternally transmitted type II diabetes mellitus and deafness. *Nat Genet* 1: 368–371, 1992.
60. **Van Maldergem L, Trijbels F, DiMauro S, Sindelar PJ, Musumeci O, Janssen A, Delberghe X, Martin JJ, Gillerot Y.** Coenzyme Q-responsive Leigh's encephalopathy in two sisters. *Ann Neurol* 52: 750–754, 2002.
61. **Vlahov D, Graham N, Hoover D, Flynn C, Bartlett JG, Margolick JB, Lyles CM, Nelson KE, Smith D, Holmberg S, Farzadegan H.** Prognostic indicators for AIDS and infectious disease death in HIV-infected injection drug users: plasma viral load and $CD4^+$ cell count. *JAMA* 279: 35–40, 1998.
62. **Weinberg JM, Venkatachalam MA, Roeser NF, Saikumar P, Dong Z, Senter RA, Nissim I.** Anaerobic and aerobic pathways for salvage of proximal tubules from hypoxia-induced mitochondrial injury. *Am J Physiol Renal Physiol* 279: F927–F943, 2000.
63. **Winn MP, Conlon PJ, Lynn KL, Farrington MK, Creazzo T, Hawkins AF, Daskalakis N, Kwan SY, Ebersviller S, Burchette JL, Pericak-Vance MA, Howell DN, Vance JM, Rosenberg PB.** A mutation in the TRPC6 cation channel causes familial focal segmental glomerulosclerosis. *Science* 308: 1801–1804, 2005.
64. **Xie LX, Hsieh EJ, Watanabe S, Allan CM, Chen JY, Tran UC, Clarke CF.** Expression of the human atypical kinase ADCK3 rescues coenzyme Q biosynthesis and phosphorylation of Coq polypeptides in yeast coq8 mutants. *Biochim Biophys Acta* 1811: 348–360, 2011.
65. **Yan K, Ito N, Nakajo A, Kurayama R, Fukuhara D, Nishibori Y, Kudo A, Akimoto Y, Takenaka H.** The struggle for energy in podocytes leads to nephrotic syndrome. *Cell Cycle* 11: 1504–1511, 2012.
66. **Ziegler CG, Peng M, Falk MJ, Polyak E, Tsika E, Ischiropoulos H, Bakalar D, Blendy JA, Gasser DL.** Parkinson's disease-like neuromuscular defects occur in prenyl diphosphate synthase subunit 2 (Pdss2) mutant mice. *Mitochondrion* 12: 248–257, 2012.
67. **Zsurka G, Ormos J, Ivanyi B, Turi S, Endreffy E, Magyari M, Sonkodi S, Venetianer P.** Mitochondrial mutation as a probable causative factor in familial progressive tubulointerstitial nephritis. *Hum Genet* 99: 484–487, 1997.

Downloaded on July 3, 2014. The Journal of Clinical Investigation. More information at www.jci.org/articles/view/69000

Related Commentary, page 4996

Research article

# *ADCK4* mutations promote steroid-resistant nephrotic syndrome through $CoQ_{10}$ biosynthesis disruption

Shazia Ashraf,[1] Heon Yung Gee,[1] Stephanie Woerner,[2,3] Letian X. Xie,[4] Virginia Vega-Warner,[5] Svjetlana Lovric,[1] Humphrey Fang,[1] Xuewen Song,[6] Daniel C. Cattran,[6] Carmen Avila-Casado,[7] Andrew D. Paterson,[8] Patrick Nitschké,[9] Christine Bole-Feysot,[10] Pierre Cochat,[11] Julian Esteve-Rudd,[12] Birgit Haberberger,[13,14] Susan J. Allen,[5] Weibin Zhou,[5] Rannar Airik,[1] Edgar A. Otto,[5] Moumita Barua,[15] Mohamed H. Al-Hamed,[16] Jameela A. Kari,[17] Jonathan Evans,[18] Agnieszka Bierzynska,[19] Moin A. Saleem,[19] Detlef Böckenhauer,[20] Robert Kleta,[20] Sherif El Desoky,[17] Duygu O. Hacihamdioglu,[21] Faysal Gok,[21] Joseph Washburn,[22] Roger C. Wiggins,[23] Murim Choi,[24,25] Richard P. Lifton,[24,25] Shawn Levy,[26] Zhe Han,[27] Leonardo Salviati,[28] Holger Prokisch,[13,14] David S. Williams,[12] Martin Pollak,[11] Catherine F. Clarke,[4] York Pei,[6] Corinne Antignac,[2,3,29] and Friedhelm Hildebrandt[1,30,31]

[1]Division of Nephrology, Department of Medicine, Boston Children's Hospital, Harvard Medical School, Boston, Massachusetts, USA. [2]Inserm U983, Necker Hospital, Paris, France. [3]Université Paris Descartes, Sorbonne Paris Cité, Imagine Institute, Paris, France. [4]Department of Chemistry and Biochemistry and Molecular Biology Institute, UCLA, Los Angeles, California, USA. [5]Department of Pediatrics, University of Michigan, Ann Arbor, Michigan, USA. [6]Division of Nephrology, University Health Network, and University of Toronto, Toronto, Ontario, Canada. [7]Department of Pathology, University Health Network, Toronto, Ontario, Canada. [8]Program in Genomic Biology, Hospital for Sick Children, Toronto, Ontario, Canada. [9]Bioinformatics Plateform, Université Paris Descartes, Paris, France. [10]Genomics Plateform, Imagine Institute, Université Paris Descartes, Paris, France. [11]Service de Néphrologie et Rhumatologie Pédiatrique, Centre de référence des maladies rénales rares, Hôpital Femme Mère Enfant, Hospices Civils de Lyon, Bron, France. [12]Jules Stein Eye Institute, UCLA School of Medicine, Los Angeles, California, USA. [13]Institute of Human Genetics, Helmholtz Zentrum Munich, Neuherberg, Germany. [14]Institute of Human Genetics, Klinikum rechts der Isar, Technical University Munich, Munich, Germany. [15]Division of Nephrology, Department of Medicine, Beth Israel Deaconess Medical Center, Boston, Massachusetts, USA. [16]Institute of Genetic Medicine, Newcastle University, Central Parkway, Newcastle upon Tyne, United Kingdom. [17]Pediatrics Department, King Abdulaziz University, Jeddah, Kingdom of Saudi Arabia. [18]Nottingham University Hospitals, Nottingham, United Kingdom. [19]Children's and Academic Renal Unit, University of Bristol, Bristol, United Kingdom. [20]UCL Institute of Child Health and Paediatric Nephrology, Great Ormond Street Hospital, London, United Kingdom. [21]Department of Pediatric Nephrology and Rheumatology, Gülhane Military Academy of Medicine, School of Medicine, Etlik, Ankara, Turkey. [22]Biomedical Research Core Facilities and [23]Department of Internal Medicine, Department of Pathology, and Department of Otolaryngology, University of Michigan, Ann Arbor, Michigan, USA. [24]Department of Genetics, Howard Hughes Medical Institute, and [25]Yale Center for Mendelian Genomics, Yale University School of Medicine, New Haven, Connecticut, USA. [26]HudsonAlpha Institute for Biotechnology, Huntsville, Alabama, USA. [27]Department of Internal Medicine — Molecular Medicine and Genetics, University of Michigan, Ann Arbor, Michigan, USA. [28]Department of Woman and Child Health, University of Padova and Istituto di Ricerca Pediatrica Città della Speranza, Padova, Italy. [29]Assistance Publique – Hôpitaux de Paris, Department of Genetics, Necker Hospital, Paris, France. [30]Department of Human Genetics, University of Michigan, Ann Arbor, Michigan, USA. [31]Howard Hughes Medical Institute, Chevy Chase, Maryland, USA.

**Identification of single-gene causes of steroid-resistant nephrotic syndrome (SRNS) has furthered the understanding of the pathogenesis of this disease. Here, using a combination of homozygosity mapping and whole human exome resequencing, we identified mutations in the aarF domain containing kinase 4 (*ADCK4*) gene in 15 individuals with SRNS from 8 unrelated families. ADCK4 was highly similar to ADCK3, which has been shown to participate in coenzyme $Q_{10}$ ($CoQ_{10}$) biosynthesis. Mutations in *ADCK4* resulted in reduced $CoQ_{10}$ levels and reduced mitochondrial respiratory enzyme activity in cells isolated from individuals with SRNS and transformed lymphoblasts. Knockdown of *adck4* in zebrafish and *Drosophila* recapitulated nephrotic syndrome-associated phenotypes. Furthermore, ADCK4 was expressed in glomerular podocytes and partially localized to podocyte mitochondria and foot processes in rat kidneys and cultured human podocytes. In human podocytes, ADCK4 interacted with members of the $CoQ_{10}$ biosynthesis pathway, including COQ6, which has been linked with SRNS and COQ7. Knockdown of ADCK4 in podocytes resulted in decreased migration, which was reversed by $CoQ_{10}$ addition. Interestingly, a patient with SRNS with a homozygous *ADCK4* frameshift mutation had partial remission following $CoQ_{10}$ treatment. These data indicate that individuals with SRNS with mutations in *ADCK4* or other genes that participate in $CoQ_{10}$ biosynthesis may be treatable with $CoQ_{10}$.**

## Introduction

Nephrotic syndrome (NS) is a chronic kidney disease that is defined by significant proteinuria (>40 mg/m$^2$/h), with resulting hypoalbuminemia, which causes edema (1). NS constitutes the second most frequent cause of end-stage kidney disease (ESKD)

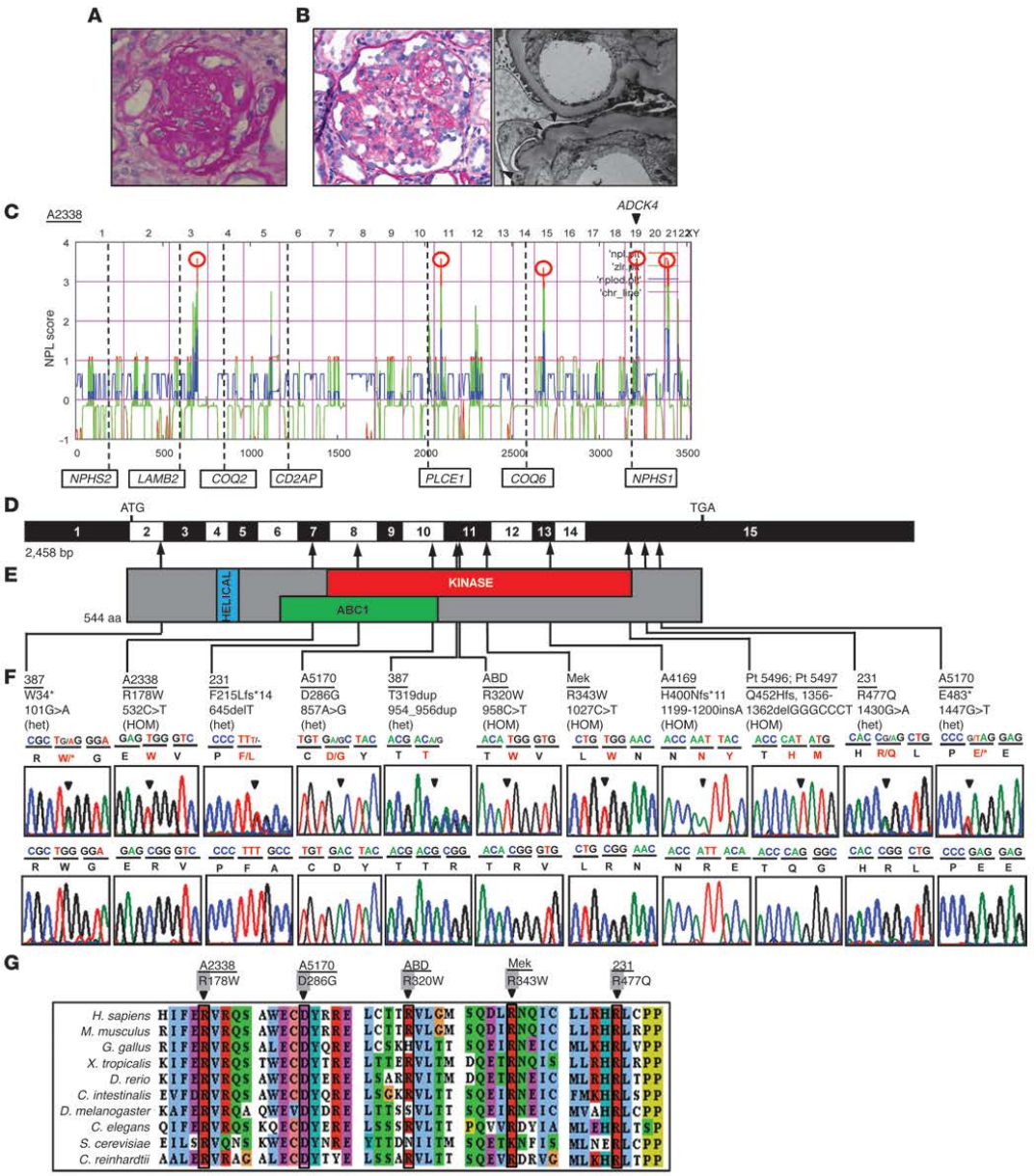
**Authorship note:** Shazia Ashraf and Heon Yung Gee contributed equally to this work.

**Conflict of interest:** The authors have declared that no conflict of interest exists.

**Citation for this article:** *J Clin Invest.* 2013;123(12):5179–5189. doi:10.1172/JCI69000.

Downloaded on July 3, 2014. The Journal of Clinical Investigation. More information at www.jci.org/articles/view/69000





Downloaded on July 3, 2014. The Journal of Clinical Investigation. More information at www.jci.org/articles/view/69000





**Figure 1**
HM and exon capture resequencing reveal *ADCK4* mutations as causes of SRNS. (**A**) Renal histology of individual A2338-21 reveals global glomerulosclerosis by excess PAS staining (red). Original magnification, ×200. (**B**) Renal histology of individual Pt5496 shows cFSGS. PAS staining (left) reveals retraction and collapse of the capillary tuft, with numerous foam cells and groups of hyperplastic and vacuolated visceral epithelial cells. Original magnification, ×40. Electron microscopy image (right) shows foot process effacement (black arrowheads). In addition, capillary basement membranes are thickened and remodeled. Original magnification, ×15,000. (**C**) Nonparametric LOD (log of the odds ratio) (NPL) score profile across the human genome in 2 siblings with SRNS of consanguineous family A2338. Five maximum NPL peaks (red circles) indicate candidate regions of homozygosity by descent. *ADCK4* is positioned (arrowhead) within a peak on chromosome (Chr) 19. Numbers at the bottom of the panels are measured in centimorgan (cM). (**D**) Exon structure of human *ADCK4* cDNA. *ADCK4* contains 15 exons. Positions of start codon (ATG) and of stop codon (TGA) are indicated. (**E**) Domain structure of ADCK4. The helical, ABC1, and kinase domains are depicted by colored bars in relation to encoding exon position. (**F**) Eleven different *ADCK4* mutations in eight families with SRNS. Family numbers and amino acid changes (Table 1) are given above sequence traces. Arrowheads denote altered nucleotides. Lines and arrows indicate positions of mutations in relation to exon D and protein domain E. (**G**) For the 5 missense mutations (p.R178W, p.D286G, p.R320W, p.R343W, and p.R477Q) conservation across evolution of altered amino acid residues is shown.

in children (2, 3). While most children with NS have steroid-sensitive NS, approximately 10%–20% of children and 40% of adults with NS do not achieve sustained remission after glucocorticoid therapy and additional immunosuppressive therapy and enter into ESKD (1). These cases of steroid-resistant NS (SRNS) manifest histologically as focal segmental glomerulosclerosis (FSGS) (4).

Recent discoveries of the single-gene causes of NS have significantly increased our understanding of glomerular filtration barrier physiology and of pathogenic mechanisms of NS (1). To date, more than 9 recessive genes that cause NS if mutated have been identified (5, 6). Overall, these genes account for up to approximately 66% of NS that starts within the first year of life (2). However, monogenic causes of a significant proportion of childhood- or adult-onset NS are still molecularly unsolved. Moreover, recently identified genes are very rare, being mutated in only one family out of hundreds (7). To overcome the limitations posed by the rarity of genes when identifying genes associated with NS, we established a strategy of combining homozygosity mapping (HM) with whole-exome resequencing (WER) (8, 9). Here, we applied this approach to sibling cases of childhood-onset NS and thereby identified mutations of aarF domain containing kinase 4 (*ADCK4*) as a single-gene cause of SRNS.

## Results

*Mutations in ADCK4 cause SRNS.* To identify further single-gene causes of SRNS, we performed HM followed by WER in a group of individuals with histology that revealed FSGS (Figure 1, A and B). In a family (A2338) of Arab origin, 2 siblings had early-onset SRNS and renal histology that revealed glomerulosclerosis (Figure 1A). HM in both affected siblings yielded 5 regions of homozygosity by descent with a cumulative genomic length of approximately 115 Mb, none of which coincided with any of 7 common recessive causes of SRNS (Figure 1C). The presence of homozygosity strongly suggested a recessive causative gene, and the lack of overlap with known NS gene loci suggested that the gene to be identified in this family would be novel. By WER in one of the affected siblings from family A2338, we detected a homozygous missense mutation (c.532C>T;p.R178W) in *ADCK4* (NM_024876.3) on chromosome 19, encoding ADCK4. This variant was the only homozygous variant remaining from the variant filtering process (Supplemental Table 1; supplemental material available online with this article; doi:10.1172/JCI69000DS1). The mutation (p.R178W) alters an amino acid residue conserved throughout evolution from *Chlamydomonas reinhardtii*. It segregated with the affected status in this family and was absent from >190 ethnically matched healthy control individuals and from >8,600 European controls in the Exome Variant Server (http://evs.gs.washington.edu/EVS/).

WER in an addtional 6 different families with SRNS also yielded 9 additional mutations in *ADCK4* (3 families with homozygous mutations and 3 families with compound heterozygous mutations) (Figure 1, D–G, and Table 1). WER of one affected individual in family 386 identified compound heterozygous mutations: c.101G>A;p.W34* and c.954_956dup;p.T319dup. We identified compound heterozygous mutations (c.645delT;p.F215Lfs*14 and c.4130G>A;p.R477Q in *ADCK4*) in 2 affected siblings from family 231 from Algeria (Figure 1F and Table 1). The missense mutation (p.R477Q) altered an amino acid residue that was continually conserved from *C. reinhardtii* to humans (Figure 1G). In a family (A5170) of 3 affected siblings, WER revealed compound heterozygous mutations: c.857A>G;p.D286G and c.1447G>T;p.E483* in *ADCK4* (Figure 1F and Table 1). This missense mutation (p.D286G) altered an amino acid residue that is continually conserved from *C. reinhardtii* to humans (Figure 1G). One of the homozygous mutations (p.R320W) in *ADCK4* was found in 2 affected siblings from the ABD family from Tunisia in an amino acid residue continually conserved throughout evolution from *C. reinhardtii* (Figure 1, F and G, and Table 1). In another family (Mek) from Morocco, we discovered a missense mutation c.1027C>T;p.R343W in this gene in 2 affected siblings (Figure 1F and Table 1). The amino acid residue R343 has been conserved from *C. reinhardtii* to humans (Figure 1G). The other homozygous mutation was an out-of-frame deletion of 7 bases (p.Q452Hfs) in exon 15 of *ADCK4* in 2 affected siblings from a family from India, with renal histology showing collapsing FSGS (cFSGS) (Figure 1F and Table 1).

To discover additional mutations in *ADCK4*, we then performed multiplex barcoded array-based PCR amplification and next-generation sequencing in an additional 400 individuals with SRNS (10). In an individual with SRNS (A4169-21), we detected a homozygous insertion of an "A" (H400Nfs*11) in exon 13 of *ADCK4* (Figure 1F and Table 1). Sequences of primers used to amplify exons and exon-intron boundaries of *ADCK4* are listed in Supplemental Table 2. All 15 affected individuals of the 8 families with recessive mutations in *ADCK4* had SRNS. Renal biopsy revealed FSGS in most cases. Interestingly, in 3 affected individuals (1146, Pt5497, and Pt5497), renal histology showed cFSGS (Figure 1B and Table 1). Moreover, the individual A4169-21, who has a homozygous truncating allele, showed the earliest onset of SRNS and also presented with developmental delay (Table 1).

*ADCK4* spans 12 kb on chromosome 19q13.1. Up to 17 different putative alternatively spliced *ADCK4* transcripts encoding different proteins have been proposed (AceView; http://www.ncbi.nlm.nih.gov/ieb/research/acembly/index.html). The longest transcript of *ADCK4* (NM_024876.3) has 14 coding exons (Figure 1D) and encodes a 60.1-kDa protein (NP_079152.3, isoform a, 544

Downloaded on July 3, 2014. The Journal of Clinical Investigation. More information at www.jci.org/articles/view/69000



**Table 1**
Recessive *ADCK4* mutations detected in individuals with SRNS

| Family–individual | Ethnic origin | Parental consanguinity | Nucleotide alteration(s)[A] | Alteration(s) in coding sequence | Exon (segregation) | Amino acid sequence conservation | Age at onset | Kidney disease | Age at ESKD | Treatment and renal transplantation | Histology (at age) | Extrarenal manifestations |
|---|---|---|---|---|---|---|---|---|---|---|---|---|
| 387 | European | No | c.101G>A | p.W34* | 2 (het, ND) | NA | | | | | | |
| 387–21 | | | c.954_956dup | p.T319dup | 11 (het, ND) | NA | 10 yr | SRNS | 12 yr | PNL, tacrolimus, first transplant (14 yr) | FSGS (10 yr) | No |
| A2338 | Arab | Yes | c.532C>T | p.R178W | 7 (HOM, M, P) | *C. reinhardtii* | | | | | | |
| A2338–21 | | | | | | | 7 yr | SRNS | 7 yr | First transplant (10 yr) | GS (7 yr) | NA |
| A2338–22 | | | | | | | 13 yr | SRNS | ND | First transplant (15 yr) | FSGS (13 yr) | NA |
| 231 | Algerian | No | c.645delT | p.F215Lfs*14 | 8 (het, P) | NA | | | | | | |
| | | | c.1430G>A | p.R477Q | 15 (het, M) | *C. reinhardtii* | | | | | | |
| 231–21 | | | | | | | 13 yr | SRNS | 13 yr | First transplant (15 yr) | FSGS (15 yr) | NA |
| 231–22 | | | | | | | 12 yr | SRNS | 12 yr | First transplant (13 yr) | FSGS (13 yr) | NA |
| A5170 | ND | No | c.857A>G | p.D286G | 10 (het, P) | *C. reinhardtii* | | | | | | |
| | | | c.1447G>T | p.E483* | 15 (het, M) | NA | | | | | | |
| A5170–21 | | | | | | | 14 yr | SRNS | 15 yr | CsA; first transplant (18 yr) | FSGS (15 yr) | HT, goiter |
| A5170–22 | | | | | | | 3 yr | SRNS | ND | ND | FSGS (13 yr) | ND |
| A5170–23 | | | | | | | 9 yr | SRNS | ND | ACE-I | FSGS (11 yr) | ND |
| ABD | Tunisian | Yes | c.958G>T | p.R320W | 11 (HOM, M, P) | *C. reinhardtii* | | | | | | |
| ABD–21 | | | | | | | 12 yr | SRNS | 17 yr | ACE-I; first transplant (17 yr) | FSGS (12 yr) | Goiter |
| ABD–22 | | | | | | | 20 yr | SRNS | 23 yr | No treatment (discovered in ESKD) | ND | ND |
| Mek | Moroccan | Yes | c.1027C>T | p.R343W | 11 (HOM, M, P) | *C. reinhardtii* | | | | | | |
| Mek–1145 | | | | | | | 20 yr | SRNS | 20 yr | ND | ND | DCM |
| Mek–1146 | | | | | | | 18 yr | SRNS | 19 yr | PNL | cFSGS (19 yr) | ND |
| A4169 | Turkish | Yes | c.1199-1200insA | p.H400Nfs*11 | 13 (HOM, M, P) | NA | | | | | | |
| A4169–21 | | | | | | | <1 yr | SRNS | ND | PNL, ACE-I, CP-R, $CoQ_{10}$[B] | FSGS (5 yr) | Neurologic developmental delay |
| | Indian | Yes | c.1356_1362del | p.Q452Hfs | 15 (HOM, M, P) | NA | | | | | | |
| | | | GGGCCCT | | | | | | | | | |
| Pt5496 | | | | | | | 16 yr | SRNS | | GsA, ACE-I | cFSGS (18 yr) | ND |
| Pt5497 | | | | | | | 21 yr | SRNS | | ACE-I | cFSGS (22 yr) | ND |

[A]All mutations were absent from >60 ethnically matched healthy control individuals and from >8,600 European controls in the Exome Variant Server. [B]Treatment-sensitive case. ACE-I, ACE inhibitor; $CoQ_{10}$, treatment with $CoQ_{10}$; CP-R, cyclophosphamide resistant; CsA, cyclosporine A; DCM, dilated cardiomyopathy; GS, global glomerulosclerosis; het, heterozygous in affected individual; HOM, homozygous in affected individual; HT, hypertension; M, heterozygous mutation identified in mother; NA, not applicable; ND, no data or DNA available; P, heterozygous mutation identified in father; PNL, prednisolone.

Downloaded on July 3, 2014. The Journal of Clinical Investigation. More information at www.jci.org/articles/view/69000



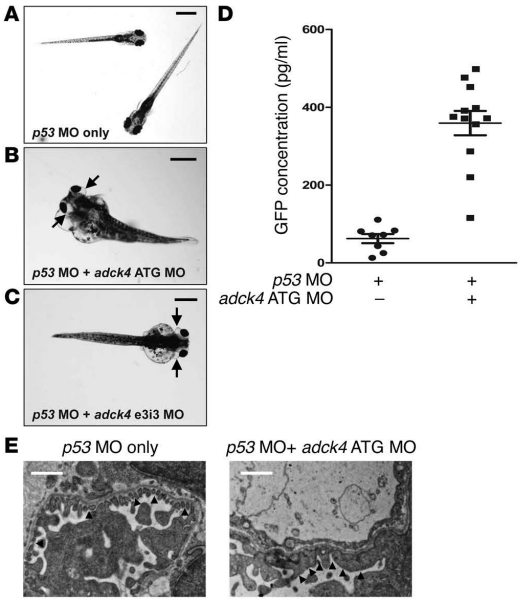



**Figure 2**
Functional analysis of *adck4* knockdown in zebrafish. (**A**) Control zebrafish were injected with *p53* MO (0.2 mM) as a control to minimize nonspecific MO effects. *p53* MO was injected into fertilized eggs at the 1- to 4-cells stage and did not produce any phenotype up to 168 hpf ($n$ >100). Scale bar: 0.5 mm. (**B**) Zebrafish coinjected with *adck4* ATG MO (0.2 mM) targeting the translation initiation site of zebrafish *adck4* and with *p53* MO. At 120 hpf, *adck4* morphants display the nephrosis phenotype of periorbital edema (arrows) and total body edema in 54.1% (193 out of 357) of embryos. (**C**) Zebrafish coinjected with *adck4* e3i3 MO (0.2 mM) targeting the donor site of intron 3 of zebrafish *adck4* and with *p53* MO. At 120 hpf, *adck4* morphants display the nephrosis phenotype (arrows) in 48.3% (274 out of 567) of embryos. Scale bar: 1 mm (**B** and **C**). (**D**) Proteinuria assay by ELISA against a fusion protein of vitamin D–binding protein and GFP in *l-fabp*::VDBP-GFP transgenic zebrafish. Note that knockdown of *adck4* causes significant proteinuria compared with that in control fish injected with p53 MO only. ($P$ < 0.001). Symbols indicate each measurements; horizontal bars indicate the average; data are presented with the average ± SEM denoted by 3 horizontal lines. (**E**) Electron microscopic ultrastructure of GBM and podocyte foot processes in *p53* MO control and *adck4* morphant zebrafish. In the control zebrafish, the foot processes are regularly spanned by slit diaphragms (black arrowheads). In contrast, the foot processes of the morphants are effaced and disorganized (black arrowheads). Scale bar: 2 μm.

amino acids) (Figure 1E). Analysis of the ADCK4 amino acid sequence yielded a helical domain and an ABC1 domain and a kinase domain (Figure 1E). ADCK4 has high sequence similarity to Abc1/Coq8 and is evolutionarily conserved to *Ciona intestinalis* (sea squirt) (XP_002126787.1), *Drosophila melanogaster* (NP_572836.1), *Caenorhabditis elegans* (NP_498014.2), *C. reinhardtii* (XP_001702520.1), and *Saccharomyces cerevisiae* (NP_011396.1), suggesting a conserved function of the domain assembly.

*Knockdown of adck4 in animal models recapitulates the nephrosis phenotype.* To further validate the causative role of *ADCK4* for the SRNS phenotype, we performed knockdown of the *ADCK4* ortholog in zebrafish. For zebrafish gene knockdown experiments, we used a *p53* morpholino oligonucleotide (MO) as a negative control to minimize nonspecific apoptotic MO effects (11). *p53* MO injection into fertilized zebrafish eggs at the 1- to 4-cell stage did not produce any phenotype through 168 hours postfertilization (hpf) (Figure 2A). However, coinjection of the *p53* control MO with an MO targeting the translation initiation site of zebrafish *adck4* caused the nephrosis phenotype of periorbital and total body edema, reminiscent of signs of NS in humans, in 54.1% of embryos at 120 hpf (Figure 2B). Similar results were obtained with 2 MOs targeting the splice donor site (e2i2 MO and e3i3 MO) (Figure 2C; Supplemental Figure 1, A–D; and Supplemental Table 3). The summary of edema phenotype observed in *adck4* morphants is displayed in Supplemental Figure 1E. The proteinuric effect of the *adck4* MO was confirmed using an established zebrafish proteinuria assay (12) by ELISA against a fusion protein of vitamin D-binding protein and GFP in *l-fabp*::VDBP-GFP transgenic zebrafish (Figure 2D). We then performed transmission electron microscopy imaging of zebrafish to permit a more direct evaluation of glomerular structures of morphants. When compared with the control (Figure 2E), we observed upon knockdown of *adck4* characteristic alterations of nephrosis (Figure 2E). These included podocyte foot process effacement and disorganization, rarefaction of slit membranes, and disorganization of the glomerular basement membranes in zebrafish glomeruli (Figure 2E, black arrowheads in right panel), as previously described in *plce1* knockdown (13).

In addition, we performed knockdown of *Drosophila coq8* (*dcoq8*) in *Drosophila* pericardial nephrocytes, which share remarkable similarities to the glomerular podocytes (14). The protein uptake assay showed that knockdown of *dcoq8* in nephrocytes reduced the uptake ability of a secreted fusion protein of rat atrial natriuretic factor (ANF) and GFP, suggesting that *dcoq8* is required for nephrocyte function in *Drosophila* (Supplemental Figure 2, A and B). The amino acid of dCoq8 has 53% sequence identity to both ADCK3 and ADCK4 *Drosophila* (Supplemental Figure 2C).

*ADCK4 localizes to the mitochondria and foot processes in podocytes.* Since most gene products that are defective in SRNS are located in glomerular podocytes, we examined the subcellular localization of ADCK4 in adult rat kidney by immunofluorescence (IF). Podocytes, as identified by expression of nuclear WT1, expressed ADCK4 at high levels in cell bodies and primary processes (Figure 3A). ADCK4 also partially colocalized with cytochrome oxidase subunit VI (COXIV) and mitochondrially encoded cytochrome c oxidase 1 (MTCO1), 2 known mitochondrial marker proteins, suggesting that ADCK4 partly localizes to the mitochondria in renal glomeruli (Figure 3, B and C). In addition, ADCK4 is detected in proximal tubules and collecting ducts (Supplemental Figure 3, A and B). To further investigate the localization of ADCK4, we performed immunogold electron microscopy in adult rat kidneys. In podocytes, ADCK4 was predominantly detected at foot processes (Figure 3D). The specificity of the anti-ADCK4 antibody used in the IF and immunogold electron microscopy studies is demonstrated in Supplemental Figure 4. We also examined the

Downloaded on July 3, 2014. The Journal of Clinical Investigation. More information at www.jci.org/articles/view/69000



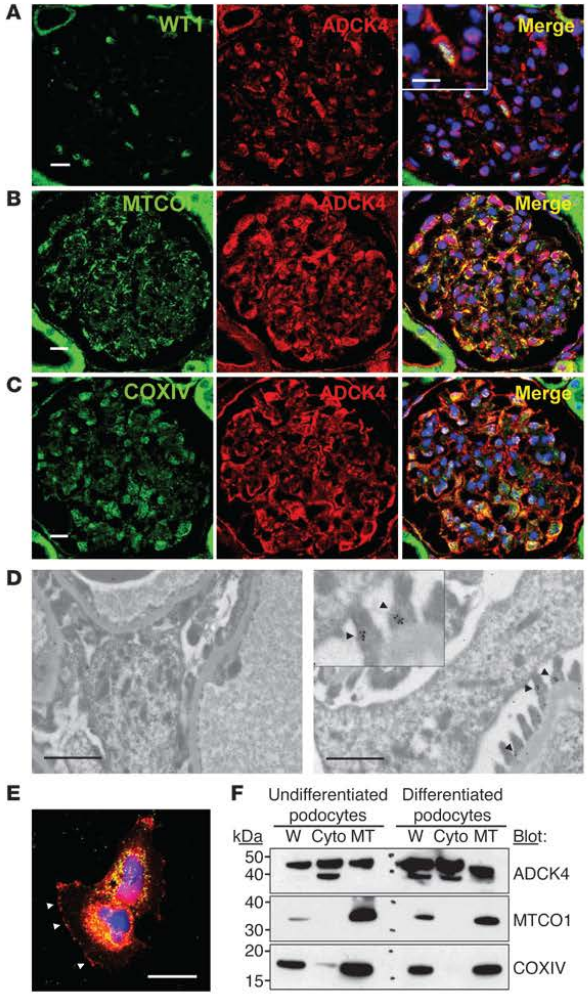



**Figure 3**
ADCK4 localizes to the mitochondria and cytoplasm of podocytes in adult rat glomeruli and also in cultured human podocytes. (**A**–**C**) Coimmunofluorescence of ADCK4 with (**A**) WT1 as well as (**B**) MTCO1 and (**C**) COXIV in adult rat glomeruli. ADCK4 partially colocalizes to mitochondria with the 2 mitochondrial markers COXIV and MTCO1. Scale bar: 10 μm. (**D**) Immunogold electron microscopy of adult rat kidney displays localization of ADCK4 (black arrowheads) at podocyte foot processes of glomeruli. A control without a primary antibody is shown on the left. Scale bar: 1 μm; ×2.5 (inset). (**E**) Podocytes were transfected with ADCK4-RFP and stained with an anti-COXIV antibody. ADCK4 partially colocalizes to mitochondria with COXIV. Note that ADCK4 also localizes along the plasma membrane (white arrowheads) in podocytes. Scale bar: 25 μm. (**F**) Subcellular fractionation of ADCK4 in undifferentiated and differentiated podocytes. Mitochondrial and cytosol fractions were prepared and immunoblotted for ADCK4, MTCO1, and COXIV, respectively. Each lane was loaded with 50 μg protein. Note that ADCK4 is present in both mitochondrial (marked by MTCO1 and COXIV), and cytosolic fractions in both undifferentiated and differentiated podocytes. W, whole cell lysates; Cyto, cytosol fraction; MT, mitochondrial fraction.

expression of ADCK4 in cultured podocytes by IF. The overexpressed ADCK4–red fluorescent protein (ADCK4-RFP) partially colocalized to mitochondria, and we also noticed that ADCK4-RFP localized to ruffles (Figure 3E) of podocytes, the equivalents of foot processes (Figure 3E and Supplemental Figure 3, C and D). Consistent with data from the cellular fractionation of cultured podocytes, these findings showed that ADCK4 is endogenously present in both the cytosolic and mitochondrial fractions (Figure 3F). Thus, in addition to its role in the mitochondrial respiratory chain, ADCK4 seems to have a very localized function at ruffles and foot processes of podocytes.

*ADCK4 is enriched in podocytes and interacts with COQ6 and COQ7.* By quantitative real-time PCR, we showed that, although ADCK3 expression exceeds that of ADCK4 in most human tissues (Supplemental Figure 5), ADCK4 is enriched in both differentiated and undifferentiated human podocytes (Figure 4A).

Furthermore, we performed coimmunoprecipitation studies in cultured podocytes to examine whether ADCK4 interacts with other proteins like COQ6 and COQ7 that are involved in the coenzyme $Q_{10}$ ($CoQ_{10}$) biosynthesis pathway. COQ6 was overexpressed in podocytes, and coimmunoprecipitation was performed. Interestingly, the protein complex precipitated by COQ6 included COQ7 and ADCK4 (Figure 4B). We also confirmed that ADCK4 and COQ6 interact endogenously in lysates from differentiated podocytes (Figure 4C).

*Levels of $CoQ_{10}$ are decreased in individuals with ADCK4 mutations.* To investigate whether the defect in *ADCK4* has any effect on $CoQ_{10}$ biosynthesis, we measured the total $CoQ_{10}$ contents in EBV-transformed lymphoblasts or cultured skin fibroblasts derived from individuals from the A2338, A4169, and Pt5496/Pt5497 families, in which *ADCK4* mutations were detected. In the case of the A2338 and A4169 families, the total $CoQ_{10}$ was found to be strongly reduced in the affected siblings, A2338-21 (81.92 ± 18.45 pmol/mg protein) and A2338-22 (75.99 ± 34.60 pmol/mg protein), who have a homozygous missense mutation (p.R178W), and in an affected individual, A4169-21 (59.12 ± 9.57 pmol/mg protein), who has a homozygous frameshift mutation (p.H400Nfs*11) (Figure 5A). In contrast, the unaffected individuals, A2338-26 and A2338-27, who have both wild-type alleles, had 784.40 ± 164.10 and 758.00 ± 286.60 pmol/mg protein of total $CoQ_{10}$, respectively (Figure 5A).

Likewise, in the case of Pt5496 and Pt5497, we confirmed similar results and found that the total $CoQ_{10}$ was reduced in fibroblasts (20.11 ± 3.41 pmol/mg protein for #50552 and 19.75 ± 4.63 pmol/mg protein for #50553) from these individuals, who have a homozygous frameshift mutation (p.Q452Hfs), and normal in fibroblasts (64.33 ± 11.92 pmol/mg protein for #50551 and 83.04 ± 20.64 pmol/mg protein for #50550) from the unaffected parents (Figure 5B).

In addition, we examined mitochondrial respiratory enzyme activity in fibroblasts by measuring maximal uncoupled oxygen

Downloaded on July 3, 2014. The Journal of Clinical Investigation. More information at www.jci.org/articles/view/69000



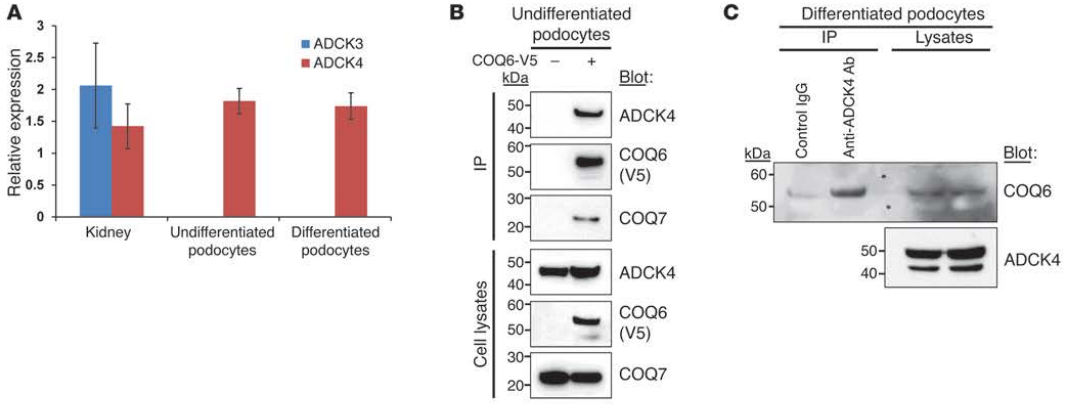



**Figure 4**

ADCK4 is enriched in podocytes and interacts with COQ6 and COQ7. (**A**) Relative expression of ADCK3 and ADCK4 in kidney tissue and podocytes, as measured by quantitative real-time PCR. Error bars indicate SD of 4 experiments. (**B**) Interaction of ADCK4 with COQ6 and COQ7 in cultured human podocytes. A C-terminally V5-tagged COQ6 construct (COQ6-V6) was transfected into the undifferentiated cultured podocytes. Coimmunoprecipitation was performed using an anti-V5 antibody and then blotting was performed with antibodies for ADCK4, COQ6, and COQ7. Note that the protein complex precipitated by COQ6 includes COQ7 and ADCK4. (**C**) Interaction of endogenous ADCK4 and COQ6 in differentiated podocytes. Podocyte lysates were precipitated with an anti-ADCK4 antibody or a control rabbit IgG. The precipitated proteins were separated by SDS-PAGE and blotted with an anti-COQ6 antibody.

consumption rate (OCR), which shows the $CoQ_{10}$ transfer of electrons from mitochondrial complex I and complex II to complex III. Maximal OCR was significantly reduced in fibroblasts from Pt5496 and Pt5497 compared with that in fibroblasts from controls or their healthy parents (Figure 5C).

*Loss of ADCK4 does not induce proliferation or apoptosis in fibroblasts or cultured podocytes.* We had previously reported that knockdown of COQ6 can cause apoptosis in podocytes (7). Since ADCK4 interacts with COQ6, we investigated the effect of loss of ADCK4 on cell proliferation and apoptosis in fibroblasts from individuals with a homozygous frameshift ADCK4 mutation (Pt5496 and Pt5497) and their healthy parents as well as in cultured podocytes. We found that fibroblasts (#50552 and #50553) from affected individuals did not show any difference in cell proliferation or apoptosis induced by hydrogen peroxide compared to parental fibroblasts (#50550 and #50551) (Supplemental Figure 6, A and B). Furthermore, in contrast to COQ6, knockdown of *ADCK4* in podocytes did not affect proliferation or apoptosis (Supplemental Figure 6, C and D).

*ADCK4 knockdown reduces podocyte migration, which is reversed by the addition of $CoQ_{10}$.* We next examined the effect of ADCK4 knockdown on podocyte migration using the xCELLigence system, which monitors cell migration in real-time (Figure 6). We found that migration of podocytes was reduced by knockdown of ADCK4 (Figure 6A). Because $CoQ_{10}$ treatment had resulted in improvement of the NS phenotype in an individual with a mutation in *ADCK4*, we tested the effect of the addition of $CoQ_{10}$ on podocyte migration. Interestingly, we found that the addition of $CoQ_{10}$ reversed the decreased migratory phenotype caused by ADCK4 knockdown (Figure 6, A and B). Similar results were obtained when 2 additional siRNAs were used for knockdown of ADCK4 in cultured human podocytes (*ADCK4* siRNAs #5 and #6) (Figure 6, C and D). We further found that decreased migration, which was caused by an *ADCK4* siRNA (*ADCK4* siRNA #6), was reversed when wild-type mouse ADCK4 was transfected into podocytes (Figure 6C). This result also confirmed that the effect on podocyte migration was caused by *ADCK4* loss of function.

## Discussion

Here, we describe the discovery of mutations in *ADCK4* as causes of SRNS. We have shown that ADCK4 is expressed in podocytes and localizes to mitochondria and foot processes and interacts with COQ6 endogenously. Knockdown of ADCK4 in podocytes reduced their migration phenotype, which could be reversed by overexpression of siRNA-resistant ADCK4 or, most importantly, by the addition of $CoQ_{10}$. By knockdown of *adck4* in zebrafish, we clearly demonstrated that the function of this gene is necessary to avoid the NS disease phenotype. The fact that ADCK4 has high sequence similarity with ADCK3, which was previously reported to be associated with $CoQ_{10}$ deficiency (15), and the fact that cells from affected individuals with *ADCK4* mutations (families A2338, A4169, and Pt5496/Pt5497) had reduced total $CoQ_{10}$ content suggests that ADCK4 is also involved in $CoQ_{10}$ biosynthesis.

$CoQ_{10}$, also known as ubiquinone, is a lipid-soluble component of virtually all cell membranes, in which it is thought to play an important antioxidant role as well as to transport electrons from complexes I and II to complex III in the respiratory chain of the mitochondrial inner membrane (16). The biochemical pathway of $CoQ_{10}$ biosynthesis is complex and has not been completely elucidated. Primary $CoQ_{10}$ deficiencies due to mutations in ubiquinone biosynthetic genes (*COQ2*, *COQ4*, *COQ6*, *PDSS1*, *PDSS2*, and *ADCK3*) have been identified (7, 15, 17–26). Clinical manifestations of $CoQ_{10}$ deficiency are variable. For example, individuals with *COQ2* mutations present with phenotypes ranging from isolated NS to catastrophic neonatal multisystem disorder with encephalomyopathy and renal involvement to a recently described multiple-system atrophy (20, 23–27). In

Downloaded on July 3, 2014. The Journal of Clinical Investigation. More information at www.jci.org/articles/view/69000



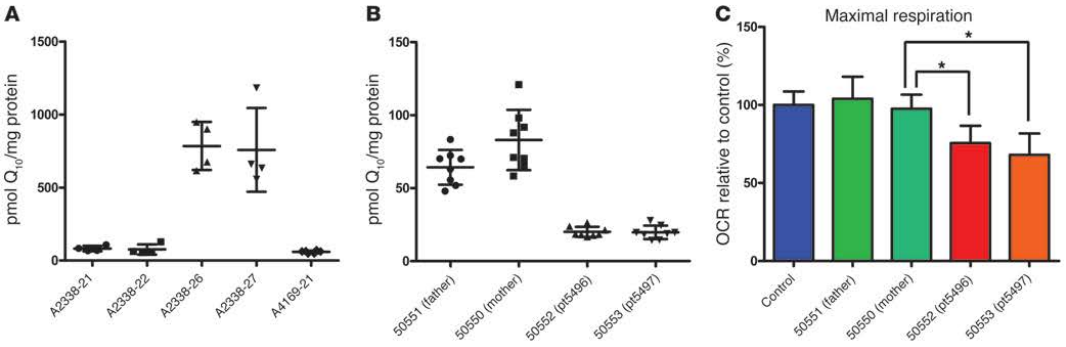



**Figure 5**

$CoQ_{10}$ content in EBV-transformed lymphoblasts and fibroblasts from SRNS families with mutations in *ADCK4*. (**A**) Scatter plot showing the total $CoQ_{10}$ content in EBV-transformed lymphoblasts derived from either healthy or affected individuals from the A2338 and A4169 families. Individuals A2338-21, A2338-22, and A4169-21 are affected with SRNS, while A2338-26 and A2338-27 have both wild-type alleles. The content of $CoQ_{10}$ is presented with the average ± SD denoted by 3 horizontal lines ($n = 4$; except $n = 6$ for A4169-21). The content from A2338-26 is significantly higher than the CoQ10 content from A2338-21, A2338-22, and A4169-21 (multiple comparison, $P < 0.0001$). Symbols indicate individual lymphoblasts; horizontal bars indicate the average. (**B**) Scatter plot showing the total $CoQ_{10}$ content in fibroblasts derived from either healthy parents or affected individuals (Pt5496 and Pt5497). The content of $CoQ_{10}$ is presented with the average ± SD denoted by 3 horizontal lines ($n = 8$). $CoQ_{10}$ content from #50551 is statistically lower than $CoQ_{10}$ content from #50550 (multiple comparison, $P = 0.0134$) and significantly higher than the $CoQ_{10}$ contents from #50552 and #50553 (multiple comparison, $P < 0.0001$). Symbols indicate individual fibroblasts; horizontal bars indicate the average. (**C**) In vivo maximal uncoupled OCR over the whole respiratory chain, including the $Q_{10}$ transfer of electrons from mitochondrial complex I and complex II to complex III. Maximal respiration was significantly reduced in fibroblasts from Pt5496 and Pt5497 compared with that in control fibroblasts. Data shown are mean ± SD ($n > 10$). *$P < 0.001$.

addition, *COQ6* (7) and *PDSS2* (19) have also been implicated in the cause of SRNS.

We as well as Montini et al. have shown previously that the individuals affected with SRNS due to mutations in $CoQ_{10}$ biosynthesis pathway genes like *COQ2* and *COQ6* can be treated with the innocuous food supplement $CoQ_{10}$ (7, 28). $CoQ_{10}$ deficiency in individuals with *ADCK4* mutations thus raises the possibility of supplementation therapy. So far, only one individual (A4169-21) with *ADCK4* mutation has been treated with $CoQ_{10}$ (15 mg/kg/d) for over 4 years. He was first treated with intravenous methylprednisolone followed by 2 mg/kg/d prednisolone over 10 weeks without achieving remission of NS. Subsequently, he was treated with 2 mg/kg/d cyclophosphamide for 3 months. The treatment resulted in partial remission, but treatment had to be stopped because of infections. Treatment with $CoQ_{10}$ was commenced at 1 year of age, giving 100 mg/d $CoQ_{10}$ orally together with 5 mg of prednisolone every other day. Then, the edema disappeared and proteinuria decreased significantly. The individual is currently being treated with $CoQ_{10}$ (15 mg/kg/d) with captopril (12.5 mg/d). Even though the effectiveness of $CoQ_{10}$ treatment cannot be generalized for individuals with *ADCK4* mutations at the moment based on this single case, we still think that the identification of molecular defects of $CoQ_{10}$ biosynthesis is important because they may represent forms of SRNS that are treatable by administration of $CoQ_{10}$.

ADCK3 and ADCK4 are highly similar members of an ancient atypical kinase family and appear to result from gene duplication in vertebrates (15). The yeast Coq8/Abc1 is required for CoQ biosynthesis (29) and is essential for the organization of high-molecular-mass Coq polypeptide complex and for phosphorylated forms of the Coq3, Coq5, and Coq7 polypeptides that perform methylation and hydroxylation steps in CoQ biosynthesis (30, 31). Considering their similarity, it is interesting that mutations in *ADCK3* result in cerebellar ataxia and seizures without renal involvement (15, 21), whereas mutations in *ADCK4* cause SRNS mostly without neurological symptoms. Currently, there is no clear explanation for this; however, this may be partially due to their differential tissue expression (Figure 4A and Supplemental Figure 5). Xie et al. previously showed that ADCK3 can rescue yeast *coq8* mutants and restore phosphorylated forms of yeast Coq polypeptides (30), but the same group observed that expression of ADCK4 failed to rescue *coq8* mutants (data not shown). On the other hand, knockdown of *Dcoq8*, which has 53% amino acid identity to both ADCK3 and ADCK4, caused defects in nephrocyte function (Supplemental Figure 2). Overall, these results suggest that ADCK3 and ADCK4 are independently required for synthesis of CoQ, yet retain distinct functions, a difference that may have evolved in vertebrates, and that ADCK3 may be closer to yeast Coq8.

cFSGS is defined morphologically by the presence of hyperplastic and hypertropic podocytes overlying collapsed capillary loops within glomerular tufts (32). Interestingly, the histology of affected individuals (1146, Pt5496, and Pt5497) with *ADCK4* mutations showed cFSGS. In addition, mutant *kd/kd* mice, which have a missense mutation in *Pdss2* and present with isolated nephropathy, have features of cFSGS (33). Therefore, it will be important to investigate whether nephropathy resulting from $CoQ_{10}$ deficiency results in cFSGS, because this may be a phenotypic criterion with which to choose individuals with SRNS that should be screened for genes involved in $CoQ_{10}$ biosynthesis, such as *COQ2*, *COQ6*, *PDSS2*, and *ADCK4*. To answer this, it is necessary to investigate more SRNS cases resulting from $CoQ_{10}$ deficiency. In addition, knockout animal models for *Coq2*, *Coq6*, and *Adck4* will be helpful.

Downloaded on July 3, 2014. The Journal of Clinical Investigation. More information at www.jci.org/articles/view/69000



*Podocyte migration and proliferation assay.* Real-time migration assays were performed using the xCELLIgence system (ACEA Biosciences) according to the manufacturer's instructions. For migration assays, 24 hours after transfection, $4 \times 10^4$ cells were plated with serum-free media in the upper chamber of the CIM-plate 16 (ACEA Biosciences). The lower chambers were filled with 10% FBS for chemoattraction or with serum-free media. For proliferation assays, $4 \times 10^4$ cells were plated with serum-free media in the E-plate 16 (ACEA Biosciences). The data obtained were analyzed with RTCA software. Results are presented as the time versus cell index curve.

*Zebrafish studies.* Zebrafish (*Danio rerio*) were maintained and reared as described previously (12). Approval for zebrafish research was obtained from the University of Michigan and the Boston Children's Hospital Committees on the Use and Care of Animals. MOs were injected into the AB* wild-type strain for phenotype analysis of morphants and transmission electron microscopy. The proteinuria assays were performed using *l-fabp*::VDBP-GFP transgenic fish and the GFP ELISA Kit (Cell Biolabs) as described previously (12).

*$CoQ_{10}$ measurements.* Cells (approximately 0.1 g) were thawed on ice and resuspended in 1.5 ml phosphate-buffered saline (0.14 M NaCl, 12.0 mM $NaH_2PO_4$, 8.1 mM $Na_2HPO_4$, pH 7.4), followed by homogenization with a polytron (Kinematica PT 2500E) for 1 minute at 15,300 *g* on ice. Lipid extracts were prepared by addition of 1.2 ml methanol, followed by 1.8 ml petroleum ether. Diethoxy-$CoQ_{10}$ served as an internal standard (39). A typical standard curve contains 5 standards with 7.2 pmol, 20 pmol, 72 pmol, 140 pmol, and 400 pmol of $CoQ_{10}$, respectively. Standard curve samples and experimental samples shared identical extractions. Each of the extraction tubes were vortexed for 45 seconds. The upper layer was removed, and the lower aqueous phase was reextracted with 1.8 ml petroleum ether. Nitrogen gas dried the combined organic phase, and 200 µl ethanol dissolved the dried lipids (USP, Apaer Alcohol and Chemical Co.). A binary HPLC solvent delivery system with a Luna Phenyl-Hexyl column (particle size 3 µm, 50 × 2.00 mm; Phenomenex) coupled with an Applied Biosystems 4000 QTRAP linear MS/MS spectrometer determined the total $CoQ_{10}$ content. The mobile phase consisted of solvent A (methanol/isopropanol, 95:5, with 2.5 mM ammonium formate) and solvent B (isopropanol, with 2.5 mM ammonium formate). The percentage of solvent B started at 0% for the first 1.5 minutes, increased linearly to 15% by 2 minutes, remained constant for the next 1 minute, and decreased linearly back to 0% by 4 minutes. The flow rate remained constant at 600 µl/min. Data acquisition and processing required Analyst software (version 1.4.2). Multiple-reaction monitoring mode detected quinone content, with the following transitions: mass-to-charge [*m*/*z*] ratio 880.7:197.0 ($CoQ_{10}$ with ammonium adduct); *m*/*z* 882.7:197.0 ($Q_{10}H_2$ with ammonium adduct); *m*/*z* 908.7:225.1 (diethoxy-$Q_{10}$ with ammonium adduct), and *m*/*z* 910.7:225.1 (diethoxy-$Q_{10}H_2$ with ammonium adduct).

*Mitochondrial respiratory enzyme activity measurement.* Fibroblasts derived from controls (NHDF-neo, Bio-Rad), healthy parents, or 2 affected individuals (Pt5496 and Pt5497) were seeded at 20,000 cells per well in 80 ml DMEM and incubated at 37°C, 5% $CO_2$ for 24 hours. In vivo maximal uncoupled OCR over the whole respiratory chain, including the $CoQ_{10}$ transfer of electrons from mitochondrial complex I and complex II to complex III, was measured using the XF96 Extracellular Flux Analyzer (Seahorse Bioscience) (40). Mitochondria membrane potential was uncoupled by the addition of carbonyl cyanide 4-(trifluoromethoxy) phenylhydrazone (FCCP, 0.4 µM). Nonmitochondrial respiration was determined after the addition of 2.5 µM rotenone/5 µM antimycin A.

*RNAi-based Drosophila nephrocyte functional assay.* The MHC-ANF-RFP transgenic flies were generated in previous studies (14, 41). Nephrocyte-specific gene knockdown was achieved by using nephrocyte-specific Gal4 and UAS-RNAi transgenes (14, 41). Nephrocyte function was measured by the amount of secreted red fluorescent proteins accumulated in nephrocytes at the second instar larvae stage (14, 41). Hand-GFP (42) was used to label the cardiac nephrocytes.

*Statistics.* Results are presented as mean ± SEM or SD for the number of experiments indicated in the figure legends. Statistical analysis of continuous data was performed with 2-tailed Student's *t* test or multiple comparison, as appropriate. $P < 0.05$ was considered statistically significant.

*Study approval.* Approval for research in human subjects was obtained from the IRBs of the University of Michigan, Boston Children's Hospital, Université Paris Descartes, University of Toronto, Yale University, and Beth Israel Deaconess Medical Center.

## Acknowledgments

The authors thank the families who contributed to this study. This research was supported by grants from the NIH to F. Hildebrandt (DK076683, DK086542), to R.C. Wiggins (DK46073 and DK081943), to E.A. Otto (DK090917), to W. Zhou (DK091405), to Z. Han (R01HL090801), to D.S. Williams (EY07042), and to R.P. Lifton (U54HG006504); by the Kidney Foundation of Canada and Nephcure Canada (to A.D. Paterson and Y. Pei); by the Nephcure Foundation (to F. Hildebrandt and M. Pollak); by the National Research Foundation (Basic Science Research Program funded by the Ministry of Education, Science and Technology) (to H.Y. Gee, 2012R1A6A3A03040212); by the American Heart Association (to Z. Han, AHA-0630178N); by the Association Francaise contre les Myopathies (to C. Antignac, GLOMGENE project: ANR-08-GENOPAT-017-01); by the Fondation pour la Recherche Médicale (to C. Antignac, project DMP 2010-11-20-386); by the European Community's 7th Framework program grant (to C. Antignac, Eurenomics 2012-305608); by a Ruth L. Kirschstein NIH Service Award (to L.X. Xie, GM 007185); by Kids Kidney Research and Garfield Weston Foundation (to D. Böckenhauer and R. Kleta); by the King Abdul-Aziz University (to J.A. Kari, D. Böckenhauer, and R. Kleta); by the Fondazione CARIPARO (to L. Salviati); by a National Science Foundation grant (to C.F. Clarke, 0919609); and by the German Network of mitochondrial disorders (to H. Prokisch, mitoNET 01GM1113C). The LC-MS/MS determination of quinones was supported in part by NIH grant S10RR024605 from the National Center for Research Resources. The authors also acknowledge with thanks the Deanship of Scientific Research; King Abdulaziz University, Jeddah, for their support; the Bloomington stock center; and the Vienna Drosophila RNAi Center for *Drosophila* stocks. H.Y. Gee is a research fellow of the American Society of Nephrology. A.D. Paterson holds a Canada Research Chair in Complex Traits Genetics. W. Zhou is a Carl W. Gottschalk Scholar. D. Böckenhauer is a Higher Education Funding Council for England Clinical Reader. D.S. Williams is an Research to Prevent Blindness Jules and Doris Stein professor. F. Hildebrandt is an investigator of the Howard Hughes Medical Institute and the Frederick G.L. Huetwell Professor.

Received for publication January 28, 2013, and accepted in revised form September 6, 2013.

Address correspondence to: Friedhelm Hildebrandt, Howard Hughes Medical Institute, Boston Children's Hospital, 300 Longwood Avenue, HU319, Boston, Massachusetts 02115, USA. Phone: 617.355.6129; Fax: 617.730.0569; E-mail: Friedhelm.Hildebrandt@childrens.harvard.edu. Or to: Corinne Antignac, Inserm U983 (ex-U574) and Department of Genetics, Necker Hospital, 149,

Downloaded on July 3, 2014. The Journal of Clinical Investigation. More information at www.jci.org/articles/view/69000



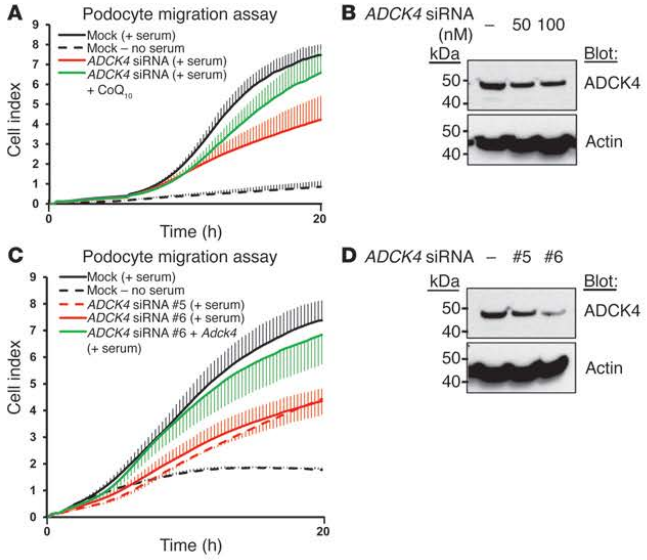



**Figure 6**
Knockdown of ADCK4 decreases the migratory phenotype of podocytes. (**A**) The effect of ADCK4 knockdown on podocyte migration. Podocytes transfected with *ADCK4* siRNA (red) exhibited decreased migration compared with podocytes transfected with scrambled siRNA (black). The decrease in podocyte migration was partially reversed by the addition of 50 μM $CoQ_{10}$ (green). Error bars are shown in only one direction for clarity and indicate SDs from 3 independent experiments. (**B**) The efficiency of *ADCK4* siRNA used in **A** was confirmed by immunoblotting with an anti-ADCK4 antibody and an anti–β-actin antibody. (**C**) Transfection of podocytes with 2 additional *ADCK4*-specific siRNAs (siRNA #5 and #6) confirmed the result from **A** that ADCK4 knockdown in human podocytes reduces migration (red dotted and solid lines) compared with podocytes transfected with the scrambled siRNA (black). The decrease in podocyte migration by ADCK4 knockdown using *ADCK4* siRNA #6 was rescued by transfection of mouse *Adck4* construct (green). Mouse ADCK4 has 5 mismatches from the siRNA target sequences. Error bars indicate SDs of 3 independent experiments. (**D**) The efficiency of *ADCK4* siRNAs used in **C** was confirmed by immunoblotting. 100 nM of each siRNA was transfected into podocytes.

In conclusion, we identified recessive mutations in *ADCK4* as novel single-gene causes of SRNS. Early recognition of this new genetic entity of SRNS will be important because it may represent a form of SRNS that can potentially be treated by $CoQ_{10}$ supplementation.

## Methods

*Subjects.* Following informed consent, we obtained clinical data and blood samples from individuals with SRNS or steroid-sensitive NS from worldwide sources. The diagnosis of NS was made by (pediatric) nephrologists based on standardized clinical and renal histological criteria (34). Renal biopsies were evaluated by renal pathologists. Clinical data were obtained using a standardized questionnaire (http://www.renalgenes.org).

*HM, WER, and mutation calling.* For the A2338 family, HM, WER, and mutation calling were performed as described previously (35). HM in the 231 and ABD families was performed using Human Mapping 250k *NspI* Array (Affymetrix), and parametric logarithm of odds (LOD) scores were calculated with MERLIN (36). For WER of the 231, ABD, and Mek families, DNA was processed using All Exon 50Mb V3 (Agilent SureSelect) to enrich for exonic sequences and a SOLiD 5500XL high-throughput sequencing machine (Applied Biosystems) (paired-end reads: 50 bases forward, 25 bases reverse). Obtained sequences were aligned to the human genome (NCBI build 37/hg19) using Lifescope suite from Lifetech. Substitution and variation calls were made with the GATK pipeline (mpileup, bfctools, vcfuitil). Variants were then annotated with an in-house software (Polyweb), which allows users to set up bioinformatic filters in order to identify the putative mutation.

*Plasmids, cell culture, and transfection.* A human *ADCK4* clone was purchased from Open Biosystems (clone accession BC013114.1). The mutant clones of *ADCK4* were generated by a PCR-based site-directed mutagenesis method. The *COQ6* clones were described previously (7). The immortalized human podocytes (37) were maintained in RPMI plus GlutaMAX-I (Gibco) supplemented with 10% FBS, penicillin (50 IU/ml)/streptomycin (50 μg/ml), and Insulin-Transferrin-Selenium-X (Invitrogen). Plasmids and siRNA were transfected into podocytes using Lipofectamine 2000 (Invitrogen). The *ADCK4*-specific and control scrambled siRNAs were purchased from Dharmacon or Sigma-Aldrich. Lymphoblasts were purified from blood samples using Ficoll-Paque PLUS (GE Healthcare) according to the manufacturer's instructions. The isolated lymphoblasts were transformed by EBV and immortalized as described previously (38). Human fibroblasts were grown in DMEM supplemented with 15% FBS, penicillin (50 IU/ml)/streptomycin (50 μg/ml), and nonessential amino acids (Invitrogen).

*Immunoblotting, immunoprecipitation, and IF staining.* These experiments were performed as described previously (13). Anti-ADCK4 (LSBio), anti-MTCO1 (Abcam), anti-COXIV (Abcam), anti-COQ6 (Santa Cruz Biotechnology Inc.), anti-COQ7 (Proteintech), and anti-V5 (Invitrogen) were used. Fluorescent images were obtained with a Leica SP5X laser scanning microscope.

*Immunogold electron microscopy.* Rat renal cortex samples were dissected and trimmed into 1-mm-thick blocks, which were fixed by immersion in 4% formaldehyde and 0.5% glutaraldehyde in 0.1 M cacodylate buffer, pH 7.4, and processed for embedment in LR White. Semithin sections (700 nm) were first obtained to locate areas that contained glomeruli. Subsequently, ultrathin sections (70 nm) were obtained from those areas and collected on formvar-coated nickel grids and etched with saturated sodium periodate for 15 minutes. Sections were blocked with 0.1 M phosphate buffer, pH 7.4, containing 1% BSA, 3% goat serum, and 0.05% Tween-20 for 1 hour at room temperature and incubated with a rabbit anti-ADCK4 antibody (LSBio) in buffer overnight at 4°C. Sections were then washed and incubated with goat anti-rabbit IgG conjugated to 18 nm gold (Jackson ImmunoResearch Laboratories) and stained with uranyl acetate. Sections in which the primary antibody was omitted during the overnight incubation were used as negative control. Sections were observed on a Zeiss 910 transmission electron microscope.

*Mitochondrial fractionation.* The mitochondrial fractionation of podocytes was done using Mitochondrial Isolation Kit for Cultured Cells (Thermo Scientific), Mitochondrial/Cytosol Fractionation Kit (Abcam), and Mitochondrial Fractionation Kit (Active Motif) according to the manufacturer's instructions.

Downloaded on July 3, 2014. The Journal of Clinical Investigation. More information at www.jci.org/articles/view/69000





rue de Sevres, 75015 Paris, France. Phone: 33.1.44.49.50.98; Fax: 33.1.44.49.02.90; E-mail: corinne.antignac@inserm.fr. Or to: York Pei, Division of Nephrology and of Genomic Medicine, University Health Network and University of Toronto, 8N838, 585 University Avenue, Toronto, Ontario, Canada M5G2N2. Phone: 416.340.4257; Fax: 416.340.4999; E-mail: York.Pei@uhn.ca.

1. Antignac C. Genetic models: clues for understanding the pathogenesis of idiopathic nephrotic syndrome. *J Clin Invest.* 2002;109(4):447–449.
2. Hinkes BG, et al. Nephrotic syndrome in the first year of life: two thirds of cases are caused by mutations in 4 genes (NPHS1, NPHS2, WT1, and LAMB2). *Pediatrics.* 2007;119(4):e907–e919.
3. Kim MS, Stablein D, Harmon WE. Renal transplantation in children with congenital nephrotic syndrome: a report of the North American Pediatric Renal Transplant Cooperative Study (NAPRTCS). *Pediatr Transplant.* 1998;2(4):305–308.
4. Benoit G, Machuca E, Heidet L, Antignac C. Hereditary kidney diseases: highlighting the importance of classical Mendelian phenotypes. *Ann N Y Acad Sci.* 2010;1214:83–98.
5. Hildebrandt F. Genetic kidney diseases. *Lancet.* 2010;375(9722):1287–1295.
6. Ozaltin F, et al. Disruption of PTPRO causes childhood-onset nephrotic syndrome. *Am J Hum Genet.* 2011;89(1):139–147.
7. Heeringa SF, et al. COQ6 mutations in human patients produce nephrotic syndrome with sensorineural deafness. *J Clin Invest.* 2011;121(5):2013–2024.
8. Hildebrandt F, et al. A systematic approach to mapping recessive disease genes in individuals from outbred populations. *PLoS Genet.* 2009; 5(1):e1000353.
9. Otto EA, et al. Candidate exome capture identifies mutation of SDCCAG8 as the cause of a retinal-renal ciliopathy. *Nat Genet.* 2010;42(10):840–850.
10. Halbritter J, et al. High-throughput mutation analysis in patients with a nephronophthisis-associated ciliopathy applying multiplexed barcoded array-based PCR amplification and next-generation sequencing. *J Med Genet.* 2012;49(12):756–767.
11. Robu ME, et al. p53 activation by knockdown technologies. *PLoS Genet.* 2007;3(5):e78.
12. Zhou W, Hildebrandt F. Inducible podocyte injury and proteinuria in transgenic zebrafish. *J Am Soc Nephrol.* 2012;23(6):1039–1047.
13. Hinkes B, et al. Positional cloning uncovers mutations in PLCE1 responsible for a nephrotic syndrome variant that may be reversible. *Nat Genet.* 2006;38(12):1397–1405.
14. Zhang F, Zhao Y, Han Z. An in vivo functional analysis system for renal gene discovery in Drosophila pericardial nephrocytes. *J Am Soc Nephrol.* 2013; 24(2):191–197.
15. Lagier-Tourenne C, et al. ADCK3, an ancestral kinase, is mutated in a form of recessive ataxia associated with coenzyme Q10 deficiency. *Am J Hum Genet.* 2008;82(3):661–672.
16. Quinzii CM, Hirano M. Primary and secondary $CoQ_{10}$ deficiencies in humans. *Biofactors.* 2011; 37(5):361–365.
17. Mollet J, et al. Prenyldiphosphate synthase, subunit 1 (PDSS1) and OH-benzoate polyprenyltransferase (COQ2) mutations in ubiquinone deficiency and oxidative phosphorylation disorders. *J Clin Invest.* 2007;117(3):765–772.
18. Quinzii CM, et al. Coenzyme Q deficiency and cerebellar ataxia associated with an aprataxin mutation. *Neurology.* 2005;64(3):539–541.
19. López LC, et al. Leigh syndrome with nephropathy and CoQ10 deficiency due to decaprenyl diphosphate synthase subunit 2 (PDSS2) mutations. *Am J Hum Genet.* 2006;79(6):1125–1129.
20. Quinzii C, et al. A mutation in para-hydroxybenzoate-polyprenyl transferase (COQ2) causes primary coenzyme Q10 deficiency. *Am J Hum Genet.* 2006; 78(2):345–349.
21. Mollet J, et al. CABC1 gene mutations cause ubiquinone deficiency with cerebellar ataxia and seizures. *Am J Hum Genet.* 2008;82(3):623–630.
22. Salviati L, et al. Haploinsufficiency of COQ4 causes coenzyme Q10 deficiency. *J Med Genet.* 2012; 49(3):187–191.
23. Diomedi-Camassei F, et al. COQ2 nephropathy: a newly described inherited mitochondriopathy with primary renal involvement. *J Am Soc Nephrol.* 2007; 18(10):2773–2780.
24. Lopez-Martin JM, et al. Missense mutation of the COQ2 gene causes defects of bioenergetics and de novo pyrimidine synthesis. *Hum Mol Genet.* 2007; 16(9):1091–1097.
25. McCarthy HJ, et al. Simultaneous sequencing of 24 genes associated with steroid-resistant nephrotic syndrome. *Clin J Am Soc Nephrol.* 2013;8(4):637–648.
26. Salviati L, et al. Infantile encephalomyopathy and nephropathy with CoQ10 deficiency: a CoQ10-responsive condition. *Neurology.* 2005;65(4):606–608.
27. Multiple-System Atrophy Research Collaboration. Mutations in COQ2 in familial and sporadic multiple-system atrophy. *N Engl J Med.* 2013;369(3):233–244.
28. Montini G, Malaventura C, Salviati L. Early coenzyme Q10 supplementation in primary coenzyme Q10 deficiency. *N Engl J Med.* 2008;358(26):2849–2850.
29. Do TQ, Hsu AY, Jonassen T, Lee PT, Clarke CF. A defect in coenzyme Q biosynthesis is responsible for the respiratory deficiency in Saccharomyces cerevisiae abc1 mutants. *J Biol Chem.* 2001; 276(21):18161–18168.
30. Xie LX, et al. Expression of the human atypical kinase ADCK3 rescues coenzyme Q biosynthesis and phosphorylation of Coq polypeptides in yeast coq8 mutants. *Biochim Biophys Acta.* 2011;1811(5):348–360.
31. Tauche A, Krause-Buchholz U, Rödel G. Ubiquinone biosynthesis in Saccharomyces cerevisiae: the molecular organization of O-methylase Coq3p depends on Abc1p/Coq8p. *FEMS Yeast Res.* 2008; 8(8):1263–1275.
32. Albaqumi M, Soos TJ, Barisoni L, Nelson PJ. Collapsing glomerulopathy. *J Am Soc Nephrol.* 2006; 17(10):2854–2863.
33. Barisoni L, Madaio MP, Eraso M, Gasser DL, Nelson PJ. The kd/kd mouse is a model of collapsing glomerulopathy. *J Am Soc Nephrol.* 2005; 16(10):2847–2851.
34. [No authors listed]. Primary nephrotic syndrome in children: Clinical significance of histopathologic variants of minimal change of diffuse mesangial hypercellularity: A Report of the International Study of Kidney Disease in Children. *Kidney Int.* 1981;20(6):765–771.
35. Gee HY, et al. ARHGDIA mutations cause nephrotic syndrome via defective RHO GTPase signaling. *J Clin Invest.* 2013;123(8):3243–3253.
36. Abecasis GR, Cherny SS, Cookson WO, Cardon LR. Merlin--rapid analysis of dense genetic maps using sparse gene flow trees. *Nat Genet.* 2002;30(1):97–101.
37. Saleem MA, et al. A conditionally immortalized human podocyte cell line demonstrating nephrin and podocin expression. *J Am Soc Nephrol.* 2002; 13(3):630–638.
38. Arnoli MM, Carthy D, Platt H, Ollier WE. EBV Immortalization of human B lymphocytes separated from small volumes of cryo-preserved whole blood. *Int J Epidemiol.* 2008;37(suppl 1):i41–i45.
39. Falk MJ, et al. Probucol ameliorates renal and metabolic sequelae of primary CoQ deficiency in Pdss2 mutant mice. *EMBO Mol Med.* 2011;3(7):410–427.
40. Haack TB, et al. Molecular diagnosis in mitochondrial complex I deficiency using exome sequencing. *J Med Genet.* 2012;49(4):277–283.
41. Zhang F, Zhao Y, Chao Y, Muir K, Han Z. Cubilin and amnionless mediate protein reabsorption in Drosophila nephrocytes. *J Am Soc Nephrol.* 2013; 24(2):209–216.
42. Han Z, Olson EN. Hand is a direct target of Tinman and GATA factors during Drosophila cardiogenesis and hematopoiesis. *Development.* 2005; 132(15):3525–3536.